Low-dose IL-2 administration and amyotrophic lateral sclerosis (ALS): understanding the transcriptional response after treatment

By

Ilaria Giovannelli

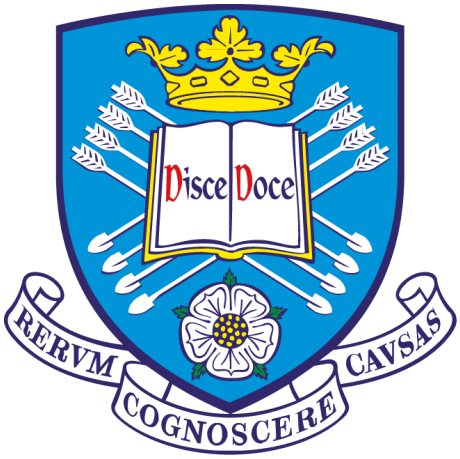

The University Of Sheffield.

Sheffield Institute for Translational Neuroscience

Department of Neuroscience

Thesis submitted for the degree of

Doctor of Philosophy (PhD)

October 2021

Table of Contents

List of figures

List of Tables

List of abbreviations

AA: Alopecia areata
AD: Alzheimer's disease
AIDs: Autoimmune diseases
ALS: Amyotrophic lateral sclerosis,
APC: antigen-presenting cells
APE1: Apurinic/apyrimidinic endonuclease 1
AUC: Area under the curve
BBB: Blood brain barrier
BDNF: Brain-derived neurotrophic factor
CCL: Chemokine ligand
CNS: Central nervous system
COX2: Cyclooxygenase-2
CR: Complement receptor
cRNA: Complementary RNA
CSF: Cerebrospinal fluid
CTLA4: Cytotoxic T lymphocytes antigen 4
CXCL: Chemokine (C-X-C motif) ligand
D: Day
DC: Dendritic cell
DEG: Differentially expressed gene
DEREG: Treg-depleted
DMSO: Dimethyl Sulfoxide
ds cDNA: Double-stranded complementary DNA
EAAT: Excitatory amino acid transporter
EMA: European Medicine Agency
ER: Endoplasmic reticulum
ETC: Electron transport chain
fALS: Familial ALS
FBS: Foetal bovine serum
FC: Fold change
FDA: U.S. Food and Drug Administration

FOV: Field of views

FOXP3: Forkhead box Protein 3

FTD: Frontotemporal degeneration

FUS: Fused in sarcoma

GDNF: Glial cell-derived neurotrophic factor

GFAP: Glial fibrillary acidic protein

GITR: Glucocorticoid-induced tumour necrosis factor receptor

GluR2: Glutamate receptor 2

GO BP: Gene Ontology biological process

GO: Gene Ontology

GVHD: Graft-versus-host disease

HCV: Hepatitis C virus

HD: Huntington's disease

hnRNP: Heterogeneous nuclear ribonucleoproteins

HSCT: Hematopoietic stem cells transplantation

iAstrocytes: iNPC-derived astrocytes

ICER: Inducible cAMP early repressor

ICOS: Inducible T cell co-stimulator

IDO: Indoleamine 2,3-dioxygenase

IFN: Interferon

IGF: Insulin growth factor

IL-2Rα or IL2RA: Interleukin-2 receptor alpha chain

IL-2Rβ or IL2RB: Interleukin-2 receptor beta chain

IL-2Rγ or IL2RG: Interleukin-2 receptor gamma chain

IL: Interleukin

IMODALS: Immuno-Modulation in Amyotrophic Lateral Sclerosis

iNOS: Inducible nitric oxygen synthase

iNPC: Induced neuronal progenitor cell

IPA: Ingenuity Pathway Analysis

IPEX: Immunodysregulation polyendocrinopathy enteropathy X-linked syndrome

iPSC: induced pluripotent stem cell

IVT: In vitro transcription

Kd: Constant of dissociation

Ld-IL-2: Low dose IL-2

LDH: Lactate dehydrogenase
LINC: Long intergenic non protein coding
LMN: Lower motor neuron
LOOCV: Leave one out cross validation
LPS: Lipopolysaccharide
MDS: Multidimensional scaling
mEB: Mouse embryonic bodies
mESC: Mouse embryonic stem cells
MHC: Major histocompatibility complex
MIU: Millions of international units
MN: Motor neuron
MND: Motor neuron disease
mSOD1: Mutant SOD1
mTOR: Mechanistic target of rapamycin
NES: Nuclear export sequence
NFAT: Nuclear factor of activated T cells
NFL: Neurofilament light chain
NGF: Nerve growth factor
NK: Natural killer cells
NKGD2: Natural killer group 2D
NMJ: Neuromuscular junction
NO: Nitric oxide
NOX2: NADPH oxidase 2
Nrf2: Nuclear erythroid 2-related factor
PAMPs: Pathogen associated molecular pattern molecules
PBS: Phosphate-buffered saline
PCA: Principal component analysis
PD: Parkinson’s disease
PGE2: Prostaglandin E2
QC: Quality control
qRT-PCR: Quantitative real-time polymerase chain reactions
R: Pearson correlation coefficient
RCC: Reporter Code Count
REVIGO: REduce and VIsualize Gene Ontology

RIN: RNA integrity number

RMSE: Root mean squared error

RNS: Reactive nitrogen species

ROC: Receiver operator curve

ROS: Reactive oxygen species

sALS: Sporadic ALS

SD: Standard deviation

SLE: Systemic lupus erythematosus

SOD1: Superoxide dismutase 1

ss cDNA: Single-stranded complementary DNA

SST-RMA: Signal space transformation robust multi-chip analysis

T1D: Type 1 diabetes

TAC: Transcriptome Analysis Console

TARDBP: Transcriptional repressor of the transactive response (TAR) DNA binding protein also referred to as TDP-43 (TAR DNA binding protein 43).

TCR: T cell receptor

TdT: Terminal deoxynucleotidyl transferase

TGF: Transforming growth factor

Th: T helper cells

TLR: Toll-like receptor

TNF: Tumour necrosis factor

TNFSF: Tumour necrosis factor superfamily

Treg: Regulatory T cell

TSDR: Treg-specific demethylated region

UDG: Uracil-DNA glycosylase

ULD: Ultra-low dose

UMN: Upper motor neuron

VEGFR2: Vascular endothelial growth factor receptor 2

VIF: Variance inflation factor

WBC: White blood cells

Acknowledgments

This work would not have been possible without the help of many, fantastic people who supported me throughout these years.

First and foremost, I am extremely grateful to my supervisors Prof Janine Kirby and Prof Dame Pamela Shaw for having given me this exceptional opportunity to undertake a PhD in their laboratory. Their invaluable guidance, constructive feedback and also personal support have been crucial throughout this journey. They always believed in me and made me grow as a researcher and a writer. I am also forever thankful to Dr Paul Heath for his exceptional academic and personal support.

I am sincerely grateful to all the individuals suffering from ALS who have generously donated their biosamples without whom this research work would not have been possible. Additionally, this PhD would not have been feasible without my funding body the NIHR Sheffield Biomedical Research Centre. I am also very grateful to the Motor Neuron Disease Association for having founded the work involving patient-derived astrocytes. I would also like to thank Abigail and Nadhim for having helped with the IMODALS sample processing, to the Bioinformatic Core for their computational support and to Dr Laura Ferraiuolo and her team for their invaluable assistance with the cell culture work.

This journey would not have been the same without all my fellow PhD colleagues at SITraN and, in particular, to my close friends: Giuseppe, Valentina, Marco, Paolo, Hubashia, Lara, Maria, I love you all! A special mention goes to Michela and my mentor Matilde, your friendship is one of the best things that happened in these years.

Despite the distance, my dearest and oldest friends from Italy: Ludovica, Michela, Eugenia, Francesca, Giulia, Beatrice, Romina, Tamara, Lara, Andrea and Luca have always been there for me…with lots of video calls!

Impossible not to mention my wonderful boyfriend Leonardo with whom I shared all this amazing journey. He is one of the most supportive, sweet and caring people I know.

Last but not least, a huge thanks goes to my family for their love and belief in me. I missed you all greatly but I have always found an exceptional support from you. A special mention goes to my aunt Anna and my little cousins Martina and Maurizio who constantly gave me love, laughter and encouragement. I would not have achieved anything without my mum, dad and brother Luca who have always been my pillars and life models. I cannot be more grateful to them for providing me with every possible opportunity in life, for all their sacrifices to get me where I am and for having filled me with love and support. I hope I made you proud.

Abstract

Background: Amyotrophic lateral sclerosis (ALS) is a fatal, neurodegenerative disease whose pathogenesis involves neuroinflammation. Regulatory T cells (Tregs) normally suppress excessive inflammation preventing the onset of autoimmune disorders. However, in ALS, Tregs are dramatically and progressively decreased, with lower levels associated with shorter survival. Low-doses of interleukin-2 (ld-IL-2) promote Treg expansion and restore the physiological immune balance. Additionally, IL-2 has been reported to penetrate the blood-brain barrier and exert protective effects on neurons and glia.

Aims: **1**) To evaluate ALS peripheral blood transcriptional changes associated with ld-IL-2 in patients participating in the IMODALS trial. **2**) To assess effects of IL-2 on patient-derived astrocytes.

Methods: 36 patients in the IMODALS trial were randomly assigned to three treatment arms: 1MIU-IL-2, 2MIU-IL-2 or placebo. At four time-points, blood was collected and gene expression profiles were generated. Patient-derived-astrocytes were differentiated from ALS or healthy volunteer fibroblasts, treated *in vitro* with IL-2 and transcriptionally profiled. IL-2 was also assessed in co-cultures of motor neurons (MN) and patient-derived-astrocytes.

Findings: Gene expression analyses revealed longitudinal changes throughout the IMODALS trial. Evidence of a broad immune suppression was provided after the first treatment cycle whilst activation of immune suppressive pathways reached a peak after the third cycle. A time-dependent and dose-dependent activation of Treg markers was identified which suggested a cumulative effect of ld-IL-2. However, inter-individual differences were found amongst patients, who were classified into high, moderate and low-responders. A predictive biomarker analysis identified two genes, whose baseline expression was able to predict patient responsiveness to ld-IL-2.

Patient-derived-astrocytes were treated with IL-2 and RNA sequencing revealed evidence of potentially protective changes including activation of axonogenesis and a reduction in oxidative stress. These findings suggest a reduction in the ALS astrocyte-mediated MN toxicity, which is in keeping with preliminary data showing an increase in MN viability when co-cultured with IL-2-treated astrocytes.

Chapter 1 – Introduction

Amyotrophic lateral sclerosis (ALS), also referred to as motor neuron disease (MND), is a devastating adult-onset neurodegenerative disease characterised by the progressive loss of both upper (UMN) and lower motor neurons (LMN) (Ingre et al., 2015). UMNs originate from the motor cortex and project their fibres to the LMNs in the brainstem and the spinal cord. UMNs control the activity of the LMNs which, themselves, innervate the skeletal muscle fibres allowing voluntary movements (Hardiman et al., 2017). The first symptom of this pathology is muscle weakness which affects a discrete body region. As the disease progresses, this spreads and the continuing degeneration leads to a range of clinical manifestations including muscle fasciculation, spasticity, muscular atrophy and, finally, paralysis. Patients lose their ability to control nearly all skeletal muscles. The only MNs relatively protected from the neurodegenerative process are neurons of the oculomotor (CNIII), trochlear (CNIV) and abducens (CNVI) nuclei which enable eye movements, and MNs of the Onuf's nucleus in the sacral spinal cord which control pelvic floor muscles (Nijssen et al., 2017, Grad et al., 2017). Interestingly, 50% of ALS patients also manifest features of neuropsychological dysfunction, while approximately 15% develop overt frontotemporal dementia (FTD) (Hardiman et al., 2017, Robberecht and Philips, 2013). Eventually the disease results in death, most commonly due to the paralysis of respiratory muscles and resultant neuromuscular respiratory failure. This usually occurs within 3 to 5 years after the diagnosis although remarkable variations are reported in patient life expectancy. Some individuals survive just a few months, while in others death occurs after several decades (Al-Chalabi et al., 2016).

The overall incidence of ALS worldwide is between 0.6 and 3.8 per 100,000 per year. This is slightly higher in Europe where between 2.1 and 3.8 new cases per 100.000 are reported annually (Longinetti and Fang, 2019). This pathology affects slightly more men than women (ratio men:women is 1.5:1) (Marin et al., 2017). The mean disease age of onset is approximately between 50 and 70 years. Juvenile forms of ALS, which exhibit before 25 years of age, are quite rare (Logroscino et al., 2010).

Despite ALS being first described by the French neurologist Jean-Martin Charcot in 1865, after almost two centuries of research, there is still no effective cure or disease-modifying treatment. Riluzole, a benzothiazole, is the only available drug which has been approved by both the U.S. Food and Drug Administration (FDA) and the European Medicine Agency (EMA) for the treatment of ALS. This is a glutamatergic antagonist and, although the precise mechanism of action is still controversial, it is believed to reduce excitotoxicity and thus has a modest neuroprotective effect on MNs. In particular, riluzole seems to block pre-synaptic sodium channels which reduces the excessive amount of glutamate released into the inter-synaptic cleft. This dampens the consequent detrimental over-stimulation of MNs. Unfortunately, riluzole extends patients survivals by only 3 months on average (Nagoshi et al., 2015, Fang et al., 2018). In 2017, Edaravone was approved only by the FDA for the treatment of ALS and it is now available with the commercial name of Radicava. It acts as a free-radical scavenger which reduces the levels of peroxyl radicals and peroxynitrite, free-radicals which cause oxidative stress. However, the long-term effect of this compound are still to be elucidated (Edaravone Writing Group, 2017).

ALS is generally classified into bulbar or spinal forms depending on the site of onset of disease symptoms. Bulbar onset, which accounts for approximately 30% of ALS cases, is characterized by an initial degeneration of the motor neurons located in the brain stem. Therefore, speech and swallowing muscles are the first affected. The majority of the patients (about 70%) have spinal disease onset. In this case, the first symptoms reported are weakness, spasticity or atrophy of the upper or lower limbs, with usually only one side being initially affected (Al-Chalabi et al., 2016, Shellikeri et al., 2017). An uncommon onset comes with respiratory symptoms which occurs in less than 3% of ALS cases. In such patients the first symptoms reported are dyspnoea (breathing difficulties) or orthopnoea (sensation of breathlessness in a lying position). This is generally associated with a poorer prognosis (Gautier et al., 2010).

1.1 ALS genes and pathological mechanisms

1.1.1 ALS genes and mutations

Another classical way of classifying ALS is by heritability and two forms of this disease are defined as:

- Familial ALS (fALS): Only 5-10% of all the diagnosed patients have a familial or hereditable ALS form. The vast majority of cases show an autosomal dominant inheritance, but autosomal recessive or X-linked patterns have also been reported in the literature (Andersen and Al-Chalabi, 2011, Byrne et al., 2011).

- Sporadic ALS (sALS): the majority of the ALS cases are sporadic (approximately 90-95%). This means that there is no evidence of family history of the disease although this does not imply the absence of genetic mutations. Sporadic ALS has been associated with several environmental factors, including some pesticides, fertilizers or the exposure to heavy metallic compounds (Paez-Colasante et al., 2015). Multiple studies suggest a correlation between ALS and intense physical exercise or professional sports, in particular football (Julian et al., 2021, Harwood et al., 2016, Chiò et al., 2005, Blecher et al., 2019). Although the relationship between sport and/or exercise and ALS is still unclear, it is believed to be at least partially due to repeated injuries and head traumas, use of drugs or dietary/ nutritional factors (Lacorte et al., 2016).

Importantly, familial and sporadic ALS are clinically indistinguishable.

In the last few decades, thanks to constantly improving sequencing technologies, new genetic factors associated with ALS have been discovered (Bettencourt and Houlden, 2015). Nearly fifty genes were identified as potentially causative or impactful in ALS disease onset and/or progression, with multiple mutations discovered in each of those (Mejzini et al., 2019). However, the genetic background of the vast majority of the ALS

cases is still unknown. In the next section, the most common genetic mutations associated with this disease are reported and briefly described (**Figure 1.1**).

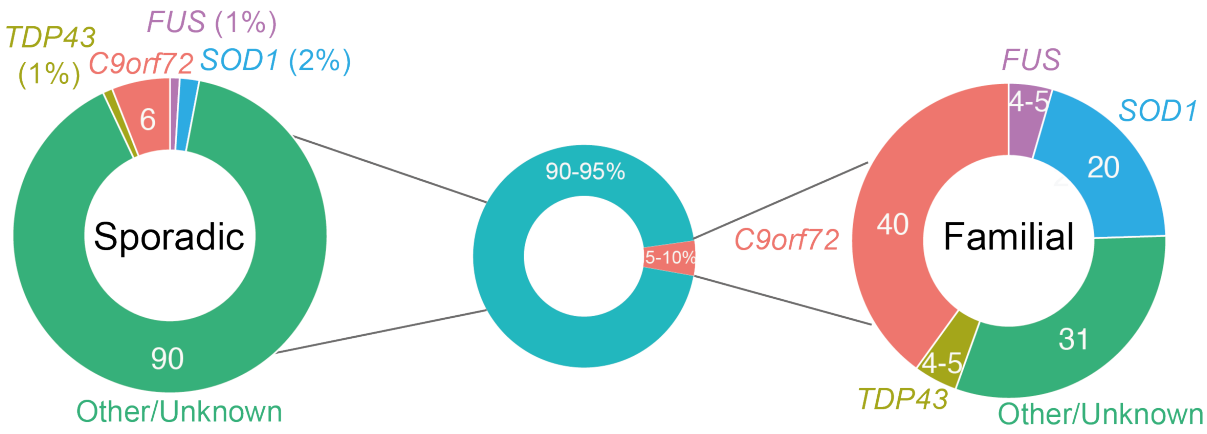

Figure 1.1. Genetics of familial and sporadic ALS.

Image showing the proportion of familial (5-10%) and sporadic (90-95%) ALS cases. For each of the two subgroups, the percentage of the four most common genes (*C9orf72*, *SOD1*, *TARDBP* and *FUS*), which mutations are associated with ALS, is reported. A considerable proportion of the sporadic cases currently do not have identified risk factors.

1.1.1.1 Superoxide Dismutase 1

In 1993, the first genetic mutations responsible for ALS were discovered. These occur in the gene coding for superoxide dismutase 1 (*SOD1*) located on chromosome 21 at position q22.11. To date, nearly 200 mutations have been identified in the *SOD1* gene (http://alsod.ac.uk). These occur in approximately 20% of fALS and in 2% of sALS patients (Mejzini et al., 2019, Zou et al., 2017). SOD1 is a ubiquitously expressed antioxidant enzyme, which functions as a homodimer made by two monomers of 16 kDa and catalyses the production of O_2 and H_2O_2 from superoxide (O_2^-) free radicals. Several mechanisms underlying SOD1 toxicity in ALS were proposed. Initially, a loss of antioxidant function was suggested with a consequent increased in superoxide concentrations, oxidative stress and cell death (Rosen et al., 1993, Deng et al., 1993). Nonetheless, knock-out SOD1 mice failed to show an evident ALS phenotype

(Reaume et al., 1996, Saccon et al., 2013), whereas the overexpression of the mutated human protein caused the expected ALS symptoms and these mice are now commonly used as ALS animal models (i.e. $SOD1^{G93A}$ mice) (Saccon et al., 2013). Therefore, it is now believed that MN injury in SOD1-ALS more likely occurs via a complex toxic gain of function mechanism which includes: (i) augmented enzymatic activity and increased H_2O_2 levels and (ii) the presence of misfolded SOD1 and the accumulation of aggregates (Kaur et al., 2016, Pansarasa et al., 2018, Barber and Shaw, 2010). Interestingly, a recent publication suggested that wild-type dismutase is also misfolded in the CSF of sALS patients in the absence of any gene mutations (Tokuda et al., 2019). Moreover, SOD1 aggregates were not exclusively found in MN but appeared also in glial cells including microglia and astrocytes (Forsberg et al., 2011).

1.1.1.2 C9ORF72

In 2011, the hexanucleotide repeat expansion (HRE) GGGGCC (G4C2) in the open reading frame 72 on chromosome 9, at position 9q21.2, was found to be associated with ALS. In particular, whilst in the healthy population the hexanucleotide is repeated less than 30 times, in the ALS patients there are usually more than 700 repeats (Kwon et al., 2014). This is the most common genetic cause of ALS, in fact the *C9orf72* HRE occurs in about 40% of fALS and in 5-7% of sALS cases (Mejzini et al., 2019, Ranganathan et al., 2020, Majounie et al., 2012).

The physiological functions exerted by C9orf72 protein are still unclear. However, considering its structural homology with the DENN (Differentially Expressed in Normal and Neoplastic cells) domain of Rab-GEF (Guanosine Exchange Factors) proteins, similar biological functions were proposed for C9ORF72. Rab-GEF proteins activate Rab-GTPases through the exchange of a GDP with a GTP (Levine et al., 2013). Recently, C9orf72 has been implicated in the regulation of the intracellular traffic linked to endosomal and autophagic protein degradation and to the autophagy initiation complex (Farg et al., 2014, Webster et al., 2016). C9orf72-mediated ALS pathogenesis is still controversial and three main mechanisms have been proposed: (i) loss of C9orf72 physiological functions, also known as haploinsufficiency; (ii) gain of a toxic function due to bidirectional (sense: GGGGCC and antisense: CCCCGG)

transcription of the repeat expansion and the formation of secondary structures that sequester RNA binding proteins leading to their loss of function; (iii) non-AUG translation of the repeat expansion with consequent formation of toxic dipeptide repeat proteins (DPRs) (Yang et al., 2020).

1.1.1.3 TARDBP

In 2006, the transcriptional repressor of the transactive response (TAR) DNA Binding Protein (*TARDBP*) was first linked to ALS. This was found as a main component of intracellular cytoplasmic inclusions, a typical feature of this disease (Arai et al., 2006). The *TARDBP* gene is located on chromosome 1, at position 1p36.22, and it encodes for a protein of 43 kDa called TDP-43 (Pesiridis et al., 2009). Even though mutations in *TARDBP* are only responsible for 4-5% of fALS and 1% of sALS (Ranganathan et al., 2020), cytoplasmic TDP-43-positive inclusions are found in over 95% of ALS cases, both familial and sporadic (Ling et al., 2013). To date, more than 60 mutations in this gene have been associated with ALS (http://alsod.ac.uk). TDP-43 belongs to the family of heterogeneous nuclear ribonucloproteins (hnRNPs), which play a crucial role in the regulation of gene expression and in RNA metabolism. In particular, it has been reported to participate in processes such as: splicing, mRNA stability, transport and in microRNA generation (Buratti and Baralle, 2010, Tollervey et al., 2011). Although mainly localized in the cell nucleus, physiologically TDP-43 is able to shuttle between the nucleus and the cytoplasm to mediated its cellular functions. The main feature of TDP-43-ALS pathology is the mislocalization of the protein, with nuclear depletion and cytoplasmic aggregation (Lee et al., 2011). However, it is still unclear whether the TDP-43 pathogenesis is mediated by a loss of physiological function in the nucleus, gain of toxic function or a combination of both (Mejzini et al., 2019).

1.1.1.4 Fused in Sarcoma

The Fused in Sarcoma (*FUS*) gene was identified in 1993 as a human oncogene involved in malignant liposarcoma (Rabbitts et al., 1993). In 2009, the protein was firstly linked to ALS because it was found in the characteristic cytoplasmic aggregates together with TDP-43 (Kwiatkowski et al., 2009, Vance et al., 2009). The gene is located on chromosome 16, at position 16p11.2, and it encodes for a protein made of

526 amino acids (Aman et al., 1996). To date, more than 50 mutations in *FUS* have been linked with ALS (https://alsod.ac.uk/output/gene.php/FUS), which are responsible for approximately 4% of fALS and less than 1% of sALS (Deng et al., 2014). FUS is a heterogeneous nuclear ribonucleoproteins (hnRNP) and shares most of its biological functions with TDP-43 as it is implicated in transcriptional regulation, splicing, mRNA transport, stability and translation. However, FUS is also involved in repair mechanisms following DNA damage (Ratti and Buratti, 2016). Similarly to TDP-43, FUS is mainly localised in the cell nucleus, where it performs most of its functions, although it can physiologically shuttle from the nucleus to cytoplasm (Calvio et al., 1995, Zinszner et al., 1997). ALS-causing mutations drive the nuclear-to-cytoplasm mislocalization of the protein and the generation of FUS-positive cytoplasmic inclusions (Ranganathan et al., 2020). A recent report suggested that the aberrant localization of the protein is a common hallmark of the disease, which can be found in the presence of other ALS-causative mutations and in sporadic cases (Tyzack et al., 2019). As for TDP-43, it is still debated whether FUS-mediated-ALS pathogenesis results from the loss of a protective nuclear mechanism, the gain of a toxic function or a combination of both (Mejzini et al., 2019).

1.1.2 ALS as a multifactorial disease

Amyotrophic lateral sclerosis is considered a multifactorial disease as a series of mechanisms and pathways are implicated in the disease onset and progression, including: alteration of proteostasis, aberrant RNA metabolism, excitotoxicity, mitochondrial damage, oxidative stress, and neuroinflammation (Cozzolino et al., 2012). A brief summary of these pathological mechanisms in ALS is provided in this section.

Protein aggregation is one of the main hallmarks of ALS, which not only affects MN but also supporting non-neural cells, such as astrocytes and oligodendrocytes. As reviewed by Blokhuis et al., several types of aggregates have been reported in ALS patients, these are known as: “Lewy body-like hyaline inclusions or skein-like inclusions” which are ubiquitinated; Bunina bodies, which are “small eosinophilic ubiquitin-negative inclusions” and neurofilamentous inclusions (Blokhuis et al., 2013). One of the main constituents of the ubiquitinated inclusions is TDP-43, which can be found in these structures in more than 95% of ALS cases (Ling et al., 2013). The underlying causative mechanism of the aggregate formation is still not completely understood. However, several cellular pathways known for impacting proteostasis have been reported to be altered in ALS, including: chaperone dysfunction (Kalmar and Greensmith, 2017), endoplasmic reticulum (ER) stress activation (Matus et al., 2013), ubiquitin-proteasome system dysfunction (Bendotti et al., 2012) and autophagy impairment (Ramesh and Pandey, 2017).

After the discovery of ALS-associated mutations in the RNA binding proteins TDP-43, FUS and the effects of HRE C9ORF72, the hypothesis of ***dysregulated RNA metabolism*** was proposed. The term RNA metabolism refers to a series of processes including: RNA transcription, translation, mRNA splicing, transport and stability, and miRNA production (Cestra et al., 2017). TDP-43 and FUS act as splicing regulators and it has been demonstrated that disease-associated mutations lead to a decrease in their splicing activity (Arnold et al., 2013, Qiu et al., 2014, Coady and Manley, 2015). Moreover, both FUS and TDP-43 can physiologically be found in stress granules in response to different cellular stresses. However, disease-associated mutations

prolong the persistence of these granules. Thus, it has been proposed that, in these structures, mRNAs and proteins are trapped, preventing them from performing their physiological functions (Coyne et al., 2017). Interestingly, ALS-C9ORF72 mutants seem to share some of these pathological mechanisms with TDP-43 and FUS leading to dysregulated RNA metabolism (Simón-Sánchez et al., 2012, Mori et al., 2013).

Excitotoxicity is a process that occurs because of the excessive persistence of glutamate in the synaptic space and the subsequent over-stimulation of neuronal glutamate receptors. This is a well-known ALS mechanism and several underlying processes have been proposed to cause it, including defects in the glutamate reuptake transporter system and glutamate receptor dysfunction (King et al., 2016). In physiological conditions, after its release, glutamate is rapidly cleared from the synaptic space. This is possible thanks to specific transporters on neuronal and astrocytic membranes such as excitatory amino acid transporter (EAAT). There are different types of EAATs but the major one implicated in ALS is EAAT2 (King et al., 2016) and its function is known to be substantially decreased in ALS patients (Fray et al., 1998, Sasaki et al., 2000). Several pieces of evidence suggest that AMPA and NMDA glutamate receptors are also dysfunctional in ALS. In particular, it appears that there is a decrease in the expression of NMDA receptor 1 (NR1) subunit of the NMDA receptor in the spinal cord ventral grey matter in ALS patients (Virgo and de Belleroche, 1995). Additionally, reduced amount of the NR2 subunit of NMDA can be observed in ALS patients' dorsal and ventral horns of the spinal cord (Samarasinghe et al., 1996). Moreover, MN have a low expression of the AMPA receptor GluR2 subunit, which means that they express calcium-permeable AMPA receptors, a known factor causing vulnerability to excitotoxicity (Geevasinga et al., 2016, Heath and Shaw, 2002).

Neurons are high energy demanding cells; in fact, the brain alone utilises about 20% of the total body ATP (Engl and Attwell, 2015). Thus, mitochondria play a pivotal role in these cells. Several studies documented ***mitochondrial dysfunction*** in ALS. Morphological abnormalities have been reported in several ALS cell and animal models. Specifically, instead of the classical oval-shaped morphology, mitochondria appear spherical, clustered, fragmented and vacuolated (Smith et al., 2019, Gao et al., 2017, Deng et al., 2015, Wang et al., 2013, Vande Velde et al., 2011, Higgins et

al., 2003). Importantly, similar structural alterations were also reported in patients (Rodríguez et al., 2012, Sasaki et al., 2007). A large body of evidence supports a dysregulation in the mitochondrial energy metabolism in animal models as well as in patients with familial and sporadic ALS (Bowling et al., 1993, Browne et al., 2006, Sasaki et al., 2007, Perera and Turner, 2016). Dysfunction in the mitochondrial electron transport chain (ETC) (Crugnola et al., 2010, Kawamata and Manfredi, 2010) and consequently reduction in the levels of ATP produced (Mattiazzi et al., 2002) were documented in ALS with evidence of decreased activities of the complexes I, II, III and IV of the ETC in post-mortem spinal cords of sALS patients (Wiedemann et al., 2002, Borthwick et al., 1999). Additionally, impairments in complex I and IV were also reported in skeletal muscle of sALS patients (Wiedemann et al., 1998, Vielhaber et al., 2000, Crugnola et al., 2010).

Oxidative stress which can be defined as an imbalance between oxidant and antioxidant factors, is a well-demonstrated hallmark of ALS. Excessive quantities of reactive oxygen species (ROS) are responsible for the oxidative damage, which includes lipid peroxidation, protein oxidation and DNA and RNA damage (Islam, 2017). Increased levels of ROS and oxidative stress biomarkers are extensively reported in the ALS literature (Barber and Shaw, 2010). In particular, increases in protein carbonyls (Shaw et al., 1995, Ferrante et al., 1997, Niebrój-Dobosz et al., 2004) and 3-nitrotyrosine levels (Abe et al., 1995, Beal et al., 1997), which indicate protein oxidation, have been detected in the post-mortem CNS tissues of both fALS and sALS patients. Moreover, markers of oxidized DNA, such as 8-hydroxy-2'-deoxyguanosine, were reported to be elevated in the plasma, urine, and cerebrospinal fluid (CSF) of ALS patients (Ferrante et al., 1997, Bogdanov et al., 2000). Additionally, a biomarker of lipid peroxidation, 4-hydroxy-2,3-nonenal, was found to be significantly increased in CSF and sera of sALS patients (Simpson et al., 2004). Oxidative stress is thought to be linked to mitochondrial dysfunctions. In fact, as the oxidative phosphorylation is the major source of ROS, the excessive amount produced could be the result of defective mitochondrial function (Cozzolino and Carrì, 2012). Additionally, evidence of an impaired antioxidant response has also been reported. In fact, reduced levels of the antioxidant glutathione (Weiduschat et al., 2014) were reported together with dysregulation in the nuclear erythroid 2-related factor (Nrf2)-antioxidant pathway (Sarlette et al., 2008, Suh et al., 2004). Nrf2 is a transcription factor which regulates

the expression of many of cytoprotective and antioxidant genes, including some involved in the biosynthesis of glutathione (Dinkova-Kostova and Kazantsev, 2017). Given this evidence, Nrf2 activation is now considered a promising therapeutic strategy for ALS (Mead et al., 2013, Johnson and Johnson, 2015).

Compelling evidence suggests neuroinflammation as another crucial mechanism participating in ALS disease onset and progression. Given its importance for this research project, a detailed description of the neuroinflammatory processes in ALS is provided in the next section.

1.2 Neuroinflammation

Neuroinflammation is an essential defensive mechanism that aims to eliminate pathogens invading the central nervous system (CNS). However, sustained inflammatory responses are detrimental and can cause cytotoxicity (Kempuraj et al., 2016). In the recent years, increasing evidence indicates an important role for neuroinflammation in the pathogenesis of ALS. Interestingly, a significant impact on disease progression was suggested as patients who had a peripheral blood phenotype comparable to healthy volunteers and had a less altered inflammatory profile seemed to survival for longer (Gustafson et al., 2017). The activation of microglia and astrocytes, production of excessive quantities of pro-inflammatory cytokines and infiltration of T lymphocytes are the main identified mechanisms contributing to the inflammatory mechanisms in this disease (Liu and Wang, 2017). Interestingly, it has been demonstrated that neuroinflammation occurs not only in ALS, but it is a common pathological mechanism in several neurodegenerative diseases including Parkinson's disease (PD), Alzheimer's disease (AD) and Huntington's disease (HD) (Stephenson et al., 2018). In fact, in the brain, CSF and serum of ALS, PD, HD and AD patients elevated levels of tumour necrosis factor (TNF-α), interleukin (IL)-1β and IL-6 have been reported (Labzin et al., 2018, Robertson et al., 2001, Sekizawa et al., 1998). In a recent report the levels of the inflammatory IL-1β, IL-6 and IFN-γ were significantly increased whereas the anti-inflammatory IL-10 was found to be reduced in ALS compared to healthy controls. Additionally, higher IL-1β levels were associated with a faster disease progression and correlated with decline in the revised ALS functional rating scale (ALSFRS-R - a questionnaire used to rate the stage and progression of the disease (Cedarbaum et al., 1999)) (Jin et al., 2020). Interestingly, IL-1β and TNF-α were also found to be elevated in the skeletal muscles of rat models of the disease, which suggested the involvement of peripheral and muscular tissue inflammation in the disease onset and/or progression (Van Dyke et al., 2016). Additionally, significant increase in the NLP3 inflammasome, a complex of cytosolic proteins that mediates the activation of inflammatory responses, was detected in the spinal cord and skeletal muscles of ALS mice models (Moreno-García et al., 2021, Johann et al., 2015, Lehmann et al., 2018) as well as in patient blood and in post mortem tissues (Moreno-García et al., 2021, Johann et al., 2015). Moreover, the expression of cyclooxygenase-

2 (COX2), an enzyme involved in prostanoid synthesis, which mediates vasodilatation and inflammation, is increased in ALS patients (Almer et al., 2001) and mouse models of the disease (Drachman et al., 2002, Pompl et al., 2003). Evidence shows that both local (or CNS) and peripheral immune system cells participate in the neuroinflammatory process (**Figure 1.2**). In the next sections, a detailed description of the involvement of each cell type in ALS inflammation is provided.

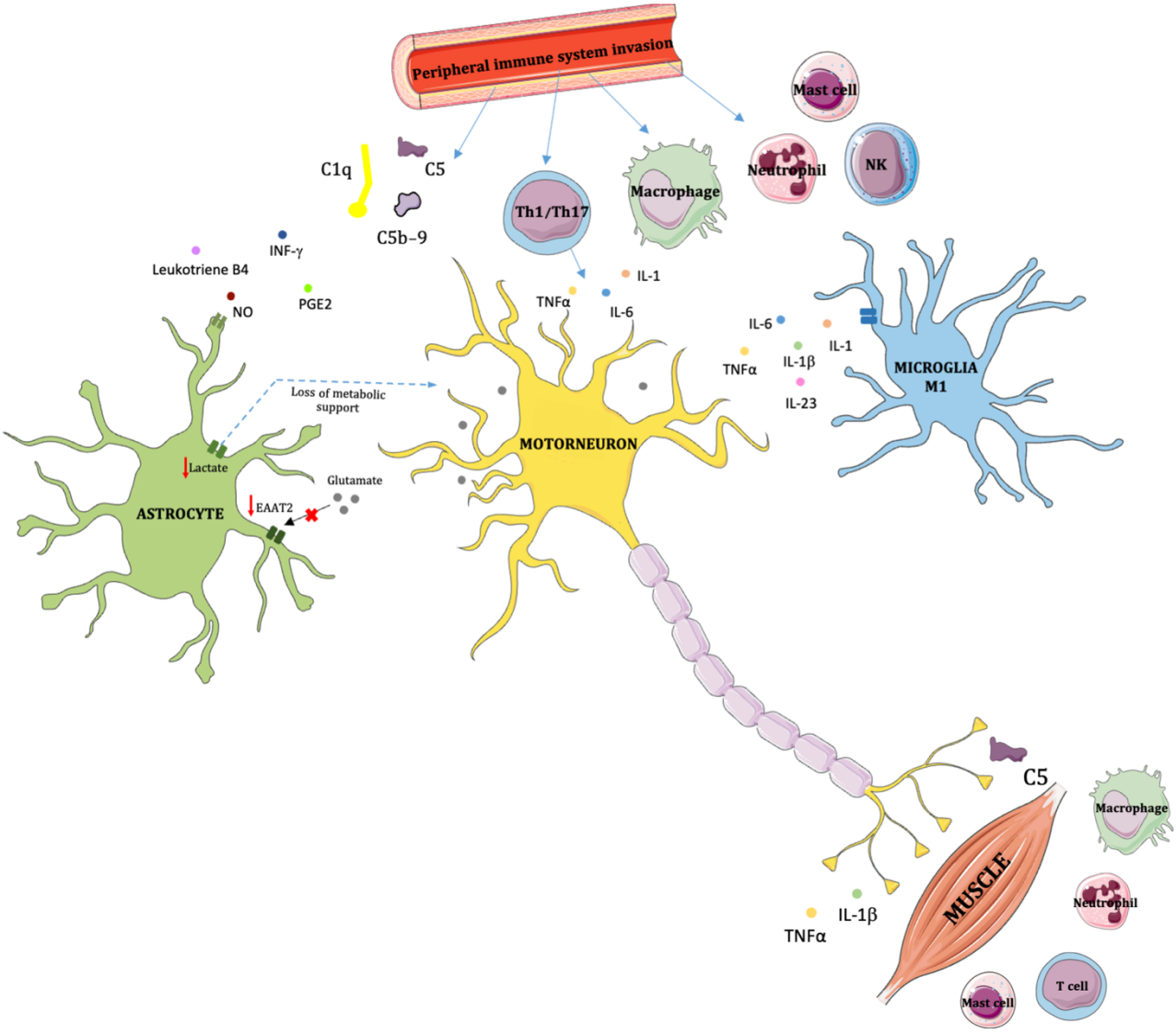

Figure 1.2: Neuroinflammation in ALS.

This figure shows an overview of major cellular components involved in the establishment of the neuroinflammatory condition characteristic of ALS.
In the CNS, microglial cells are activated in an M1 pro-inflammatory phenotype and release several pro-inflammatory cytokines such as: IL-1 β, IL-6, IL-23 and TNF-α. Astrocytes are also known to contribute to this pathological mechanism by producing pro-inflammatory mediators, including IFN-γ, PGE2, leukotriene B4 and NO. Given the importance ALS astrocytes in pathogenesis of the disease, other mechanisms of astrocyte-mediated MN toxicity are also reported in the figure including: decreased production and release of lactate and downregulation of EAAT2 transporters which lead to a reduction in glutamate reuptake. Additionally, components of the peripheral immune system (T-cells, macrophages, complement system proteins, neutrophils, natural killers and mast cells) are recruited and infiltrate the CNS participating to neuroinflammation. Lastly, immune cells (T cells, macrophages, neutrophils, complement system proteins and mast cells) and cytokines (IL-1β and TNF- α) reported to be involved in the inflammation at the skeletal muscle level are also displayed.

1.2.1 CNS immune cells

a. Microglia

Microglia are the brain and spinal cord-resident macrophages and the major component of the innate immune system in the CNS. They represent this organ's first line of defence in response to a multitude of stimuli and injuries (Baufeld et al., 2017). Microglia are generally classified into resting and activated populations. Despite the name, resting or M0 microglia are highly dynamic cells that exert a crucial surveillance function, patrolling the CNS microenvironment for any injuries or infections (Nimmerjahn et al., 2005). If a homeostatic disturbance is detected, microglia switch into an active state modifying their morphology and acquiring an amoeboid shape (Labzin et al., 2018, Geloso et al., 2017). Two distinctive activated microglial phenotypes have been identified: M1 and M2. Also known as the “classically activated” microglia, M1 cells have pro-inflammatory functions and their phenotype switching is generally due to increased levels of inflammatory agents such as pathogen associated molecular pattern molecules (PAMPs), lipopolysaccharide (LPS) or interferon (IFN)-γ (Du et al., 2017). Interestingly, microglial activation seems to be also triggered by protein aggregates (Labzin et al., 2018). Once in their M1 state, a downstream signalling cascade leads to the activation of several transcription factors, including NF-kβ, and the consequent production and release of multiple pro-inflammatory mediators including: IL-1β, IL-6, IL-12, IL-23, TNF-α, chemokines, prostaglandin E2, ROS and inducible nitric oxygen synthase (iNOS) (Geloso et al., 2017, Du et al., 2017). In contrast, M2 or “alternatively activated” microglia, which are induced by cytokines like IL-4, IL-10 or IL-13, have anti-inflammatory and protective properties. In particular, they secrete anti-inflammatory mediators including IL-10 and TGF-β (Du et al., 2017), mediate tissue repair by producing extracellular matrix components (Michell-Robinson et al., 2015) and promote oligodendrocyte differentiation during CNS remyelination (Miron et al., 2013).

A condition of microgliosis, meaning an increased accumulation of activated microglial cells in the CNS, was extensively documented in ALS both in mouse models of the disease (Alexianu et al., 2001) and in patients’ post mortem tissues (Engelhardt and

Appel, 1990, Kawamata et al., 1992). In particular, this was observed in the motor cortex, brainstem motor nuclei, anterior horn of the spinal cord and in the corticospinal tracts of ALS patients (Kawamata et al., 1992). Additionally, PET imaging of individuals living with this disease showed a widespread microgliosis in different CNS areas with particular involvement of the motor cortex (Turner et al., 2004, Corcia et al., 2012). Moreover, one of the most reproducible results found in ALS CSF samples is an increased level of chemokine ligand 2 (CCL2), also referred to as monocyte chemoattractant protein 1 (MCP-1), which is a well-known marker of microglial activation (Wilms et al., 2003, Henkel et al., 2004, Baron et al., 2005, Tanaka et al., 2006). This protein was proposed not only as a biomarker of ALS, but also as a marker of disease progression as it correlated with the revised ALS functional rating scale (ALSFRS-R) (Tanaka et al., 2006, Mitchell et al., 2009, Tateishi et al., 2010).

Several pieces of evidence suggest an alteration in the ALS microglia population during disease progression. During early stages, upregulation of M2 markers, such as CD206 and Ym1, was reported in the spinal cord of mutant SOD1 (mSOD1) transgenic mice. As the disease progressed, a gradual and progressive increase in the M1 population was observed together with elevated levels of NADPH oxidase 2 (NOX2) and IL-1β, suggesting the establishment of an inflammatory milieu (Beers et al., 2011b). Moreover, in a different study, Liao and colleagues obtained consistent results using microglia isolated from mSOD1 mice indicating a preponderance of M2 cells in the first stage of ALS and a shift toward the M1 phenotype over time (Liao et al., 2012). Hence, it has been proposed that at an early stage M2 cells prevail, releasing anti-inflammatory mediators and trophic factors, including glial cell-derived neurotrophic factor (GDNF) and insulin growth factor (IGF-1), which promote a neuroprotective response (Appel et al., 2010). However, later during the course of the disease, a shift towards the M1 phenotype occurs due to the release of different danger signals, which possibly includes misfolded and aggregated proteins. This leads to the release of pro-inflammatory agents and ROS, to the establishment of inflammatory conditions and ultimately to neurotoxicity (Zhao et al., 2013, Hooten et al., 2015).

Nonetheless, the traditional and physiological dual classification of microglia into M1 and M2 subtypes has been recently perceived as an oversimplification (Ransohoff, 2016). In the context of ALS, in an in-depth RNA sequencing study of microglia

isolated from the spinal cord of ALS mouse models, Chiu and colleagues showed that the gene expression profiles were not consistent with either M1 or M2 microglia and that genes with both potentially protective and toxic functions were upregulated. Thus, a new neurodegenerative or ALS-specific microglial phenotype was proposed (Chiu et al., 2013).

b. Astrocytes

Astrocytes represent the largest glial population in the CNS. Although not definable as immune-system cells, astrocytes are able to modulate the immune response and they are known to contribute to neuroinflammation (Hovden et al., 2013).

Physiologically, astrocytes are crucial for CNS homeostasis exerting a range of essential functions and providing neurons with the necessary molecules to supply their trophic, metabolic and structural support to neighbouring neurons (Vargas and Johnson, 2010). In particular, they influence MN survival by secreting neurotrophic factors such as glial cell line-derived neurotrophic factor (GDNF) and brain-derived neurotrophic factor (BDNF) (Yamanaka and Komine, 2018); maintain glutamate homeostasis by tightly regulating glutamate release and uptake (Mahmoud et al., 2019) and are essential for the formation and maintenance of the blood brain barrier (Cheslow and Alvarez, 2016). Additionally, astrocytes appear to be crucial for MN trophic support and energy metabolism. Specifically, these cells are pivotal for CNS energy and glucose storage being the main brain source of glycogen and, according to the astrocyte-to-neuron lactate shuttle hypothesis, lactate is primarily produced by astrocytes from glucose and subsequently transported to the MNs where it is converted to pyruvate and used by mitochondria for aerobic energy production (Deitmer et al., 2019). More recently and importantly to this research project, astrocytes were found to physiologically influence the function of immune system cells including the anti-inflammatory regulatory T cells (Tregs). In a study involving normal rat cells, *in vitro* astrocyte-Treg co-cultures reduced Treg apoptosis suggesting a probable pro-survival effect of astrocytes on these cells. In addition, the same authors reported increased FOXP3 expression (a crucial transcription factor for Treg function and differentiation) in co-cultures compared to Tregs monocultures (Xie et al., 2015).

Astrocytes were proposed as a substitute source of IL-2, an essential cytokine for Treg differentiation and activation, for CNS Tregs. In fact, this cytokine was found in the supernatant from astrocytes and the reported pro-survival effects on Tregs appeared to be dependent on the IL-2/STAT5 pathway (Xie et al., 2015, Xie and Yang, 2015). Moreover, Treg-depleted (DEREG) mice showed increased levels glial fibrillary acidic protein (GFAP) suggesting that astrocytes were in their reactive state (Ito et al., 2019, Krämer et al., 2019). In contrast, the passive transfer of Tregs in DEREG mice suppressed excessive astrocytic activation (Ito et al., 2019).

Astrocytes are known to respond to CNS damage or injury via a protective mechanism called astrogliosis. These reactive astrocytes are characterized by increased levels of markers such as GFAP, vimentin and nestin (Pehar et al., 2017). This is a hallmark of multiple neurodegenerative diseases as well as ALS, including Alzheimer's and Parkinson's disease (Verkhratsky et al., 2014). In ALS patients, astrogliosis features were reported in several white matter regions (Kushner et al., 1991), including the motor cortex, in the cortical grey matter (Nagy et al., 1994) and in the spinal cord (Schiffer et al., 1996).

Moreover, ALS-mutant genes appeared to be expressed not exclusively in MNs, but also in astrocytes. Mutations in the SOD1 genes were found in ALS patients astrocytes (Bruijn et al., 1997, Forsberg et al., 2011) and, interestingly, several studies demonstrate that such cells secrete several toxic factors able to induce Bax-dependent MN death (Nagai et al., 2007). Furthermore, the presence of TDP-43 inclusions in ALS patient astrocytes was shown in the grey matter of the spinal cord and motor cortex, in the neostriatum, and in the white matter of frontal and temporal cerebral cortex (Tan et al., 2007, Zhang et al., 2008, Neumann et al., 2007).

Several pieces of evidence suggest that ALS astrocytes are toxic to MN (Haidet-Phillips et al., 2011, Meyer et al., 2014, Yamanaka and Komine, 2018) and different mechanisms were proposed to drive astrocyte-mediated pathology, which are summarised below:

- *Impaired glutamate reuptake*. Glutamate is the major excitatory neurotransmitter of the CNS that acts through ionotropic and metabotropic receptors responsible for excitatory neurotransmission. However, excessive stimulations and activation of glutamate receptors cause intracellular Ca^{2+} overload and cell death (Ankarcrona et al., 1995). Multiple studies demonstrate a severe impairment in the glutamate uptake process due to the loss of EAAT2 transporter in mouse models (Howland et al., 2002, Pardo et al., 2006) and in both familial and sporadic ALS cases (Rothstein et al., 1995, Rothstein et al., 1992). Interestingly, glutamate receptors are expressed on immune system cells including T cells and this molecule is now considered an immunomodulator (Pacheco et al., 2007). One study suggested that glutamate favours the inflammatory Th1 differentiation over the anti-inflammatory Tregs (Beurel et al., 2014). Although, these results were not from ALS patients, this could potentially represent an additional mechanism by which astrocytes indirectly regulate the immune system.

- *Oxidative stress and mitochondrial dysfunction*. Astrocytes are crucial components of the antioxidant system in the CNS being the main source of glutathione and ascorbic acid, both key ROS scavengers (Verkhratsky and Nedergaard, 2018). Nonetheless, one study reported decreased levels of glutathione in fibroblasts and astrocytes derived from ALS patients carrying a TDP-43 mutation (Moujalled et al., 2017). In addition, ALS astrocytes show evidence of defects in mitochondrial respiration with increased production of ROS and reactive nitrogen species (RNS) leading to nitroxidative stress and MN death (Cassina et al., 2008). In particular, elevated levels of induced nitric oxide synthase (iNOS), an enzyme that is responsible for the production of the ROS nitric oxide (NO), were reported (Almer et al., 1999, Sasaki et al., 2001). Evidence shows that the exposure of astrocytes to NO promotes cellular death in MN (Cassina et al., 2002).

- *Loss of MN metabolic support*. As previously mentioned, astrocytes are responsible for MN trophic support providing them with lactate, which is fundamental for MN mitochondrial energy production. Whilst both cell types express lactate dehydrogenase 1 (LDH1), an enzyme that converts lactate to

pyruvate, astrocytes are the only source of lactate dehydrogenase 5 (LDH5), which catalyses the opposite reaction leading to lactate production (Bittar et al., 1996). Thus, the “astrocyte-neuron lactate shuttle” theory has been proposed by which lactate consuming cells (neurons) depend on lactate-producing cells (astrocytes) for their metabolic needs and therefore this molecule is shuttled between the two (Magistretti and Allaman, 2018). ALS mSOD1 mice showed decreased levels of the lactate efflux transporter and reduced amount of lactate in the spinal cord (Ferraiuolo et al., 2011, Madji Hounoum et al., 2017). In addition, lactate supplementation increased MN survival when co-cultured with ALS defective astrocytes (Ferraiuolo et al., 2011). More recently, several other metabolic alterations were reported in ALS astrocytes. Adenosine deaminase, a crucial enzyme for purine metabolism which catalyses the conversion of adenosine to inosine, was significantly reduced in astrocytes reprogrammed from both sporadic and C9ORF72-mutant ALS fibroblasts (Allen et al., 2019b, Allen et al., 2019a). Inosine supplementation was found to be beneficial and able to increase healthy MN survival when co-cultured with ALS astrocytes (Allen et al., 2019a). In addition, the same group provided evidence of an impairment in the fructose and glycogen metabolism in induced neuronal progenitor-derived astrocytes carrying a C9ORF72 mutation. In particular, both mRNA and protein levels of two glycogen mobilization enzymes (glycogen phosphorylase and phosphoglucomutase) appeared to be decreased in C9ORF72 ALS (Allen et al., 2019b). These findings were in line with evidence showing reduction in glycogen degradation to glucose, increased accumulation of glycogen in lumbar spinal cord of mSOD1 mice and elevated mRNA levels of glycogen synthase (Li et al., 2019, Dodge et al., 2013).

- *Release of pro-inflammatory mediators*: Several pieces of evidence demonstrate that ALS astrocytes contribute to neuroinflammatory processes by secreting several types of pro-inflammatory mediators that contribute to MN injury. Astrocytes from mSOD1 rats or mice were shown to secrete IFN-γ, which activated a death signaling pathway in MNs via tumour necrosis factor superfamily member 14 (TNFSF14, also referred to as LIGHT)-mediated lymphotoxin-b receptor LIGHT activation (Aebischer et al., 2011). In line with this, IFN-stimulating genes were found to be upregulated in astrocytes

surrounding MNs in the spinal cord of mSOD1 mice and the reduction or deletion of IFN-γ receptor 1 extended their life span (Wang et al., 2011).

Other pro-inflammatory agents were reported to be produced and secreted by ALS astrocytes including prostaglandin E2 (PGE2), leukotriene B4 and nitric oxide (Hensley et al., 2006) Moreover, a recent study showed that the exposure of primary rat astrocytes to ALS CSF significantly enhanced the production and secretion of different pro-inflammatory mediators including IL-6, TNF-α, cyclooxigenase-2 (COX-2) and PGE2 whilst decreasing the anti-inflammatory IL-10 (Mishra et al., 2016). This is in line with findings showing elevated IL-6 in ALS astrocytes exosomes, levels of which correlated with disease progression (Chen et al., 2019). COX-2 is a pivotal enzyme for the biosynthesis of the pro-inflammatory mediators prostanoids. In a transgenic mSOD1 mice model of ALS, COX-2 was found to be significantly increased both in MNs and astrocytes. In particular, a time dependent elevation in the expression of this enzyme level was reported, with end-stage mice showing a widespread COX-2 immunoreactivity (Almer et al., 2001). Consistent with this, spinal cord from post-mortem ALS CNS tissues showed a dramatic upregulation COX-2 mRNA and protein levels (Yasojima et al., 2001, Maihöfner et al., 2003). In addition, PGE2, a major product of COX-2 activity and a pro-inflammatory mediator, was reported to be increased in post-mortem specimens (Almer et al., 2001) and in ALS CSF (Almer et al., 2002, Maihöfner et al., 2003). The COX-2 inhibitor celecoxib significantly reduced PGE2 levels in mSOD1 mice, reduced spinal MN death by diminishing astrogliosis and microglial activation and prolonged survival by 25% (Drachman et al., 2002). Nonetheless, a clinical trial evaluating the effect of this drug in ALS patients failed to show any significant evidence of clinical improvement (Cudkowicz et al., 2006). In a more recent study, a different COX-2 inhibitor, refecoxib was tested in mSOD1 mice. The authors reported activation of COX-2 and its downstream signalling targets (IL-1β and TNF-α) in untreated mice as a result of glial activation, which was reversed by refecoxib treatment. Additionally, MN loss was partially rescued and evidence was shown of reduction in the rate of disease progression (Zou et al., 2020).

1.2.2 Peripheral immune system

a. Complement system

The complement system consists of a series of 30 proteins with antimicrobial functions. Their role is to opsonize pathogens and recruit macrophage and neutrophil cells to drive an efficient immune response. Depending on the type stressor, complement can be activated in three different ways following the classical, lectin or alternative pathways (Morgan, 2015). Complement system factors are present in the CNS and primarily produced by neurons, astrocytes, oligodendrocytes and microglia (Barnum, 1995).

Evidence of elevated levels of complement system proteins has been reported in ALS. Analysis of post-mortem spinal cord and motor cortex tissues revealed increased mRNA and protein levels of C1q and C4, proteins involved in the classical pathway, and also of the downstream C3 and C5b-9 proteins (Sta et al., 2011). Similarly, brain and spinal cord autopsies showed reactive microglia with increased levels of the complement receptors (CR) 3 and 4 as well as C3d and C4d positive neurites in disease affected areas. Consistently with this, increased CSF levels of C3 and C4 were reported in multiple studies (Annunziata and Volpi, 1985, Ganesalingam et al., 2011, Tsuboi and Yamada, 1994) whereas C1q, C5a and C5b-9 were elevated in the plasma, CSF and spinal cord of ALS patients and mouse models (Heurich et al., 2011, Woodruff et al., 2008, Mantovani et al., 2014). Moreover, Ferraiuolo and colleagues provided evidence of increased expression of genes involved in the first step of complement activation (C1q and C4) in laser-captured murine mSOD1 MNs. These findings suggested that MNs can actively contribute to activation of the complement cascade in ALS (Ferraiuolo et al., 2007). C5a and its receptor, C5aR1, have also been implicated in ALS. Their increased levels in mSOD1 mice were associated with macrophage recruitment and infiltration into degenerating skeletal muscles (Wang et al., 2017). Similar results were found in a different ALS mice model carrying a TDP-43 mutation, where C5aR1 levels were elevated whilst those of CD55, a negative regulator of the complement system were reduced (Lee et al., 2018). Additionally, evidence of complement alterations at the neuromuscular junction were provided in

an ALS mice model ($SOD1^{G93A}$ mice), where deposits of C3b and C1q were detected as early as at the presymptomatic stage (47 days) and were maintained following symptoms onset (Heurich et al., 2011). Consistent with this, one study in ALS post-mortem tissues showed an increased level of C1q, C3 and also of the membrane attack complex (MAC), a structure made of different complement proteins which localizes on the cell membrane of pathogens causing cell death (Bahia El Idrissi et al., 2016).

The involvement of the complement system in ALS pathogenesis, however, is still debated. Lobsiger and colleagues proposed that neither the C1q-induced classical pathway of complement activation, nor the C3-induced alternative pathway can mediate MN toxicity in ALS. In fact, in their mSOD1 transgenic mouse model, the genetic ablation of C1q and C3 did not affect disease progression (Lobsiger et al., 2013). In contrast, two different studies showed that pharmacological inhibition of C5a-C5aR1 signalling slowed disease progression and extended mSOD1 mice survival (Lee et al., 2017, Woodruff et al., 2008).

b. Neutrophils

In the recent years, increasing evidence suggests an impact of neutrophils on ALS inflammation. These cells are the most abundant type of leukocyte and constitute the first line of defence against infections. Following pathogen recognition, neutrophils destroy the microorganism either via phagocytosis, degranulation (release of antimicrobial proteins from the neutrophil granules) or through the formation of neutrophil extracellular traps (formed by DNA fibres that trap and kill microorganisms) (Rosales, 2018).

Several pieces of evidence suggest that neutrophil counts and percentage are increased in the peripheral blood of ALS patients compared to healthy controls (Murdock et al., 2016, Murdock et al., 2017). Interestingly, this increment significantly correlated with a higher ALSFRS-R score and was associated with a shorter survival, which was more evident in female patients compared to male (Murdock et al., 2021b). More recently, a high neutrophil-to-lymphocyte ratio was found to be significantly

associated with shorter disease duration and the authors proposed this this measurement as a new prognostic biomarker for ALS (Choi et al., 2020). Additionally, CD16 expression in peripheral blood neutrophils was also positively correlated with disease severity and rate of ALS progression. As this protein has been linked with neutrophil oxidative burst and phagocytic activity, the authors speculated that increased neutrophil activation and function may lead to additional ROS production and stress, exacerbating the neurodegeneration (McGill et al., 2020). Furthermore, post-mortem skeletal tissues from ALS patients showed a significantly increased proportion of infiltrating neutrophils. This was associated with neuromuscular junction denervation, suggesting the involvement of this immune cell type in axon degeneration and neuromuscular compromise (Trias et al., 2018). Similarly, neutrophils, together with mast cells, were found to be infiltrating in the motor axon located in the muscles of mSOD1 mice (Trias et al., 2018).

c. Mast Cells

Mast cells are bone marrow hematopoietic progenitor-derived immune cells that are crucial in mediating host defence against parasites (Mukai et al., 2016) and allergic reactions (Amin, 2012). These cells are characterised by cytosolic granules that contain a variety of factors including inflammatory mediators (e.g. leukotrienes, prostaglandins, cytokines and chemokines), NO and ROS (Harcha et al., 2021). Following stimulation, mast cells degranulate and secrete the aforementioned factors mediating the recruitment of various immune system cells (eosinophils, monocytes and neutrophils) and they can also act as antigen-presenting cells to induce T cell activation (Skaper et al., 2018).

Mast cells were first linked to ALS in 2004 when an immunocytochemistry study showed both macrophage and mast cell infiltration in the post-mortem spinal cord of affected individuals (Graves et al., 2004). In mSOD1 rat models, mast cells were found to massively infiltrate skeletal muscles (extensor digitorum longus), in particular they were localised in close proximity with motor nerve endings and NMJs, with their number progressively augmenting over disease progression. These cells appeared to be increased in size, to display features of explosive degranulation and to express the

tyrosine kinase receptor c-Kit, a growth factor receptor crucial for survival, differentiation and degranulation of mast cells (Trias et al., 2017). Interestingly, the same authors reported mast cells to be interacting with CD11b/Iba1$^+$ and CD68$^+$ macrophages, suggesting an important interplay between these two immune system cell types (Trias et al., 2017). In a more recent report, the same group showed concomitant infiltration of both mast cells and neutrophils in extensor digitorum longus muscle, sciatic nerve, and ventral roots of symptomatic mSOD1 rats (Trias et al., 2018). Interestingly, mast cells were also found nearby microvascular elements, which showed characteristic pathological abnormalities in mSOD1 rat and mouse models. The authors proposed that the aberrant trafficking and infiltration of these cells was at least partially due to a defective microvasculature. In fact, intravenous administration of bone marrow-derived c-Kit$^+$ mast cell precursors were able to infiltrate the spinal cord of ALS mice but not that of control littermates (Kovacs et al., 2021). In line with this, ALS patient biopsies showed evidence of mast cell infiltration in skeletal muscles (quadriceps) and in spinal cords. These were found to be enlarged, degranulating (Kovacs et al., 2021) and interacting with neutrophils forming large extracellular traps (Trias et al., 2018). More interestingly, masitinib, a c-Kit receptor inhibitor, reduced the number of infiltrating mast cells and neutrophils, improved aberrant microvasculature, alleviated NMJ denervation and reduced motor deficit in mSOD1 symptomatic mice (Trias et al., 2017, Trias et al., 2018, Kovacs et al., 2021). Given these encouraging preclinical results, masitinib has been trialled in a phase II/III clinical study assessing its efficacy in 394 ALS patients (NCT02588677). A significant survival benefit of 25 months was reported in 4.5mg/kg/day treated slow ALS progressors (ALSFRS-R decrease/month < 1.1) (Mora et al., 2021). These findings have led to the design of an additional phase III clinical trial (NCT03127267), which is currently recruiting, evaluating the effects of either 4.5 or 6mg/kg/day masitinib in a larger cohort of 495 patients (https://www.clinicaltrials.gov/ct2/show/NCT03127267).

d. Natural Killer Cells

Natural killer cells (NK) are granular cytotoxic cells that are components of the innate immune system. These share a similar function to cytotoxic T cells, however, the term "natural" suggests that NK are capable of killing cells without prior antigen

presentation. In fact, they are able to exert their cytotoxic functions naturally when cells do not express the self-marker major histocompatibility complex (MHC) class I (Vivier et al., 2008).

The role of NK in ALS is still to be fully understood with contradictory results being reported in the literature. Several studies reported elevated NK levels in the peripheral blood of ALS patients (Rentzos et al., 2012, Murdock et al., 2017, Jin et al., 2020) and one report also showed a progressive increase of the mean number of these cells over time (Murdock et al., 2017). In particular, Jin and colleagues provided evidence of the $CD56^{bright}$ NK population being increased in ALS whereas $CD56^{dim}$ NK were reduced (Jin et al., 2020). This is surprising considering that $CD56^{dim}$ is primarily a marker of NK with cytotoxic effects whilst $CD56^{bright}$ is associated with immunomodulatory functions. In contrast with this, Rolfes and colleagues provided evidence of intrathecal $CD56^{brigh}$ NKs being significantly reduced in ALS, which was particularly evident in rapidly progressive patients (Rolfes et al., 2021). Additionally, Garofalo and colleagues did not report an increase in both $CD56^{bright}$ and $CD56^{dim}$ NK cells in patient peripheral blood. However, they found NKs in postmortem spinal cord and motor cortex of sALS individuals whereas this infiltration was not present in matched controls (Garofalo et al., 2020). The same group also reported a CCL2-dependent recruitment of these cells in the motor cortex and spinal cord of mSOD1 mice at an early disease stage (with a peak at 10-13 weeks) whilst a decline was evident later during the disease course. Importantly, the cytotoxic activities of NK seemed to be mediated by MNs themselves, which expressed high levels of natural killer group 2D (NKG2D), a crucial protein for their activation and cytotoxicity (Garofalo et al., 2020). In addition, they provided evidence of pro-inflammatory microglia activation and impairment of regulatory T cells (Tregs) induced by NK-secreted IFN-γ. Interestingly, NK depletion in mice carrying either SOD1 and TDP-43 mutations delayed disease onset and paralysis although it did not produce a significant effect on disease progression (Garofalo et al., 2020). A more recent study showed that only female mSOD1 mice with depleted NKs showed extended survival whereas these results were not replicated in male mice. Moreover, the same group studied longitudinal NK counts in the peripheral blood of ALS patients and found significant correlations between NK surface markers and the ALSFRS-R. In addition, increased expression of several cytotoxic and migration markers was reported in ALS, although age-related variations were reported (Murdock et al.,

2021a). These findings suggested that NK cells may contribute to ALS progression in an age and gender-specific manner and therefore this could also explain the contradictory results reported so far in the literature.

e. Monocytes/Macrophages

Macrophages are phagocytic cells differentiated from monocytes that internalize and digest pathogens, foreign substances and cellular waste. Similarly to microglia, macrophages can be classified into the pro-inflammatory M1 and the anti-inflammatory M2 subset (Italiani and Boraschi, 2014).

The role of peripheral monocytes/macrophages in ALS pathogenesis is still not completely understood. However, elevated levels of MCP-1 in both the blood and CSF samples of ALS patients, suggest an involvement of these cell types in disease progression (Kuhle et al., 2009). Moreover, different studies showed functional activation of monocytes in ALS patient serum and monocyte/macrophage invasion into the CNS (Butovsky et al., 2012, Zondler et al., 2016). It has been proposed that peripheral monocyte infiltration into the CNS could exert a neuroprotective effect at the early stages of ALS. Nonetheless, as the disease progresses, a detrimental and inflammatory effect prevails (Zondler et al., 2016). Consistent with this, Zhao and colleagues reported that ALS monocytes had an inflammation-prone gene expression profile and this correlated with disease progression. In fact, ALS patient monocytes showed increased expression of IL-8, chemokine (C-X-C motif) ligand 1 (CXCL1) and CXCL2 compared to healthy controls. Moreover, this upregulation was more pronounced in rapidly compared to slowly progressing patients, thus reinforcing the hypothesis of a role for monocytes in disease progression (Zhao et al., 2017). A study involving rats overexpressing mutant SOD1 indicated that macrophages may play an active role in skeletal muscle denervation given the increased macrophage activation reported in neuromuscular junctions (NMJs) of this animal model of the disease (Van Dyke et al., 2016). Additionally, the number of infiltrating macrophages was found to progressively increase in the skeletal muscles of mSOD1 mice during disease progression and this mechanism appeared to be at least partially mediated by the C5a complement system protein, whose receptor is expressed on macrophages (Wang et

al., 2017). Consistent with this, muscular biopsies from a subset of ALS patients showed evidence of low grade inflammation and chronic monocyte/macrophages infiltration (Al-Sarraj et al., 2014). Two recent groups studied the specific functions of ALS M1 and M2 macrophages. Interestingly, Du and colleagues reported that M1 macrophages differentiated from ALS peripheral monocytes showed an increased inflammatory phenotype. In particular, evidence of augmented production and secretion of different pro-inflammatory cytokines, including IL-6 and TNF-α, was provided in ALS compared to healthy control M1 macrophages (Du et al., 2020). However, induced pluripotent stem cell (iPSC)-derived M2 microglia from fibroblasts of ALS patients showed comparable anti-inflammatory activities similar to heathy controls. In particular, iPSC-M2 cells were able to suppress the pro-inflammatory M1 macrophages and cytotoxic T cells whereas they were capable of sustaining and inducing Tregs (Zhao et al., 2020). This evidence suggests that, while ALS M1 macrophages are more inflammatory prone, M2 cells retain their anti-inflammatory functions and may constitute an interesting therapeutic target to induce immunosuppression.

f. T Lymphocytes

T lymphocytes play a crucial role in adaptive cell-mediated immunity. They consist of a large and heterogeneous population of cells which can be divided into subgroups according to the markers expressed on their surface. The major distinction is between T cells carrying CD4, termed $CD4^+$ cells (T helpers and regulatory T cells) and those expressing CD8, termed $CD8^+$ cells (cytotoxic T cells) (Male M., 2006). Like macrophages and microglia, $CD4^+$ cells can be further classified in two major subgroups depending on the cellular inflammatory properties. The first one has anti-inflammatory properties and consists of T helper 2 (Th2) and regulatory T cells (Treg), which secrete immune-modulating cytokines, such as IL-4, IL-10 and TGF-β. The latter subgroup is made of pro-inflammatory lymphocytes: T helper 1 (Th1) and T helper 17 (Th17) which release inflammatory mediators including IL-1, IL-6 and IFN-γ (Crisafulli et al., 2018).

T lymphocytes are known to contribute to the ALS pathology. Several studies reported alterations in the T-cell population in the peripheral blood of ALS patients and infiltrating T lymphocytes in the CNS and skeletal muscles (Engelhardt et al., 1993, Graves et al., 2004, Zhang et al., 2005, Mantovani et al., 2009, Rolfes et al., 2021, Al-Sarraj et al., 2014). In particular, regional and temporal differences were found in infiltrating T cells. Specifically, analysis of ALS postmortem tissues revealed that $CD4^+$ T helpers were found predominantly in the corticospinal tract whereas $CD8^+$ cytotoxic T cell were localized mainly in the ventral horns (Engelhardt et al., 1993). Interestingly, the major histocompatibility complex I (MHC I), crucial for antigen presentation to cytotoxic T cells, was found to simultaneously exert protective and harmful effects in ALS mSOD1 mice (Nardo et al., 2018). Whilst the ubiquitarian or sciatic nerve-specific lack of MHC I caused denervation, anticipated disease onset and atrophy; the same depletion in spinal cord resulted in lesser infiltrating T cells, reduced inflammation and preserved MNs. Therefore, the authors proposed a dual role of MHC I and cytotoxic T cell in peripheral vs central nervous system and this can potentially explain the failure of clinical trials aiming to promote a systemic immune suppression in ALS (Nardo et al., 2018). Additionally, in an early disease phase, $CD4^+$ T cells seemed to prevail whereas at later stages the number of $CD8^+$ lymphocytes increased (Beers et al., 2008). Interestingly, $CD4^+$ cells were found to be protective in several rodent models of ALS. In fact, mSOD1 mice lacking of these cells showed an accelerated disease progression and shorter survival (Beers et al., 2008) whilst the passive transfer of activated $CD4^+$ lymphocytes extended their survival (Banerjee et al., 2008). Additional reports also suggested an alteration within the $CD4^+$ subset over the disease course in mSOD1 mice. Specifically, at an early stage of the disease, Th2 and Treg cells predominate, however, as the disease progresses, a shift towards the inflammatory Th1 and Th17 cells was reported (Beers et al., 2011b). Neurotoxic effects were particularly associated with IL-6 released by Th1 (Beers et al., 2011b) and interestingly this cytokine has been shown to inhibit the protective Tregs (Bettelli et al., 2006). In line with this, a pro-inflammatory-skewed T cell phenotype was registered in the blood (but not in the CSF) of ALS patients where Th1/Th17 prevailed over Th2/Treg. Additionally, a significant negative correlation was found between Th1/Th17 and the ALSFRS-R or forced vital capacity, a measurement to evaluate lung function (Jin et al., 2020). Evidence showed that in the blood, CSF and spinal cord of ALS patients there is a significant increase in the expression of IL-17 and IL-23, cytokines produced

by Th17 cells, which further reinforces the hypothesis of an extensive activation of this cell type in ALS (Rentzos et al., 2010, Saresella et al., 2013).

1.3 The role of regulatory T cells

Given the importance of the regulatory T cells in this thesis, in the next section, the physiological role of these cells is extensively discussed together with their pathopathological alteration in ALS. This section was published as a review article (Giovannelli et al., 2020) in the journal *Amyotrophic Lateral Sclerosis and Frontotemporal Degeneration*.

1.3.1 Physiology of regulatory T cells

Regulatory T cells (Tregs) are fundamental modulators of the immune response: they maintain self-tolerance and homeostasis, preventing the onset of autoimmune disorders. These cells are generally classified into two subgroups: thymus-derived and peripheral inducible Tregs (Male M., 2006). The first type is produced in the thymus during the negative selection process; these cells then migrate into peripheral tissues to perform their functions. They are also known as naturally occurring or $CD4^+CD25^+$ Tregs because of the surface molecules they express. The presence of $CD25^+$, also referred to as interleukin-2 receptor alpha chain (IL-2Rα or IL2RA), indicates the importance of IL-2 for Treg functions (Male M., 2006). Another key feature of these cells is the expression of Forkhead box Protein 3 (FOXP3) (Mills, 2004). The second type of Tregs are peripheral in origin. These cells are derived by antigen-exposed $CD4^+$ T cells in peripheral tissues following the exposure to specific molecules. Induced $CD4^+$ Tregs can be further classified into $FOXP3^+$ or $FOXP3^-$ cells (Yadav et al., 2013). Finally, another type of peripheral induced Tregs are $CD8^+$. They are generated by the stimulation of $CD8^+$ cells with antigen and IL-10 and, once active, they express FOXP3 (Male M., 2006).

Clearly, FOXP3 plays a crucial role in CD8+, CD4+ and CD4+CD25+ Tregs. It is a transcriptional regulator which is fundamental for their development and function. It can act both as a transcriptional activator or repressor because it interacts with several transcription factors and proteins involved in epigenetic regulation (Vent-Schmidt et al., 2014). In particular, it prevents the transcription of pro-inflammatory cytokines such

as IL-2 and IFN-γ and it concomitantly activates immune suppressors including cytotoxic T lymphocyte antigen 4 (CTLA4) (Vent-Schmidt et al., 2014).

Other key markers for Tregs are glucocorticoid-induced tumour necrosis factor receptor (GITR) and inducible T cell co-stimulator (ICOS). GITR, also referred to as TNFRSF18, plays a role in Treg suppressive activities, in fact, antibodies against GITR can abrogate Treg immune modulatory functions, and it is also crucial for the differentiation process of thymus Tregs (Shimizu et al., 2002, McHugh et al., 2002, Ronchetti et al., 2015). ICOS is a costimulatory molecule which is known to exert various roles within the immune system, participating in both inflammatory and suppressive processes (Wikenheiser and Stumhofer, 2016). However, ICOS appears to play a role in Treg functions. In fact, the blockage of the interaction of ICOS with its ligand (ICOSL) causes a decrease in the expression of CTLA4 and ICOS deficiency induces a reduction in FOXP3 expression (Zheng et al., 2013, Landuyt et al., 2019).

Interleukin-2 is a crucial mediator of Treg activity. This cytokine is known to be essential for the development and survival of these cells (Garg et al., 2012). Although IL-2 exerts pleiotropic functions on the immune system, evidence demonstrates that this cytokine has crucial immune suppressive functions as IL-2 or IL-2 receptor knockout mice do not develop immune deficiency syndromes, but they do show signs of autoimmune diseases (Malek, 2008). IL-2 administration promotes activation of different pathways in effector T cells (Teffs) and Tregs and, at low doses, it is able to induce expansion and activation of Tregs without having similar effects on Teffs (more details on IL-2 are provided in the following section) (Matsuoka et al., 2013).

Regulatory T cells exert several immunosuppressive functions: they suppress Teffs, B cells, natural killer cells (NKs) and antigen-presenting cells (APC) by inhibiting their activation, proliferation and function (Duffy et al., 2018). Moreover, they can alter the activation state of microglia/macrophages promoting the M2 (or anti-inflammatory) phenotype (Liu et al., 2011). Several mechanisms have been proposed to mediate these functions (**Figure 1.3**):

- **Inhibitory cytokine release**: Tregs can secrete anti-inflammatory cytokines including IL-10, IL-35 and TGF-β which suppress the functions of Teffs (Vignali et al., 2008).

- **Cytolysis induction**: Tregs are able to produce and release granzyme B and perforin which induce cytolysis and apoptosis in Teffs, B cells and NKs (Gondek et al., 2005, Zhao et al., 2006, Cao et al., 2007).

- **Metabolic disruption**: This proposed mechanism is based on the consumption of local IL-2 by Tregs. This would cause a depletion of this cytokine which is necessary for the function of Teffs (de la Rosa et al., 2004), leading to an IL-2-deprivation-mediated apoptosis of Teffs (Pandiyan et al., 2007).

- **CTLA4-mediated mechanism**: Tregs can physically interact with dendritic cells (DC) due to the binding of CTLA4 on the Treg surface and the co-stimulatory molecules CD80/CD86 expressed by DC. This leads to the production of indoleamine 2,3-dioxygenase (IDO) in DC, which is a potent immune regulator which suppress T cells and NKs (Fallarino et al., 2003, Mellor and Munn, 2004). Moreover, Tregs can also mediate the downregulation of CD80/CD86 (Cederbom et al., 2000).

- **cAMP-mediated mechanism**: Tregs express high levels of cAMP and this molecule can be transferred to Teffs through gap junctions. This provokes the activation of inducible cAMP early repressor (ICER) which inhibits nuclear factor of activated T cells (NFAT), a transcription factor which is necessary for IL-2 production. Thus, this can lead to IL-2 deprivation-mediated apoptosis (Bopp et al., 2007, Schmidt et al., 2012).

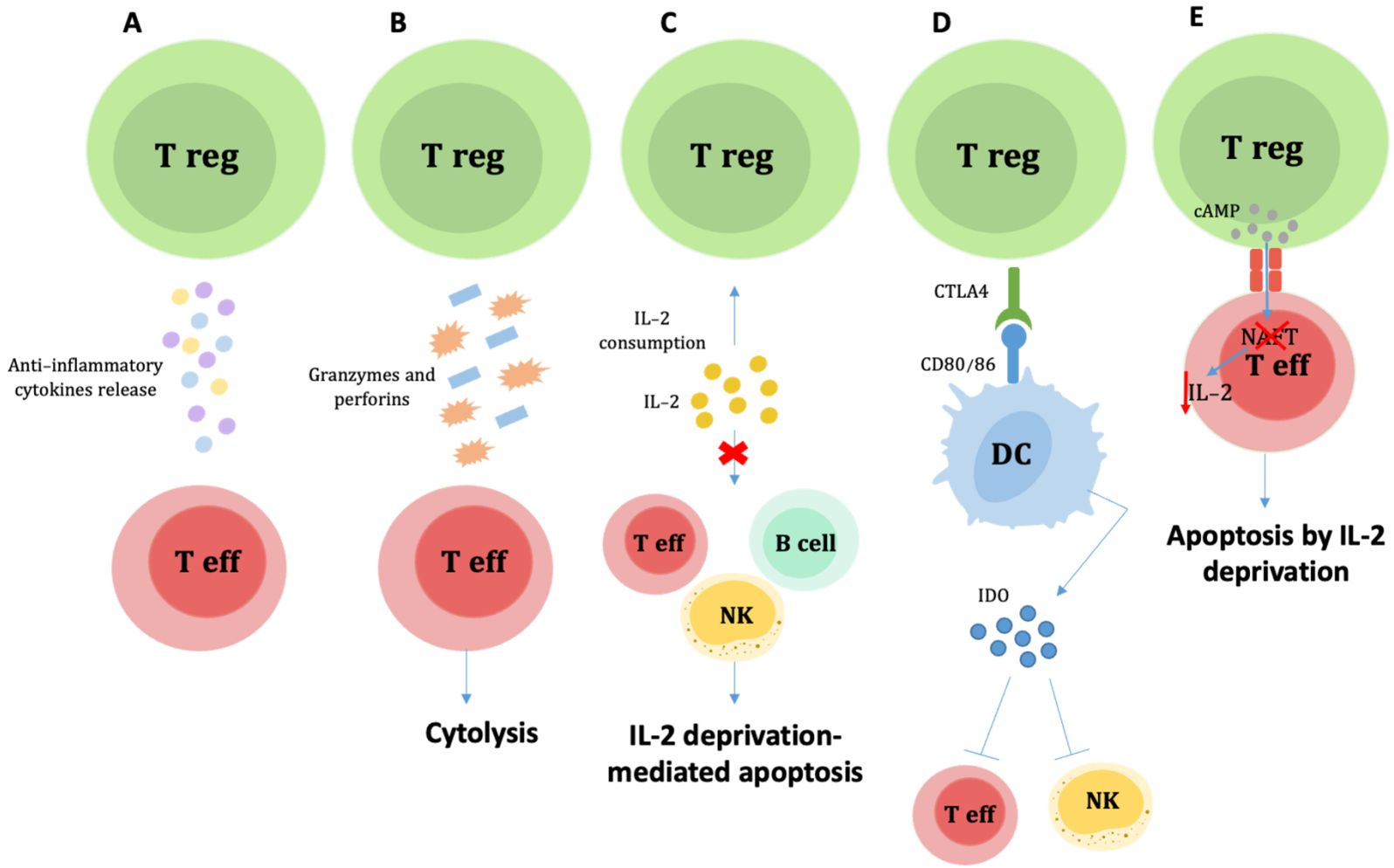

Figure 1.3: Mechanisms of Treg suppressive actions.

This image shows a summary of the different mechanisms of Treg-mediated immune suppression. **A**: Inhibitory cytokine release, **B**: Cytolysis induction, **C**: Metabolic disruption, **D**: CTLA4-mediated mechanism, **E**: cAMP-mediated mechanism.

1.3.2. Regulatory T cells in ALS

Several pieces of evidence demonstrate a key role of regulatory T cells in ALS onset and progression. In 2009, Mantovani and colleagues first reported a dramatic decrease in the number of CD4+CD25+ Tregs in sALS patients' peripheral blood (Mantovani et al., 2009). Since then, several laboratories have studied these cell types and their possible role in ALS.

Changes in the Treg population over the disease course were demonstrated in mSOD1 mouse models. In particular, in an early stable phase of the disease the number of CD4+CD25+ and CD25+FOXP3+ Tregs is increased while, as the disease progresses, they gradually decrease. More precisely, in 18-week old mice, which represents a late disease phase, a shift from the neuroprotective Treg/Th2 and M2 microglia population to a neurotoxic Th1/M1 microglial phenotype was observed, and this led to an acceleration in disease progression (Beers et al., 2011a, Zhao et al., 2012). In particular, increased expression of NOX2, IL-1β and IL-12, which are markers of M1 microglia activation, and of IFN-γ, secreted by Th1 was detected at later time points together with an elevation in the levels of IL-6, a cytokine that can completely inhibit Treg functions (Beers et al., 2011a). Interestingly, the passive transfer of healthy Tregs to mSOD1 mice seemed to prolong the stable phase of the disease and extend survival. After the treatment, increased levels of FOXP3, IL-4 and Gata-3, a key transcription factor of Th2 cells, were reported (Beers et al., 2011a). Furthermore, a different study using the same mSOD1 mouse model showed that Tregs were able to inhibit the activation of microglia through the secretion of IL-4. Specifically, this inhibition appeared to be independent from CTLA-4, IL-10 or TGF-β and mediated by a mixture of IL-4, IL-10 and TGF-β. Intriguingly, IL-4 was not entirely secreted by Tregs but also by Th2, hence this cytokine and Th2 were proposed as other crucial mediators of neuroinflammation suppression (Zhao et al., 2012).

Given this background, it was questioned what was the role of Tregs in ALS patients. In an early disease phase, Tregs were found to be significantly decreased in the peripheral blood, perhaps as an attempt of the CNS to suppress neuroinflammation as this correlated with a Treg increase in the CNS (Rentzos et al., 2012). However, as

the disease progresses, this compensatory attempt fails and Tregs were inhibited and decreased in number (Rentzos et al., 2012) (**Figure 1.4**). Moreover, the quantity of Tregs negatively correlated with the ALSFRS-R score. Hence, reduced Treg numbers are associated with a poor ALSFRS-R score and a more aggressive disease course (Beers et al., 2011a, Rentzos et al., 2012). The percentage of Tregs in patient blood also negatively correlated with ALS progression expressed in terms of AALS (Appel ALS score (Appel et al., 1987)) an ALS clinical rating scale (Beers et al., 2017, Henkel et al., 2013). This score is independent from ALSFS-R and thus this finding reinforces the hypothesis of a Treg dysfunction occurring over time in ALS patients.

Interestingly, Tregs were found not only to be reduced in number but they also appeared dysfunctional and less effective in promoting Teffs suppression and this impairment was more evident in rapidly progressing patients (Beers et al., 2017). In fact, the expression of *FOXP3*, *CD25*, *GATA3* and some anti-inflammatory cytokines, including *TGF-β, IL-10* and *IL-4*, were found to be downregulated in the peripheral blood of rapidly progressive ALS patients. In particular, their expression levels were found to be inversely correlated with the disease progression rate (Henkel et al., 2013). In contrast, increased expression of *Tbx21*, a transcription factor crucial for Th1 functions, was reported in the spinal cord of both rapidly and slowly progressive ALS patients whilst augmented levels of inflammatory mediators such as IFN-γ and NOX2, were found only in the rapidly progressive cases (Henkel et al., 2013). FOXP3 was proposed as a prognostic factor since its levels can efficiently predict the speed of disease progression (Henkel et al., 2013). Furthermore, evidence of epigenetic alteration in the Treg-specific demethylated region (TSDR), a CpG-rich regulatory region within the first intron of FOXP3 gene, was documented in ALS. This element is physiologically demethylated only in Tregs which stably express *FOXP3* but it is fully methylated in $CD4^+$ T cells. TSDR is partially methylated in ALS patients and this modification occurred more significantly in rapidly progressive cases (Beers et al., 2017).

Recently, evidence showed that Tregs isolated from ALS cases are not permanently impaired but their function can be restored by culturing them *in vitro* in the presence of IL-2 and rapamycin (Alsuliman et al., 2016). This latter compound is known to inhibit

the activity of Th1 and Th17 because it suppresses the mechanistic target of rapamycin (mTOR) signalling, which is crucial for these cells. In contrast, rapamycin promotes Treg differentiation and proliferation because their activities are independent from mTOR (Delgoffe et al., 2009). After the treatment with IL-2 and rapamycin, Tregs from ALS subjects and healthy volunteers had comparable suppressive functions. Evidence was provided of the generation of a large-scale GMP-compliant method for Treg isolation and expansion in the presence of IL-2 and rapamycin (Alsuliman et al., 2016). Safety, tolerability and benefits of this therapy were assessed in a phase I clinical trial (Thonhoff et al., 2018) (https://clinicaltrials.gov/ct2/show/NCT03241784).

More recently, specific Treg subtypes have been correlated with ALS progression rate (ALSFRS-R). Tregs can be classified into $CD45RO^+$, functionally active Tregs, and $CD45RA^+$, which are resting Tregs. In rapidly progressive patients, reduction in the number of $CD45RO^+$ Tregs was reported, and the amount of this cell type can be correlated with disease progression (Sheean et al., 2018). Furthermore, intraperitoneal injection of rapamycin and IL-2c (IL-2 combined with its monoclonal antibody which increases the magnitude and duration of IL-2 activity) in mSOD1 mice promoted CD45RO+ Treg expansion and prolonged their survival. In addition, a reduction in astrogliosis and microgliosis by 40 and 50% respectively was demonstrated together with an increase in FOXP3 and M2 microglia in the spinal cord and the sciatic nerve, and increased levels of GATA3 in sciatic nerve of these treated mice. Thus, these latter findings establish that Tregs can not only promote neuroprotection in the CNS, but they can also exert an equivalent function in the periphery (Sheean et al., 2018).

This body of evidence demonstrates a key role of Tregs and a dual trend during the disease course: these cells seem to be increased in an early disease phase, probably as an anti-inflammatory attempt made by the CNS, but as disease progresses, Tregs progressively and dramatically decrease leading to a worsening degree of neuroinflammation. Moreover, Treg levels can be considered as a prognostic factor of the disease progression and survival and the expansion of these cells was proposed as a promising therapeutic strategy for ALS. Several clinical trials testing different molecules but with the same molecular aim are currently active to try and elucidate any beneficial effect of Treg expansion in ALS (Giovannelli et al., 2020).

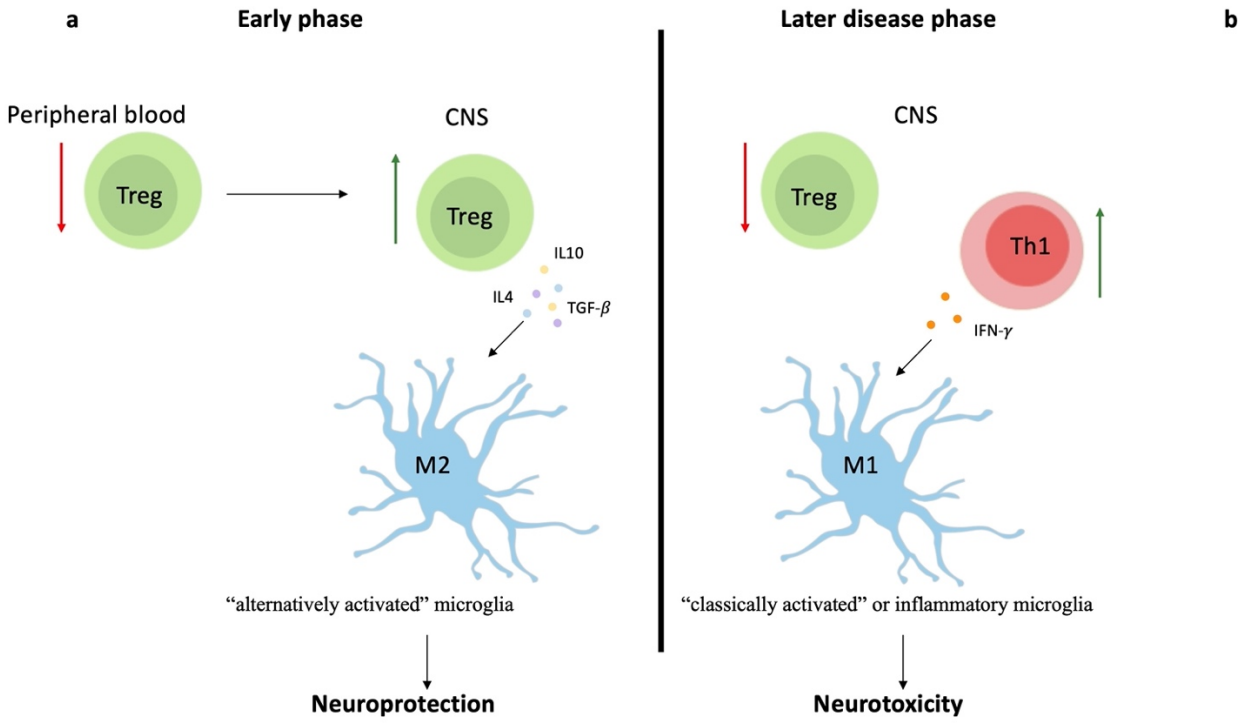

Figure 1.4: The role of Tregs in the early versus the later phase of the disease

The early disease phase is characterized by a recruitment of regulatory T cells in the CNS from the periphery (**a**). This is perceived as a neuroprotective attempt made by the CNS to reduce neuroinflammation. At this stage, Tregs secrete anti-inflammatory molecules which promote the activation of M2 microglia, known for their anti-inflammatory properties. In the later stage, as the disease progresses, the number of Tregs in the CNS decreases, while inflammatory mediators prevail (**b**). This includes Th1, which secretes cytokines that activate M1 microglia and promote inflammation and neurotoxicity.

1.4 Interleukin 2

IL-2 is known to be a crucial mediator of Treg differentiation and survival (Garg et al., 2012). Despite its pleiotropic functions on the immune system, it has been shown that IL-2 treatment causes specific FOXP3+Treg development and expansion, both in mouse models (Tang et al., 2008, Grinberg-Bleyer et al., 2010) and in humans (Zorn et al., 2006). Moreover, evidence shows that following IL-2 administration, different pathways are activated in Teffs and Tregs. In fact, the binding of this cytokine with its receptor in Teffs results in the activation of STAT5 and subsequently of S6 kinases, which triggers PI3K-Akt and mTOR pathways. In contrast, in Tregs, IL-2 binding mediates a direct activation of STAT5 and then FOXP3 becomes functional (Malek and Castro, 2010). Interestingly, it seems that treatment with low dose IL-2 (ld-IL-2) induce a selective increase in the phosphorylation, and thus activation, of STAT5 in Tregs, which corresponds to a decrease in the same modification in Teffs (Matsuoka et al., 2013). More importantly, the threshold for IL-2 receptor (IL2R) activation in Teffs appears to be much higher than in Tregs, which in turns require lower concentration of IL-2 for their stimulation. This can be explained by the different IL-2 receptors these two cell types show on their surface membranes. In fact, whilst Tregs constitutively express high-affinity IL2R (made of three subunits: IL2RA, IL2RB and IL2RG, which has a constant of dissociation Kd ~10^{-11} M), Teffs express it only after T cell receptor (TCR) activation. Without this stimulus, Teffs constitutively express only the intermediate-affinity receptor (made of IL2RB and IL2RG subunits and has a Kd ~10^{-9} M). This means that Teffs require higher IL-2 concentrations to become active compared to Tregs (Matsuoka et al., 2013). In particular, a recent study showed that the amount of IL-2 needed for the activation of Teffs is about 5000 greater than the dose required for Tregs (Dupont et al., 2014). In addition, as reviews by Spolski and colleagues, another type of IL2R is reported in humans, which is composed exclusively of the subunit IL2RA and is characterized by a low affinity of IL-2 (Kd ~10^{-8} M) (**Figure 1.5**).

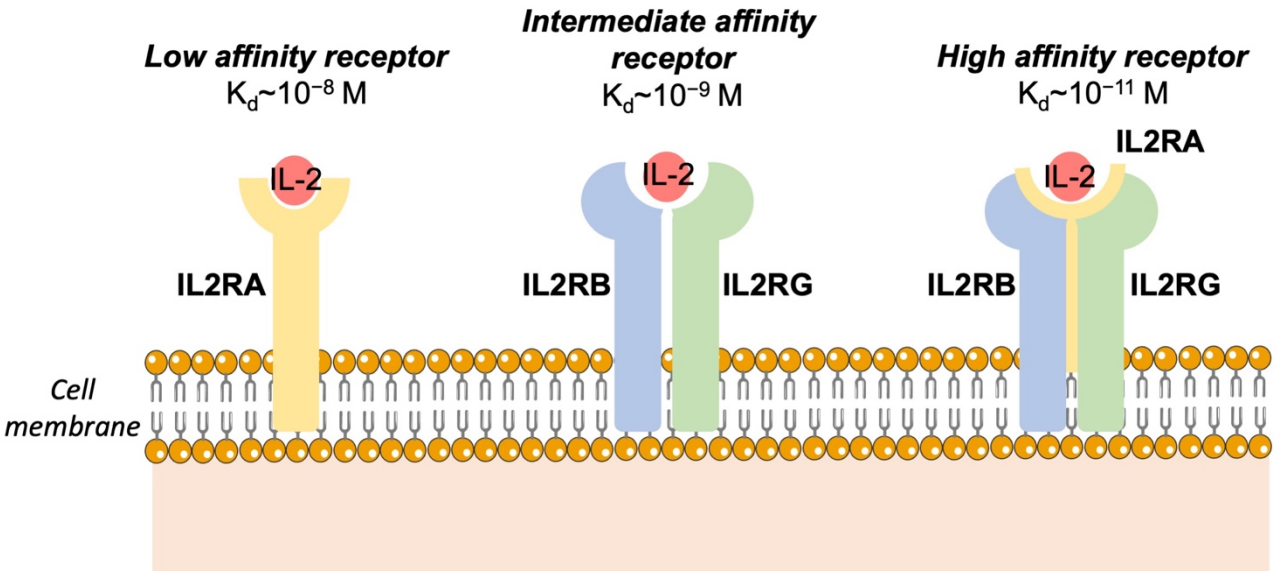

Figure 1.5: Different IL-2 Receptors

Schematic representation of the three different IL-2 receptors: low affinity (Kd ~10^{-8} M), intermediate affinity (Kd ~10^{-9} M) and high affinity (Kd ~10^{-11} M). The different receptor subunits characteristic of each receptor type are clearly displayed.

Given this background, ld-IL-2 has been proposed as a drug to treat different autoimmune disorders characterised by a Treg dysfunction. Several clinical trials have been carried out and, in the following paragraphs, these studies are grouped according to the disease for which the trial has been designed and their results are summarised.

- **Graft-versus-host disease (GVHD) caused by allogeneic haematopoietic stem cell transplantation (HSCT).** HSCT evokes host immune response which can result in GVHD, a chronic autoimmune disorder in which Tregs are known to be decreased in number. The safety and efficacy of ld-IL-2 (different dosages from 1x10^5 international units (IU)/m^2 to 3x10^6 IU/m^2) were evaluated in multiple clinical studies involving GVHD patients. No serious adverse events were reported, whilst an increase in the Treg count and Treg:Teff ratio were documented in phase I (Koreth et al., 2011, Whangbo et al., 2019a, Matsuoka et al., 2013) and phase II trials (Kennedy-Nasser et al., 2014, Koreth et al., 2016). In particular, one study showed that the number of Treg

cells in the blood peaked after four weeks of daily administration but the levels declined following cessation of treatment (Koreth et al., 2011). Additionally, this cytokine appeared to be able to increase functional activation of Tregs, mediate their expansion, increase thymic export and reduce Treg apoptosis (Matsuoka et al., 2013). However, while nearly all the patients showed an increase in their Treg subset, significant improvements in their clinical manifestations were reported in 50% of the study cohort (Koreth et al., 2011, Koreth et al., 2016). The authors proposed that this was probably due to inter-individual differences, concomitant medications and/or underlying pathologies (Koreth et al., 2011). A more recent study showed that ld-IL-2 induced increases in the diversity of the T cell receptor (TCR) repertoire and clinical improvements were associated with a rapid turnover of the TCR (Whangbo et al., 2019b).

- **Vasculitis induced by Hepatitis C virus (HCV).** Vasculitis is a remarkable extrahepatic presentation of HCV. The presence of autoantibody, T cells in the vascular infiltrates and the reduced number of circulating Tregs suggest an autoimmune process underlying in the disease onset (Boyer et al., 2004). In 2011, ld-IL-2 was evaluated for the first time as a possible treatment for vasculitis HCV-related vasculitis in a phase I/IIa study. The study population was treated with 1.5MIU IL-2 for 5 days (cycle 1) and, after a period of wash out, the dose was increased to 3MIU per day for 5 days (cycle 2-3-4). Results indicated that the treatment led to a significant increase in the percentage of Tregs in all patients. Moreover, clinical responses and improved symptoms were reported in the majority of patients. Adverse events were minor and transient (Saadoun et al., 2011).

- **Type 1 diabetes (T1D).** Ld-IL-2 treatment has been proposed as a treatment for this pathology, which is characterized by an autoimmune-mediated destruction of pancreatic β-cells. Several disease-associated mutations have been reported in genes involved in the IL-2 pathway (including IL2RA and IL2RB) and a Treg deficiency was demonstrated in these patients (Rosenzwajg et al., 2015). In 2013, a phase I/IIa study evaluated the safety and efficiency of 0.33, 1 or 3MIU IL-2 per day for 5 days in T1D patients. The authors reported the cytokine to be safe with no serious adverse events registered, and a dose-dependent increase in the Treg counts in the treated cohort was documented (Hartemann et al., 2013). In addition, the duration of the Treg

increase seemed to be also dose-dependent and treated patients showed elevated levels of CTLA-4, CD25, GITR and pSTAT5, all markers of Tregs activation (Rosenzwajg et al., 2015). However, at the 3MIU-IL-2 dose, an activation of NK cells, a trend towards chemokine and cytokine increase and more frequent mild to moderate adverse reactions were reported, therefore 1MIU-IL-2 was indicated as the prefered cytokine dosage for these patients (Rosenzwajg et al., 2015). More recently, in a different phase I/IIa trial, ld-IL-2 (0.125, 0.25 and 0.5 MIU/m^2) was shown to be well tolerated in newly diagnosed children with T1D. Nonetheless, although the cytokine efficiently promoted a dose-dependent Treg expansion, significant variations were reported amongst patients who were classified into high and low responders. Interestingly, the more responsive subjects were associated with a higher expression of soluble IL2RA (sIL2RA) and vascular endothelial growth factor receptor 2 (VEGFR2) (Rosenzwajg et al., 2020).

- **Alopecia areata (AA).** AA is one of the most frequent autoimmune diseases. This is characterize by a localized hair loss due to the autoimmune destruction of the hair follicles mediated by infiltrating $CD4^+$ and $CD8^+$ T cells (Castela et al., 2014). In a pilot study, five patients with severe AA (<50% of the scalp without hair) received 1.5MIU of IL-2 for 5 days (cycle 1) and then, 3MIU IL-2 (cycles 2-3-4). None of those patients achieved a complete regrowth of hair but a partial response was obtained in four out of five patients. Interestingly, these four responding patients showed a recruitment of Tregs into the lesioned skin of the scalp, while no Tregs infiltration was found in the non-responding patient (Castela et al., 2014).

- **Systemic lupus erythematosus (SLE).** SLE is a complex autoimmune disorder characterized by dysfunction of both the innate and the adaptive immune systems and by reduced levels of Tregs (Ohl and Tenbrock, 2015). Ld-IL2 was tested in SLE in a phase I/IIa study where participants received a subcutaneous injection of this cytokine (1.5 MIU-IL2 in the first cycle with possibility of increment in subsequent ones) for 5 consecutive days over 4 treatment cycles. Consistently with other studies, ld-IL-2 appeared to be well-tolerated and was able to expand Tregs in a dose-dependent manner. Clinical improvements were detected only in 8 out of 12 participants and, interestingly, a significant correlation between the changes in the Treg proportion and clinical scores was reported (Humrich and Riemekasten, 2019).

Additionally, in a different trial involving a larger cohort of SLE patients, 1MIU-IL2 was able to induce a partial remission in almost 77% of patients, whilst a complete remission of lupus nephritis was observed in 54% of the cohort (He et al., 2020).

- **Other autoimmune diseases (AIDs).** In 2018, Rosenzwajg and colleagues published their results related to an extensive clinical trial which aimed to assess the efficacy of ld-IL-2 on 11 different AIDs (rheumatoid arthritis, ankylosing spondylitis, SLE, psoriasis, Behçet's disease, granulomatosis with polyangiitis, Takayasu's disease, Crohn's disease, ulcerative colitis, autoimmune hepatitis and sclerosing cholangitis). Patients were treated with 1MIU-IL-2 for 5 consecutive days followed by fortnightly injections for a total of 6 months. Their results showed a consistent, significant and robust expansion of Tregs in all patients regardless of the specific AIDs. Moreover, an increase in the $CD56^{bright}$ NK cells or regulatory NK was also reported (Rosenzwajg et al., 2018). This particular type of NK produce high amounts of cytokines, such as IFN- γ, TNF-α, IL-13 and IL-10 depending on their stimulation (Poli et al., 2009). Finally, the same authors also reported a significant improvement in several clinical tests and patients' symptoms (Rosenzwajg et al., 2018).

- **Healthy volunteers.** One study evaluated the molecular and proteomic changes associated with ultra-low dose (ULD) IL-2 treatment (0.05 to 0.2 MIU/m^2/day) in healthy volunteers (Ito et al., 2014). As expected, after the administration of the drug, a significant expansion in the Treg subset was observed. In particular, both Helios-positive and Helios-negative Tregs appeared to be equally expanded. Helios (also known as IKZF2) is a transcription factor proposed as a marker of thymic-derived Tregs. This suggested that both thymic and peripheral Tregs were increased. Additionally, cytokine profiling and gene expression analysis were also performed to assess molecular variation following the treatment. A significant increase in CXCL10, which is known to be induced by IFN-γ and functions as a chemoattractant for monocytes, T cells and NKs, was reported. Given this, authors proposed that ULD-IL2 induced a type 1-related immune effect *in vivo*. Consistent with this, *STAT1*, *IRF9*, *GBP1* and *IFITM3*, all genes associated with IFN-γ pathway and type 1-immune response, were significantly increased. Nonetheless, at the same time, microarray analysis revealed a significant upregulation of both *FOXP3* and *IL2RA*. Moreover, *CISH*, a cytokine which plays an important role in the negative feedback of cytokine

signal transduction, was also found to be upregulated after the treatment. These findings suggest that ULD IL-2 promote an apparently paradoxical response: on the one hand it promotes IFN-γ immunity, while on the other hand it induces FOXP3+ Tregs immunosuppressive functions. This apparent paradox can be explained by the fact that this drug is not aimed to generally suppress the immune response but to modulate the immune system and restore its normal homeostasis. These treatments promote the maintenance of immune system functions in response to pathogens, while preventing excessive autoimmunity (Ito et al., 2014).

Taken together, these findings suggest that ld-IL-2 is well-tolerated and capable of expanding the Treg population in a dose-dependent manner in both healthy volunteers and in patients suffering from different autoimmune disorders. However, remarkable differences were reported and clinical improvements may be limited to a subset of responding individuals.

Since the role of the immune system in ALS has been documented, different drugs, aiming to suppress neuroinflammation, have been investigated as treatments for this disease. In particular, prednisone, celecoxib, minocycline and thalidomide have been evaluated as immunosuppressive agents for ALS. Unfortunately, all of them failed to slow disease progression and some of these agents caused serious adverse reactions (Tan et al., 1994, Cudkowicz et al., 2006, Gordon et al., 2007, Stommel et al., 2009). These compounds negatively regulate the overall function of the immune system, and thus, it is now believed that indiscriminate immunosuppression is not a suitable therapeutic strategy for ALS. In contrast, drugs which exert immunomodulatory effects aiming to restore the normal neuroimmune homeostasis, are considered promising. In this respect, Tregs represent a new therapeutic target in ALS and, given the large body of evidence suggesting the expansion and activation of the Treg compartment promoted by ld-IL-2, this cytokine has been proposed as a treatment for ALS.

The safety and clinical effects of 1 or 2MIU-IL2 was evaluated for the first time in ALS in a randomized, placebo-controlled pilot phase II clinical trial called Immuno-Modulation in Amyotrophic Lateral Sclerosis (IMODALS). Recently, our collaborators published the clinical results of this study and reported a significant and dose-dependent increase in both the absolute number and the frequency of Tregs in the

two treated arms compared to placebo (Camu et al., 2020). However, 2MIU-IL-2 administration was able to promote a higher Treg peak compared with the lower amount of the drug. In addition, the suppressive functions of Tregs were evaluated by *in vitro* co-culture of patient FACS-sorted Tregs and Teffs. These results suggested increased immunosuppressive functions of regulatory T cells following ld-IL-2 treatment, although statistical significance was only reported in the 1MIU-IL-2 group. This was due to a considerable variation in the response of individuals treated with the 2MIU-IL-2 dose. Moreover, a significant and dose-dependent reduction in the plasma levels of the inflammatory CCL2 was registered following ld-IL-2 treatment together with an increase in CCL17 and CCL18, two chemokines associated with the protective M2 macrophage/microglia phenotype. Nonetheless, no differences in the plasma concentration of neurofilament light chain (NFL), or in clinical parameters (such as ALSFR-R and slow vital capacity) were detected following drug administration. NFL, a constituent of the axonal cytoskeleton which is released into the CSF and in the blood following neuronal damage or death, has been proposed as a diagnostic and prognostic biomarker of ALS (Zucchi et al., 2020). The lack of variations in this protein levels or in the clinical readouts may have been due to the trial design, as patients were treated for only 3 months and monitored during a follow-up period for 3 additional months. Therefore, the study was perhaps underpowered in detecting changes in neurofilament biomarkers in such a limited period of time. However, further investigations are scheduled as part of different randomized, placebo-controlled, double-blind phase II clinical trial called MIROCALS (NCT03039673) that is currently active and aims to evaluate the effect of 2MIU-IL-2 in a larger ALS cohort of 220 participants over a longer period of 18 months.

Notably, it is important to stress that rapamycin was not used as additional treatment for the IMODALS clinical. As previously mentioned, Alsuliman and colleagues are currently exploring the efficacy of the *in vitro* expansion of Treg cells isolated from ALS patients in the presence of both IL-2 and rapamycin in a phase I clinical trial (Alsuliman et al., 2016, Thonhoff et al., 2018). In addition, a phase II trial is currently ongoing evaluating the effect of rapamycin as add-on therapy to riluzole in 63 ALS individuals (https://clinicaltrials.gov/ct2/show/NCT03359538). Importantly, besides its role in promoting Treg differentiation, rapamycin was shown to exert an important role in autophagy by being involved in the formation of autophagosomes and by

promoting the clearance of pathological protein aggregates, which are a prominent feature in ALS (Mandrioli et al., 2018). However, conflicting pre-clinical results have been reported. In fact, while some studies showed rapamycin to be neuroprotective by promoting the elimination of aggregates in cellular and animal models; another report found this drug to be harmful for ALS mSOD1 mice causing increase in motor disfunctions, acceleration in MN degeneration and decreased survival (Caccamo et al., 2009, Staats et al., 2013, Cheng et al., 2015, Madill et al., 2017, Zhang et al., 2011). Therefore, further research is needed to clearly elucidate the beneficial or detrimental effects of rapamycin in ALS. Lastly, as previously reported (pages 53-56), accumulating and compelling evidence suggest that low-dose IL-2 alone is able to efficiently promote a robust and dose-dependent Treg expansion in several autoimmune disorders characterised by decreased count of these protective T cell type. For this reason, the aim of the IMODALS study was to assess the potential of low-dose IL-2 in monotherapy in mediating Treg expansion and possibly in reducing the neuroinflammatory burden in ALS patients.

1.5 Interleukin-2 in the CNS

Given the neurological nature of ALS, a literature review focusing on the role of this cytokine within the nervous system was also conducted and previous studies investigating the role of IL-2 in the CNS are reported in this section.

Evidence shows that blood-derived IL-2 is able to penetrate the blood brain barrier (BBB), and it enters the CNS intact and in its bioactive form. Moreover, both blood-to-brain and brain-to-blood transport of this cytokine have been reported (Hanisch and Quirion, 1995, Banks et al., 2004, Waguespack et al., 1994). However, the way in which IL-2 penetrates the CNS is still to be elucidated. Given its high aqueous nature and its high molecular weight (15.5 kDa) it is very unlikely that it penetrates the barrier by diffusion (Banks et al., 1995). At the same time, it has been demonstrated that this cytokine does not cross the BBB through a saturable transport system (Waguespack et al., 1994). The rate of entry of radioactively labelled mouse IL-2, injected intravenously in mice is about 0.142 ± 0.044 μl/g-min and its half-life is of approximately 22 minutes. Moreover, a saturable CNS-to-blood efflux system has been discovered in these mice (Banks et al., 2004), potentially representing a protective mechanism through which IL-2 accumulation is avoided given that high dosage of the cytokine is known to cause detrimental effects such as the activation of brain endothelial cells and destabilization of the BBB (Wylezinski and Hawiger, 2016).

Several pieces of evidence show that IL-2 is also produced in the CNS by resident cells and that the IL-2 receptor (IL2R) is expressed in a wide range of brain regions. This cytokine appears to be produced primarily by neurons (Meola et al., 2013). Nevertheless, astrocytes and microglia involvement in IL-2 production have also been reported (Eizenberg et al., 1995, Hanisch and Quirion, 1995). In particular, as previously mentioned in section 1.2.1b, recent studies proposed astrocytes as one the major sources of brain IL-2, essential for CNS Tregs. Moreover, Meola and colleagues evaluated the presence of brain-derived IL-2 and its receptor in different CNS regions. They demonstrated a wide expression in different nuclei including: cingulate, dorsal endopiriform nucleus, lateral septum, nucleus of the solitary tract, magnocellular/gigantocellular reticular formation, red nucleus, entorhinal cortex,

mammilary bodies, cerebellar fastigial nucleus, and posterior interposed nucleus. These areas are all involved in the regulation of the sensorimotor gating nucleus (Meola et al., 2013). Moreover, IL2R expression was also reported in the motor cortex, anterior and lateral aspects of the striatum, interposed nuclei, red nuclei, inferior olivary nuclei, and the gigantocellular reticular nucleus, which are involved in motor control; as well as in the somatosensory cortex, fastigial nucleus of the cerebellum, vestibular nuclei, and the mesencephalic nucleus of the trigeminal nerve, fundamental areas for proprioception (Meola et al., 2013). Furthermore, IL2R has also been found to be expressed in the hippocampus influencing learning and memory processes (Petitto et al., 1998, Petitto et al., 1999). Interestingly, unpublished data generated in our Department by Dr Chloe Allen and Dr Laura Ferraiuolo suggested that ALS-patient derived astrocytes express all the three IL2R subunits (alpha, beta and gamma) although IL2RG appeared to be significantly downregulated in sporadic ALS compared to healthy control astrocytes.

IL-2 has already been shown to influence the activity, growth and survival of different non-immune system CNS cells in *in vitro* cultures:

- **Oligodendrocytes**: IL-2 appears to have a growth controlling function on immature oligodendrocytes: it exerts a positive proliferative action on these cells and it induces upregulation of myelin basic protein (Benveniste et al., 1987, Benveniste and Merrill, 1986, Hanisch and Quirion, 1995). However, negative control properties have been documented on oligodendrocytes at a later stage of development (Hanisch and Quirion, 1995).

- **Astrocytes**: IL-2 is considered an astrocytic mitogen which is able to promote astrocytic DNA synthesis and proliferation (Hunter et al., 1993). However, the administration of high-dose IL-2 (2ul of 10U/ul IL-2) to neonatal mice results in astrogliosis in the brain (Balasingam et al., 1994).

- **Neurons**: IL-2 appeared to have a survival-promoting effect on cultured neurons from various regions of the rat and murine brain, such as: hippocampal, cortical, septal, striatal, cerebellar and sympathetic neurons (Moroni and Rossi, 1995, Awatsuji et al., 1993, Sarder et al., 1993, Shimojo et

al., 1993). This response is concentration dependent (higher response dose: 200 U/ml) (Awatsuji et al., 1993). For this reason, IL-2 has been proposed as a neurotrophic factor. Moreover, IL-2 is able to induce morphological changes in neurons: it induces increased length and branching index of the axons (Sarder et al., 1993). Notably, Sarder et al propose that while the morphological changes are induced by a direct effect of IL-2 on cultured neurons, the pro-survival effect is indirectly mediated by soluble factors released from glial cells (Sarder et al., 1993). More recently, an IL-2-mediated effect on dendrites was demonstrated. This cytokine increased dendritic arborization and growth in cultured rat neurons. Furthermore, IL-2 is able to increase dendritic filopodia, and, the treatment in the early stages of development, is able to increase spine density (Shen et al., 2010). Moreover, IL-2 modulates the release of neurotransmitters such as acetylcholine (Hanisch et al., 1993, Seto et al., 1997), dopamine (Lapchak, 1992) and noradrenaline (Lapchak and Araujo, 1993). This effect is dependent on the concentration of IL-2: very low concentrations (pM) of this cytokine seem to promote a release of the neurotransmitters, while higher (nM) doses inhibit neurotransmitter release.

Interestingly, several pieces of evidence show that the downregulation or knock-down of IL-2 in the brain causes a series of detrimental consequences. First of all, the deletion of the *IL-2* gene seems to promote learning and memory impairment and reduction in the sensorimotor gating (Petitto et al., 1999). Moreover, knock-down of *IL-2* in mice corresponds to a significant decrease in the concentration of brain-derived neurotrophic factor (BDNF) and increased quantity of nerve growth factor (NGF) in the hippocampus (Petitto et al., 2012). Furthermore, IL-2 deficiency has been associated with the development of CNS autoimmune and degenerative diseases such as multiple sclerosis and Alzheimer's disease. In particular, it seems that reduction in the expression of this cytokine in the CNS leads to an increased invasion of T cell into the brain which can mediate autoimmunity (Huang et al., 2011, Huang et al., 2009). In a recent report, Alves and colleagues demonstrated that the administration of an AAV containing *IL-2* for 5 months in an Alzheimer's disease mouse model improved amyloid pathology. In particular, the treatment increased the number of Tregs and decreased the level of several proinflammatory markers. Furthermore, the group also reported an increased astrocytic activation which correlated with a reduction in the number of

amyloid plaques and in the ratio amyloid β42/β40 which suggests the involvement of astrocytes in the clearance of amyloid plaques. Lastly, a recovery in the memory deficit was also observed (Alves et al., 2017).

Hypothesis and aims

Given the large body of evidence suggesting a significant effect of ld-IL-2 in promoting Treg expansion and considering the impairment of these cells in the disease, this cytokine at low concentrations was proposed as an immunomodulatory treatment for ALS. We hypothesise that the Treg expansion in the peripheral blood is accompanied by significant changes in the patient transcriptome with evidence of activation of immunosuppressive pathways together with an inhibition of inflammatory processes. The expected effect was assessed through a transcriptomic analysis of the white blood cells from the IMODALS clinical trial cohort. Moreover, we propose that IL-2 has the potential to exert protective effects on CNS cells. In particular, given the contribution of astrocytes to neuroinflammation but also considering their physiological influence on Tregs as they maintain and sustain their functions, we hypothesise that low doses of IL-2 will be beneficial, possibly by reducing the astrocytic non-cell autonomous toxicity with a resultant a pro-survival effect on MNs. Additionally, we propose that healthy MN also react to the treatment by changing their morphology, increasing their branching index and arborization. To this end, induced neuronal progenitor cell (iNPC)-derived astrocytes reprogrammed from ALS patients and healthy controls were transcriptionally profiled following IL-2 treatment and co-cultured with normal murine MNs.

Given these hypotheses, **the specific aims** of this project are:

1. To evaluate microarray gene expression changes that occur in the leukocyte population of the IMODALS trial participants. In particular, differences between the two treatment doses will be assessed in order to examine a dose-dependent expression of key transcripts including Treg-specific markers. Additionally, longitudinal transcriptional changes throughout the trial will be evaluated by contrasting gene expression profiles of treated and untreated patients at different time points. Lastly, we aim to investigate whether the transcriptional effects of the ld-IL-2 are sustained after the end of the IMODALS administration period.

2. To investigate possible inter-individual differences in response to ld-IL-2 in the IMODALS participants. As reported in previous ld-IL-2 trials and from our collaborator's clinical data, considerable variations were reported in the ability of individuals to react to the cytokine. Therefore, differences in the levels of key transcripts will be examined in the trial cohort with the aim of stratifying patients and identifying specific genes whose expression at baseline could predict patient responsiveness at the end of the administration period.

3. To evaluate whether this cytokine has any beneficial effect on CNS cells. In particular, following IL-2 exposure, iNPC-derived astrocytes from ALS patient and healthy controls will be transcriptionally profiled through the use of the Oxford Nanopore cDNA-sequencing technique. Additionally, pro survival effects of IL-2 on MNs mediated by astrocytes will be assessed using a co-culture *in vitro* system. Lastly, IL-2-mediated changes in the morphology of MNs will also be investigated.

Chapter 2. Materials and Methods

2.1. IMODALS study Materials and Methods

2.1.1 Trial design

IMODALS (NCT02059759) was a three-arm, randomized, placebo-controlled pilot phase IIa clinical trial. Thirty-six participants between 18 and 75 years of age, with probable, laboratory-supported or definite ALS, were recruited at the Centre Hospitalier Universitaire de Montpellier, France (Camu et al., 2020). They were randomly assigned to one of the three treatment arms: 1 million international units (MIU) or 2MIU of IL-2 (Proleukin®, Novartis) or placebo (5% glucose solution). Patients received subcutaneous injections once daily for five days every 28 days for a total of three administration cycles (3 months). A three month follow-up period was also carried out. Notably, participants had been taking riluzole for at least three months prior to the inclusion visit and they continued this treatment with no interruptions during the trial. After the inclusion and randomization (day 1 or D1), four more visits were arranged over the course of the treatment administration period (days 8, 29, 57 and 64) and two were scheduled throughout the follow up period (days 85 and 169). During all these visits, clinical assessments were performed and blood samples were collected. For the purpose of transcriptome profiling, four time points during the course of the trial were selected: D1 or baseline, D8 (day 8, three days after the first injection cycle), D64 (day 64, three days after the last treatment cycle), and D85 (day 85, 24 days after the last injection and at the beginning of the follow-up period) (**Figure 2.1**).

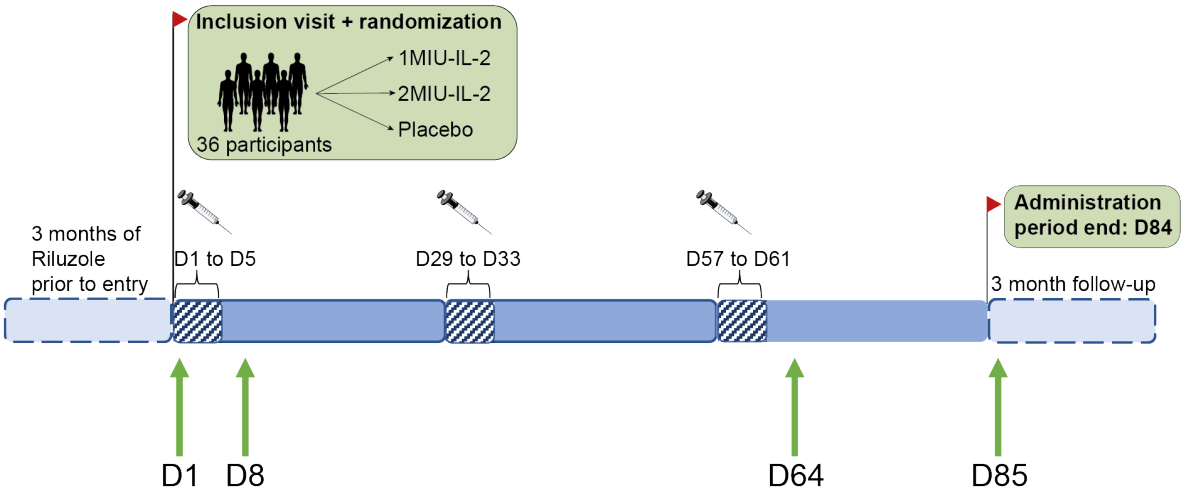

Figure 2.1: Timeline of the IMODALS clinical trial and Biosampling Time Points.

Schematic representation of the IMODALS clinical trial timeline. Patients were treated with riluzole for at least three months prior to their inclusion and randomization. Subcutaneous injections of either 1MIU, 2MIU-IL-2 or placebo were performed once daily for five days every month for a total of three months. Moreover, a three month follow-up period was arranged at the end of the administration period. For transcriptomic purposes, four time points were selected: D1, D8, D64 and D85 (indicated with green arrows).

2.1.2 Blood collection, processing and RNA extraction

Blood samples were collected from each patient at each study visit in the Centre Hospitalier Universitaire de Montpellier (France). LeukoLOCK™ filters (Ambion™, Thermofisher Scientific) were used to isolate the total leukocyte population (both lymphoid and myeloid cells), also referred to as white blood cells (WBCs). These were captured on the filters in RNAlater (Thermofisher Scientific) for stabilization and stored at -80°C before shipping to Sheffield for further processing. Total RNA was extracted from the filters by Dr Nadhim Bayatti and Abigail Brown using the LeukoLOCK™ Total RNA isolation kit (Ambion™, Thermofisher Scientific) according to manufacturer's instructions. Firstly, WBCs were lysed using a pH-adjusted lysis/binding solution.

Then, proteinase K in nuclease-free water solution was added to allow protein degradation. Subsequently, binding beads were added to the mix. RNA binds to the beads and following centrifugation (200xg for 3 min), the RNA-beads complexes were collected and resuspended in Wash Solution 1. Following a further centrifugation (16,000xg for 30 sec), samples were washed using Wash Solution 2/3 and centrifuged (16,000xg for 30 sec) to remove impurities from the beads. Pellets were air-dried for 2 min to allow any remaining alcohol from the Wash Solution to evaporate. TURBO DNase was then added and incubated for 10 min to remove any DNA contaminant. The DNase activity was stopped using a mixture of Lysis/Binding Solution and 100% isopropanol. To improve RNA purity, two more washes were performed using Wash Solution 2/3, followed by centrifugation (16,000xg for 1min) and removal of the supernatant. Subsequently, the pellet was air dried and 50µl of Elution solution was added wherein the RNA was released from the beads. A last centrifugation (16,000xg for 2min) enabled RNA separation from the beads which formed a pellet. The supernatant RNA was collected and stored at -80°C.

2.1.3 RNA quantity and quality assessments

Nanodrop ND-1000 (Thermo Scientific) was used to assess RNA quantity and purity. This is a UV spectrophotometer which is able to measure the absorbance of 1µl of RNA samples loaded between two optic pedestals. The analysis is based on the principle that nucleic acids can absorb light in the ultraviolet spectrum. The instrument is able to calculate both the concentration of the nucleic acid (ng/µl), using the Beer-Lamber law, and its purity, thanks to the measurement of two absorbance ratios: 260/280 and 260/230. The first one is the most important indicator and a value ~2 is generally accepted as pure RNA. Lower scores might indicate the presence of protein, phenol or other contaminants which absorb at wavelengths near 280nm. A secondary measure is 260/230 ratio which should be ~2 and lower values indicate the presence of contaminants absorbing at 230nm such as phenol, carbohydrates or salt.
Before initiating the sample read, the instrument was washed by adding 1µl of RNase-free water on the lower optic pedestal. Then, a blank measurement was performed to set the baseline for subsequent reads. This was carried out by loading and reading

1µl of the substance in which RNA is diluted (either elution buffer or RNase-free water). At this point, 1µl of RNA was added and the sample read. To avoid sample carryover, both upper and lower pedestals were wiped upon completion of each sample before loading the following one.

The quality of RNA samples was also assessed using Agilent 2100 Bioanalyser (Agilent Technologies), an automatised electrophoretic analysis tool to inspect biomolecule integrity. Microfabricated chips are used to perform an electrophoretic separation of RNA samples whose fluorescence signals are detected. Electropherograms and spectra are then generated which allow a visual assessment of the RNA quality (**Figure 2.2)**. Sample integrity can be monitored by analysing 18S and 28S ribosomal RNA and their spectra peaks. In particular, as degradation proceeds, a decrease in the ratio of the 18S to 28S signals is detected together with an increase in the baseline signal between the two ribosomal peaks. To allow standardization and easier interpretation, the instrument uses ribosomal ratios to compute the RNA integrity number (RIN) by using a complex and non-publicly available algorithm. This metric indicates the quality of the extracted nucleic acids; a value equal to 10 means that the RNA is highly intact, while, if it is equal to 1, the RNA is very likely to be degraded. Dr Nadhim Bayatti and Abigail Brown assessed the integrity of the IMODALS RNA samples whilst the same analysis on RNA extracted from cells was performed by myself. The Agilent RNA 6000 Nano kit (Agilent Technologies) was used following the manufacturer's instructions. First of all, a gel dye was mixed to RNA gel matrix. The mixture was then vortexed and centrifuged at 13000g for 10 min. Subsequently, an RNA chip was inserted into the chip priming station and the gel-dye mix was pipetted into the appropriate well. The priming station was then closed to force the gel to spread across the chip. After exactly 30s, the station was re-opened and 9µl of gel-dye mix was loaded into two predefined wells. Next, the RNA marker was pipetted into all 12 sample wells and in the ladder well. Subsequently, 1µl of ladder and 1µl of RNA sample were loaded into each of the designated sample wells. The chip was vortexed in the IKA® MS3 basic vortexer (IKA Works Inc.) for 1 min and scanned using the Agilent 2100 Bioanalyzer (Agilent Technologies) and the Eukaryotic Total RNA Nano assay programme was used to calculate the RIN.

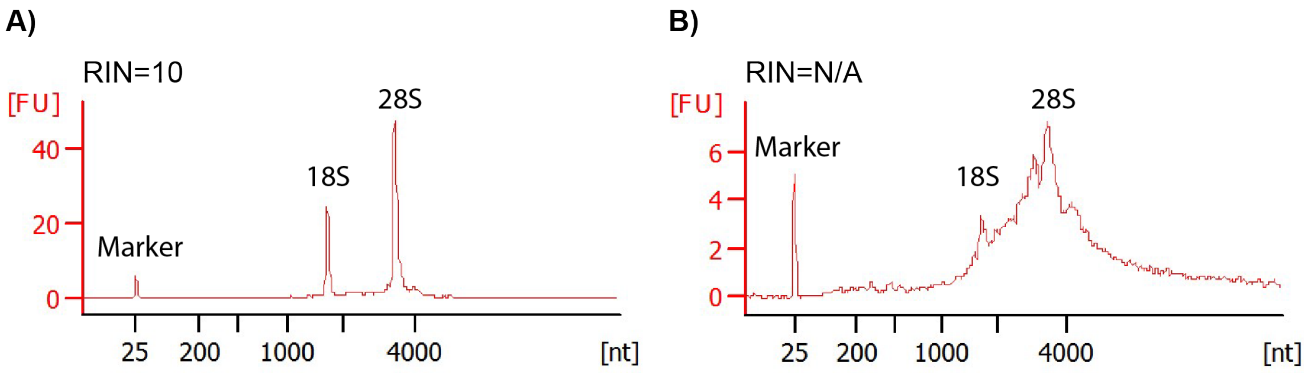

Figure 2.2: Representative Bioanalyser Spectra from High and Low Quality RNA samples.

Examples of spectra from (**A**) an intact RNA sample (RIN=10) and (**B**) a likely degraded RNA sample (RIN=N/A) obtained with the Agilent 2100 Bioanalyser. While in the first graph peaks form 18S and 28S ribosomal subunits are clearly recognizable, evidence of RNA degradation is visible in the second one. X-axis: number nucleotide estimated, Y-axis: fluorescence units.

2.1.4 Microarray preparation, normalization and quality control

Affymetrix Clariom D human microarrays (Applied Biosystem™, Thermofisher Scientific) are useful tools to conduct transcriptome expression profiling. Single sense-stranded DNA copies are generated from total RNA samples and hybridized onto a microarray GeneChip where probes for coding and non-coding (such as lincRNA, pre-miRNA, miRNA etc) transcripts as well as for different splicing isoforms, annotated and speculative sequences are included. This allows gene-level, exon-level and alternative splicing expression analyses.

Gene expression profiles from Clariom D human microarrays were generated using total RNA extracted from IMODALS participants' WBCs as per manufacturer's instructions. Prior to the start of my PhD, Dr Nadhim Bayatti processed IMODALS samples from D1 and D85 whilst D8 and D64 gene expression profiles were produced by myself. Reagents used were provided from GeneChip™ WT PLUS Reagent Kit

GeneChip™ hybridization and Wash and Stain Kit (Applied Biosystems). The microarray protocol can be divided in 16 steps which are summarized below:

1. *Total RNA preparation.* 200ng of high quality total RNA was diluted in nuclease-free water to reach a final volume of 3µl.
2. *Preparation of poly-A RNA controls.* To provide exogenous positive controls, each array contains a set of *B. subtilis* genes which are absent in eukaryotic samples. These controls were amplified and labelled together with RNA samples. Their hybridization allowed monitoring of the labelling process. Poly-A RNA controls were diluted with the poly-A control buffer and added to RNA samples.
3. *First-strand cDNA synthesis.* In this procedure, RNA was retrotranscribed to cDNA using primers containing a T7 promoter sequence. Thus, a single-stranded complementary DNA (ss cDNA) with a T7 promoter sequence at its 5' end was produced. Total RNA/poly-A RNA controls were mixed with the first strand enzyme and its buffer and the mixture was incubated for 1 hour (h) at 25°C, 1 h at 42°C and 2 min at 4°C.
4. *Second-strand cDNA synthesis.* At this stage, double-stranded cDNA (ds cDNA) was obtained generated by the second strand enzyme mix. This contained a DNA polymerase, which synthesizes the second strand, and RNase H which simultaneously degraded the original RNA. First strand cDNA, second strand enzyme and buffer were incubated at 16°C for 1 h, then 65°C for 10 min and finally 4°C for 2 min to cool the solution.
5. *In vitro transcription (IVT).* Antisense or complementary RNA (cRNA) was produced using T7 DNA-dependent RNA polymerase. The solution of ds cDNA, T7 polymerase and buffer was incubated at 40°C for 16 h.
6. *cRNA purification.* cRNA was then purified from enzymes, salts, inorganic phosphates and unincorporated nucleotides using magnetic purification beads. These beads bound cRNA and, by utilising a magnetic stand, cRNA-bead complexes were isolated and washed with 80% ethanol to remove impurities. Finally, pre-heated (65°C) nuclease-free water was added to elute the purified cRNA.
7. *Second-cycle single-stranded cDNA.* Fifteen nanograms of cRNA was retro-transcribed to single-stranded (ss) cDNA using second cycle primers in the

presence of appropriate buffer and primers (incubation: 10 min at 25°C, then 90 min at 42°C, 10 min at 70°C and finally 2 min at 4°C). This reaction produced ss cDNA containing a fixed ratio of dUTP:dTTP.

8. *RNA hydrolysis using RNaseH.* To degrade RNA previously used to generate ss cDNA, the enzyme RNaseH was added and the solution was incubated at 37°C for 45 min, 95°C for 5 min and 4°C for 2 min.
9. *Ss cDNA purification.* Similarly to step 6, ss cDNA was purified using magnetic purification beads.
10. *Ss cDNA fragmentation.* Single-stranded cDNA was fragmented by uracil-DNA glycosylase (UDG) and apurinic/apyrimidinic endonuclease 1 (APE1) at the unnatural dUTP residues added in step 7. Ss cDNA (5.5µg) was combined to the fragmentation master mix (containing 10X cDNA fragmentation buffer, 1µl of UDG, 1µl of APE1 in nuclease-free water) and incubated for 1 hr at 37°C, 2 min at 93°C and 2 min at 4°C.
11. *Fragmentation control.* To check if the fragmentation process was successful, samples were run on an Agilent RNA 6000 Nano chip (Agilent Technologies) using the Agilent 2100 Bioanalyzer (Agilent Technologies) (as described in section 2.1.3). Spectra showing a peak around 40-70 nt and a RIN ~2 indicated that samples were successfully fragmented.
12. *Ss cDNA labelling.* At this stage, ss cDNA was labelled using terminal deoxynucleotidyl transferase (TdT) with an Affymetrix proprietary DNA labelling reagent which was covalently bound to biotin. To this end, fragmented ss cDNA was mixed with the 5X TdT buffer, DNA labelling reagent and TdT and incubated for 1 h at 37°C, 10 min at 70°C and 2 min at 4°C.
13. *Labelling control.* The labelling process efficiency was assessed using the gel-shift assay which monitored the addition of biotin residues. This step is crucial as biotin is needed for the binding of streptavidin phycoerythrin to each of the ss cDNA molecule and for the subsequent detection of fluorescent signals which are proportional to the level of expression of each mRNA molecule. For each sample to be tested, two solutions containing 1µl of sample and either NeutrAvidin solution (5µl of 2mg/ml in PBS) or PBS only (5µl) were prepared. The solutions were incubated at room temperature for 5 min. Then, 5µl of loading dye was added and samples were loaded into an agarose gel which was run at 150V for 1h. Following ethidium bromide staining, the gel was placed

into UV light G-box (Syngene) and the success of the labelling process was visually assessed.

14. *Hybridization.* Fragmented and labelled ss cDNA was hybridized on Affymetrix® chips. For each sample, a hybridization cocktail was prepared (3.7µl of control oligo B2, 11µl of pre-heated 20X hybridization controls, 110µl of 2X hybridization mix, 15.4µl of DMSO, 19.9µl of nuclease-free water and 5.2µg of fragmented and labelled ss cDNA). The mixture was incubated at 99°C for 5 min and at 45°C for 5 min in the thermal cycler and then centrifuged at 13'000rpm for 1.30min, using 1- 15PK centrifuge (Sigma-Aldrich, St Louis, MO). Subsequently, the solution was injected into one of the septa of the GeneChip® which was then incubated with rotation at 60 rpm at 45°C for 16 h in the Affymetrix® oven (Affymetrix GeneChip®) to allow hybridization.
15. *Wash and stain.* Following hybridization, unbound components and debris were washed away using the Fluidics Station 450 (Affymetrix GeneChip®). Subsequently, streptavidin-phycoerythrin staining was performed using Stain cocktail 1 and 2 and the array holding buffer.
16. *Scan.* Fluorescent signals, proportional to the level of expression of each transcript in a sample, were detected by the Affymetrix GeneChip® scanner. CEL files containing expression data for each of the probes on the arrays were obtained.

Microarray data were normalized using signal space transformation robust multi-chip analysis (SST-RMA) method. Expression Console™ (Affymetrix, Thermofisher Scientific) software was used to perform quality control (QC) and specific metrics were used to investigate the quality of the arrays including:

- **Positive and negative area under the curve (AUC)**: AUC is defined as the area under a receiver operator curve (ROC). Generally, this assesses the accuracy of a test considering two possible types of errors: false positive and false negative. A ROC curve, in fact, plots the true positive rate (sensitivity) against the false positive rate (specificity). The overall performance of a classifier can be assessed using the AUC which variates between 0.5 (random guessing) to 1 (perfect classifier). Affymetrix arrays contain a set of control probes for housekeeping genes. In particular, probes matching in the exon

regions of these genes are considered positive controls while, probes in their introns are negative controls. The assumption is that negative and positive controls are a measure of false positive and true positive respectively. A ROC is generated by assessing the ability of the probe set summary in separating positive from negative controls (exon vs intron). Samples showing AUC>0.7 were considerate to have passed this QC metric.

- **Spike or hybridization control:** Whilst preparing the hybridization cocktail, 20x Eukaryotic Hybridization Controls (AFFX-r2-Ec-BioB, AFFX-r2-Ec-BioC, AFFX-r2-Ec-BioD, AFFX-r2-P1-Cre) were added. As these were mixed only prior to the addition of samples onto the microarrays, spiked controls did not interfere with RNA sample preparation and thus they can be used to assess the efficiency of the hybridization process. Fixed and increasing relative concentrations are characteristic of Affymetrix Eukaryotic Hybridization Controls and therefore they should exhibit a signal intensity pattern with BioB's signal < BioC < BioD < Cre.

- **Labelling control.** To assess the quality of the labelling process, fixed concentrations of poly-A RNA controls were mixed and processed alongside the RNA extracted from patient samples. These are exogenous positive controls made of a set of four *B. subtilis in-vitro* synthesized genes (Lys, Phe, Thr, Dap) which are absent in the eukaryotic genome and contain an artificial poly-A tail to their 3'-ends in order to enable their labelling. Lys was added at the lowest concentration (1:100.000) which is closed to the level of sensitivity of the microarray, therefore its detection in at least half of the microarrays processed in any experiment, indicated a successful procedure (Jaksik et al., 2015). Moreover, given the staggered concentrations of the four *B. subtilis* genes (Lys= 1:100.000; Phe= 1:50.000; Thr=1:25.000; Dap=1:6.667), their expected signal intensities should be: Lys < Phe < Thr < Dap.

- **Signal intensity histogram and relative signal box plot.** Although not strictly considered as QC metrics, signal intensity histograms and relative signal box plots were considered useful tools to identify potential outliers.

2.1.5 Microarray data analysis

2.1.5.1 Differential expression analysis

Microarray data from D64 were analyzed using Transcriptome Analysis Console (TAC) 4.0 (Affymetrix, Thermofisher Scientific) to identify differential expression between 1MIU IL-2 treated and placebo patients (referred to as 1MIU_vs_Placebo) and between 2MIU IL-2 and placebo (2MIU_vs_Placebo). Gene level analyses with p-value≤0.05 (F-test statistics) and fold change (FC) ≤-1.2 or ≥1.2 cut-offs were performed. The formula used to compute FCs by the software is reported below:

$$FC = 2^{ABS\,(Expression\ comparison)}$$

Formula 2.1: Fold changes calculation.

Mathematical calculation to retrieve fold changes or differential expression of specific transcripts in two patient groups. Importantly, if negative values are obtained from the exponential term, the sign of the computed FC is changed to negative to clearly indicate downregulation. ABS: absolute value. Expression comparison: microarray signal intensity of Gene X in patient group Y subtracted to microarray signal intensity of Gene X in patient group Z.

To accomplish complex multifactorial-designed differential expression analyses with multiple sample groups to compare, the Limma software package in R was used (https://www.bioconductor.org/packages/release/bioc/html/limma.html, (Ritchie et al., 2015). Empirical Bayes statistical methods were applied by the software in order to identify significantly differentially expressed genes (DEGs) (cut-offs: p-value ≤0.05 and FC ≤-1.2 or ≥1.2). SST-RMA normalized data were imported into the software and RefSeq gene filtering was applied before launching the analyses.
Three analyses were performed using Limma in which treated patient transcriptomes at specific time points (D8, D64 and D85) were compared to their baseline levels (D1) and normalised to the same comparison within the placebo group. FC were computed as per Formula 2.1 and the three produced expression comparisons were: (T8-T1)-(P8-P1); (T64-T1)-(P64-P1); (T85-T1)-(P85-P1), (T1, 8, 64, 85= intensity signal of a certain gene in the 2MIU-IL2 treated group at D1, 8, 64, 85; P1, 8, 64, 85= intensity

signal of a certain gene in the placebo group at D1, 8, 64, 85). These analyses will be referred to in the text as: ΔD8; ΔD64; ΔD85 respectively.

Following the import of microarray data into Limma, a PCA analysis was carried out and two batches were recognisable (D1 and D85 were spatially separated from D8 and D64). This was probably due to the fact that samples were shipped and received at different times and the samples were processed in 2 batches. Evidence shows that methods that remove batch effect prior to Limma statistical analysis may lead to exaggerated and unreliable results (Nygaard et al., 2016). For this reason, batch effect identifiers were instead included as a variable to our statistical model (Nygaard et al., 2016, Ritchie et al., 2015). In this way, we took into account the variation resulting from the batches obtaining reliable results. Therefore, microarray data were categorized into factors, namely treatment type (placebo or 2MIU IL-2), time point (D1, D8, D64, D85) and batch (1 and 2). Then, linear models were used to fit to the three factors. Given that RNA extracted from patient C01P011 at D8 failed RNA QC checks and a microarray was not generated, array data from that participant at D1 and D64 were also excluded from the ΔD8 and ΔD64 analyses. Notably, for these analyses, we assumed patients belonging to the same treatment group to be replicates even though variability within participants was reported. This setting was chosen because, considering the small sample size, more complex mixture models would probably have generated inconclusive results.

2.1.5.2 Gene enrichment and pathway analysis

To investigate which pathways or biological processes were altered as an effect of the drug administration over time, an enrichment analysis was carried out. Gene enrichment is a computational method used to cluster an input list of genes into functional groups in order to better understand the underlying biological processes being altered as a consequence of a disease or a treatment.

Importantly, to perform enrichment analyses RefSeq filtering was applied to the identified DEGs. This was done because Affymetrix microarrays include probes for a considerably large number of novel, uncharacterized and putative transcripts which

are not included in any gene set libraries given that their functions in cellular pathways are currently unknown. Therefore, because of the large proportion of such non-annotated genes, the input of gene lists including all transcripts would have affected the statistical power of the enrichment analysis and very few significantly enriched terms would be retrieved. This means that a large number of type II statistical errors (false negatives: when researchers conclude that there is not a significant effect, when there actually is) would have been made. In contrast, transcripts included in the RefSeq databases are known and annotated, therefore this selection increased the power of the statistical tests.

Different gene enrichment software programmes were used to conduct different investigations. These are summarised in the list below and a description of the analyses and statistical tests they perform is also reported:

- **Enrichr**: This is an open-source web-based bioinformatic software which integrates several databases or gene set libraries (including KEGG, Reactome, Wikipathway and GO) (Chen et al., 2013, Kuleshov et al., 2016). Given a gene list, Enrichr compares and computes the overlap between the user's input and existing annotated lists in each library. Then, a Fisher's exact statistical test is performed by the software to identify statistically significant (p-value <0.05) enriched terms. Lists of upregulated and downregulated DEGs, previously obtained from either TAC or Limma, were separately imported and analysed using Enrichr. Outputs from Gene Ontology (GO) databases were investigated in detail. However, long lists of GO biological processes resulted as altered from this type of analysis with often redundant terms being identified.

- **REVIGO**: To allow summarisation and easier interpretation of data obtained from Enrichr and to gain more biologically relevant results, the software REduce and VIsualize Gene Ontology (REVIGO), was used (Supek et al., 2011). Briefly, this is an open-source web-server software which groups GO terms into clusters depending on their semantic similarity. It searches for Uniprot proteins included in each GO process and finds closely related or ancestral terms. Then, it chooses a cluster representative which is a GO process that recapitulates a group of similar terms. This selection is based on the frequency score, which is

the percentage of Uniprot proteins included in a GO process - thus the higher the more general is the term - and on the p-value of overlap (in our case this was obtained with Enrichr and inputted by the user in REVIGO). The semantic similarity level can be customised to obtain shorter or larger summarised GO lists depending on the user's needs. For our analysis, given the long lists retrieved from Enrichr, a similarity cut-off of 0.5 was chosen.

- **Metascape**: This is an open-source, user-friendly gene enrichment software. Unlike Enrichr which performs different enrichment analyses for each database, Metascape considers all gene libraries together and generates a p-value-ranked list of enriched terms from different databases (KEGG Pathway, GO Biological Processes, Reactome Gene Sets, Canonical Pathways, CORUM, TRRUST, DisGeNET, PaGenBase, Transcription Factor Targets and COVID) (Zhou et al., 2019). It calculates the enrichment factor (ratio between the number of genes observed in the user input list and the counts expected by chance), p-value (computed using hypergeometric test) and q-value (Benjamini-Hochberg) to correct for multiple testing. Following the identification of enriched processes, the software clusters related terms depending on their similarity. In particular, pairwise similarities between terms are assessed using the Kappa-test and processes with scores > 0.3 are considered similar and grouped together in a cluster. The most significant term in a group is used as cluster representative. Unlike REVIGO, this software provides an extra analysis tool: it identifies relationships between terms and generates network plots where intra and inter-cluster relationships can be visually inspected. In these enrichment networks, each term is represented as a node and two processes having Kappa similarity score > 0.3 are connected by edges. To reduce complexity, only the top 20 most significant clusters are shown in a network map with a maximum of 15 terms per cluster. This function provides a simple and effective way to capture relationships between processes. Lastly, Metascape allows simultaneous analysis of multiple gene lists to identify similarities and differences among them. In particular, heatmaps showing top enriched clusters are generated to visualise shared or unique altered pathways and, in the case of the enrichment network maps, each node is represented as a pie chart where each sector size represents the percentage of genes included

in the corresponing gene list. Separate lists of upregulated and downregulated DEGs, previously obtained from either TAC or Limma, were imported and analysed using Metascape.

- **Ingenuity Pathway Analysis® (IPA®)** (Qiagen Inc.): This commercially available web-based software application uses the Ingenuity Knowledge Base®, which includes millions of findings published in the peer-reviewed literature, to retrieve significant (p-value ≤0.05, Fisher's exact test) altered pathways in a data set (https://www.qiagenbioinformatics.com/products/ingenuitypathway-analysis). Unlike the previous reported software, IPA® also allows the user to make predictions on processes' activation or inhibition following the calculation of z-scores (activation: z-score > 0, inhibition: z-score <0) (Krämer et al., 2014). This prediction is particularly valuable as it allows the import of a single gene list for each comparison that includes both up and downregulated genes. This is not possible with the software mentioned above which requires two separate gene lists containing transcripts with positive and negative FCs to be imported separately and different analyses to be performed. Hence, IPA allows a more complete enrichment analysis, predicting the overall activation state of a single pathway considering all the DEGs present in the process regardless of their FC direction. Complete lists of DEGs (with the associated p-values) from the Limma ΔD8 and ΔD64 comparisons were imported in IPA and analysed. IPA provides several analysis features including: 1) canonical pathway, 2) upstream regulators and 3) disease and function analyses.
  The first tool allows the identification of canonical pathways included in the Ingenuity Knowledge Base® that are enriched in the user's data set. For each of the identified pathways, prediction of activation or inhibition is computed. The second tool, the IPA upstream regulator analysis, allows the identification of key regulatory molecules (i.e. transcription factors, miRNAs or small molecules) which are capable of recapitulating the observed gene expression changes in a data set. In fact, IPA investigates the number of transcription regulator targets that are present in a user's input file and it also evaluates the direction of change in their expression to retrieve the activation status of a master expression regulator. Lastly, the diseases and function tool was used to identify relevant

terms associated with common human disorders or biological functions that are over-represented in the ΔD8 and ΔD64 comparisons.

To visualise and summarise results obtained from these analyses, volcano plots, heatmaps and bar plots were generated using ggplot2 or gplots R packages. Treemaps were also produced with the treemap library in R.

2.1.6 cDNA synthesis and quantitative Real Time PCR

To perform quantitative real-time polymerase chain reactions (qRT-PCR), total RNA (200-500ng) was retrotranscribed to cDNA using 5x qScript™ DNA Supermix (Quantobio) by incubating samples in Peltier Thermal Cycler PTC-200 (MJ Research) at 25°C for 5 min, then at 42°C for 30 min and finally at 85°C for 5min. Subsequently, cDNA were mixed with 20X predesigned PrimeTime® qPCR Assay (Integrated DNA Technologies Inc., see **Table 2.1**), which contains primers and a probe for each target transcript, and 2X Luna® Universal qPCR Master Mix (New England BioLabs® Inc.) in nuclease-free water solution. Samples (prepared in triplicate) were loaded into Hard-Shell PCR 384-well plates (Bio-Rad Hercules, CA) (10µl of qRT-PCR master mixture per well) and centrifuged at 1760 rpm for 1 min using an ALC PK120 centrifuge (DJB Labcare, Newport Pagnell, UK). Samples were incubated at 95°C for 3 min to allow denaturation and then 40 cycles of amplification at 95°C for 10 sec and 60°C for 30 sec were performed using C1000 Touch™ Themal cycler (Bio-Rad).
Raw Ct values were retrieved using CFX Maestro™ software (Bio-Rad). Afterwards, ΔCt, ΔΔCt and relative concentration (R) values were computed as follows:

$$\Delta Ct = Ct_{\text{gene of interest}} - Ct_{\text{reference gene}}$$

$$\Delta\Delta CT = \Delta CT - (\text{average } \Delta CT_{\text{placebo sample}})$$

$$R = 2^{-\Delta\Delta Ct}.$$

GraphPad Prism 8.4 was used for statistical analysis and for plot generation.

qRT-PCR experiments were conducted with different aims: to validate microarray gene expression data, to identify blood transcripts that could act as predictive biomarkers to forecast Treg-response in ld-IL-2 treated patients and to optimise IL-2 treatment in iNPC-derived astrocytes (iAstrocytes). For microarray validation, all samples from the 4 time points and from the 12 2MIU IL-2 and 12 placebo patients were screened by qRT-PCR. Three technical replicates were produced for each condition. To identify possible biomarkers, samples at D1 from all 12 2MIU IL-2 and 3 placebo patients - C01P006, C01P012 and C01P025 - were screened for 6 transcripts and three technical replicates were produced for each sample. To optimise IL-2 treatment in iAstrocytes, three biological replicates were produced for each experimental condition (healthy control, sporadic ALS and C9orf72 mutant ALS astrocytes). Importantly, GAPDH was used as a reference gene across all these experiments as its expression from microarray data was found to be stable across all the time points and no variations were reported amongst patient groups. Moreover, astrocytic expression data previously generated in Dr Laura's Ferraiuolo team by Dr Chloe Allen suggested no substantial transcriptional differences amongst different ALS patient lines.

Table 2.1. qRT-PCR primer/probe summary.

In this table, a list of all the PrimeTime® qRT-PCR primers/probes (Integrated DNA Technologies Inc.) used for different experiments is reported. For each transcript target, the product ID is indicated together with the RefSeq accession number which specifes the recognised mRNA molecule. A separate column illustrates whether the PrimeTime® primer/probe detects all the splicing variants of a gene of interest. Finally, the targeted exon location is also reported and, in particular, our chosen primer/probes anneal multiple exons and the junction regions between them.

Experimental aim	Target	Product ID	RefSeq accession number	Detects all variants	Exon location
Reference gene	GAPDH	Hs.PT.39a.22214836	NM_002046	Yes	2-3
Microarray validation	CTLA4	Hs.PT.58.3907580	NM_005214	Yes	3-4
	FOXP3	Hs.PT.58.3671186	NM_001114377 NM_014009	Yes	10-11
	IKZF2	Hs.PT.58.2960172	NM_001079526 NM_016260	Yes	6-7
	IL2RA	Hs.PT.58.2187899	NM_000417	Yes	4-5
Biomarker identification analysis	BLNK	Hs.PT.58.1645191	NM_001114094 NM_001258442 NM_001258441 NM_001258440 NM_013314 NR_047683 NR_047682 NR_047681 NR_047680	Yes	10-12
	BTLA	Hs.PT.58.20005939	NM_001085357 NM_181780	Yes	2-5
	CD27	Hs.PT.56a.27441991	NM_001242	Yes	2-3
	SBNO2	Hs.PT.58.14833003	NM_001100122 NM_014963	Yes	27-28
	TLR9	Hs.PT.58.40576968	NM_017442	Yes	1-2
	TRAF2	Hs.PT.58.3116982	NM_021138	Yes	9-10
IL-2 treatment optimization in iAstrocytes	CASP3	Hs.PT.56a.25882379.g	NM_004346 NM_032991	Yes	4-5
	CCND2	Hs.PT.58.28257	NM_001759	Yes	1-2
	IL2RA	Hs.PT.58.2187899	NM_000417	Yes	4-5
	IL2RB	Hs.PT.58.19340846	NM_000878	Yes	5-6
	IL2RG	Hs.PT.58.4465361	NM_000206	Yes	4-5
	MYB	Hs.PT.58.264008	NM_001130172 NM_005375 NM_001161660 NM_001161659 NM_001161658 NM_001161657 NM_001161656 NM_001130173	Yes	5-6

2.1.7 NanoString

To further validate microarray data and also to investigate on inter-individual dissimilarities in patient Treg-response to 2MIU-IL-2 treatment, nanoString analyses were conducted. In fact, our expression data, consistently with flow cytometry measurement obtained from our collaborators, suggested that the rate of Treg expansion is different across different ALS patients treated with 2MIU-IL-2. For this reason, we wanted to investigate the immunological gene expression signature of those patients showing the highest increase in Treg numbers with those with little or no Treg increase following ld-IL-2 treatment. 2MIU-IL-2-treated patients were classified depending on their Treg counts measured at D64. In particular, three participant sub-groups were defined in relation to their Treg-response to ld-IL-2:

- High responders: patients with Treg level at D64 > 250 cells/µl of blood
- Mild responders: Treg level at D64 between 150 and 250 cells/µl
- Low responders: Treg levels at D64 < 150 cells/µl.

A list of the patients and their Treg response is provided in **Table 2.1**.

Table 2.2: Patient characteristics and response type.

This table illustrates age, gender, disease decline and treatment regimen of each participant. Moreover, Treg count at D64 is displayed and these data have been used to classify the patient response to 2MIU-IL-2 (high responders: Treg level at D64 > 250 cells/µl; moderate responders: between 150 and 250 cells/µl; low responders: < 150 cells/µl). Disease decline per month was computed using the formula below:

$$Decline\ per\ month = \frac{48 - ALSFRSR_{at\ recruitment(D1)}}{Duration\ from\ symptom\ onset\ to\ recruitment\ (month)}$$

where ALSFRSR indicated the revised ALS functional rating score and 48 is the maximum total score which is generally observed at symptom onset.

Patient ID	Gender	Treatment type	Age at D1 (years)	Disease decline/month (ALSFRS-R/month)	Treg count at D64 (cell/µl of blood)	2MIU-treated response classification
C01P001	Male	1MIU-IL-2	40.2	0.114	115.14	-
C01P005	Male	1MIU-IL-2	42.5	0.514	145.97	-
C01P008	Female	1MIU-IL-2	47.7	0.400	120.59	-
C01P010	Female	1MIU-IL-2	65.4	0.378	151.50	-
C01P013	Male	1MIU-IL-2	44.7	0.643	114.18	-
C01P020	Female	1MIU-IL-2	46.4	0.296	160.49	-
C01P023	Male	1MIU-IL-2	53.8	0.075	87.79	-
C01P024	Female	1MIU-IL-2	55.8	0.600	156.26	-
C01P027	Male	1MIU-IL-2	64.4	0.800	154.40	-
C01P033	Male	1MIU-IL-2	59.1	0.250	91.62	-
C01P035	Female	1MIU-IL-2	75.4	0.424	146.48	-
C01P038	Male	1MIU-IL-2	64.4	0.224	81.65	-
C01P003	Male	2MIU-IL-2	36.5	1.000	406.72	High
C01P004	Female	2MIU-IL-2	47.3	0.688	169.13	Moderate
C01P009	Female	2MIU-IL-2	68.8	0.692	434.47	High
C01P011	Male	2MIU-IL-2	76.6	1.500	144.34	Low
C01P016	Male	2MIU-IL-2	63.4	0.375	88.99	Low
C01P018	Male	2MIU-IL-2	59.8	0.444	117.88	Low
C01P021	Female	2MIU-IL-2	62.7	0.226	505.70	High
C01P026	Male	2MIU-IL-2	72.5	0.417	222.66	Moderate
C01P028	Male	2MIU-IL-2	63.4	0.148	176.08	Moderate
C01P032	Male	2MIU-IL-2	44.4	0.667	181.13	Moderate
C01P036	Male	2MIU-IL-2	56.5	0.209	52.22	Low
C01P037	Male	2MIU-IL-2	40.3	1.375	263.93	High
C01P002	Male	Placebo	47.5	0.375	30.08	-
C01P006	Male	Placebo	44.2	0.277	34.22	-
C01P007	Male	Placebo	49.2	0.351	55.14	-

C01P012	Female	Placebo	64.6	0.455	35.41	-
C01P014	Male	Placebo	52.6	0.350	90.37	-
C01P017	Male	Placebo	42.2	0.143	60.33	-
C01P022	Male	Placebo	63.6	0.429	32.99	-
C01P025	Male	Placebo	61.7	0.909	84.88	-
C01P030	Male	Placebo	58.5	0.313	25.63	-
C01P031	Male	Placebo	53.9	1.600	46.73	-
C01P034	Female	Placebo	69.7	0.579	57.52	-
C01P039	Female	Placebo	69.7	0.241	32.49	-

Following these auto-defined criteria, 4 high Treg-responsive patients (C01P003, C01P009, C01P021, C01P036), 4 low Treg-responder patients (C01P018, C01P011, C01P016, C01P036) and 4 patients from the placebo group (C01P012, C01P017, C01P022, C01P031) were investigated through nanoString at D1, D8 and D64. This enzyme-free technique consists in the direct counting of each mRNA molecule in a sample based on two types of probes: capture and reporter probes. The first one is made of a hybridization region, which binds a target sequence in the mRNA of interest, and a biotin tag which allows RNA samples to be immobilised to a streptavidin coated slide. The second probe consists of a hybridization region and a unique sequence of fluorescent tags specific for each transcript. The assay does not measure the fluorescence signal intensities, instead, it simply counts individual barcodes which is equivalent to directly counting the different mRNA molecules. This technique, also called molecular barcoding technology, allows the generation of highly reproducible and robust expression data.

Briefly, 300ng of total RNA were mixed with the capture and reporter probes (included into the Autoimmune Discovery panel) in the presence of the Hybridization buffer and incubated at 65°C for 16 hours. Subsequently, samples were loaded into cartridges which were then scanned using nCounter® SPRINT profiler (NanoString Technologies Inc.). The Autoimmune Discovery panel was used which contains probes for 755 mRNA targets: 740 immune-related transcripts with both pro and anti-inflammatory functions and 15 housekeeping genes used for data normalization. Moreover, both positive and negative controls were added according to manufacturer's instructions to

allow quality control analysis. Notably, a higher concentration of RNA (300ng) was used compared to what is generally recommended (~100ng). This was chosen because preliminary NanoString data obtained from collaborators at SITraN, who used the suggested amount of RNA, showed low yields, poor QC and housekeeping genes were barely or not detectable. This made their downstream analysis very difficult and therefore, to avoid this troubleshooting, we were advised to increase the starting concentration of the nucleic acids.

Once the scanning was completed, one Reporter Code Count (RCC) file was generated for each of the samples screened. This file contains the barcode counts of each gene and controls in the CodeSet which correspond to the number of mRNAs counted by the machine for each transcript.

Data normalisation was done using a two-step process. Firstly, data were normalized on positive controls included in the panel. This is to reduce variation due to different cartridges, reagents used or different processing days. Secondly, housekeeping gene standardization was performed.

The nSolver^{TM} 4.0 software (NanoString Technologies Inc.) was used to conduct quality control (QC) analysis and four metrics were evaluated:

- **Imaging QC**: this parameter measures the ratio of field of views (FOVs: area of the cartridge successful scanned and imaged by the instrument) that the nCounter successfully counts over the number of FOVs attempted. A threshold of 0.75 is generally accepted which means that 75% of the cartridge was successfully detected.

- **Binding density**: this metric evaluates the concentration of barcodes read by the instrument. Ideally, it should not exceed the range of 0.1-2.25 spots per square micron.

- **Positive control QC**: this parameter indicates the correlation between the known concentration of positive controls included in the panel and the counts measured by the instrument. The computed R^2 should be not lower than 0.9.

- **Limit of detection** (or positive control limit of detection): this metric computes the limit of detection of the assay and indicates whether counts of a positive

control (POS_E) are significantly above the counts of the negative controls. As mentioned before, positive controls were included as per the manual. In particular, six positive controls (indicated as POS_A to POS_E, while POS_F is below the limit of detection) were mixed in as per manufacturer's instructions at decreasing standard concentrations. This QC metric indicates if the raw counts of 0.5fM positive control probe (POS_E) is greater than the mean counts of the negative controls. If this is at least two standard deviations higher, the sample is considered as having passed this QC metric.

To identify which selection of transcripts amongst these 740 were responsible for patient group differences, nanoString data was inputted into Qlucore Omics Explorer (Qlucore) and multi-group comparison statistical analysis (p-value≤0.05) was performed. Variables (transcripts) accounting for groups' separation were selected and plotted separately using nSolver™ 4.0. Finally, a pathway scoring analysis was performed using nCounter Advanced Analysis 2.0 (NanoString Technologies Inc.). This technique allows the summarization of biologically and functionally related gene expression changes. Transcripts are grouped into pathways and a score is computed for each sample as the first principal component of the pathway genes' normalized expression. Despite the complexity of the score calculation, this is a reliable technique which is able to detect trends in pathway alterations due to mild gene expression changes. Positive scores indicate pathways being generally activated as the majority of its genes are upregulated, while the opposite applies for negative values.

2.1.8 Predictive biomarker analysis

A predictive analysis was carried out to try and identify biomarkers of the outcome of the treatment which might be able to forecast patient Treg-response given their gene expression at time of recruitment. To this end, a preliminary screening was conducted by correlating the expression level at D1 of all the 740 targets included into the Autoimmune Discovery nanoString panel with i) the Treg counts at D64 (as measured by flow cytometry at Kings College London by our collaborators Dr Timothy Tree and Dr Marius Mickunas. (Camu et al., 2020)) and ii) with the expression of IL2RA at D64 (nanoString data). In particular, Pearson's correlation tests were performed with

associate t-test statistics. Significant correlations were studied and transcripts were ranked according to their computed p-values (rank 1= transcript showing the lowest p-value). Subsequently, a consensus screening was conducted to identify transcripts which were found to be commonly significantly correlated with the two chosen variables measured at D64. Lastly, a combined score was computed by adding the two ranks computed for the Treg and IL2RA correlations. Low scores reflected transcripts behind most significantly correlated with both the variables. Six biomarker candidates (*SBNO2*, *BTLA*, *CD27*, *TRAF2*, *BLNK*, *TLR9*) were selected as they were amongst the commonly and most significantly correlated transcripts with the best ranked combined scores.

Given that nanoString experiments were conducted only on a selection of eight patients, qRT-PCRs were performed on all 12 2MIU IL-2 treated patients and on three placebos as controls (C01P006, C01P012 and C01P025, randomly chosen). The averaged qRT-PCR expression values from three technical replicates for each sample were correlated (Pearson's correlation) with their associated Treg counts at D64. This analysis was performed using the programming language R (caret package) and plots were generated using the ggplot2 package. Two of the six candidates (TLR9 and CD27) were selected as they showed good and significant correlation scores when qRT-PCR expression data from all the patients were analysed. Subsequently, a multiple linear regression model using the two promising transcripts was generated and statistically tested using "linear model()" function in R. To visualise the two-variable-linear regression model, scatterplot3d package in R was used.
Linear regression models are generally based on four key assumptions:

- ***Linearity of the data***: it is assumed that the relationship between the Y predictors and the X outcome is linear.
- ***Normality***: data, and in particular the residuals (difference between observed and predicted values), follow a normal distribution.
- ***Homoscedasticity****:* the variance of the residual is constant.
- ***Independence****:* there is no relationship between the residuals and the Y variable. This is particularly important in longitudinal or time series data sets and no correlation between consecutive residual is assumed.

To test the reliability of the model, diagnostic tests were conducted in order to verify that all the aforementioned linear assumptions were met. Moreover, given that a multiple linear model was chosen, an extra analysis was performed to exclude the existence of collinearity. This phenomenon occurs when two or more predictor variables are correlated to each other. It is crucial to rule out this possibility as if two predictors are correlated, they cannot independently forecast the dependent variable hence an interpretation of the model would be impossible. Several R packages were used to perform these tests which are summarised in the **Table 2.3**.

Table 2.3: R Packages for Multiple Linear Model Tests.

This table lists the different R packages used to test the reliability of the multiple linear model. The R package or library names and the specific R functions used to carry out the analyses are reported together with the kind assumption tested and the obtained output (plots or values).

R package or library name	R function	Assumption tested	Output
Global Validation of Multiple Linear Model Assumption	gvmla()	All linear model assumption	Scores and p-values
R base function	plot()	All linear model assumption	Diagnostic plots
Caret	vif()	Collinearity	Variance inflation factor (VIF) values

Finally, a cross validation was carried out to test the robustness of the model. Specifically, this is a resampling method which allows the assessment of the performance of a given predictive model on new and unseen data. To this end, the original data are split into: i) a training set, which is used to build or train the model, and ii) a test set which is needed to validate the model by estimating the prediction error. In this case, a k-fold=12 cross-validation or leave one out cross validation (LOOCV) was performed. This method consists of the random splitting of the data into 12 K-equal sized subsets. One of these subsamples is reserved each time and, while

the others are used as training data to build the model, the excluded one serves to test and validate the model and the prediction error is recorded. These steps are repeated K-times and the average of K-errors is computed. The package caret in R was used to perform this type of validation and compute the cross-validation metric root mean squared error (RMSE).

2.2. Effects of IL-2 in CNS cells - Materials and Methods

2.2.1 Astrocyte differentiation from iNPCs and IL-2 treatment

Induced neuronal progenitor cells (iNPCs) are tripotent cells capable of differentiating into oligodendrocytes, neurons or astrocytes. These are reprogrammed from human adult fibroblasts using a mixture of retroviral agents containing four reprogramming factors (*Sox4*, *KLF4*, *Oct3/4* and *c-Myc* (Stopford et al., 2019, Meyer et al., 2014)).

For the purpose of this thesis, nine skin fibroblast lines (3 ALS patients carrying a C9orf72 mutation, 3 sporadic ALS patients and 3 healthy volunteers) were reprogrammed into iNPCs and then differentiated into patient-derived astrocytes (or iAstrocytes) by culturing them in the appropriate medium for five days by Dr Laura Ferraiuolo and her team according to the published protocols (Stopford et al., 2019, Meyer et al., 2014) (**Table 2.4**).
Specifically, at D0 of differentiation, iNPCs were seeded into a 10cm petri dish coated with fibronectin (Millipore) and cultured into the human iAstrocyte differentiation media containing: DMEM (Fisher Scientific), 0.2% of N2 (Gibco), 1% of penicillin-streptomycin mixture (Lonza) and 10% foetal bovine serum (FBS) (Life Science Production). Following receipt of the cells from Dr Ferraiuolo's team, after 72 hours, the cells were fed with fresh human iAstrocyte differentiation media and incubated for 2 more days at 37°C/5% CO_2. At D5 of differentiation, iAstrocytes were harvested using accutase (StemPro® Accutase® Cell Dissociation Reagent, Gibco) and plates were incubated at 37°C/5% CO_2 for 4 min. Accutase was diluted in PBS, cells were collected and spun at 200 x g for 4 min. Subsequently, iAstrocytes were seeded into 6-well plates (400.000 cells per well) and incubated for 24h at 37°C/5% CO_2 to allow cells to adhere to the plates. At D6 of differentiation, iAstrocytes were treated with IL-2-supplemented media (containing either 1 or 10% FBS). Lyophilised IL-2 (PeproTech) was reconstituted in 100nM acetic acid to a concentration of 100µM as per manufacturer's instruction. To allow extended storage at -80°C, IL-2 was diluted in PBS containing 0.1% bovine serum albumin (Sigma Aldrich) to reach a final stock concentration of 50µM. Different treatment times (1h, 4h and 24h) and IL-2

concentrations (1nm to 100nM diluted in 5% glucose-PBS) were tested. Control samples were treated with media containing 5% glucose-PBS solution (1:1000). Finally, iAstrocytes were washed with PBS to remove medium and harvested by cell scraping. Cell pellets were stored at -80°C.

Table 2.4. Fibroblast donors.

This table summarises details of fibroblast donors which cells have been used to generate iAstrocytes. For each cell lines, ALS patient or healthy control age at skin biopsy collection is reported together with gender details, disease type and duration.

Cell line	Diagnosis	Age at biopsy collection (years)	Gender	Disease duration (months)
AG86620	Non-ALS	64	Female	-
155v2	Non-ALS	40	Male	-
161	Non-ALS	31	Male	-
78	C9orf72 ALS	66	Male	31.7
183	C9orf72 ALS	50	Male	27
201	C9orf72 ALS	66	Female	19.4
009	Sporadic ALS	61	Female	21
12	Sporadic ALS	29	Male	90
17	Sporadic ALS	47	Male	72

2.2.2 RNA extraction from astrocytes

RNA was extracted from iAstrocytes using the RNeasy® Mini Kit (Qiagen). This technique employs the use of a spin column containing a silica-based membrane to isolate and purify RNA molecules. Briefly, cell pellets were lysed using the appropriate RTL buffer (350µl) which contains guanidine-thiocyanate to prevent RNAse-mediated RNA degradation. Subsequently, 70% ethanol solution was added (350µl) to promote the nucleic acid binding to the column membrane. All sample volume (700µl) was

loaded into the RNeasy Mini spin column and centrifuged at 10,000 x g for 15 s. Total RNA bound to the membrane and contaminants were washed away through several washing steps (700µl of RW1 buffer was added and sample were centrifuged at 10,000 x g for 15 s; and two washes were performed with 500µl of RPE buffer and centrifugation 10,000 x g for 15 s). The spin column membranes were dried to ensure ethanol evaporation to avoid the presence of alcohol contaminants in the final samples. High-quality RNA was eluted using 50µl of RNAse-free water. RNA quantity and quality was assessed through nanodrop and Agilent 2100 Bioanalyser respectively (see section 3.1.3). RNA samples were stored at -80°C.

2.2.3 LDH cytotoxicity assay

Lactase dehydrogenase (LDH) is a cytosolic enzyme which catalyses the conversion of lactate to pyruvate via NAD^+ reduction to NADH. LDH concentration in the medium is an indicator of cell death as this protein is released when plasma membranes are damaged. The LDH assay is a colorimetric method to assess and quantify cell cytotoxicity using a tetrazolium salt (INT). Upon cell damage, LDH is released in the medium, NADH is produced and used by the enzyme diaphorase to reduce INT to formazan. The concentration of fromazan can be measured spectrophotometrically at 490nm. This quantity is proportional to the amount of LDH released and therefore to the amount of dying cells.

The CyQUANT™ LDH cytotoxicity assay kit (Invitrogen) was used. At D5 of differentiation iAstrocytes were seeded into 96-well fibronectin-coated plates (10,000 cells per well). After 24 hours, cells were treated with either IL-2 supplemented media (10nM IL-2 in 1% FBS iAstrocyte media) or 5% glucose-PBS solution (1:1000) media for 4 hours. Then, 10µl of 10X lysis buffer was added to a set of triplicates to determine the maximum LDH activity controls while 10µl of dH_2O was included in the other samples to monitor spontaneous LDH released. After 45 min of incubation at 37°C/5% CO_2, 50µl of sample medium was transferred into a new 96-well plate and reaction mixture (50µl) was added. Samples were incubated at room temperature for 30 min protected from light. Finally, the stop solution (50µl) was added and absorbances at

490nm and 680nm were measured using the PHERAstar FS plate reader (BMG Biotech). Plain medium absorbances were also detected and used to normalise spontaneous LDH or maximum LDH samples to their medium background signal. To calculate LDH activity, absorbance values at 690nm (background) were subtracted from the 490nm one and then the percentage of cytotoxicity is calculated using the formula below:

$$\% = \frac{Absorbance\ (IL-2\ treated/control\ samples) - Avarege\ absorbance\ (medium\ background\ )}{Avarege\ absorbance\ (Max\ LDH\ release) - Avarege\ absorbance\ (medium\ background)} * 100$$

Formula 2.2. Method for Calculation of Percentage of Cytotoxicity.

This formula was used to retrieve the percentage of sample cytotoxicity. In particular, this calculation allowed the quantification of the number of cells which died because of the IL-2 administration compared to the ones that have died because of the treatment with the lysis buffer. Absorbance: 490-680nm value.

Data were analysed using GraphPad Prism 8.4 and to conduct statistical analysis (Unpaired T tests, p-value<0.05 were considered significant).

2.2.4 cDNA library generation and Oxford Nanopore sequencing

Total RNA was extracted from iAstrocytes belonging to 3 ALS patients carrying a C9orf72 mutation, 3 sporadic ALS patients and 3 healthy volunteers using the RNeasy® Mini Kit (Qiagen, see section 2.2.2). Quantity and quality of RNA was assessed using Nanodrop and Bioanalyzer, respectively, as described in section 2.1.3. In particular, for each cell line, two treatment conditions were performed: control (1:1000, 5% glucose PBS solution in iAstrocytes differentiation media containing 1% FBS) or IL-2 treated (10nM IL-2 in iAstrocytes differentiation media containing 1% FBS). Therefore, a total of 18 RNA samples (50ng) were used to generate sequencing libraries.

Given COVID-19 restrictions and the Department policy on limited working hours to allow social distancing, library preparation was performed by Matthew Wyles. The

Oxford Nanopore PCR-cDNA barcoding kit (SQK-PCB109, Oxford Nanopore Technologies) was used and libraries were prepared as per manufacturer instructions (**Figure 2.3**). This method allows the sequencing of long-read RNA molecules, which provides several advantages over short-read techniques, usually considered a gold standard for RNA sequencing giving their affordable prices and high accuracy. Human transcripts have an average length of 200-300 base pairs (bp). Short reads (usually 50 bp), characteristic of sequencing techniques such as Illumina, can only partially cover the mRNA's length making difficult the bioinformatic process of reconstructing the entire sequence. Moreover, because the reads are short, multimapping is also frequently observed. In contrast, using Oxford Nanopore, the entire transcript of a gene can be sequenced end-to-end in a single read making this technique ideal for splicing isoform analysis. Additionally, whilst short-read sequencing is characterized by the so-called GC bias (sequences with low and high GC content are usually underrepresented), Oxford nanopore technology has been shown to provide accurate representation of mRNA molecules with different GC contents. The different steps in the library preparation are briefly described in this section. Firstly, poly T primer with a known extra sequence at the end were annealed on the poly A tail on the eukaryotic mRNA. Reverse transcriptase produced first strand cDNA which subsequently underwent a process called strand switching. Specifically, when the retro-transcriptase reached the 5' end of the mRNA, three cytosine residues (3xC) were added at the end of the newly synthesised cDNA. In this reaction, strand switching primers were also present. These contained three 2-oxymethyl guanine bases which are known to have a higher affinity for DNA than RNA and to be resistant to nucleases. In addition, a synthetic known 5' tail sequence was also present in the strand switching primer. This primer hybridised to the 3xC present on the cDNA and the retrotranscriptase synthesised the reverse complement of the known 5' synthetic sequence. Therefore, the strand switching process and the poly- T primers allowed to have known sequences on both ends of the newly synthesised cDNA. These were then employed by the PCR to amplify the nucleic acids as primers were designed to be complementary to those ends. Importantly, PCR primers also contained a barcode, which was unique for each RNA and allowed multiple samples to be run on the same flow cell, and rapid attachment chemistries, which aid the attachment of sequencing adapters in the last step of library preparation. PCR mixes were incubated in the thermal cycler for 30sec at 95°C and then 14 cycles of 15 sec at 95°C to allow

denaturation, 15sec at 62°C for primers annealing, 50sec at 65°C for primer extension were performed followed by 6 min at 65°C to allow a final extension. Finally, 100fM of the double stranded cDNA library was carried over and sequencing adapters were added, which allow cDNA to reach nanopores and facilitate sequencing. Given that the Oxford Nanopore kit provides only 12 unique barcodes, our samples were divided and processed in two batches of 9 RNA each. Each library was loaded onto three different SpotOn flow cells to maximize the quantity of reads obtained and samples were then sequenced using the GridION machine (Oxford Nanopore Technologies). The sequencing lasted approximately 2.5 days and half way through the process extra libraries were loaded to increase the read depth. The software called MiniKNOW, which is installed onto the GridION, automatically performs basecalling, a process that allows the conversion of electric signals detected by the nanopores into nucleic acid base sequences. Additionally, it automatically recognises and removes sequencing adapters and it also performs demultiplexing by which unique barcodes are detected and sequencing data of each sample is saved into separate fastq files.

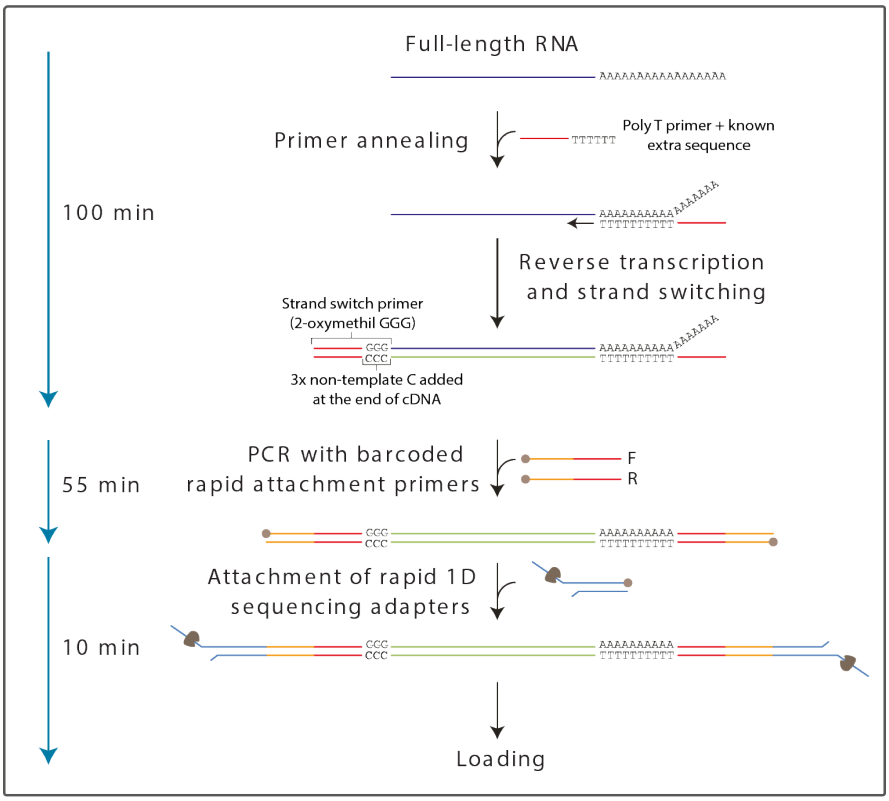

Figure 2.3: Oxford Nanopore library preparation.

Schematic representation of the Oxford Nanopore library preparation using the PCR-cDNA barcoding kit (SQK-PCB109). Figure modified from the kit protocol available from: https://community.nanoporetech.com/protocols/pcr-cdna-barcoding_sqk-pcb109/. The different steps of the library preparation are reported which are: reverse transcription, strand switching, PCR and sequencing adapter attachment.

2.2.5 cDNA sequencing data analysis

Following the generation of fastq files, data were pre-processed in order to obtain human readable gene expression profiles. Given the extremely large amount of data obtained (approximately 3 Tb of sequencing data were retrieved from all the 18 samples), the pre-processing was performed using the high performing computing clusters available within the University of Sheffield by Dr Matthew Parker, a bioinformatician from the Sheffield Bioinformatics Core. Briefly, data belonging the same sample but obtained from the three flow cells were merged to obtain a single fastq file per sample. Subsequently, the sequence reads were aligned onto the reference human genome (Hg.38) using the software minimap2 (version 2.17-r941). Lastly, counting was performed in order to calculate the number of reads present in each sample for every gene (Ensembl gene IDs). Quality control analysis was also conducted using the software MultiQC (version 1.9).

Gene-level expression data were used by myself to carry out differential expression analysis using the software package DESeq2 (version 1.30.0) in R (Love et al., 2014). In particular, three different analysis were performed:

- **HC_IL2vsG**: within the healthy control derived astrocytes, IL-2 (10nM) treated cells were contrasted to the control condition (1:1000, PBS + 5% glucose solution).

- **C9_IL2vsG**: within the astrocytes derived from ALS patient carrying a C9orf72, IL-2 (10nM) treated cells were contrasted to the control condition (1:1000, PBS + 5% glucose solution).
- **SALS_IL2vsG**: within the astrocytes derived from sporadic ALS patient, IL-2 (10nM) treated cells were contrasted to the control condition (1:1000, PBS + 5% glucose solution).

DESeq2 firstly allows to normalise data by sequencing depth (adjusting for differences in library sizes) and library composition (adjusting for transcriptional variations in different tissues or in treated/untreated samples). It utilises the median of ratios method by which original read counts are divided by a computed scaling factor for each sample. Briefly, the scaling factor is calculated as follows:

- Step 1: for every gene, calculate the geometric mean across all the samples.
- Step 2: For each gene in each sample, divide the raw counts by the geometric mean (these resulting values are also referred to as ratios).
- Step 3: calculate the median value of all the ratios (1 for each gene) for a given sample. These are the scaling factors for each sample.

Subsequently, differentially expressed genes were identified by DESeq2 using a negative binomial generalized linear model and Wald statistical tests were used for hypothesis testing. Significant differential expression was defined for genes showing p-value <0.05 and $\log_2$FC ≤ -0.58 or ≥ 0.58 (which is equal to a FC ≤ -1.5 or ≥ 1.5). Importantly, the FC cut off was increased for these analyses compared to those performed using microarray gene expression data (for which the cut off was FC =1.2). A more stringent setting was chosen because, as reported in the results chapter 5, two samples (161 and P201) generated more variable results compared to the rest of the sequenced astrocytes. Therefore, to reduce the proportion of false positive (differential expressed genes) results, this cut off was increased. Subsequently, gene enrichment and pathway analyses were carried out using different software programmes (Enrichr, REVIGO, Metascape and IPA®) as described previously in section 2.1.5.2.

2.2.6 Co-cultures of iNPC-derived astrocytes and mouse MNs

The viability of mouse MNs following culture in the presence of iNPC-derived ALS astrocytes and after treatment with IL-2 was assessed through a co-culture assay. This has been optimized by Dr Laura Ferraiuolo and her team and a complete description of the protocol is available in their published paper (Stopford et al., 2019). For information, a schematic representation of the procedure is provided in **Figure 2.4**. iNPC-derived astrocytes were produced as described in section 2.2.1. At D5 of differentiation, cells were seeded in 96-well plates (10.000 cells per well) in the presence of iAstrocyte differentiation media and were incubated for 24h at 37°C/5% CO_2 to allow cells to adhere to the plates. At D6 of differentiation, iAstrocytes were treated with IL-2-supplemented media (10nM IL-2 in iAstrocyte differentiation media containing 1% FBS) whilst negative controls were obtained by treating cells with either anhydrous DMSO (1:1000) or with PBS + 5% glucose solution (1:1000). Simultaneously, Dr Laura Ferraiuolo's team produced mouse MNs expressing green fluorescent protein (GFP) under the MN-specific promoter Hb9 (also referred to as GFP-Hb9$^+$ MN) from mouse embryonic stem cells (mESC). Briefly, mESC were seeded into a 10cm Petri dish and, in order to stimulate their differentiation to mouse embryonic bodies (mEBs), on D1 cells were cultured in the ADFNB differentiation medium (25 ml of Advanced DMEM/F12 (Gibco), 25 ml of Neurobasal Medium (Gibco), 0.5mL of 100x Pen/Strep (Gibco), 0.5mL of 200mM L-Glutamine (Gibco), 1mL of 50x NeuroBrew-21* supplement (Miltenyi), 0.5mL of 100x N-2 supplement (Gibco), 50µL of 1000x (55mM) 2-mercaptoethanol (Gibco), 1mL of 7,5% sterile BSA (Sigma)). Subsequently, from D2 to D6, mEB were media changed daily with fresh ADFNB + 2uM of retinoic acid and + 1uM of SAG. On day 7, mEB were dissociated using 100 µl of 200 U/ml papain (Sigma-Aldrich) into GFP-Hb9$^+$ MNs as per the protocol reported previously (Stopford et al., 2019). Following receipt of the cells from Dr Ferraiuolo's team, MNs (10,000 cells per well) were seeded on top of iAstrocytes. On D8, fresh ADFNB medium + BDNF (1:10,000), CNTF (1:10,000) and GDNF (1:10,000) was added to the cells and, in the wells containing IL-2-treated astrocytes, the medium was supplemented with other IL-2 (10nM). Additionally, on D9, 20µl of either PBS + 5% glucose solution or IL-2 (10nM, diluted in PBS + 5% glucose solution) was added. This was done in order to expose both astrocytes alone and astrocyte/ MNs to the cytokine.

Lastly, on D8 and D10 (also referred to as D1 and D3 following MN plating), plates were scanned using the microscope In Cell Analyzer 2000 and, given that these MNs express GFP, live-imaging was performed with the following criteria: objective = Nikon 10x; number of fields = 9 per well; wavelength = FITC; exposure = 0.5s; focus = laser autofocus at 10% power; deconvolution = enhanced ratio method, 5 cycles; plate temperature = 37 °C. Lastly, the software Columbus Image Data Storage and Analysis System was used to analyse imaging data and to quantify the number of viable MN and neurites. Details of the software settings were reported in (Stopford et al., 2019). Briefly, MNs showing at least one axon were considered as live whilst cells without visible axons were classified as dead and therefore filtered out from the analysis. Data were plotted and statistically analysed (One-way ANOVA with Tukey's correction for multiple comparisons) using GraphPad Prism 8.4.

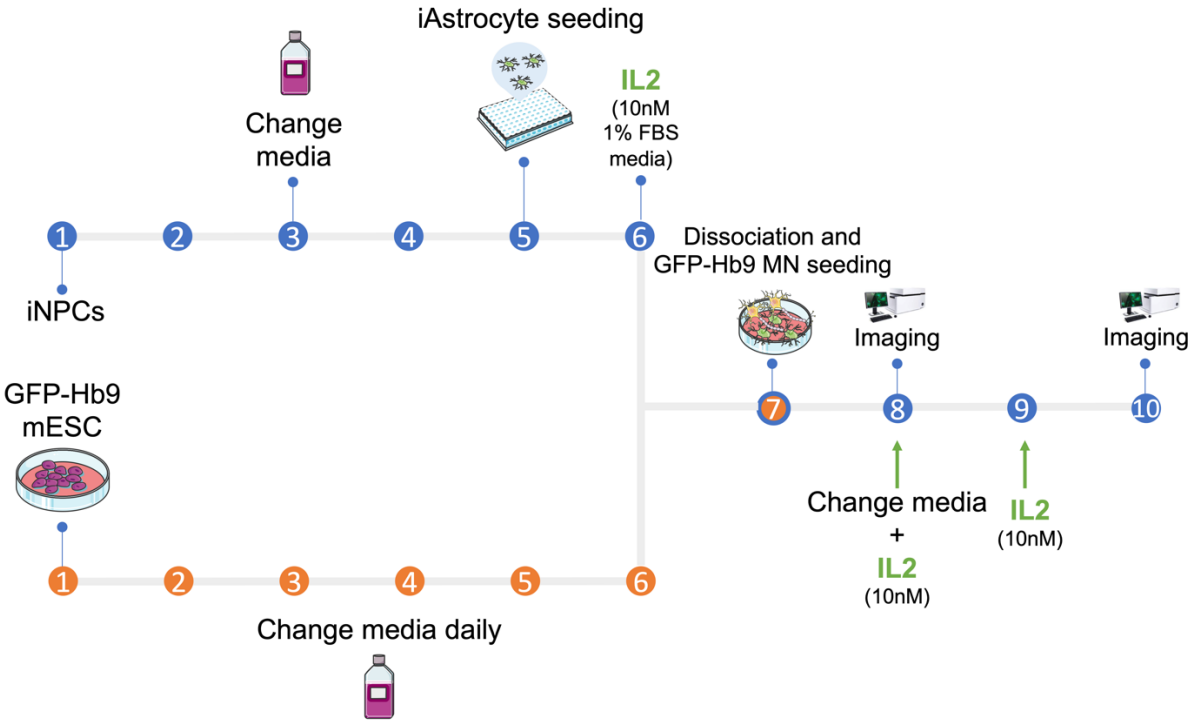

Figure 2.4: Schematic representation of the co-culture protocol.

This image summarises the co-culture protocol. From day 1 to day 6, astrocyte differentiation from iNPCs (iAstrocytes) was carried out and, simultaneously, GFP-Hb9^{+} mESC were differentiated into mEB (this is highlighted in orange as mEBs were generated by Dr Laura Ferraiuolo's team). On day 7, mEBs were dissociated, MNs were isolated and seeded on top of iAstrocytes (the blue and orange colours indicate that the dissociation was performed by Dr Laura Ferraiuolo's team whilst cells were seeded by myself). On day 8, cells were media changed and, where appropriate, they were supplemented with IL-2 (10nM). One last IL-2 treatment (10nM) was undertaken on day 9 while at day 8 and 10 the plates were imaged using the In Cell Analyzer 2000.

Chapter 3 – Results: Microarray analysis of IMODALS samples

The overall aim of the work described this chapter was to perform microarray analysis to evaluate transcriptomic changes in the white blood cells (WBCs) of patients enrolled in the IMODALS clinical trial. Several analyses were carried out in order to investigate the effect of low-dose IL-2 in the blood of ALS participants, compared to placebo, at selected time points and longitudinally throughout the trial. Some of the results reported in this chapter were published as an original article in the journal *Brain Communications* (Giovannelli et al., 2021). The full manuscript is provided as **Appendix 1**.

Gene expression profiles using Affymetrix Clariom D chips were produced at four time points: day 1 or D1 (also referred to as baseline), D8 (three days after the first injection cycle); D64 (three days after the last treatment cycle) and D85 (during the follow-up period, 24 days after the last treatment) (see **Figure 2.1**, page 61). The D1 and D85 microarrays were run by Dr Nadhim Bayatti prior to the start of my PhD, whilst D8 and D64 arrays were generated by myself. Subsequently, I performed quality control on all the arrays before any comparative analyses. Overall, gene expression profiles from a total of 107 blood samples were produced which can be classified as follows:

- 24 arrays from samples at D1: twelve placebo and twelve 2MIU IL-2.
- 23 microarrays from samples at D8: twelve placebo and eleven 2MIU IL-2. Unfortunately, the RNA sample from a treated patient (C01P011) at this time point could not be used to generate a microarray due to its very poor RNA quality.
- 36 arrays from samples at D64: twelve placebo, twelve 1MIU IL-2 and twelve 2MIU IL-2.
- 24 microarrays from samples at D85: twelve placebo and twelve 2MIU IL-2.

3.1 Summary of RNA Samples and RNA Quality Control

Total RNA was extracted from white blood cells (WBCs) by Abigail Brown and Dr Nadhim Bayatti. Prior to processing the samples ready for hybridisation to the microarrays, RNA quantity and quality were evaluated using Nanodrop ND-1000 and Agilent 2100 Bioanalyser, respectively. A summary of each patient's sample characteristics and total RNA quantity and quality parameters is provided in **Table 3.1**. Importantly, in order to process samples in an unbiased way, patient IDs and treatment information were blinded to the researches while extracting RNA and producing the microarrays. For this reason, a code was assigned to each sample which is also reported in **Table 3.1**. Overall, good quality RNA was obtained with acceptable concentrations (average= 122.8 ng/ul), 260:280 ratios (average= 2.14) and RIN values (average= 7.85). Importantly, the mean value of the RINs suggested that the extracted RNA was of high integrity. Despite some having lower RIN scores, microarrays were successfully generated from all the samples except for 68WKU83 from patient C01P011, whose RNA failed QC (concentration= 124.55 and RIN= n/a which suggested that RNA was degraded and therefore the Bioanalyser could not compute the RIN).

Table 3.1: IMODALS RNA samples' characteristic

In this table, RNA concentration (ng/ul), 260:280 ratio and RIN values are reported for each total RNA sample extracted from the WBCs of the IMODALS patients. Moreover, patient IDs are assigned together with their sample ID, time point of blood collection and treatment regimen.

Patient code	Sample ID	Time point	Treatment type	RNA concentration (ng/ul)	260/280 ratio	RIN value
C01P001	23MXS57	**64**	**1MIU IL-2**	91.75	2.17	7.4
C01P002	16NM22	**1**	**Placebo**	121.61	2.17	8.9
C01P002	83QCF22	**8**	**Placebo**	114.86	2.15	8.9
C01P002	34CJU23	**64**	**Placebo**	131.4	2.14	9.1
C01P002	44FGS45	**85**	**Placebo**	125.88	2.16	9
C01P003	17MA49	**1**	**2MIU IL-2**	156.19	2.1	8.6
C01P003	72WPD58	**8**	**2MIU IL-2**	219.62	2.09	4.9
C01P003	38QCW65	**64**	**2MIU IL-2**	307.03	2.12	7.8
C01P003	99WQZ38	**85**	**2MIU IL-2**	144.87	2.14	8.1
C01P004	92XZK83	**1**	**2MIU IL-2**	215.14	2.12	8.7
C01P004	29DXU82	**8**	**2MIU IL-2**	132.92	2.11	2.8
C01P004	56JIT63	**64**	**2MIU IL-2**	163.27	2.12	7.4
C01P004	57KHM43	**85**	**2MIU IL-2**	168.86	2.13	8.8
C01P005	83VXX85	**64**	**1MIU IL-2**	176.32	2.12	7.8
C01P006	92QND85	**1**	**Placebo**	71.75	2.1	8
C01P006	56UWH39	**8**	**Placebo**	84.57	2.19	8.7
C01P006	96OKC39	**64**	**Placebo**	98.31	2.14	8.9
C01P006	96GFO65	**85**	**Placebo**	108.3	2.13	9.1
C01P007	98NFA86	**1**	**Placebo**	142.74	2.17	3.4
C01P007	92NTM59	**8**	**Placebo**	94.81	2.13	8.7
C01P007	57TOS36	**64**	**Placebo**	43.15	2.11	2.6
C01P007	36VVR32	**85**	**Placebo**	92.84	2.15	9.4
C01P008	26UIR45	**64**	**1MIU IL-2**	105.79	2.2	7.7
C01P009	66ADE25	**1**	**2MIU IL-2**	131.95	2.16	9.3
C01P009	44AZD87	**8**	**2MIU IL-2**	152.16	2.1	8.4

C01P009	55WDE55	**64**	**2MIU IL-2**	248.48	2.14	7.4
C01P009	22DSY33	**85**	**2MIU IL-2**	140.65	2.18	8.6
C01P010	47AVU82	**64**	**1MIU IL-2**	152.11	2.14	7.8
C01P011	72YOV58	**1**	**2MIU IL-2**	60.12	2.01	6.6
C01P011	68WKU83	**8**	**2MIU IL-2**	124.55	2.17	n/a
C01P011	95HNE98	**64**	**2MIU IL-2**	161.96	2.08	7.8
C01P011	47NSH95	**85**	**2MIU IL-2**	11.09	2.19	1.9
C01P012	95TBM69	**1**	**Placebo**	92.06	2.13	5.9
C01P012	24TTF82	**8**	**Placebo**	108.06	2.15	8.4
C01P012	76UCI87	**64**	**Placebo**	109.46	2.15	8.2
C01P012	44PBR28	**85**	**Placebo**	90.21	2.04	8
C01P013	75UQO22	**64**	**1MIU IL-2**	103.26	2.14	9.1
C01P014	75ABF54	**1**	**Placebo**	66.08	2.09	6.5
C01P014	89ERK87	**8**	**Placebo**	132.36	2.1	9.1
C01P014	98DAD98	**64**	**Placebo**	131	2.17	7.5
C01P014	72EBF68	**85**	**Placebo**	103.79	2.09	8.3
C01P016	33DGN54	**1**	**2MIU IL-2**	142.04	2.14	9.4
C01P016	53WYU63	**8**	**2MIU IL-2**	116.14	2.15	8.1
C01P016	23KVR46	**64**	**2MIU IL-2**	177.05	2.12	9.2
C01P016	24WMJ33	**85**	**2MIU IL-2**	75.67	2.14	6.8
C01P017	23BDT37	**1**	**Placebo**	110.05	2.13	9.2
C01P017	94GRV28	**8**	**Placebo**	115.48	2.17	8.6
C01P017	87FSD36	**64**	**Placebo**	131.23	2.16	8.3
C01P017	94RYH63	**85**	**Placebo**	26.54	2.14	8.2
C01P018	44JRQ89	**1**	**2MIU IL-2**	198.64	2.08	8.5
C01P018	48ZSZ47	**8**	**2MIU IL-2**	127.72	2.14	9.1
C01P018	93GXQ33	**64**	**2MIU IL-2**	73.45	2.19	n/a
C01P018	35PXK56	**85**	**2MIU IL-2**	144.99	2.02	8.6
C01P020	83QAN59	**64**	**1MIU IL-2**	146.71	2.03	n/a
C01P021	54HYO55	**1**	**2MIU IL-2**	71.05	2.1	7.6
C01P021	54SIW45	**8**	**2MIU IL-2**	248.88	2.1	8.4
C01P021	36UVF76	**64**	**2MIU IL-2**	154.78	2.15	5.5
C01P021	73XJQ42	**85**	**2MIU IL-2**	79.38	2.2	6
C01P022	66TDV96	**1**	**Placebo**	184.33	2.08	5

C01P022	48CFV44	**8**	**Placebo**	142.85	2.17	8.9
C01P022	33UVN85	**64**	**Placebo**	178.57	2.12	8.5
C01P022	63VCW65	**85**	**Placebo**	94.13	2.17	8.4
C01P023	67CNF42	**64**	**1MIU IL-2**	85.27	2.21	9.5
C01P024	87VON76	**64**	**1MIU IL-2**	167.4	2.14	7.6
C01P025	34SBH78	**1**	**Placebo**	119.98	2.07	8.3
C01P025	37TMZ28	**8**	**Placebo**	109.98	2.15	9.3
C01P025	48BFT76	**64**	**Placebo**	160.29	2.16	9
C01P025	49KHX86	**85**	**Placebo**	133.18	2.08	5.9
C01P026	78TJC44	**1**	**2MIU IL-2**	118	2.11	8.7
C01P026	88NWQ96	**8**	**2MIU IL-2**	140.98	2.19	8.5
C01P026	29DUQ88	**64**	**2MIU IL-2**	147.52	2.08	8.6
C01P026	97MAY94	**85**	**2MIU IL-2**	64.87	2.15	8.6
C01P027	87RXK32	**64**	**1MIU IL-2**	131.11	2.1	8.6
C01P028	38TPQ86	**1**	**2MIU IL-2**	145.97	2.31	7.5
C01P028	45XVK33	**8**	**2MIU IL-2**	195.63	2.16	8.7
C01P028	82AII97	**64**	**2MIU IL-2**	145.74	2.15	8.3
C01P028	59ZAQ99	**85**	**2MIU IL-2**	134.25	2.09	6.1
C01P030	79OHS63	**1**	**Placebo**	101.96	2.11	8.4
C01P030	28TBF72	**8**	**Placebo**	20.7	2.27	6.1
C01P030	85ORI83	**64**	**Placebo**	99.11	2.22	8.9
C01P030	63ORT67	**85**	**Placebo**	41.5	2.23	6.2
C01P031	47XAT27	**1**	**Placebo**	62.36	2.13	5.4
C01P031	28BMD36	**8**	**Placebo**	140.82	2.15	8.7
C01P031	77WZO64	**64**	**Placebo**	106.37	2.22	8.9
C01P031	45XNH76	**85**	**Placebo**	115.98	2.12	8.7
C01P032	29ZCQ57	**1**	**2MIU IL-2**	155.53	2.14	8.3
C01P032	96HQV85	**8**	**2MIU IL-2**	210.36	2.14	8.4
C01P032	46DHR29	**64**	**2MIU IL-2**	167.47	2.18	9.3
C01P032	35NXS97	**85**	**2MIU IL-2**	94.79	2.08	6.9
C01P033	46XDM67	**64**	**1MIU IL-2**	95.83	2.23	8.7
C01P034	55MKH26	**1**	**Placebo**	24.82	2.08	7.6
C01P034	88TWF48	**8**	**Placebo**	100.47	2.11	8.1
C01P034	76ABW86	**64**	**Placebo**	95.82	2.19	8.7

C01P034	77PVZ38	**85**	**Placebo**	80.29	2.03	7.6
C01P035	77NSV37	**64**	**1MIU IL-2**	167.24	2.17	9
C01P036	88FRZ35	**1**	**2MIU IL-2**	111.43	2.11	9.2
C01P036	24ZOV85	**8**	**2MIU IL-2**	191.58	2.06	5.1
C01P036	23TKJ93	**64**	**2MIU IL-2**	150.46	2.17	9
C01P036	83VZK65	**85**	**2MIU IL-2**	25.68	2.25	5.5
C01P037	37QNW23	**1**	**2MIU IL-2**	107.08	2.23	7.9
C01P037	25SJK94	**8**	**2MIU IL-2**	145.54	2.14	8.4
C01P037	98HXI86	**64**	**2MIU IL-2**	125.85	2.15	8.4
C01P037	53HHI65	**85**	**2MIU IL-2**	64.42	2.14	8.2
C01P038	87NSF26	**64**	**1MIU IL-2**	115.78	2.26	8.4
C01P039	46XWM36	**1**	**Placebo**	121.6	2.15	8.6
C01P039	44IKD34	**8**	**Placebo**	125.52	2.19	8.6
C01P039	33IEV23	**64**	**Placebo**	80.49	2.17	8.2
C01P039	53UCM47	**85**	**Placebo**	46.77	2.09	6.2

3.2 Microarray Quality Control

In order to ascertain data quality, once gene expression profiles were generated and prior to any comparative analyses, quality control (QC) was performed using the Expression Console (Affymetrix) software. Several QC metrics were evaluated:

- **Positive vs negative area under the curve (AUC).** The AUC or the area under a receiver operator curve (ROC), was computed for each array. Typically, an AUC threshold is set to 0.7. Given that all our microarrays showed values greater than 0.8, they all passed this QC metric (**Figure 3.1**).

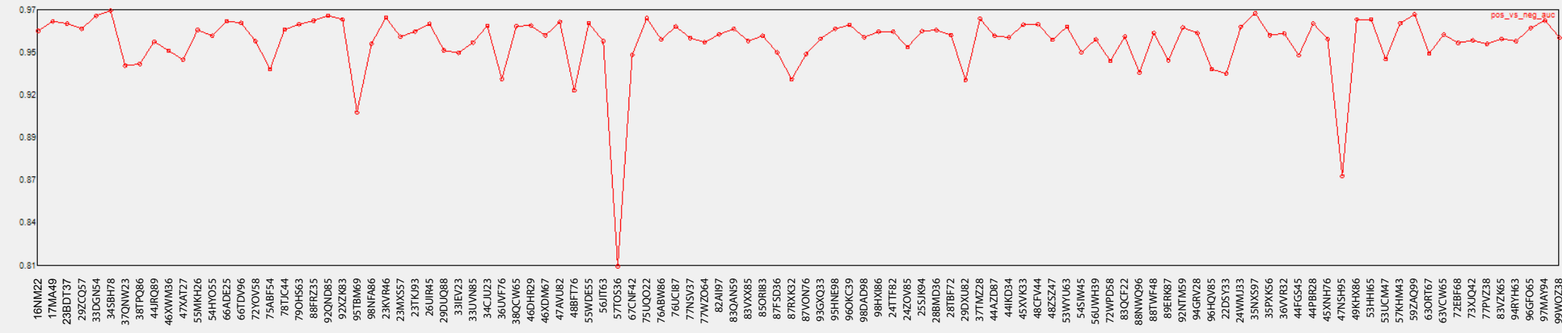

Figure 3.1: Microarray Positive vs Negative AUC.

In this graph, AUC value computed for each of the IMODALS sample microarrays is displayed. This is one of the metrics used to assess the quality of the generated gene expression profiles and, generally, a threshold of 0.7 is accepted to consider samples as having passed this QC metrics. All the microarrays show an AUC>0.8 and therefore passed this metric. X-axis: array ID; Y-axis: AUC value.

- **Spike or hybridization control.** 20x Eukaryotic Hybridization Controls (AFFX-r2-Ec-BioB, AFFX-r2-Ec-BioC, AFFX-r2-Ec-BioD, AFFX-r2-P1-Cre) were included in the hybridization cocktails at staggered relative concentrations (BioB < BioC < BioD < Cre). Our results were in line with this signal pattern which suggested that all the arrays passed the hybridization quality control (**Figure 3.2**).

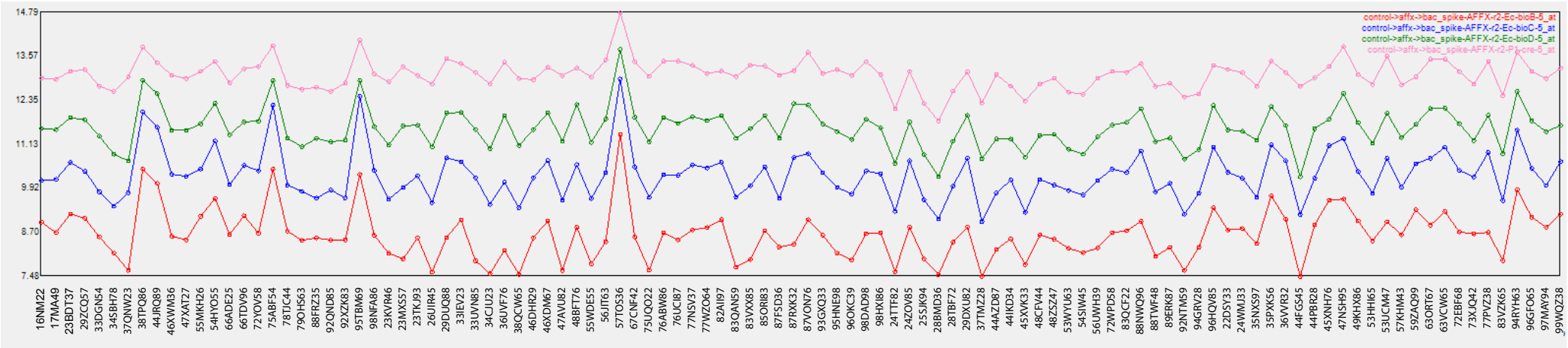

Figure 3.2: Microarray Eukaryotic Hybridization Controls.

Signal intensities of four eukaryotic hybridization controls (BioB is displayed in red, BioC in blue, BioD in green and cre in pink) are reported in this plot. All the arrays show the expected BioB < BioC < BioD < cre signal pattern. X-axis: array ID; Y-axis: signal intensity.

- **Labelling control.** The quality of the labelling process was inspected through the addition of the poly-A RNA controls. These were mixed at fixed and increasing concentrations (Lys= 1:100.000; Phe= 1:50.000; Thr= 1:25.000; Dap= 1:6.667) and processed alongside the RNA extracted from patient samples. As expected, the signal Lys < Phe < Thr < Dap was visible for the majority of the microarrays suggesting a satisfactory labelling process. However, some small variations were visible in a reduced number of arrays (e.g. 23TKJ93, 46DHR29 or 46XDM67) (**Figure 3.3**). Nonetheless, given that Lys (the lowest concentrated control from which the levels are close to the detection limit of the arrays) was visible in all samples and that the other QC metrics were encouraging, the entire set of microarrays were included in the subsequent gene expression analyses.

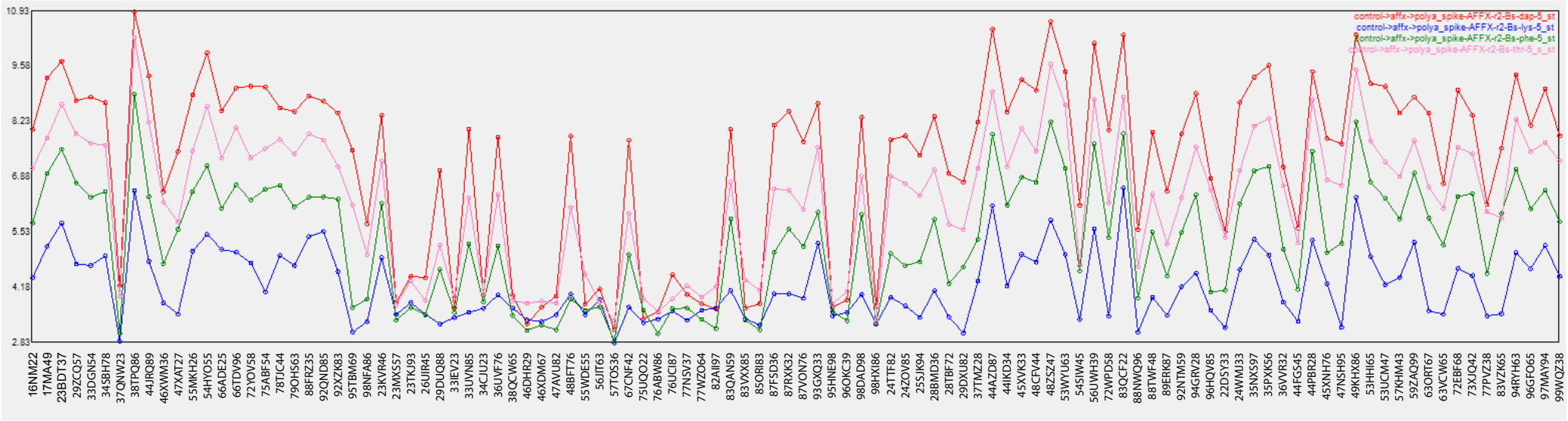

Figure 3.3: Microarray Labelling Controls.

This graph shown signal intensities of exogenous *B. subtilis* gene probes included in the microarrays as labelling controls. Four controls are visible (Lys displayed in blue, Phe in green, Thr in pink and Dap in red) for each microarray. X-axis: array ID, y-axis: signal intensities. Most of the arrays show the expected Lys < Phe < Thr < Dap signal pattern.

- **Signal intensity histogram and relative signal box plot.** Although not strictly considered as QC metrics, these are useful tools to inspect for potential outliers. Histograms displaying the distribution of microarray signals were generated and all the curves showed a homogeneous and similar pattern suggesting that no microarray had a substantially different intensity distribution (**Figure 3.4A**). A relative signal box plot was also generated (**Figure 3.4B**). Each transcript probe signal in one array is divided by the median probe signal across all the arrays in the study and the distribution of the ratios of all the probes is displayed in a box plot. If comparable, each array's distribution should lie on a reference red line, while outliers would detectably deviate. In this case, microarrays did not appear to have a substantially divergent signal distribution. The array 57TOS36 was the only one to show a slightly different distribution, however, it was still positioned on the reference line. Taken together, these results indicated that no clear outlier was identified.

A)

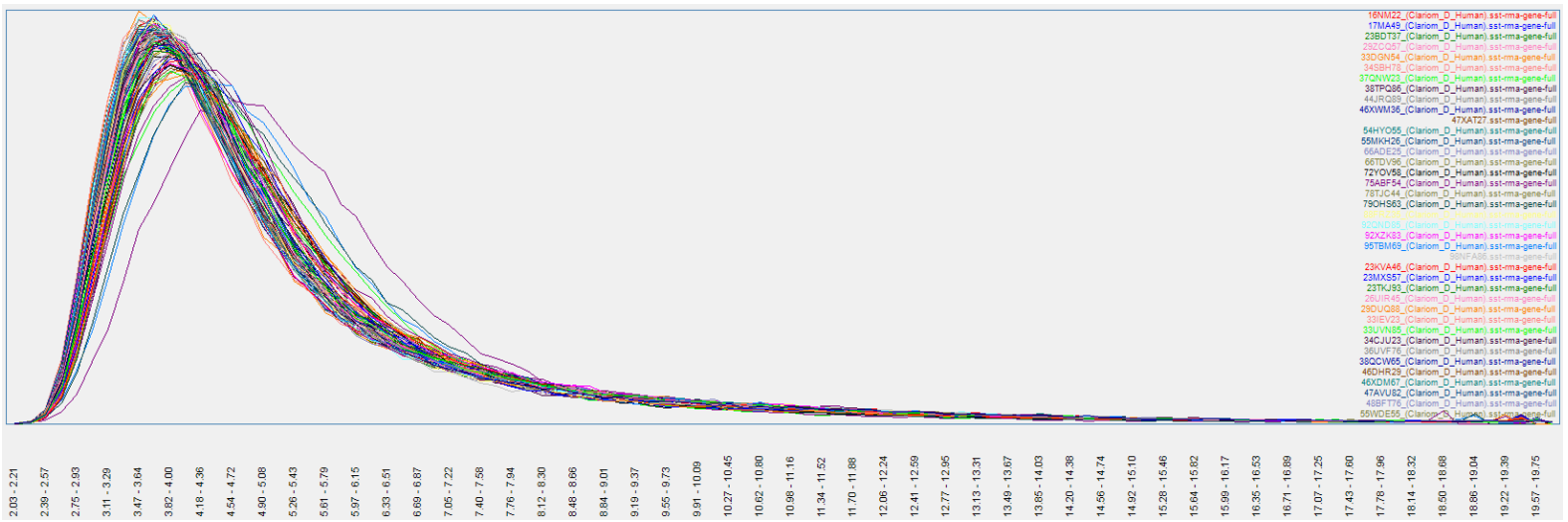

B)

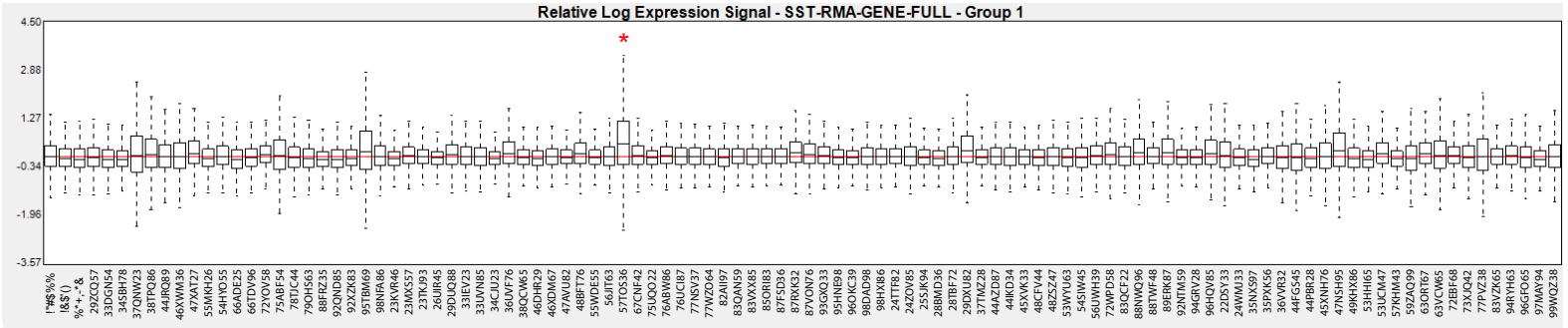

Figure 3.4: Microarray Signal Intensity Histograms and Relative Signal Box Plots.

(A) Histogram showing signal intensity microarray curves. Each microarray is displayed using a different colour. No evident distribution differences amongst arrays are reported. (B) Relative signal box blot shows signal distribution of each produced microarray. Each array name is reported on X-axis and a red reference line is also displayed. Sample 57TOS36 is marked with a red asterisk.

3.3 Differential expression and dose-dependency at D64

The first aim of this section of the study was to establish patient transcriptional response to ld-IL-2 following the three administration cycles when the drug effect was hypothesised to have reached a peak. Moreover, to assess whether there was a dose-dependency in this response, the gene expression profiles from patients treated with 1MIU and 2MIU-IL2 were compared to those on placebo at D64.

Firstly, D64 gene expression profiles were evaluated through a principal component analysis (PCA). This technique performs dimensionality reduction allowing easier interpretation of large datasets whilst minimizing information loss. PCA uses orthogonal linear transformation to transform the data into a new set of variables or principal components (PCs). The first PC is generated as a linear combination of the original variables so that it explains most of the variance within the dataset. The remaining variation is accounted for by the second and subsequent PCs. Principal components can be used to create a coordinate system where data points are reported and can be visually inspected. Spatial separation indicates data being substantially different from each other while closely displayed points suggest similarities. A multigroup comparison (p-value<0.05) was performed using the software Qlucore Omics Explorer (Qlucore) and a three component PCA was generated (**Figure 3.5**). Three groups were clearly visible. This spatial separation suggested that the gene expression of the placebo patients was significantly different from the profile of treated participants. Importantly, the reported distance between 1MIU and 2MIU-IL-2 groups indicated transcriptomic dissimilarities amongst the two different dosages. The sample 57TOS36 seemed to be slightly more distanced from the rest of the placebo group arrays. Interestingly, this sample showed also a moderately different distribution in the relative signal box plot (**Figure 3.4B**) and it was also amongst the samples showing the lowest RNA quality and quantity (**Table 3.1**). However, as previously discussed, 57TOS36 was not considered as an outlier, and thus was not excluded from the analysis.

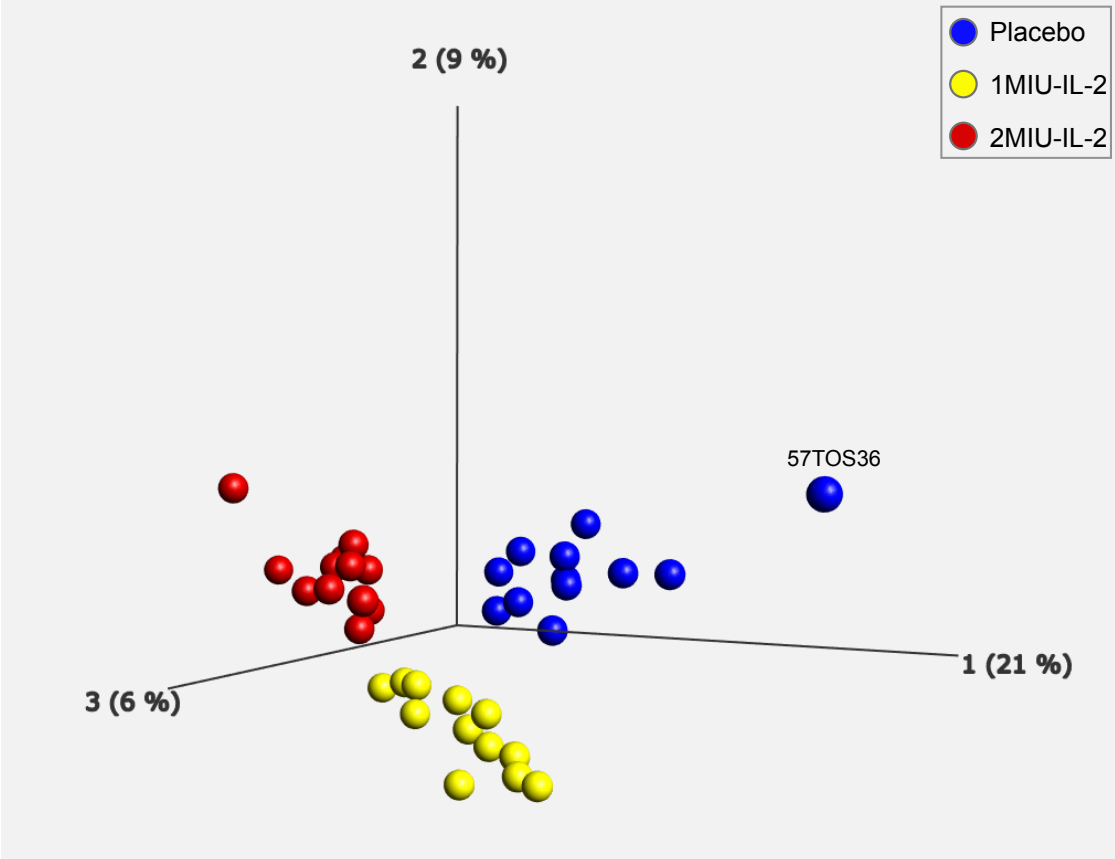

Figure 3.5: Principal Component Analysis of D64 Microarrays.

Cartesian plane displaying the first three principal components identified through a multigroup comparison performed with the software Qlucore. Spatial separation of the three treatment groups (Placebo in blue, 1MIU-IL-2 in yellow and 2MIU-IL-2 in red) is visible. X-axis: first PC (accounting for 21% of the variance), Y-axis: second PC (9% of the variance), Z-axis: third PC (6% of the variance).

To identify differentially expressed genes (DEGs) characteristic of each participant group at the end of the last treatment cycle (D64), two comparative analyses were carried out using the TAC software. Microarrays from 1MIU-treated patients were compared to placebo (1MIU_vs_Placebo) and, similarly, 2MIU-treated and placebo (2MIU_vs_Placebo) were compared. Using arbitrary cut offs ($1.2 \leq FC \leq -1.2$ and p-value <0.05), 3873 transcripts were identified as significantly differentially expressed (2097 decreased, 1776 increased) in 1MIU_vs_Placebo whilst 6352 (3530 decreased,

2822 increased) were retrieved from 2MIU_vs_Placebo comparison. Of importance, 1160 transcripts were commonly differentially expressed (**Figure 3.6**). More stringent p-value cut offs reduced the number of DEGs (though, 1.2 ≤ FC ≤ -1.2 cut off was always applied) (**Table 3.2**). Interestingly, regardless of the settings used, the comparison 2MIU_vs_Placebo showed a considerably greater number of DEGs compared to 1MIU_vs_Placebo. Although there is still no consensus on the ideal cut off for gene expression analysis, evidence in the literature suggests that different criteria influence data interpretation (Dalman et al., 2012). This needs to be cautiously balanced as a more stringent setting (e.g. using tight thresholds for false discovery rate, also referred to as FDR) reduces the number of false positive results but this also leads to an unacceptably high level of false negative results. This would mean that a potentially large proportion of truly differentially expressed genes would not be identified. For this reason, it has been previously proposed in the literature to combine significance level with fold change cut offs to obtain more reliable data by increasing the number of detectable DEGs whilst not exceeding in the number of false positive results (Park and Mori, 2010). Therefore, a decision was made to set as thresholds: 1.2 ≤ FC ≤ -1.2 and p-value< 0.05 for further analyses. Notably, these settings have been previously used in our Department and the obtained results were published in peer-reviewed journals (including: (Fadul et al., 2020, Ratcliffe et al., 2018, Bury et al., 2021).

Table 3.2. The effect of different p-value cut-offs on the numbers of DEGs

In this table a summary of the DEGs retrieved using different significance level criteria is provided. More stringent settings drastically reduces the number of identified DEGs. Nonetheless, regardless of the criterion used, a considerably greater number of DEGs was identified in the comparison 2MIU_vs_Placebo compared to 1MIU_vs_Placebo. Notably, in all the cases the FC cut offs was always applied. Full lists of DEGs from the two comparisons are provided in **Appendix 2** and **3**.

Comparison	P value<0.05	P value<0.01	FDR<0.2	FDR<0.05
1MIU_vs_Placebo	3873	802	1	0
2MIU_vs_Placebo	6352	1790	125	19

To investigate the biological functions associated with the reported DEGs, lists of genes were imported into Enrichr to perform gene ontology (GO) analyses, focusing on Biological Process (BP). Redundant GO BP terms were summarised and clustered using the software REVIGO. Importantly, only transcripts which were RefSeq annotated (and met the criteria: $1.2 \leq FC \leq -1.2$ and p-value <0.05) were included in such analyses. In fact, as previously discussed in Chapter 2 (section 1.5.2), Affymetrix microarrays contain probes for a vast amount of unannotated, putative and uncharacterized transcripts. Therefore, given that their functions are unknown, they are not included in any of the gene set libraries included in Enrichr and therefore this considerably impacts on the statistical power of the GO analysis. 760 RefSeq-annotated DEGs were found in the 1MIU_vs Placebo, 1764 in 2MIU_vs Placebo comparison and 375 were commonly differentially expressed in both.

GO analysis of the unique list of DEGs characteristic of 1MIU_vs_Placebo highlighted sixty-two significantly enriched biological processes (BPs) which were summarised in 27 functional clusters using the software REVIGO (**Figure 3.6** and **Figure 3.7A**). Changes in the expression of genes involved in the metabolism and transport of cholesterol and phospholipids were identified in this comparison, together with variation in nucleoside catabolism. Only a few transcriptional variations in immune-related biological processes (such as regulation of T cell differentiation and regulation

of leukocyte activation and adhesion) were reported in 1MIU_vs_Placebo (**Figure 3.6** and **Figure 3.7A**).

In contrast, transcripts exclusively differentially expressed in 2MIU_vs_Placebo comparison were enriched in 129 GO BPs and 35 REVIGO clusters. Importantly, more evidence of immune-modulation was provided in the 2MIU_vs_Placebo gene lists compared to the 1MIU one (**Figure 3.6** and **Figure 3.7B**). In particular, alterations in genes involved in B, T cell and antigen receptor signalling pathways, in the regulation of T cell and granulocyte differentiation and in innate immunity were reported. Moreover, enrichment of cell cycle regulation processes, intra-cellular transport and RNA metabolism was documented.

The import in Enrichr of the RefSeq list containing commonly DE transcripts in both comparisons resulted in 138 GO BPs being significantly enriched which were summarised in 26 clusters by REVIGO. Interestingly, the large majority of these clusters and processes were involved in immune modulation. In fact, differential expression of genes involved in the regulation of activation and differentiation of T cell types, including Treg, and B cells was evident. Moreover, an extensive modulation of different cytokines (such as IL-4, 10, 12, 15 and 17) production, secretion and signalling pathways was also observed (**Figure 3.6** and **Figure 3.7C**). Interestingly, amongst the enriched non-immunological processes, alterations (upregulation) in ganglioside, ceramide and lipid metabolism and in membrane raft distribution and polarization were identified. These mechanisms, especially ganglioside biosynthesis, have been implicated in the pathogenesis of ALS (Moll et al., 2020) and thus their IL-2-mediated modulation may contribute to a neuroprotective drug effects on patients.

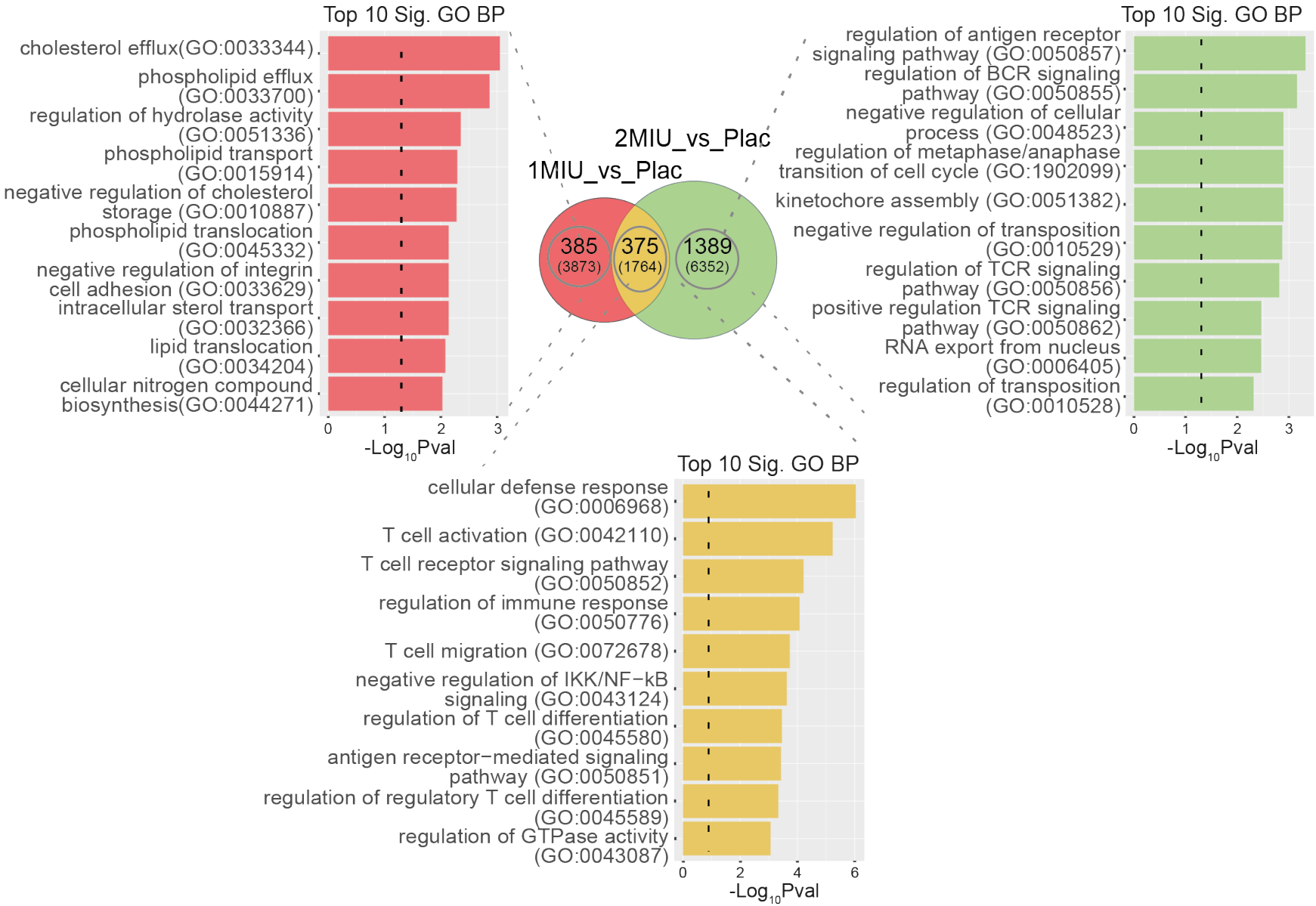
Top 10 Sig. GO BP
cholesterol efflux(GO:0033344)
phospholipid efflux (GO:0033700)
regulation of hydrolase activity (GO:0051336)
phospholipid transport (GO:0015914)
negative regulation of cholesterol storage (GO:0010887)
phospholipid translocation (GO:0045332)
negative regulation of integrin cell adhesion (GO:0033629)
intracellular sterol transport (GO:0032366)
lipid translocation (GO:0034204)
cellular nitrogen compound biosynthesis(GO:0044271)
0 1 2 3
-Log10Pval
2MIU_vs_Plac
1MIU_vs_Plac
385 (3873)
375 (1764)
1389 (6352)
Top 10 Sig. GO BP
regulation of antigen receptor signaling pathway (GO:0050857)
regulation of BCR signaling pathway (GO:0050855)
negative regulation of cellular process (GO:0048523)
regulation of metaphase/anaphase transition of cell cycle (GO:1902099)
kinetochore assembly (GO:0051382)
negative regulation of transposition (GO:0010529)
regulation of TCR signaling pathway (GO:0050856)
positive regulation TCR signaling pathway (GO:0050862)
RNA export from nucleus (GO:0006405)
regulation of transposition (GO:0010528)
0 1 2 3
-Log10Pval
Top 10 Sig. GO BP
cellular defense response (GO:0006968)
T cell activation (GO:0042110)
T cell receptor signaling pathway (GO:0050852)
regulation of immune response (GO:0050776)
T cell migration (GO:0072678)
negative regulation of IKK/NF−kB signaling (GO:0043124)
regulation of T cell differentiation (GO:0045580)
antigen receptor−mediated signaling pathway (GO:0050851)
regulation of regulatory T cell differentiation (GO:0045589)
regulation of GTPase activity (GO:0043087)
0 2 4 6
-Log10Pval

Figure 3.6: Differential expression analyses at D64.

Venn diagram showing significant (1.2 ≤ FC ≤ -1.2 and p-value <0.05, F-test) differentially expressed genes (DEGs) from either 1MIU_vs_Placebo (in red) or 2MIU_vs_Placebo (in green) TAC (Transcriptome analysis console) comparisons. All altered transcripts are reported in brackets while RefSeq annotated transcripts are shown in bold. Overlapping common DEGs are also shown in yellow. For each RefSeq transcript list shown in the Venn diagram, the top 10 significant enriched Gene Ontology (GO) biological processes are shown in a bar plot. X axis: $-Log_{10}$ (enrichment p-value); y axis: GO term.

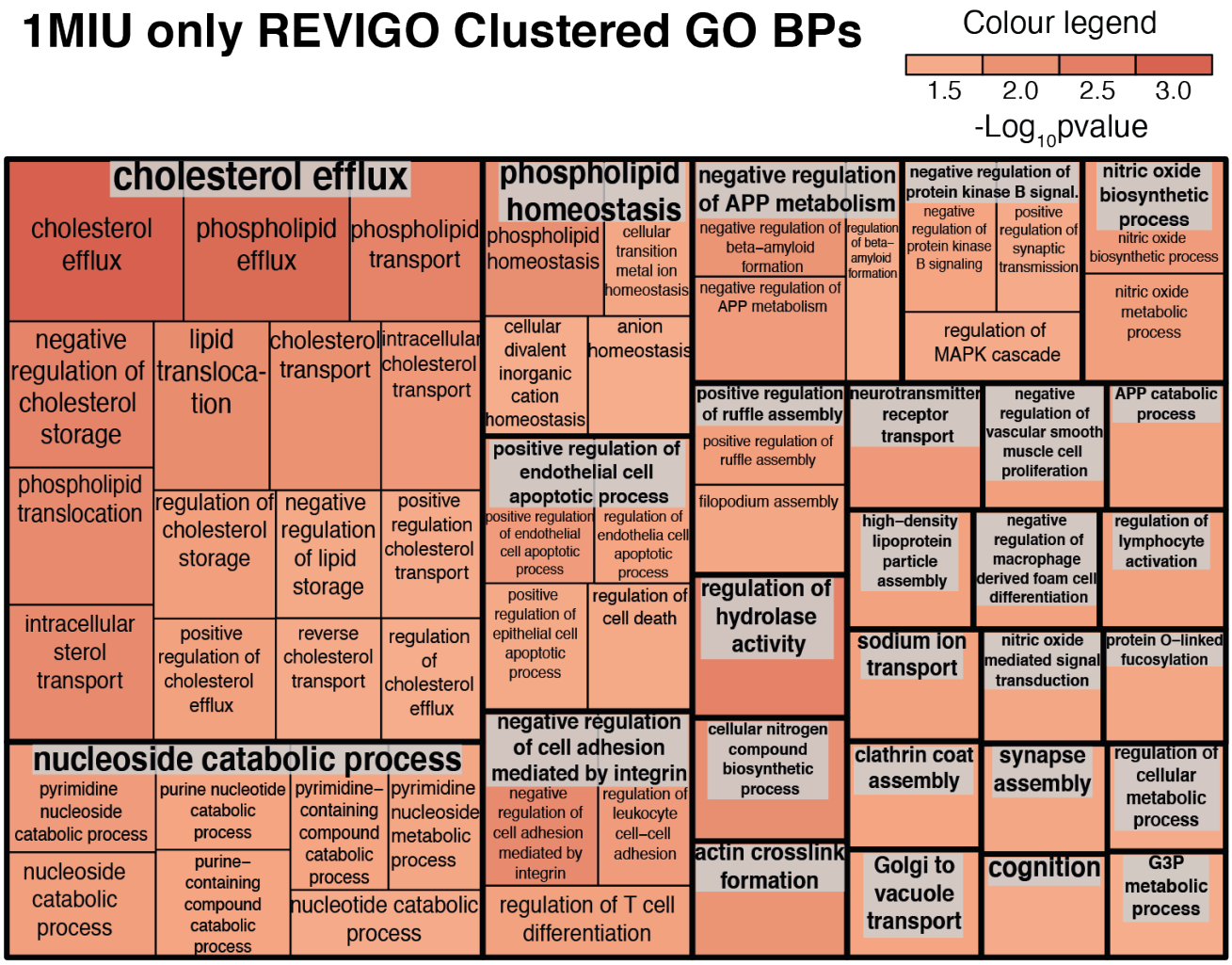

Figure 3.7A: REVIGO-clustered Enriched GO Biological Processes from the Comparison 1MIU_vs_Placebo.

Treemap showing REVIGO clustered Gene Ontology biological processes (GO BPs) obtained from the unique list of differentially expressed genes characteristic of 1MIU_vs_Placebo. GO BP terms belonging to the same REVIGO cluster are grouped and displayed in the same rectangle and cluster representatives are reported with grey tags. GO BP terms are sized and colour-coded depending on their significance levels (-Log10pvalue).

2MIU only REVIGO Clustered GO BPs

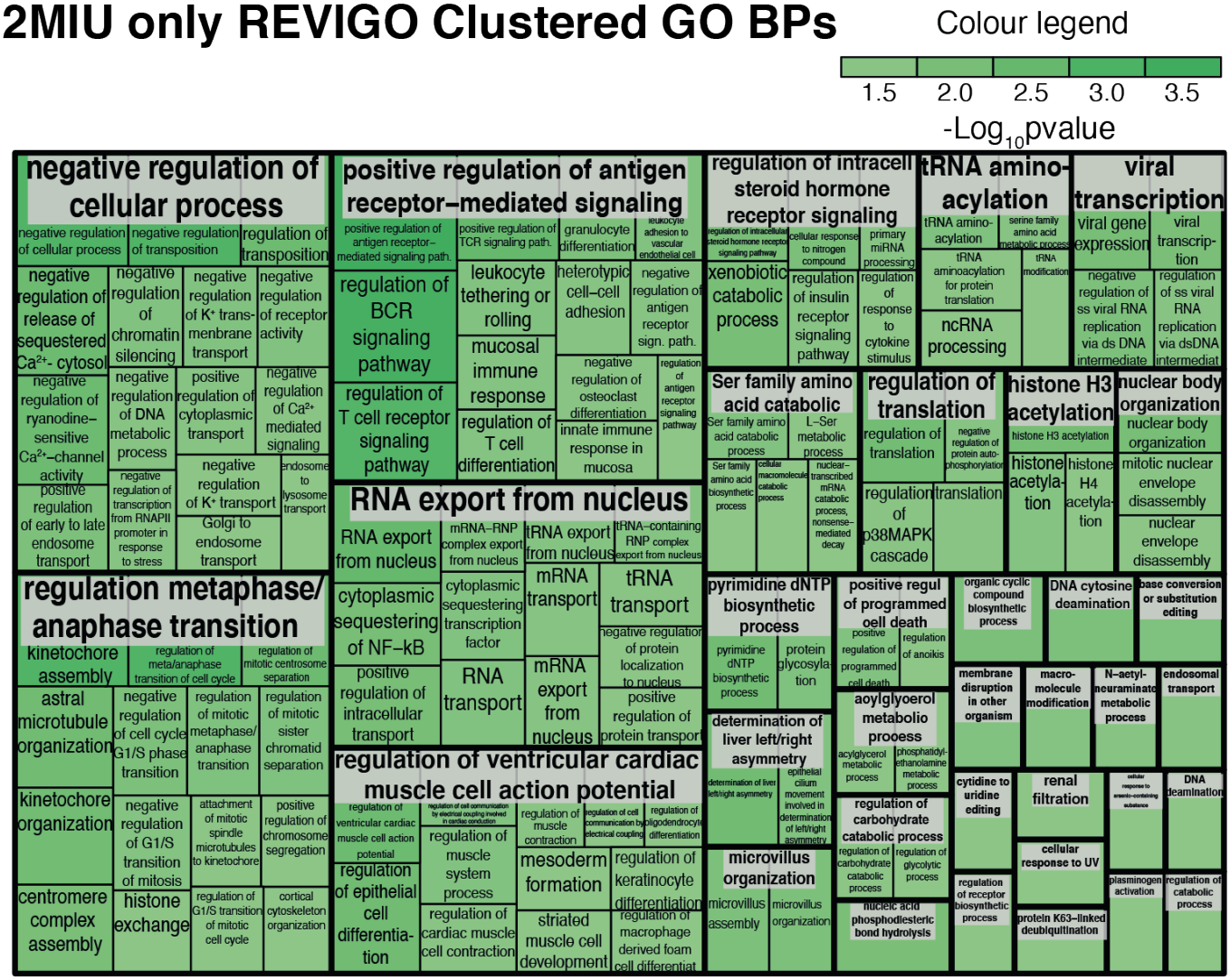

Figure 3.7B: REVIGO-clustered Enriched GO Biological Processes from the Comparison 2MIU_vs_Placebo.

Treemap showing REVIGO clustered Gene Ontology biological processes (GO BPs) obtained from the unique list of differentially expressed genes characteristic of 2MIU_vs_Placebo. GO BP terms belonging to the same REVIGO cluster are grouped and displayed in the same rectangle and cluster representatives are reported with grey tags. GO BP terms are sized and colour-coded depending on their significance levels (-Log10pvalue).

Common DEGs
REVIGO Clustered GO BPs

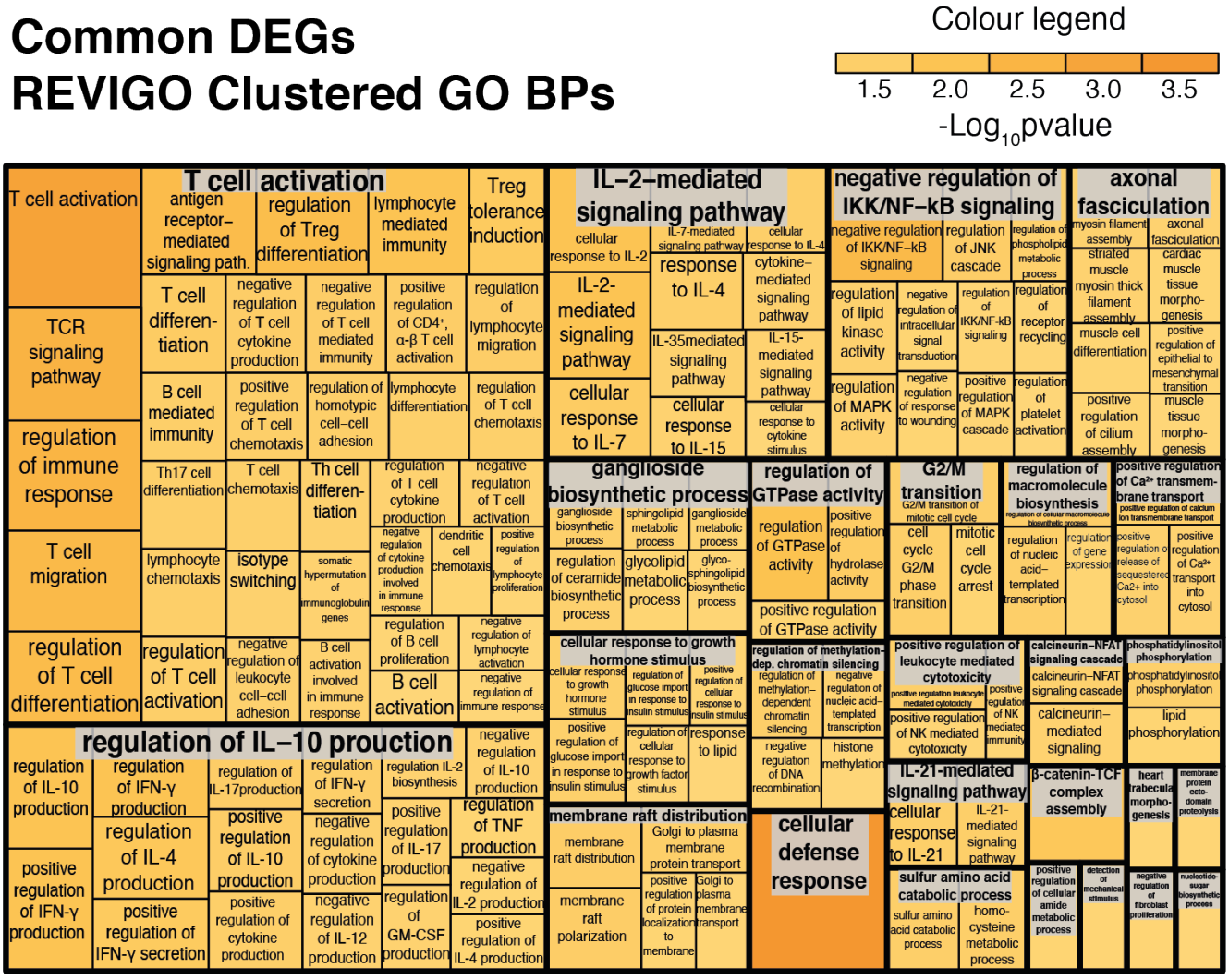

Figure 3.7C: REVIGO-clustered Enriched GO Biological Processes of the DEGs in Common Between the 1MIU and the 2MIU treatment groups.

Treemap showing REVIGO clustered Gene Ontology biological processes (GO BPs) obtained from the list of commonly DEGs in both comparisons. GO BP terms belonging to the same REVIGO cluster are grouped and displayed in the same rectangle and cluster representatives are reported with grey tags. GO BP terms are sized and colour-coded depending on their significance levels (-Log10pvalue).

Subsequently, to further analyse data from 1MIU_vs_Placebo and 2MIU_vs_Placebo, significant ($1.2 \leq FC \leq -1.2$ and p-value <0.05) RefSeq-annotated DEGs from both comparisons were inputted into Metascape. In particular, the two lists were analysed simultaneously to visualise differences and similarities in altered mechanisms. A heatmap and an enrichment network were generated. Interestingly, immune regulatory processes were significantly altered in both comparison lists (**Figure 3.8**). These included terms such as: "RUNX1 and FOXP3 control the development of regulatory T lymphocytes", "Immunoregulatory interaction between lymphoid and non-lymphoid cell", "negative regulation of immune system process" and "PID IL2 STAT5 signaling pathway"; which suggested an activation of Treg and regulatory processes following ld-IL-2 administration. However, other immunological pathways, including "regulation of antigen receptor-mediated signaling pathway", were uniquely altered in the 2MIU_vs_Placebo list.

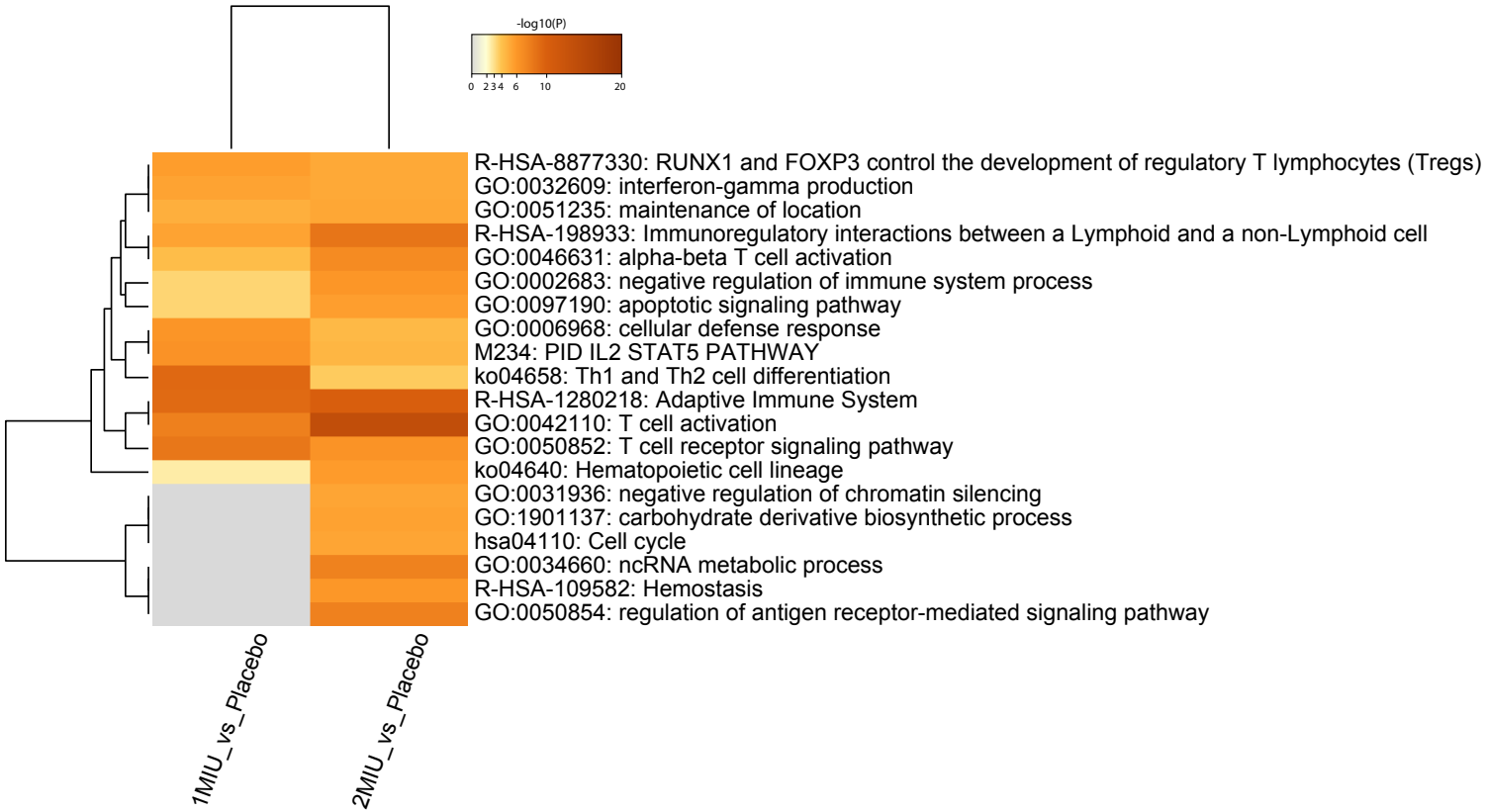

Figure 3.8: ***Heatmap of Metascape Enriched Processes at D64***

Enrichment heatmap generated by Metascape showing the top 20 significant enriched clusters. The names of cluster representatives are reported together with their significance level (Log10(P), calculated using hypergeometric test). Clusters are colour-coded depending on their Log10(P) while grey colour denotes lack of significance.

Moreover, an enrichment network was also generated using Metascape to visualise relationships between the top 20 most significant altered processes/pathways (**Figure 3.9**). The main identified cluster clump reflected a considerable alteration in immune regulatory processes and it was evident that Treg-specific processes (mentioned above) were closely related to the more general T cell activation and differentiation processes. This suggested a modulation within the immune system occurring with both treatment regimens, although generally more DEGs were observed among the 2MIU_vs_Placebo comparison. Moreover, from this analysis it seemed that processes involved in the regulation of the adaptive immune system were altered almost exclusively following the administration of the higher (2MIU) dose of the drug. Consistently with our REVIGO data, processes involved in cell cycle, apoptosis, chromatin regulation and ncRNA processing were reported amongst the differentially expressed clusters solely identified in the 2MIU_vs_Placebo comparison.

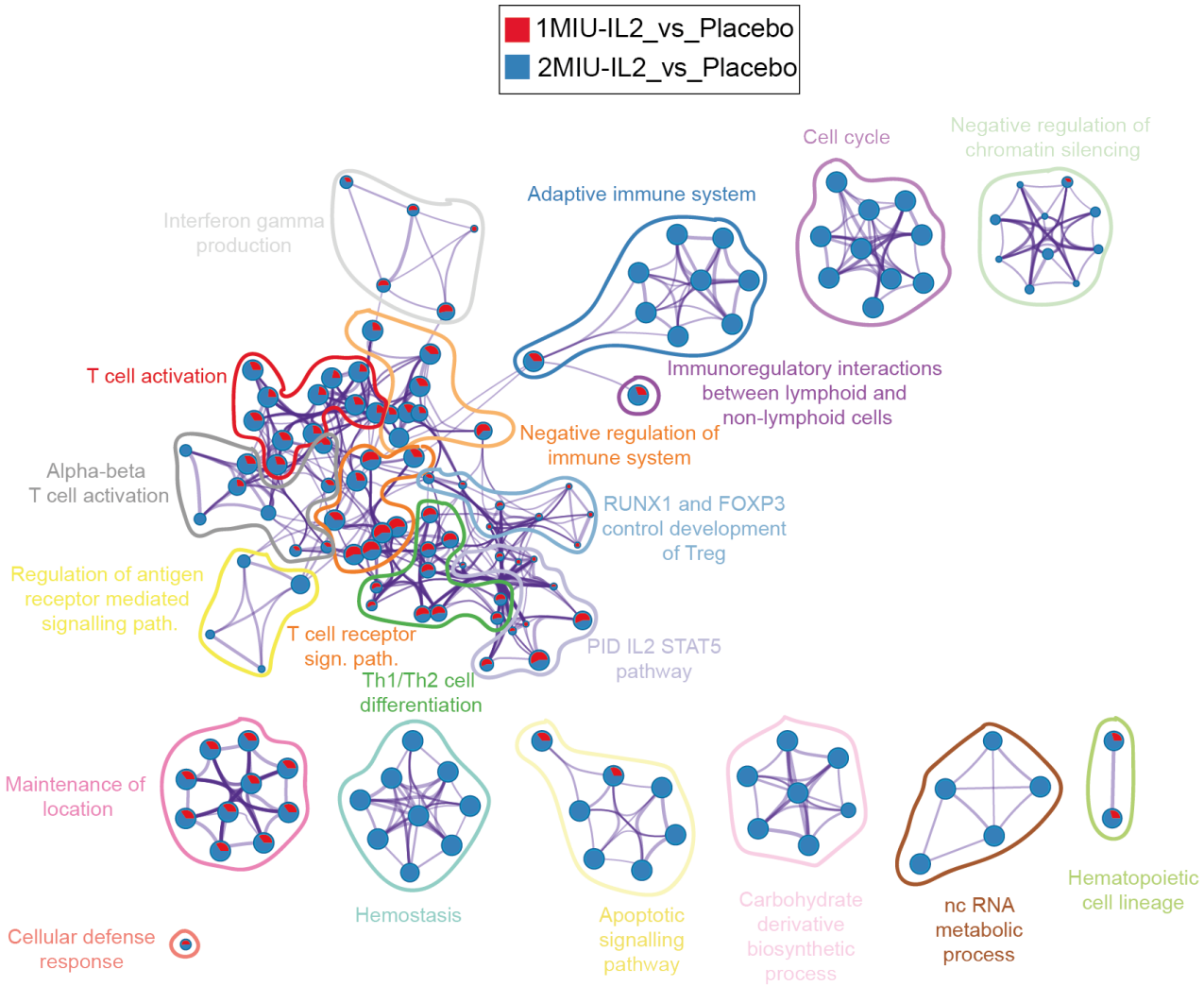
1MIU-IL2_vs_Placebo
2MIU-IL2_vs_Placebo
Cell cycle
Negative regulation of chromatin silencing
Interferon gamma production
Adaptive immune system
T cell activation
Immunoregulatory interactions between lymphoid and non-lymphoid cells
Negative regulation of immune system
Alpha-beta T cell activation
RUNX1 and FOXP3 control development of Treg
Regulation of antigen receptor mediated signalling path.
T cell receptor sign. path.
PID IL2 STAT5 pathway
Th1/Th2 cell differentiation
Maintenance of location
Hemostasis
Apoptotic signalling pathway
Carbohydrate derivative biosynthetic process
nc RNA metabolic process
Hematopoietic cell lineage
Cellular defense response

Figure 3.9: Pathway Enrichment Network Suggests Differential Effects of Ld-IL-2 Doses at D64.

This image shows an enrichment network generated using the software Metascape. This type of graph is useful to investigate and identify closely related pathways (displayed in the figure as nodes) as terms having a Kappa similarity score > 0.3 are connected by edges. In particular, this image shows the top 20 most significant enriched clusters of pathways (no more that 15 terms into each cluster are displayed to reduce complexity). In addition, this graph allows the visual inspection of the proportion of differentially expressed genes belonging to a certain gene list included into each pathway. This is possible because each pathway or node is reported as a pie chart within which sectors indicate the number of transcripts included into different gene lists (red= 1MIU IL-2_vs_Placebo and blue= 2MIU IL-2_vs_Placebo). This is tool is useful to investigate whether a particular pathway was altered as a result of a specific treatment dosage (e.g. genes involved into the “adaptive immune system” appeared to be differentially expressed only in 2MIU IL-2_vs_Placebo) or if processes were modified by both doses (e.g. “T cell action”).

Overall, these results suggested that both treatment doses were able to promote a Treg expansion and/or activation. Given that the majority of the Treg-associated genes were commonly differentially expressed following treatment with both ld-IL-2 doses (as shown in **Figures 3.6** and **3.7C**), these transcripts were further investigated. In particular, to evaluate if there were differences in terms of the magnitude of Treg response, the fold changes of the commonly DEGs from the two comparisons (1MIU_vs_Placebo and 2MIU_vs_Placebo) were compared. A dose-dependent reaction was found for 260 out of 375 (69.3%) commonly differentially expressed RefSeq genes. In fact, increased transcripts showed a greater level of upregulation, and similarly, decreased DEGs were more downregulated following the higher dose of IL-2 administered (**Figure 3.10**). Consistently with this, looking at microarrays' expression data of four key Treg and immune suppression markers (*FOXP3*, *CTLA4*, *IKZF2* and *IL2RA*) a dose-proportional upregulation was evident (**Figure 3.11**).

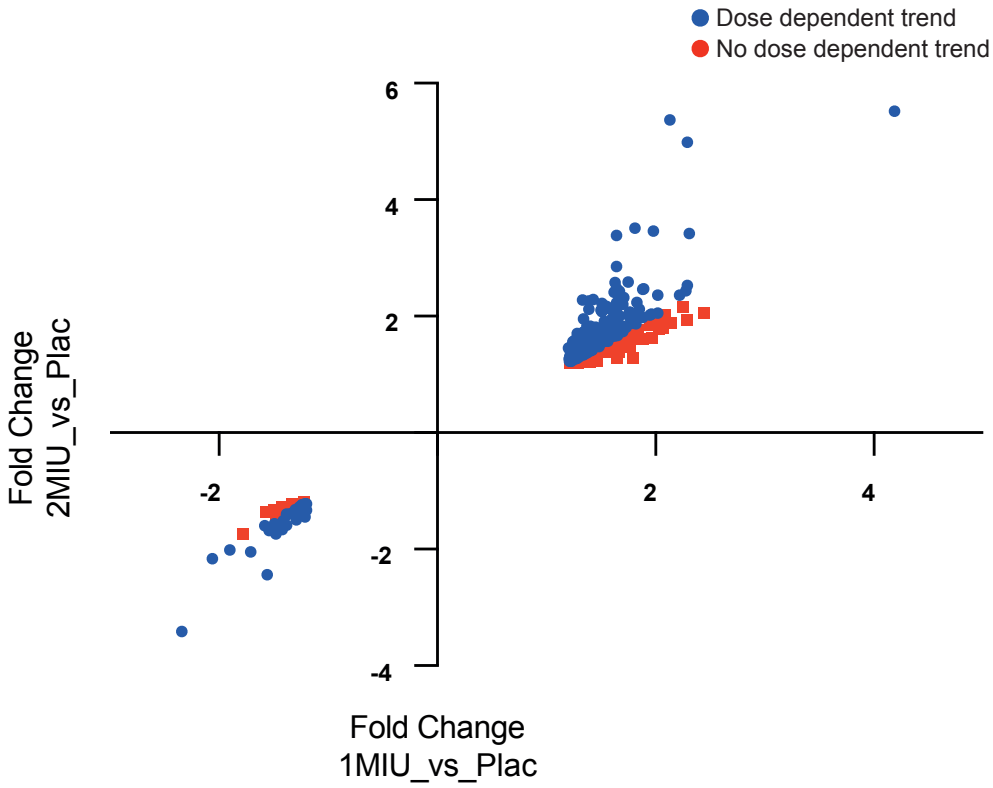

Figure 3.10: Dose-Dependency at D64.

Scatter plot displaying 375 RefSeq DEGs altered in common within the two treatment groups and their fold changes resulting from either 1MIU_vs_Placebo or 2MIU_vs_Placebo comparisons. 260 out of 375 genes (69.3%) exhibit a dose-dependent expression (in blue, while transcripts showing no dose-dependent trend are represented in red).

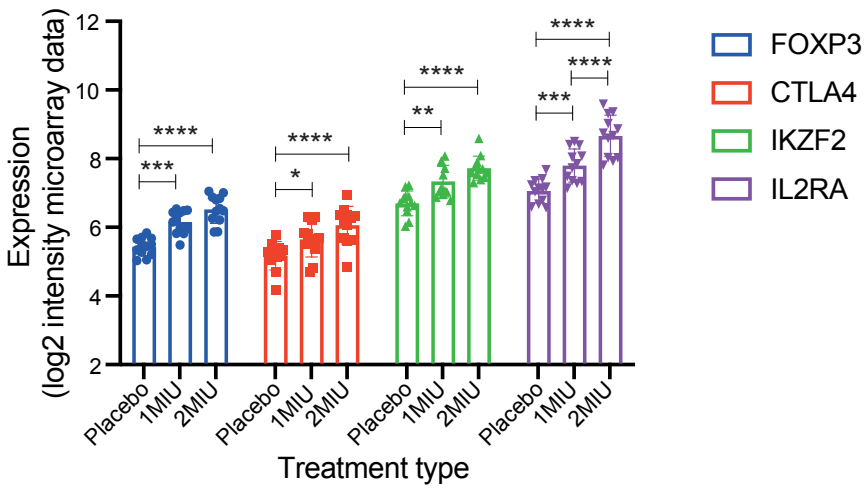

Figure 3.11: Dose-Dependent Expression of Treg markers at D64.

The expression levels (log_2 of signal intensity from the microarrays) of 4 Treg and immune suppression markers – *FOXP3*, *CTLA4*, *IKZF2* and *IL2RA* – are shown. A significant dose-dependent upregulation of these transcripts is detected. Box plots show mean ± SD. A two-way ANOVA with Turkey correction for multiple comparisons was conducted. *: Adjusted p-value<0.05, **: Adjusted p-value<0.01, ***: Adjusted p-value<0.001, ****: Adjusted p-value<0.0001.

Collectively, these results indicated evidence of immune modulatory gene expression changes following ld-IL-2 administration. However, a broader immune-regulation seemed to be promoted by the higher dose and, for this reason, further analyses were conducted comparing only 2MIU-IL-2-treated participants to placebo.

3.4 Longitudinal gene expression changes throughout the administration period

The second aim of this subsection of the study was to evaluate the longitudinal transcriptional changes occurring throughout the administration period in the 2MIU-IL-2-treated patient compared to placebo. In particular, three time points were selected over the course of the trial: D1, D8 and D64 and gene expression data were compared. To this end, complex and multifactorial comparisons were performed using the Limma package in R.

Firstly, data were imported into Limma and visually inspected using multidimensional scaling (MDS). Similarly to PCA, MDS is a technique that allows dimensionality reduction and visual representation of the data, highlighting similarities and differences among samples which are displayed in a Cartesian space. Unlike PCA, which uses original data, MDS builds a similarity matrix to generate the plot. This matrix is produced by calculating Euclidean distance for each pair of samples in a data set. In the case of microarray data, distance is computed as leading log fold changes (which is the average of the root mean square deviation of expression) of the top genes between samples. These are the genes that show the largest variations between samples. Gene expression profiles from both placebo and 2MIU-IL-2 treated samples from D1, D8, D64 and also D85 (24 days after the last injection and at the beginning of the follow-up period) were inspected with an MDS plot to gain a general overview of the complete dataset. Transcriptomic profiles from D1 and D85, generated by Dr Nadhim Bayatti (NB), clustered together and they were spatially separated from the profiles produced by myself (D8 and D64), regardless of their treatment type (**Figure 3.12**). Thus, the main source of variation was probably the result of a batch effect which was due to the fact that Leukolock^{TM} filters were shipped to SITraN at different times and therefore the microarrays were generated by two researchers.

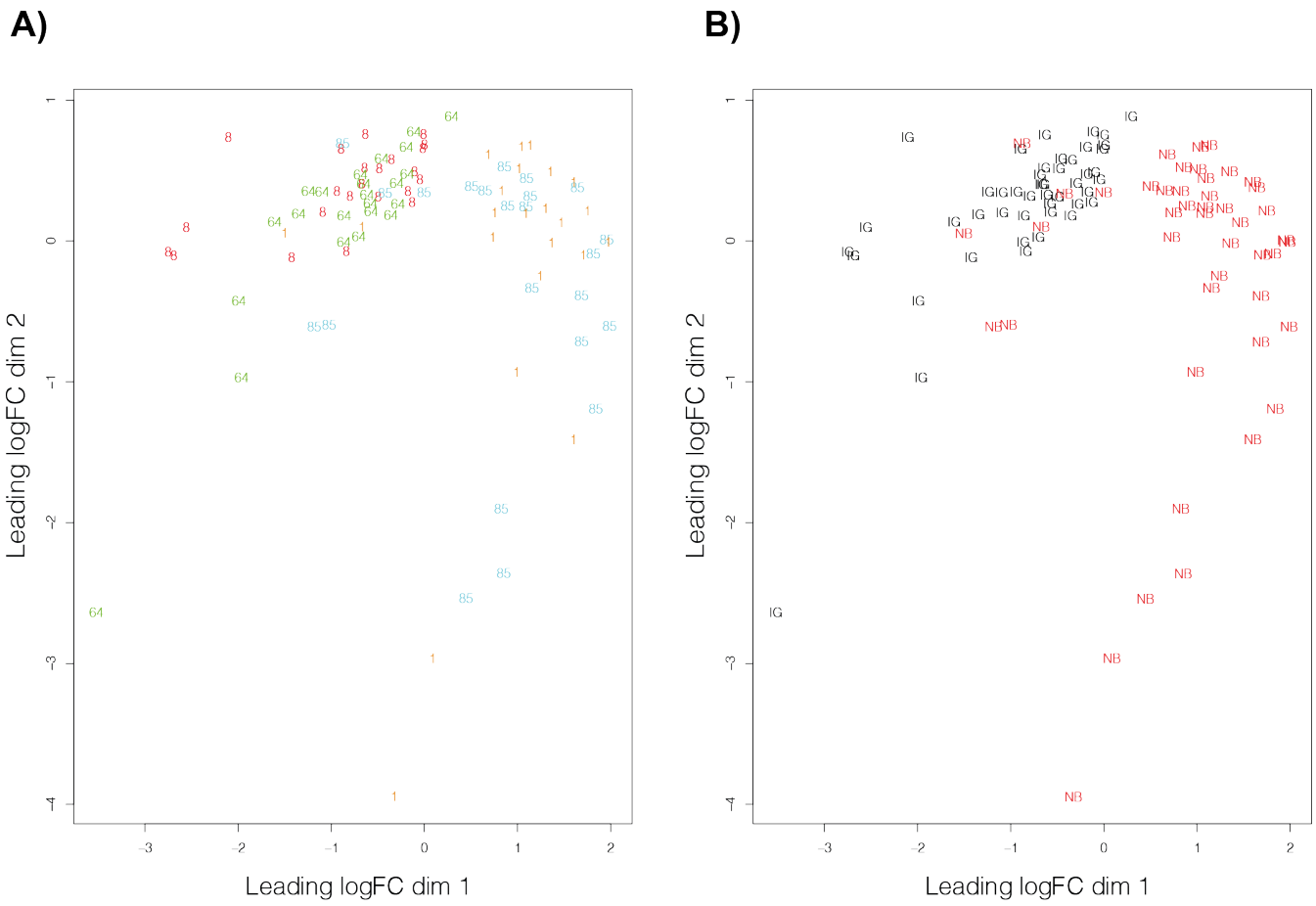

Figure 3.12: Multidimensional Scaling Plots of IMODALS Microarrays from D1, D8, D64 and D85.

Multidimensional scaling plot showing all the placebo and 2MIU-IL-2 treated samples at D1, D8, D64 and D85. Samples are colour-coded and labelled by time point (D1=orange, D8=red, D64=green, D85=light blue) (**A**) or by the operator who generated the microarrays (IG= Ilaria Giovannelli, in black and NB= Nadhim Bayatti, in red) (**B**). A clear batch effect is visible.

As mentioned in Chapter 2 (section 1.5.1), the removal of the batch effect may lead to exaggerated and unreliable results. For this reason, this was neither removed nor ignored, instead, batch identifiers were incorporated in our Limma statistical models leading to the production of two reliable gene expression comparisons: namely ΔD8, ΔD64. These were conducted with the aim of identifing transcriptional differences characteristic of the first and the last treatment cycles. In each of those, 2MIU-IL2 treated patients' transcriptome was compared to their baseline level and normalised to the same comparison within the placebo group. The two comparisons were studied and analysed alongside to identify similarities and differences in the gene expression alterations at D8 and D64.

The comparison ΔD8 identified 2635 RefSeq genes as significantly ($1.2 \leq FC \leq -1.2$ and p-value <0.05) differentially expressed (1953 decreased, 682 increased), while only 525 RefSeq genes (198 decreased, 327 increased) resulted from ΔD64 (**Figure 3.14A** and **B**). A widespread decrease in gene expression was reported after the first treatment cycle, while this effect seemed to be no longer present at the later time point. In contrast, at D64 a more pronounced upregulation of gene expression was documented. Interestingly, in both comparisons, one of the most significant DEG is *FOXP3*, crucial transcription factor for Treg implicated in the establishment and maintenance of their suppressive phenotype. This suggests an activation of Tregs starting from the first cycle and continuing throughout the administration period. However, other Treg markers (such as IL2RA and CLC) were visible with the upregulated genes only in the ΔD64 comparisons.

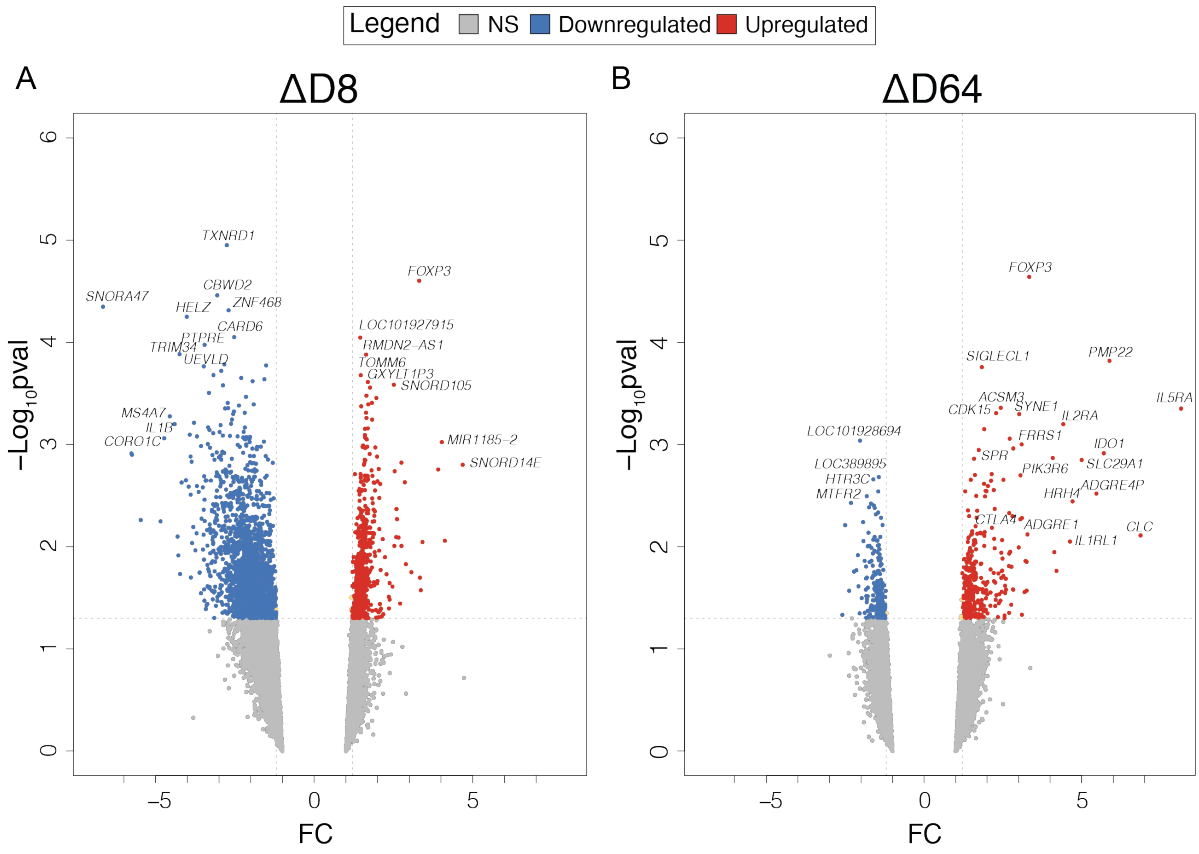

Figure 3.13: Comparison of Differentially Expressed Genes at ΔD8 and ΔD64.

Volcano plots displaying DEGs resulting from the comparisons ΔD8(**A**) and ΔD64 (**B**). DEGs are plotted and colour-coded depending on their fold change (FC) and their significance levels (-Log_{10} p-value): non-significant or transcripts that failed the FC cut-off are reported in grey, significant and with FC ≤-1.2 in blue and significant and with FC ≥1.2 in red. Three black lines are also shown: the horizontal one indicates the significance threshold (-Log_{10} p-value=1.3) and two vertical dotted lines mark the FC cut-off at -1.2 and 1.2 respectively. A widespread downregulation is detectable at D8, while at D64 an increased upregulation is reported amongst which some Treg makers are recognisable. (Empirical Bayesian statistics were conducted using Limma to determine significant DEGs).

To understand the biological functions exerted by the identified DEGs, upregulated and downregulated lists of transcripts from the two comparisons were imported separately into Enrichr and gene ontology analyses were carried out. As expected, a large number of downregulated GO BPs (448 processes) were significantly enriched in the ΔD8 comparison while, only 35 downregulated biological processes were identified in ΔD64. In contrast, analysis of upregulated DEGs identified 35 significantly enriched GO BPs in the ΔD64 comparison while, only 10 were observed in ΔD8.

The most significant ΔD8 GO BPs revealed an extensive alteration (both increase and decrease) in different processes involved in the RNA metabolism. These included variations in both non coding RNA and mRNA processing, splicing and gene expression regulation (**Figure 3.15A and 3.15B**). Moreover, evidence of inflammatory suppression was also documented, with neutrophil activation and degranulation being significantly decreased. In contrast, the top 10 significant GO BPs from ΔD64 did not show a clear downregulation of inflammatory processes, while inhibition of other biological mechanisms including iron transport and lipid processing were reported. However, several immune regulatory processes, especially involved in Treg-activation and differentiation, were upregulated at D64. Interestingly, enrichment in muscle regulatory process was also documented, together with an upregulation in membrane raft polarization and distribution (**Figure 3.15C and 3.15D**). Full lists of enriched GO BPs from the two comparisons are reported in **Appendix 4** (ΔD8) and **5** (ΔD64), respectively.

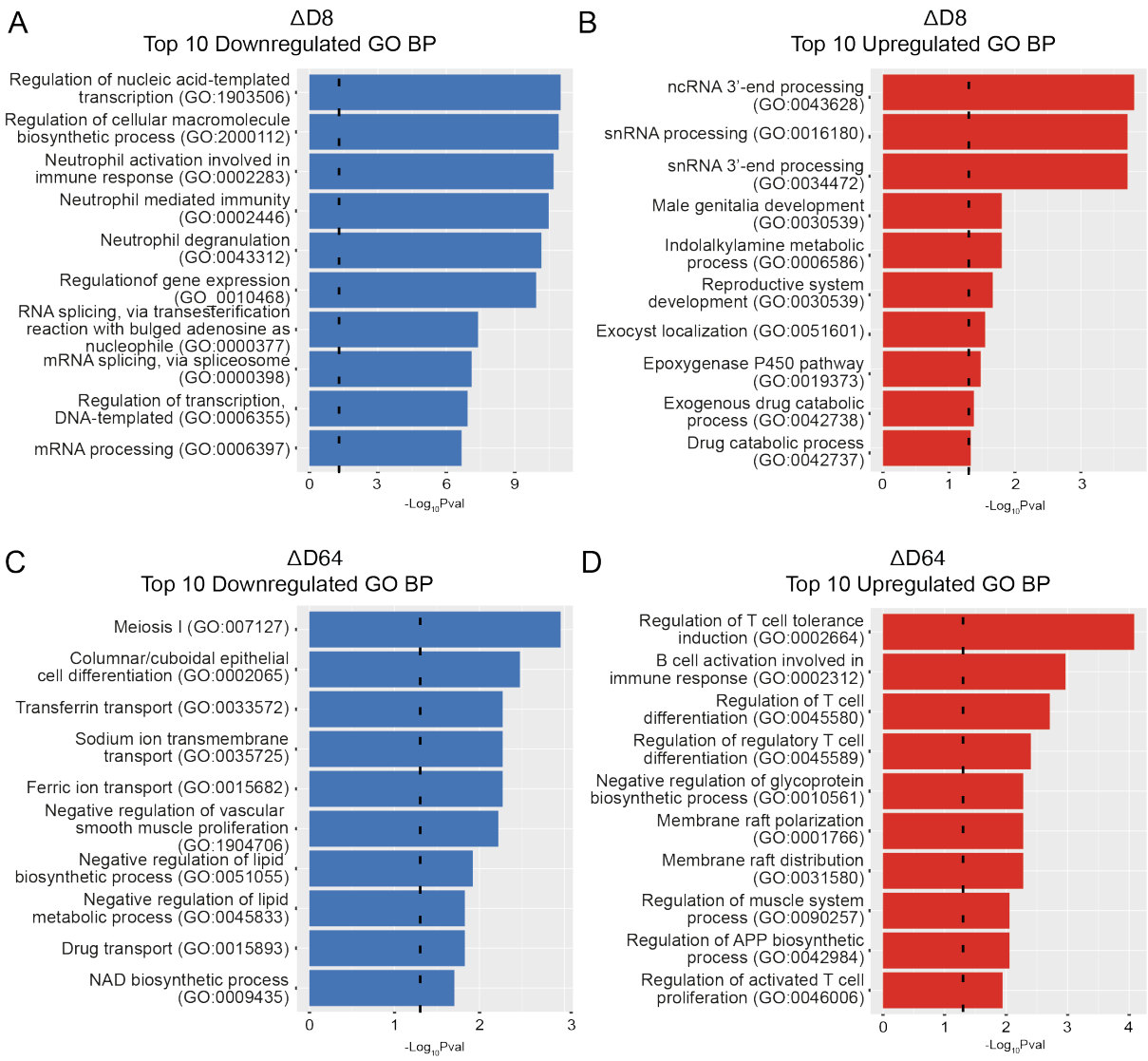

Figure 3.14: Gene Ontology Analyses of ΔD8 and ΔD64 DEGs

Bar plots displaying the top 10 significant downregulated (**A**) and upregulated (**B**) GO Biological Processes (GO BPs) from ΔD8 and top 10 significant downregulated (**C**) and upregulated (**D**) GO BPs from ΔD64. Significance threshold lines are reported in black ($-Log_{10}$ p-value=1.3). A downregulation of pro-inflammatory processes involving neutrophils and an alteration in the RNA metabolism are observed at D8 while, later during the course of the trial, a significant upregulation of Treg processes is documented. (Fisher's exact statistical test was performed using Enrichr to cluster transcripts into GO BP terms).

Given our interest in evaluating the effect on the immune system promoted by ld-IL-2 in the IMODALS cohort, all the previously described significant GO BPs were summarised using REVIGO and immune-related clusters were isolated and studied separately. While no upregulated immunological clusters were reported in the analysis ΔD8, GO summarisation showed a broad downregulation of inflammatory processes at this time point. The larger cluster, which included 10 immunological GO BP terms, showed evidence of an extensive reduction in the expression of genes involved in granulocyte (in particular neutrophil) activation and functions. Moreover, other inflammatory mechanisms were reduced following the first injection cycle, this included several cytokine production and downstream signalling pathways and different immune cell differentiation and migration (**Figure 3.16A**). A different immunological phenotype was reported at D64 when no clear immune-related clusters were found to be downregulated, but a widespread activation of regulatory processes, which particularly involved T cells, was documented (**Figure 3.16B**).

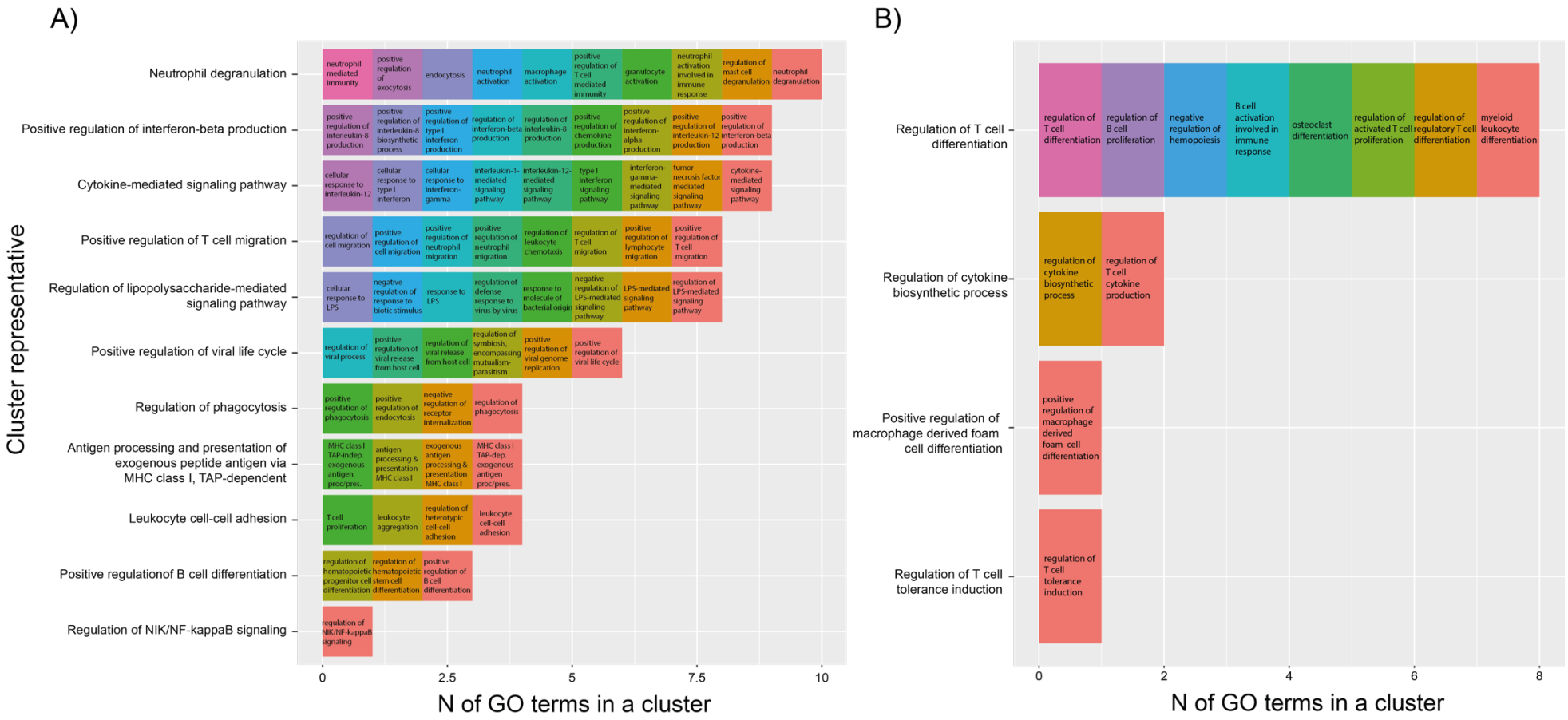
A)
Cluster representative
Neutrophil degranulation
Positive regulation of interferon-beta production
Cytokine-mediated signaling pathway
Positive regulation of T cell migration
Regulation of lipopolysaccharide-mediated signaling pathway
Positive regulation of viral life cycle
Regulation of phagocytosis
Antigen processing and presentation of exogenous peptide antigen via MHC class I, TAP-dependent
Leukocyte cell-cell adhesion
Positive regulationof B cell differentiation
Regulation of NIK/NF-kappaB signaling
neutrophil mediated immunity
positive regulation of exocytosis
endocytosis
neutrophil activation
macrophage activation
positive regulation of T cell mediated immunity
granulocyte activation
neutrophil activation involved in immune response
regulation of mast cell degranulation
neutrophil degranulation
positive regulation of interleukin-8 production
positive regulation of interleukin-8 biosynthetic process
positive regulation of type I interferon production
regulation of interferon-beta production
regulation of interleukin-8 production
positive regulation of chemokine production
positive regulation of interferon-alpha production
positive regulation of interleukin-12 production
positive regulation of interferon-beta production
cellular response to interleukin-12
cellular response to type I interferon
cellular response to interferon-gamma
interleukin-1-mediated signaling pathway
interleukin-12-mediated signaling pathway
type I interferon signaling pathway
interferon-gamma-mediated signaling pathway
tumor necrosis factor mediated signaling pathway
cytokine-mediated signaling pathway
regulation of cell migration
positive regulation of cell migration
positive regulation of neutrophil migration
positive regulation of neutrophil migration
regulation of leukocyte chemotaxis
regulation of T cell migration
positive regulation of lymphocyte migration
positive regulation of T cell migration
cellular response to LPS
negative regulation of response to biotic stimulus
response to LPS
regulation of defense response to virus by virus
response to molecule of bacterial origin
negative regulation of LPS-mediated signaling pathway
LPS-mediated signaling pathway
regulation of LPS-mediated signaling pathway
regulation of viral process
positive regulation of viral release from host cell
regulation of viral release from host cell
regulation of symbiosis, encompassing mutualism-parasitism
positive regulation of viral genome replication
positive regulation of viral life cycle
positive regulation of phagocytosis
positive regulation of endocytosis
negative regulation of receptor internalization
regulation of phagocytosis
MHC class I TAP-indep. exogenous antigen proc/pres.
antigen processing & presentation MHC class I
exogenous antigen processing & presentation MHC class I
MHC class I TAP-dep. exogenous antigen proc/pres.
T cell proliferation
leukocyte aggregation
regulation of heterotypic cell-cell adhesion
leukocyte cell-cell adhesion
regulation of hematopoietic progenitor cell differentiation
regulation of hematopoietic stem cell differentiation
positive regulation of B cell differentiation
regulation of NIK/NF-kappaB signaling
0
2.5
5
7.5
10
N of GO terms in a cluster
B)
Regulation of T cell differentiation
Regulation of cytokine biosynthetic process
Positive regulation of macrophage derived foam cell differentiation
Regulation of T cell tolerance induction
regulation of T cell differentiation
regulation of B cell proliferation
negative regulation of hemopoiesis
B cell activation involved in immune response
osteoclast differentiation
regulation of activated T cell proliferation
regulation of regulatory T cell differentiation
myeloid leukocyte differentiation
regulation of cytokine biosynthetic process
regulation of T cell cytokine production
positive regulation of macrophage derived foam cell differentiation
regulation of T cell tolerance induction
0
2
4
6
8
N of GO terms in a cluster

Figure 3.15: REVIGO-Clustered Enriched Immunological GO Biological Processes

Box plots showing immunological REVIGO clustered downregulated GO BPs in ΔD8 (**A**) and immunological REVIGO clustered upregulated GO BPs in ΔD64 (**B**). Each bar represents a cluster which summarises a number of GO BPs the names of which are displayed inside each box. A wide inhibition of inflammatory processes is evident after the first treatment cycle while, upregulation of Treg-related mechanisms is reported at the end of the treatment. X-axis: number of GO BPs included in each cluster, Y-axis: GO cluster representatives.

Subsequently, Ingenuity Pathway Analysis® (IPA) was also used. Unlike Enrichr, REVIGO or Metascape, this software provides advanced analysis capabilities including the prediction of the activation/inhibition state of identified altered pathways and the discovery of key upstream regulators which allows the researcher to hypothesize casual relationships associated with experimental data. Limma ΔD8 and ΔD64 gene lists were imported into IPA to identify pathways longitudinally altered throughout the trial.

Seventy-seven pathways were altered at ΔD8 (**Figure 3.17**). An inhibition of inflammatory mechanisms was identified, with functions of both innate (phagocytic cells, neutrophils, eosinophils, macrophages/monocytes and natural killers) and adaptive immune cells (cytotoxic T lymphocytes and B cells) being decreased. Moreover, inhibition of NF-kB and signalling related to several cytokines was documented. Interestingly, negative regulation of pathways subserving autoimmune diseases, such as multiple sclerosis and systemic lupus erythematosus, were also found. Taken together, these results suggest a broader suppression of inflammatory processes, which are known to be activated in ALS, and also involved in other autoimmune pathologies. Additionally, two processes linked to the CNS homeostasis, neuregulin and glioma signalling pathways, were decreased.

In contrast, only 16 pathways were altered at ΔD64 (**Figure 3.18**). The majority of these were involved in the metabolism of several molecules including amino acids and sulphate-containing compounds. However, two mechanisms implicated in T-cell subset modulation were altered. In particular, activation of the Th2 pathway was

observed. Importantly, Th2 cells share some anti-inflammatory properties with Tregs mediated by IL-4 secretion (Beers et al., 2011a, Zhao et al., 2012).

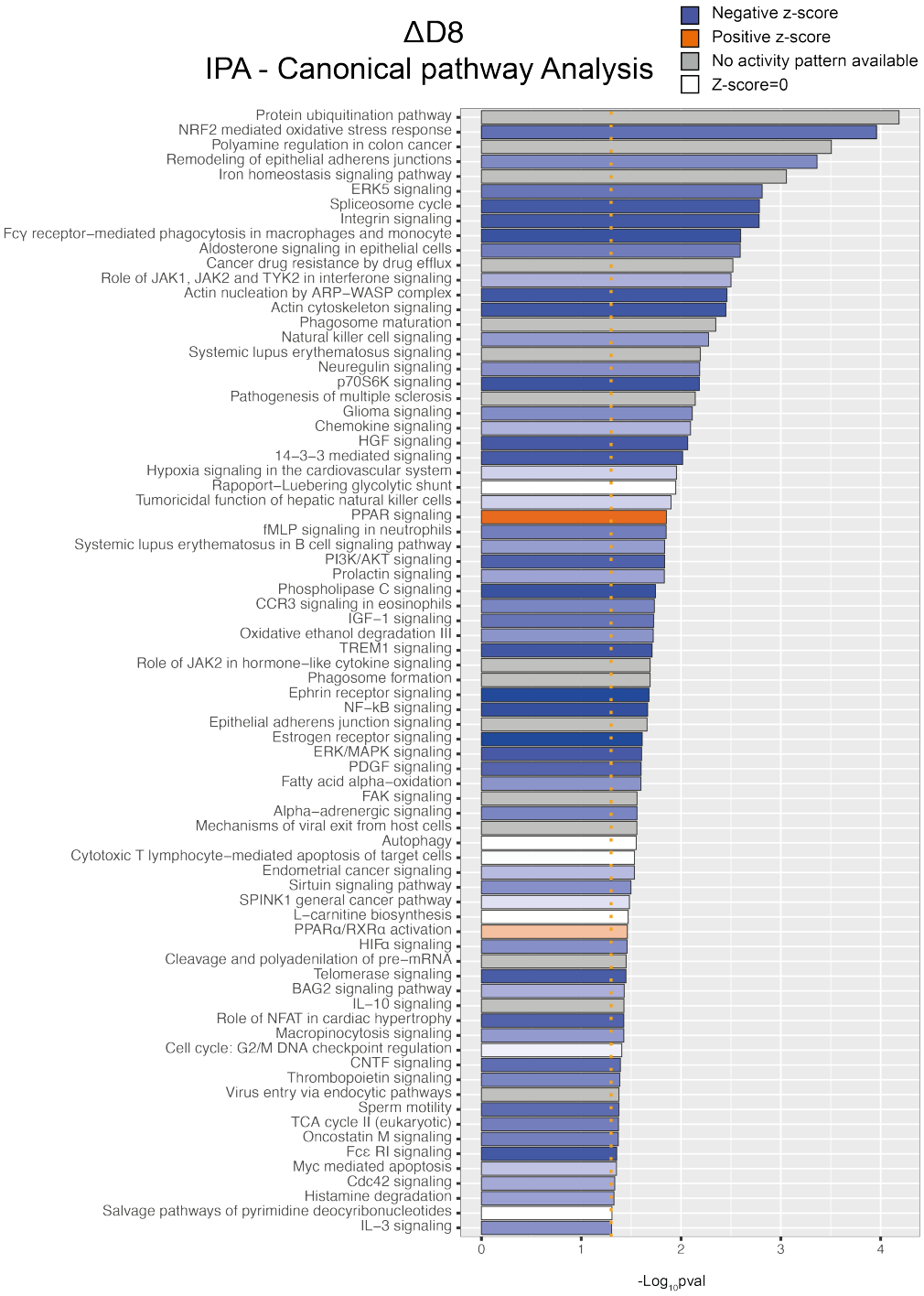

Figure 3.16: IPA Canonical Pathway Analysis at D8.

Bar plot displaying IPA canonical pathway analysis retrieved from the ΔD8 gene list. Activated (z-score>0, in orange) or inhibited pathways (z-score<0, in blue) are shown. Significant pathways but with z-score equal to 0 (in white) or with no activation prediction available in the software (in grey) are also reported. A significance threshold is displayed as a dotted orange line (-Log_{10} p-value=1.3).

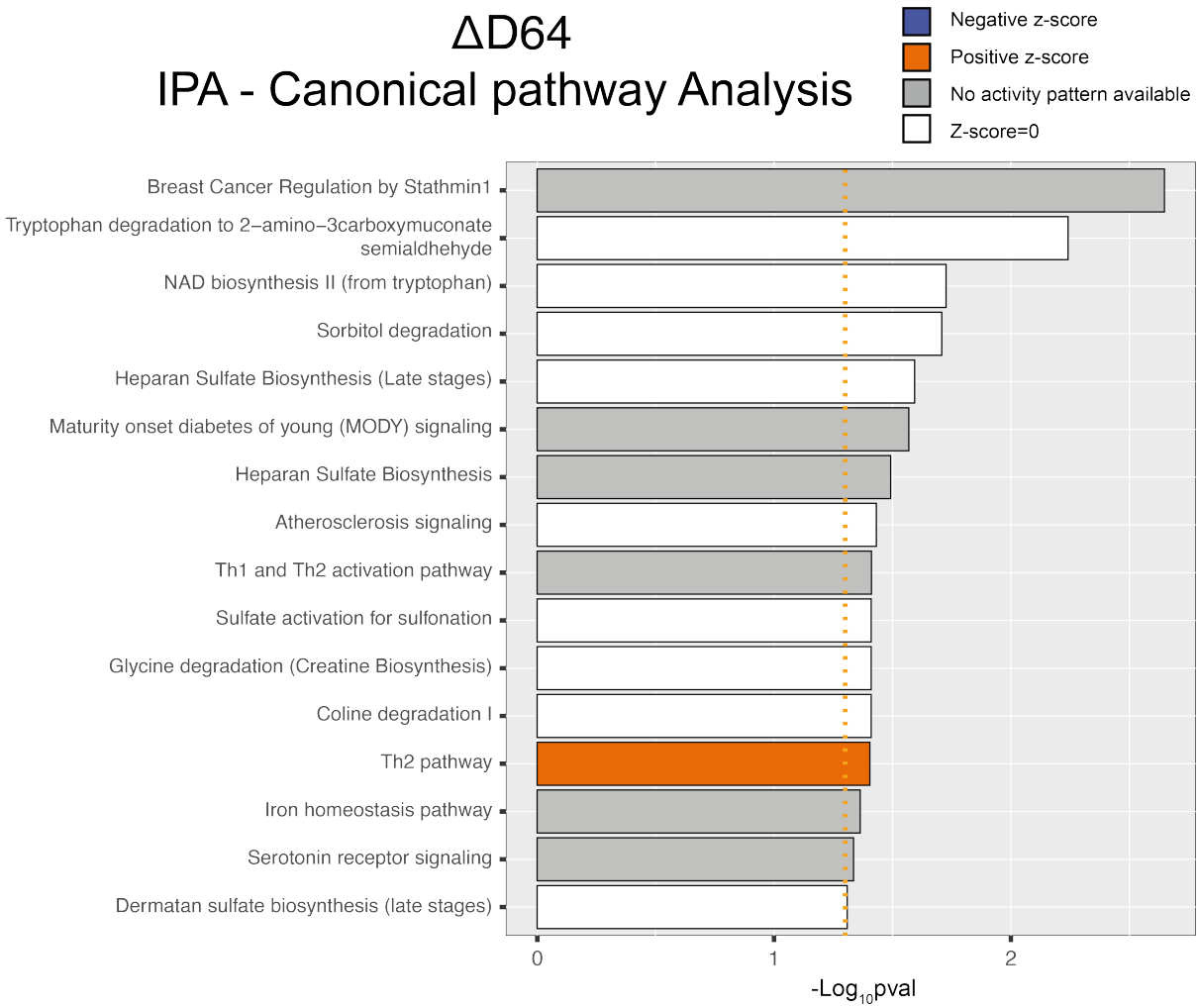

Figure 3.17: IPA Canonical Pathway Analysis at D64.

Bar plot displaying IPA canonical pathway analysis retrieved from the ΔD64 gene list. Activated (z-score>0, in orange) or inhibited pathways (z-score<0, in blue) are shown. Significant pathways but with z-score equal to 0 (in white) or with no activation prediction available in the software (in grey) are also reported. A significance threshold is displayed as a dotted orange line (-Log_{10} p-value=1.3).

Interestingly, the top two significant pathways altered at ΔD8 were "protein ubiquitination pathway", for which the activation status could not be predicted, and the "NRF2-mediated oxidative stress response", which appeared to be inhibited. The first mechanism is crucial for protein degradation and turnover. Proteostasis dysregulation and formation of aggregates are well characterized ALS pathological mechanisms (Malik and Wiedau, 2020). Moreover, excessive ROS generation, oxidative stress and consequently oxidative damage are other key processes involved in the pathophysiology of ALS (Barber and Shaw, 2010). NRF2 is a transcription factor which promotes a cytoprotective response, including induction of anti-oxidant and anti-inflammatory gene expression and its dysregulation has been reported in ALS (Sivandzade et al., 2019, Sarlette et al., 2008). Given the identification of these pathways as altered following the first treatment cycle, genes included in those processes were analysed in detail to elucidate possible short-term detrimental effects of 2MIU-IL-2.

Fifty transcripts were included in the IPA pathway called "protein ubiquitination pathway" and the expression of all these genes was significantly downregulated in the ΔD8 comparison, while none of them reached statistical significance in ΔD64. Eight functional clusters were identifiable in this group of transcripts (**Figure 3.19**). As expected, the majority of the genes coded for proteins involved in the ubiquitination process and subunits of the proteasome. However, heat shock and major histocompatibility complex (MHC) proteins were also recognisable. Consistently with this, the analysis of the same fifty transcripts using Metascape revealed a close relationship between ubiquitination processes and MHC antigen processing and presentation which is crucial for the immune response (**Figure 3.20**). Moreover, evidence from the literature highlights the importance of the ubiquitin-proteasome system in immune cells and the formation of the so-called immuneproteasome for the presentation of antigens and the initialization of the host immune response (Kammerl and Meiners, 2016, Çetin et al., 2021). Hence, the downregulation of these transcripts may be the result of a prompt inhibition of immune system processes rather than a detrimental effect. However, further investigation would be needed to exclude similar effects in ALS motor neuron or glial cells which are characterized by an already impaired proteostasis and the downregulation of these genes could potentially result in further protein aggregation.

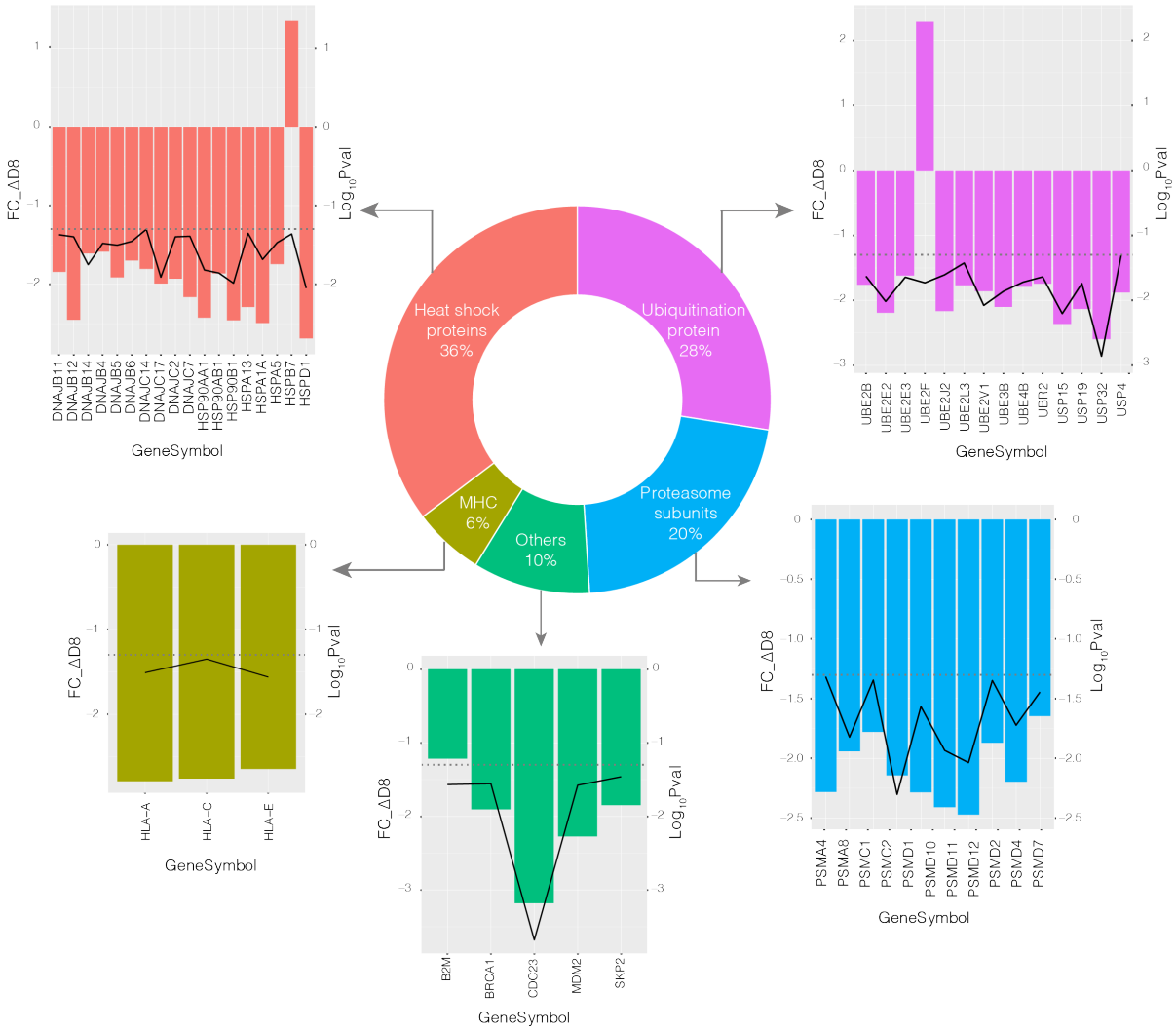

Figure 3.18: Classification of Transcripts Included in the IPA Protein Ubiquitination Pathway.

A donut plot shows the classification of the transcripts included in the IPA protein ubiquitination pathway. For each category, the fold change (FC) expression of each gene is displayed in a bar plot while the Log_{10}(Pval) is shown as a black line. A dotted grey line is also reported to mark the statistical significant threshold (Log_{10}(Pval)= -1.3). X-axis: gene symbol, Y-axis: FC and Log_{10}(Pval).

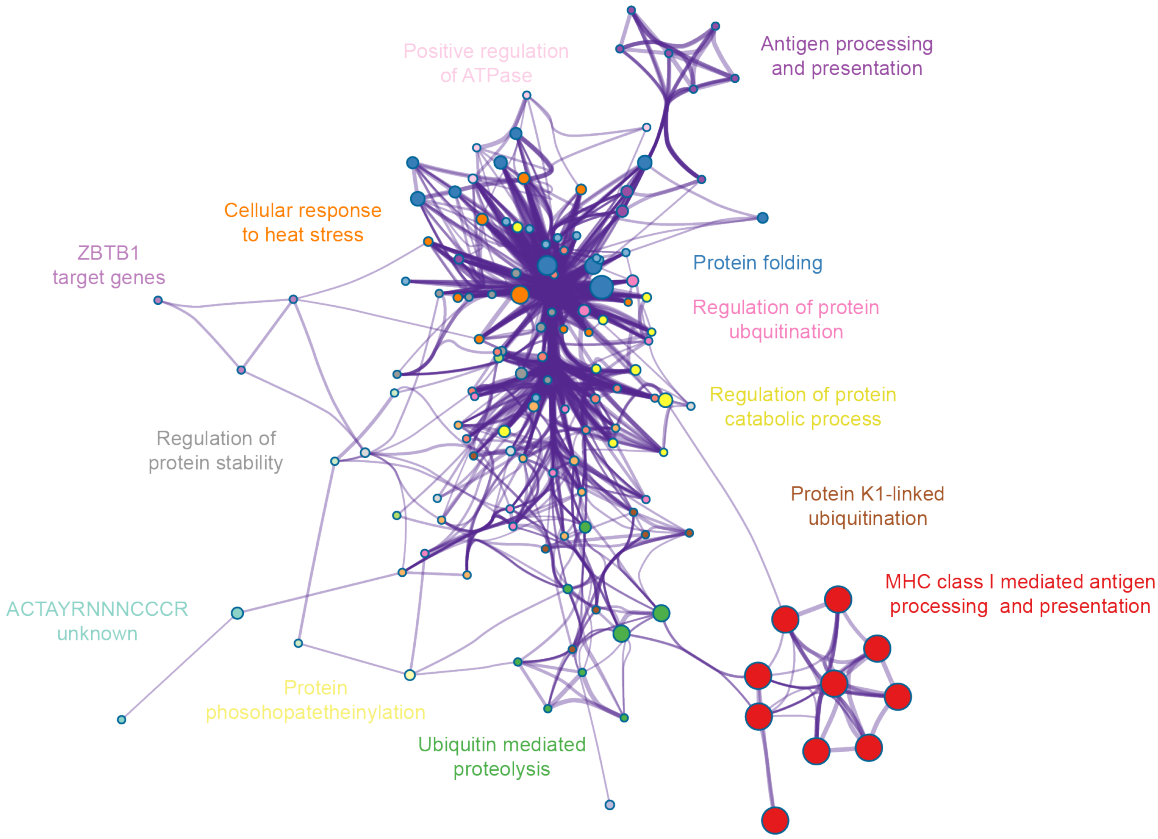

Figure 3.19: Metascape Analysis of the Transcripts Included in the Protein Ubiquitination Pathway.

Enrichment network produced by Metascape following the input of the list of genes included in the protein ubiquitination pathway identified with IPA. Each node represents a pathway and terms showing a Kappa similarity score > 0.3 are connected by edges. Clusters are labelled and marked using different colours.

Thirty-six transcripts (32 downregulated and 4 upregulated) were differentially expressed in the ΔD8 comparison and included in the IPA "NRF2 mediated oxidative stress response" pathway (z-score= -2.982), while none of them were significantly altered in ΔD64. To investigate the role of the transcripts in the oxidative response, a network displaying a selection of the most important proteins was generated with IPA (**Figure 3.21**). NRF2 is implicated in various cellular mechanisms but, expression changes associated with the end of the first administration cycle mostly affected genes

involved in chaperones/stress response or antioxidant genes. The repression of these latter genes can be interpreted either as a detrimental short-term effect of ld-IL-2, given that this suppression was not detected at D64, or it can be also speculated that ld-IL-2 can instead have an anti-oxidant effect by dampening the production of ROS and therefore reducing the need for the NRF2-associated stress response. However, further investigation is necessary to verify this hypothesis, especially in CNS cells.

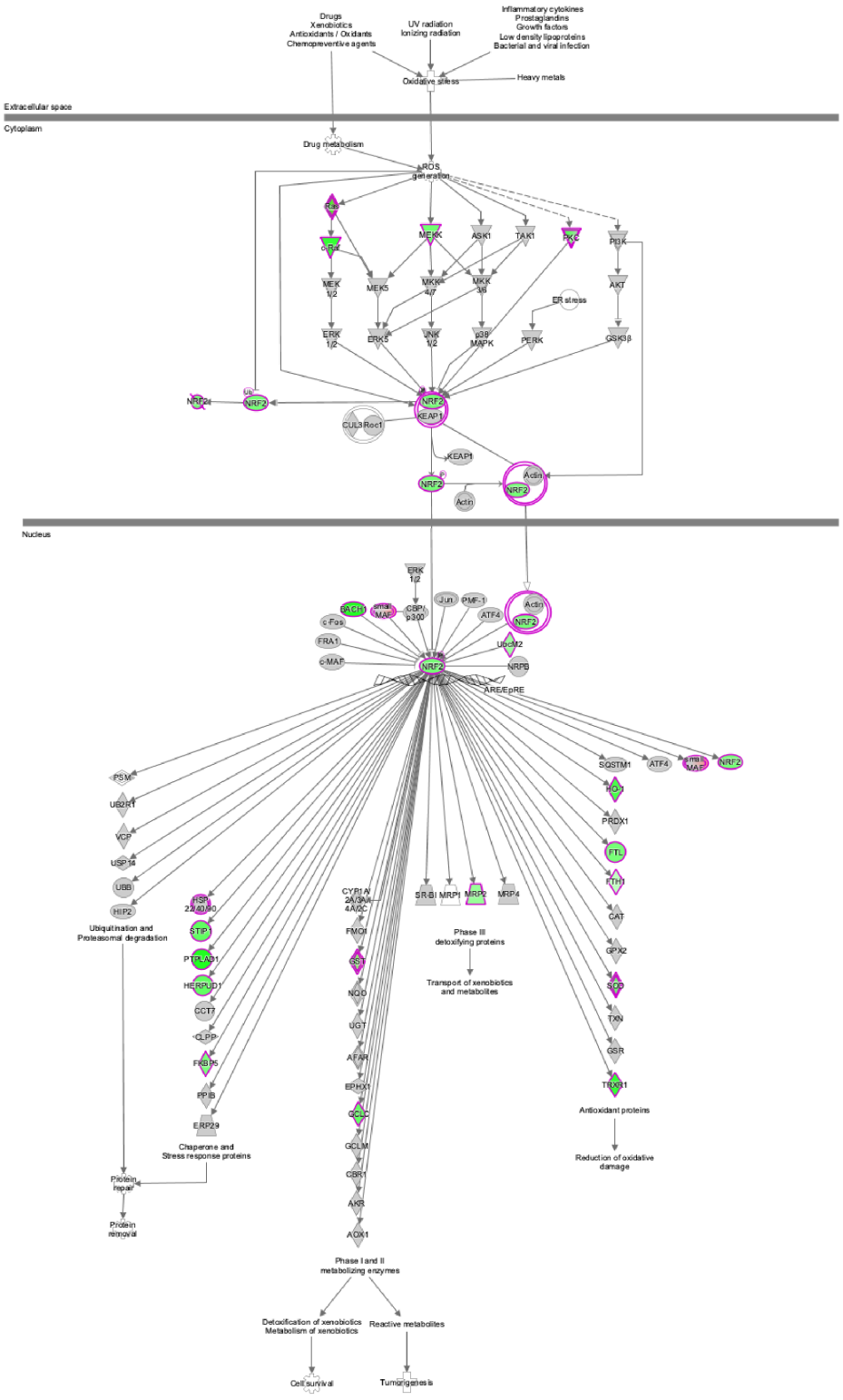

Figure 3.20: NRF2-Mediated Oxidative Stress Response IPA Pathway.

Graph generated with IPA showing the most important proteins involved in the NRF2 pathway. Downregulated genes are shown in green while red indicates upregulation. The colour magenta indicates the transcripts present in the data set.

Another tool provided by IPA, called diseases and functions, was used to further investigate molecular mechanisms altered following ld-IL-2 administration. This analysis revealed an almost opposite phenotype occurring at D8 and D64. In fact, while the vast majority of the pathways showed negative z-scores, which indicates inhibition, after the first cycle, a trend towards inversion was visible at the later time point with a positive z-score-skewed phenotype (**Figure 3.22** and **3.23**). This analysis reinforces previous observations indicating a rapid inhibition of inflammatory mechanisms after the first cycle. In fact a repression of diapedesis of leukocytes - including phagocytes, monocytes, granulocytes and neutrophils- as well as developmental and functional inhibition of these cells was shown (**Figure 3.22**). Cell death mechanisms were also found to be activated in leukocytes. This may indicate a reorganization within immune cells happening at this time point. Concomitantly, downregulation of cell death processes in neurons and brain cells ("cell death of brain", " cell death of brain cells", "apoptosis of cortical neurons") was observed, together with a mild activation of the pro-survival "protection of cortical neurons" which is particularly interesting in the context of ALS (**Figure 3.22** and **Appendix 6**). Furthermore, processes involved in metabolism, synthesis and production of reactive oxygen species (ROS) were inhibited at this time point. This latter result is particularly interesting and, considering previous findings involving the NRF2 pathway, it could be speculated that the treatment promoted a reduction in the production of oxidative species therefore diminishing the need of the protective NRF2 pathway, which appeared to be inhibited at D8.

In contrast, ΔD64 analysis revealed an extensive activation of regulatory processes ("regulation of cells", "suppression of lymphocytes", "differentiation of induced Tregs", "regulation of mononuclear leukocytes" and "activation of Tregs") and concomitant activation of leukocyte apoptosis (**Figure 3.23**). This suggested a more evident expansion of protective Tregs following the third treatment cycle. However, unlike D8, processes involved in immune cell movement and recruitment seemed to increase at this time point. The reported activation of the "inflammatory response" process may be perceived as counter intuitive. However, when investigating the transcripts included in this process by the software, it was clear that several anti-inflammatory agents (such as *FOXP3*, *IDO1*, *IL2RA*) were also incorporated and thus "inflammatory response" included both pro and anti-inflammatory modulators (**Appendix 7**). Notably, only the

diseases and functions for which the z-score was ≠ 0 are reported in **Figure 3.22**. The completed list with all the enriched terms is reported in **Appendices 7** and **8**.

ΔD8

IPA - Diseases and Functions

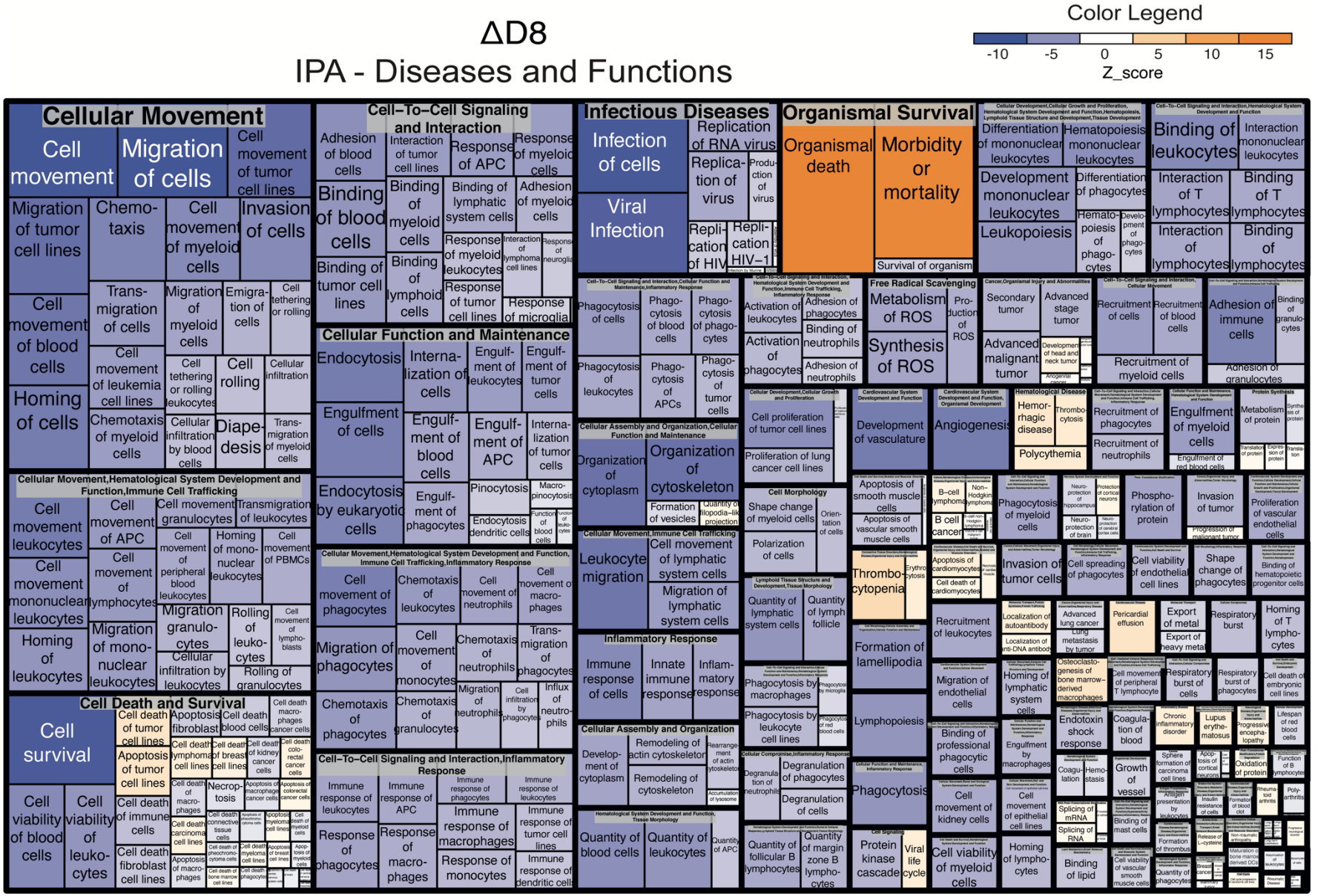

Figure 3.21: ΔD8 IPA disease and function analysis.

Treemap summarising altered IPA diseases and biological functions resulting from the ΔD8 comparison. Each box represents a biological function or a disease and they are sized and coloured by their z-score (z-score > 0 in the orange colour scale or < 0 in the blue scale). Diseases and functions are clustered by IPA into master categories for which the name is displayed by a grey label. A widespread downregulation of immunological processes was reported at D8.

ΔD64

IPA - Diseases and Functions

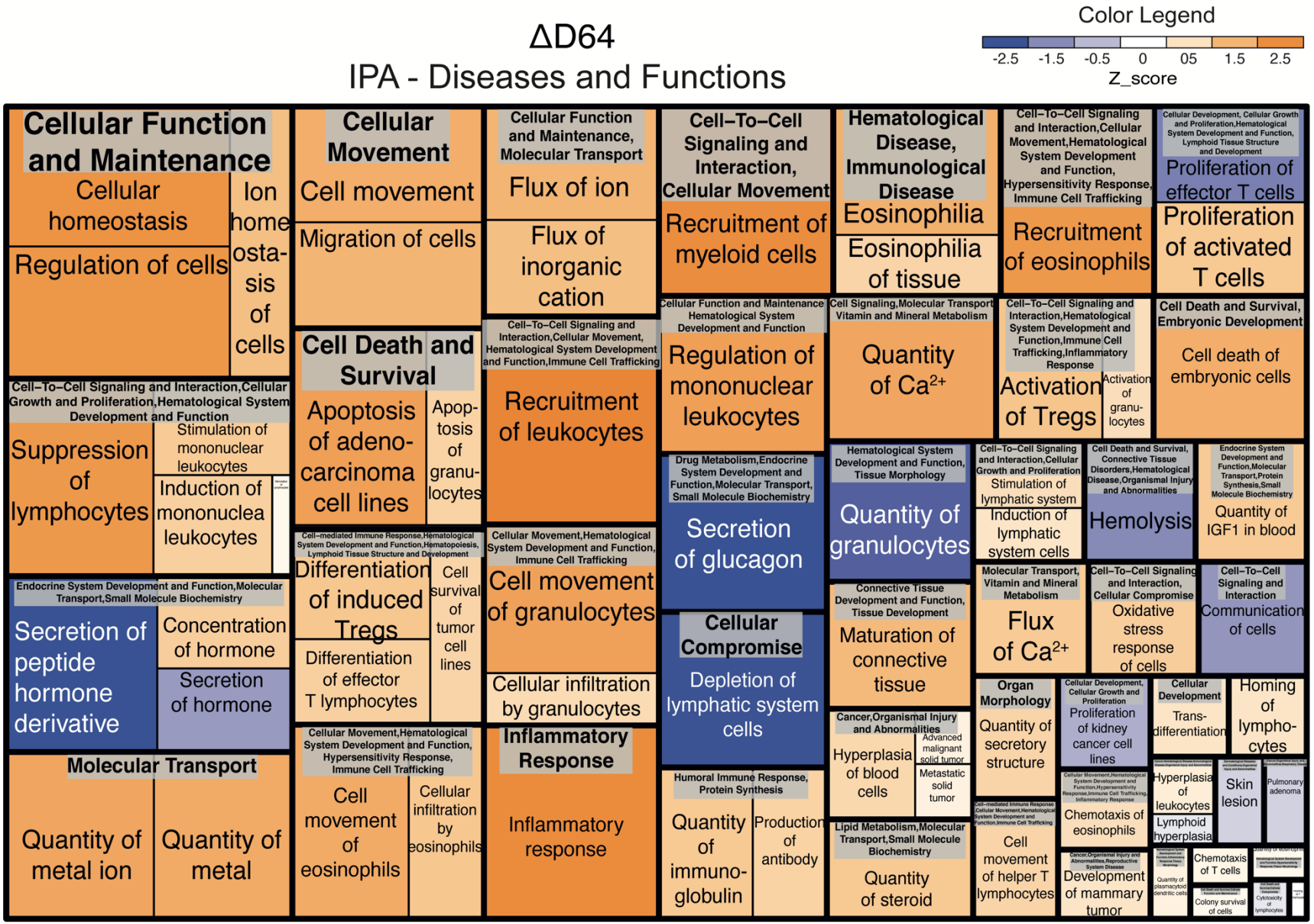

Figure 3.22: ΔD64 IPA disease and function analysis.

Treemap summarising altered IPA diseases and biological functions resulting from the ΔD64 comparison. Each box represents a biological function or a disease and they are sized and coloured by their z-score (z-score > 0 in the orange colour scale or < 0 in the blue scale). Diseases and functions are clustered by IPA into master categories for which the name is displayed by a grey label. An opposite phenotype was visible at D64 where most of the processes appeared to be upregulated. Evidence of increase activation of immune suppressive mechanisms was provided at this time point.

The last analysis tool used in IPA was the upstream regulator. This allows the identification of transcriptional regulators which are molecules (e.g. transcription factors, miRNAs or drugs) known to be capable of modulating expression of downstream genes. Therefore, their alteration can explain the overall observed transcriptional status of a dataset. Moreover, IPA® allows the researcher to make predictions on the activation status of each identified transcription regulator. In particular, a factor is predicted as activated if the majority of downstream genes known to be induced by it are upregulated or if downregulation is detected for genes whose expression is reduced by a transcriptional regulator. An opposite condition is reported if a molecule with regulatory action is predicted as inhibited.

The top ten most significant upstream regulators from ΔD8 and ΔD64 comparisons are displayed in **Table 3.3**. Most of them showed a significant p-value of overlap but an insignificant Z-score (Z-score is considered significant if it is either <-2 or >2). This suggested that genes downstream to a certain regulator were significantly differentially expressed in our dataset but their expression pattern was not sufficient to confidently predict its overall activation/inhibition.

Amongst the top ten most significant upstream regulators identified in the ΔD8 comparison, five showed also a significant Z-score consistent with an inhibition pattern. In particular, TGFB1, IFNG and NFE2L2 exhibited the lowest Z-scores. Transforming growth factor beta 1 (TGFB1) is involved in numerous cellular process but it has a central role in immunity having both pro- and anti-inflammatory effects. In particular, it regulates Treg or Th17 development in a concentration-dependent manner where high levels promote Treg whilst low concentration favours Th17, the

Treg inflammatory counterpart (Zhou et al., 2008, Sanjabi et al., 2017). Although TGFB1 expression was increased in ΔD8, it was predicted to be inhibited. We can speculate that this discrepancy can be due to a lag time between change in TGFB1 gene expression and downstream effects on transcriptional regulation. Interferon-gamma (IFNG) is a well characterized pro-inflammatory cytokine secreted by both innate and adaptive immune system cells with pleiotropic functions (Kopitar-Jerala, 2017). Following the first treatment cycle, given the expression changes of downstream genes, IPA identified IFNG as a significantly inhibited regulator suggesting a reduction in inflammatory mechanisms. Moreover, NFE2L2, also known as NRF2, showed a negative Z-score and, consistently with previous data, its expression is reduced and predicted to be inhibited. Finally, significant and negative Z-scores were also reported for FLT1 and TCL1A. The first one is also known as VEGFR1 and it is a receptor for vascular endothelial growth factor and involved in angiogenesis (Fischer et al., 2008), while T cell leukaemia/lymphoma 1A (TCL1A) is an oncogene involved in the maturation and development of T and B cells (Paduano et al., 2018).

Within the top 10 upstream regulators from the ΔD64 comparison, the only one showing also a significant Z-score was IL-21 which was predicted as activated. This cytokine exerts a wide range of biological functions including several immune suppressive effects such as IL-10 induction, promotion of B cell and DCs inhibition and reduction in the expression of LPS-induced pro-inflammatory cytokines. Moreover, IL-21 alterations have been associated with several autoimmune disorders (Leonard and Wan, 2016). Interestingly, although not showing a significant Z-score, several other transcriptional regulators with known anti-inflammatory properties were identified. In particular, the most significant (highest p-value of overlap) was FOXP3 but also GATA3 and IL10RA were reported. Overall, these results are in line with previous analysis indicating a broad immune suppression at D8, although a more evident immune regulation was evident at D64.

Table 3.3: Top 10 most significant upstream regulators.

This table illustrates the top 10 upstream regulators identified by IPA® in our two data sets: ΔD8 and ΔD64. For each regulator, its fold change (FC) is reported together with the Z-score, the prediction of its activation status (activated if Z-score>2 and inhibited if <-2) and p-value of overlap (Fisher's Exact statistical test).

ΔD8					ΔD64				
Upstream Regulator	FC	Z-score	Predicted activation	Overlap p-value	Upstream Regulator	FC	Z-score	Predicted activation	Overlap p-value
TP53	-1.54	-1.92	-	6.7E-07	FOXP3	3.34	0.68	-	4.0E-04
IL10	-1.25	0.09	-	1.3E-06	CBFB	1.22	-	-	9.8E-04
HNFA4	1.25	-0.92	-	3.4E-06	IL21	1.26	2.49	Activated	1.6E-03
TGFB1	1.25	-5.53	Inhibited	4.1E-06	GATA3	1.40	0.84	-	1.9E-03
FLT1	-1.51	-2.71	Inhibited	5.3E-06	IL10RA	1.93	0.91	-	2.1E-03
TCL1A	-1.48	-2.0	Inhibited	6.3E-06	RNASE2	4.20	0.78	-	2.1E-03
NFE2L2	-1.98	-5.46	Inhibited	9.7E-06	IL6	-1.35	0.98	-	3.2E-03
MTOR	-1.51	-1.65	-	1.7E-05	MAFB	-1.66	0.81	-	4.6E-03
IFNG	-1.60	-5.54	Inhibited	2.4E-05	STAT6	-1.39	1.36	-	5.1E-03
NLRP12	-2.00	-0.134	-	3.3E-05	PRKAA1	1.25	0.37	-	5.8E-03

3.5 Gene expression changes during the follow-up period

Transcriptional changes occurring in IMODALS patients during the follow-up period were analysed to investigate whether the ld-IL-2 effect was sustained once treatment ceased. The Limma package in R was used to generate a comparison called ΔD85. Similarly to what was done for ΔD8 and ΔD64, the transcriptome of 2MIU-IL2-treated patients at D85 was compared to their baseline (D1) and normalised to the same comparison within the placebo group. In this way, gene expression variation during the follow up period of the trial was analysed.

A total of 508 RefSeq transcripts were found to be significantly ($1.2 \leq FC \leq -1.2$ and p-value <0.05) differentially expressed (281 upregulated, 227 downregulated) (**Figure 3.24**). Interestingly, four main Treg and immune suppression markers (*FOXP3*, *IL2RA*, *CTLA4*, *IKZF2*) were no longer significantly differentially expressed at this time point. The comparison of their fold change (FC) from ΔD85 with the results retrieved from the previous analyses during the drug administration period (ΔD8 and ΔD64) showed that the expression of these markers progressively increased during the treatment cycles, but it dramatically decreased once it ceased (**Figure 3.25**). This suggested that 2MIU-IL-2-promoted Treg activation was no longer preserved at D85.

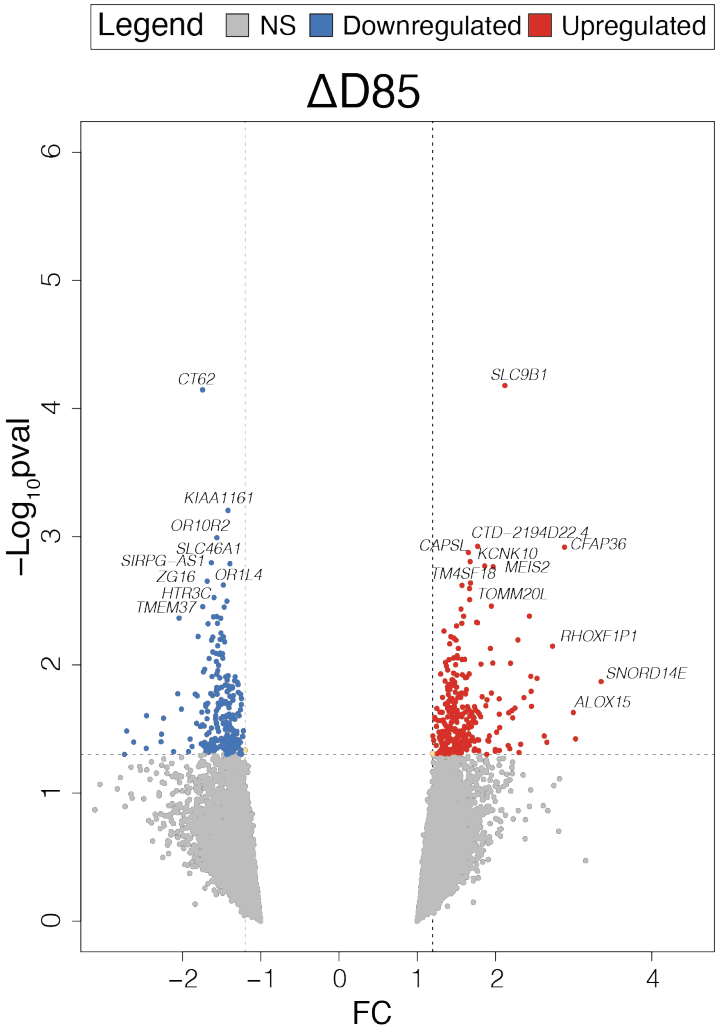

Figure 3.23: Transcriptional Changes During the Follow-up Period.

Volcano plot showing DEGs resulting from the comparisons ΔD85. DEGs are colour-coded depending on their fold change (FC) and their significance levels ($-Log_{10}$ p-value): non-significant transcripts or transcripts that failed the FC cut-off are reported in grey, significant and with FC ≤-1.2 in blue and significant and with FC ≥1.2 in red. Three black lines are also shown: the horizontal line indicates the significance threshold ($-Log_{10}$ p-value=1.3 or p-value=0.05) and the two vertical dotted lines mark the FC cut-offs at -1.2 and 1.2 respectively. (Empirical Bayesian statistics were conducted using Limma to find significant DEGs).

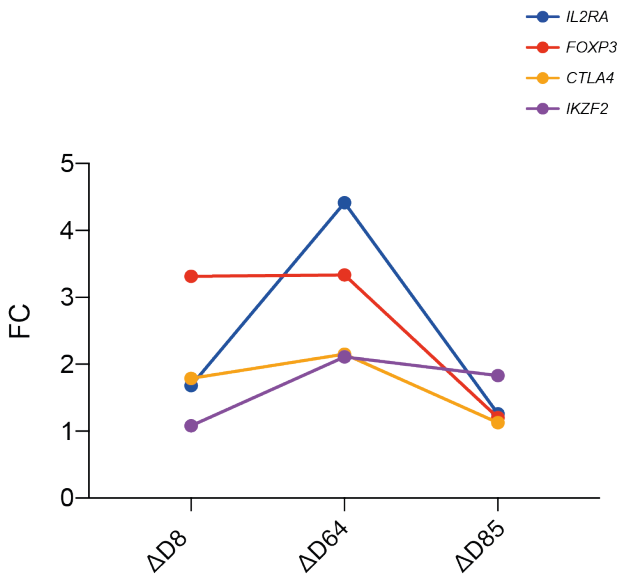

Figure 3.24. Longitudinal Comparison of Treg Marker Expression.

Plot displaying the variation in the expression of 4 key Treg activation and immune suppressive markers – *FOXP3*, *IL2RA*, *CTLA4* and *IKZF2*- throughout and after the administration period. Their expression increases during the 2MIU-IL-2 treatment and peaks at D64 but it decrease at D85. On the x-axis the different Limma comparisons are shown while on the y-axis each transcript FC is reported.

Furthermore, to investigate the biological functions of the upregulated and downregulated DEGs observed in ΔD85, a GO analysis was carried out using Enrichr. Twenty-five upregulated and 23 downregulated significantly enriched GO BPs were found and none of these were related to immunological processes (**Figure 3.27**). Interestingly though, an upregulation in mechanisms involved in CNS development, including neural tube development and neuron differentiation, were observed, while downregulation of neurotransmitter transport and axonogenesis was documented.

A

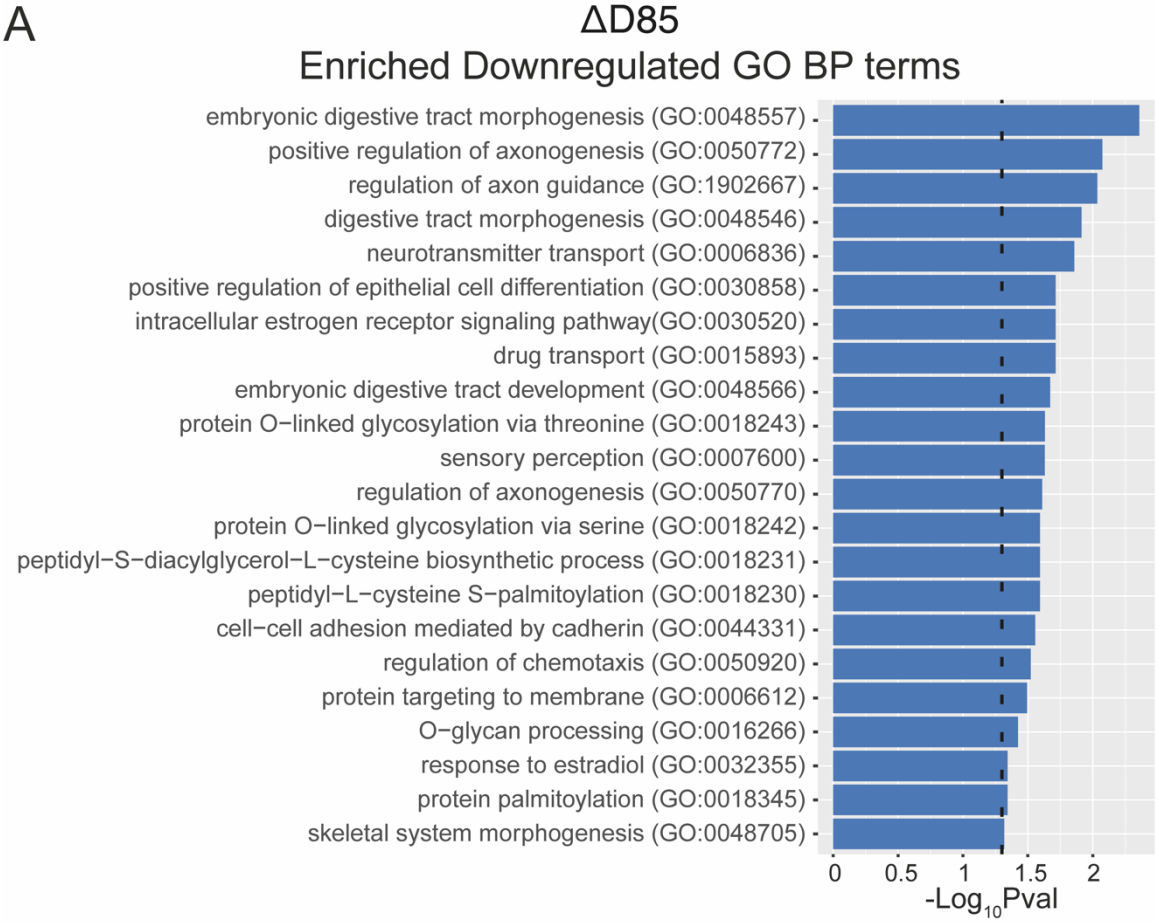
ΔD85
Enriched Downregulated GO BP terms
embryonic digestive tract morphogenesis (GO:0048557)
positive regulation of axonogenesis (GO:0050772)
regulation of axon guidance (GO:1902667)
digestive tract morphogenesis (GO:0048546)
neurotransmitter transport (GO:0006836)
positive regulation of epithelial cell differentiation (GO:0030858)
intracellular estrogen receptor signaling pathway(GO:0030520)
drug transport (GO:0015893)
embryonic digestive tract development (GO:0048566)
protein O−linked glycosylation via threonine (GO:0018243)
sensory perception (GO:0007600)
regulation of axonogenesis (GO:0050770)
protein O−linked glycosylation via serine (GO:0018242)
peptidyl−S−diacylglycerol−L−cysteine biosynthetic process (GO:0018231)
peptidyl−L−cysteine S−palmitoylation (GO:0018230)
cell−cell adhesion mediated by cadherin (GO:0044331)
regulation of chemotaxis (GO:0050920)
protein targeting to membrane (GO:0006612)
O−glycan processing (GO:0016266)
response to estradiol (GO:0032355)
protein palmitoylation (GO:0018345)
skeletal system morphogenesis (GO:0048705)
0
0.5
1
1.5
2
-Log10Pval

B

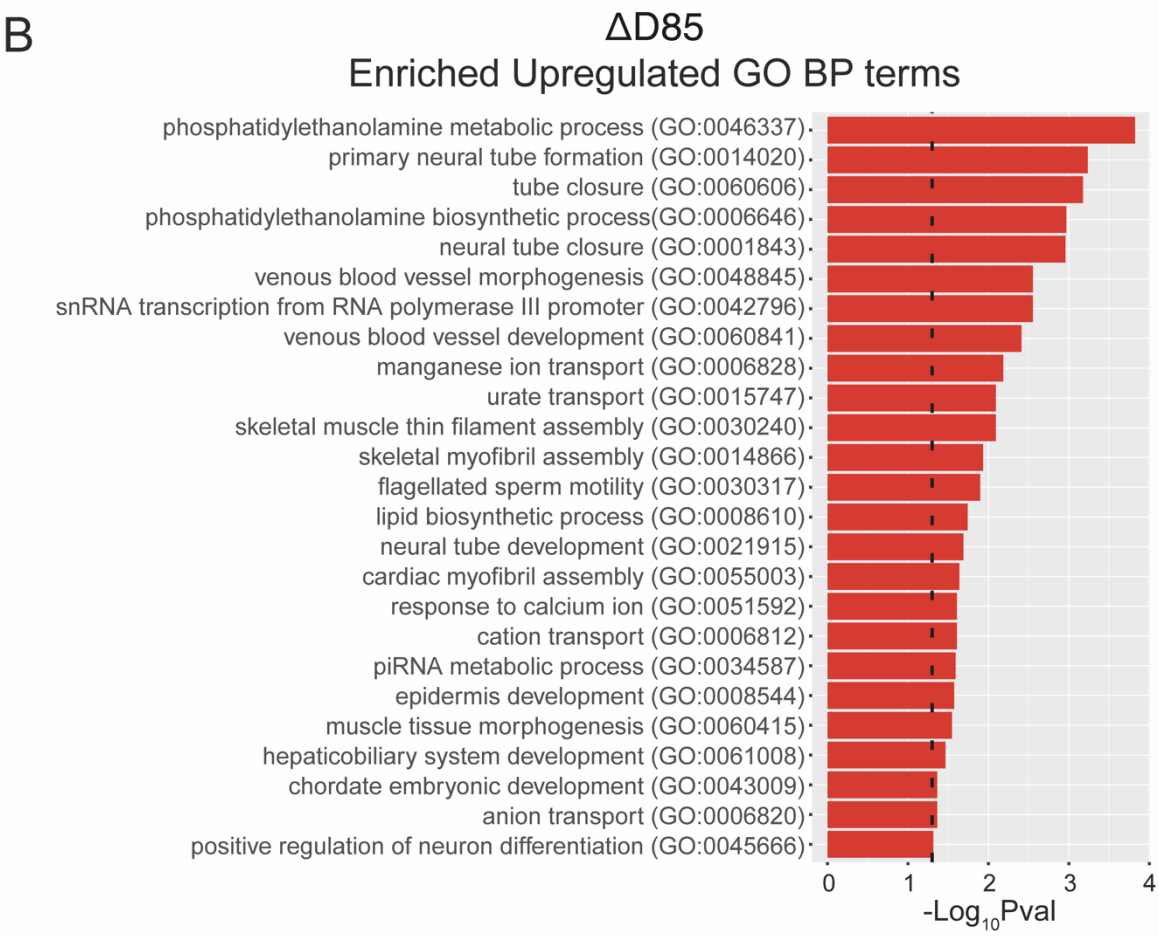
ΔD85
Enriched Upregulated GO BP terms
phosphatidylethanolamine metabolic process (GO:0046337)
primary neural tube formation (GO:0014020)
tube closure (GO:0060606)
phosphatidylethanolamine biosynthetic process(GO:0006646)
neural tube closure (GO:0001843)
venous blood vessel morphogenesis (GO:0048845)
snRNA transcription from RNA polymerase III promoter (GO:0042796)
venous blood vessel development (GO:0060841)
manganese ion transport (GO:0006828)
urate transport (GO:0015747)
skeletal muscle thin filament assembly (GO:0030240)
skeletal myofibril assembly (GO:0014866)
flagellated sperm motility (GO:0030317)
lipid biosynthetic process (GO:0008610)
neural tube development (GO:0021915)
cardiac myofibril assembly (GO:0055003)
response to calcium ion (GO:0051592)
cation transport (GO:0006812)
piRNA metabolic process (GO:0034587)
epidermis development (GO:0008544)
muscle tissue morphogenesis (GO:0060415)
hepaticobiliary system development (GO:0061008)
chordate embryonic development (GO:0043009)
anion transport (GO:0006820)
positive regulation of neuron differentiation (GO:0045666)
0
1
2
3
4
-Log10Pval

Figure 3.25: Gene Ontology Analysis During the Follow-up Period.

Bar plots showing 23 downregulated (**A**) and 25 upregulated (**B**) enriched Gene Ontology biological processes. Significance threshold lines are reported in black ($-Log_{10}$ p-value=1.3). (Fisher exact statistical test was performed using Enrichr and enrichment $-Log_{10}$ p-value is reported in these graphs).

Moreover, a different analysis was conducted with Metascape to visualise relationships between altered enriched processes. Upregulated and downregulated significantly ($1.2 \leq FC \leq -1.2$ and p-value <0.05) differentially expressed terms from ΔD85 were imported and analysed separately with this software (**Figure 3.27A** and **B**). Interestingly and differently from the Enrichr GO analysis, two immunological processes were identified to be downregulated, namely "chemotaxis" and "cytokine-cytokine receptor interaction". Amongst the upregulated pathways, several mechanisms involved in the development and differentiation of different organs and tissues was reported. Notably and consistently with the GO analysis, five processes involved in the positive regulation of neuron differentiation were upregulated which might suggest a possible effect of the three 2MIU-IL-2 treatment cycles on CNS cells.

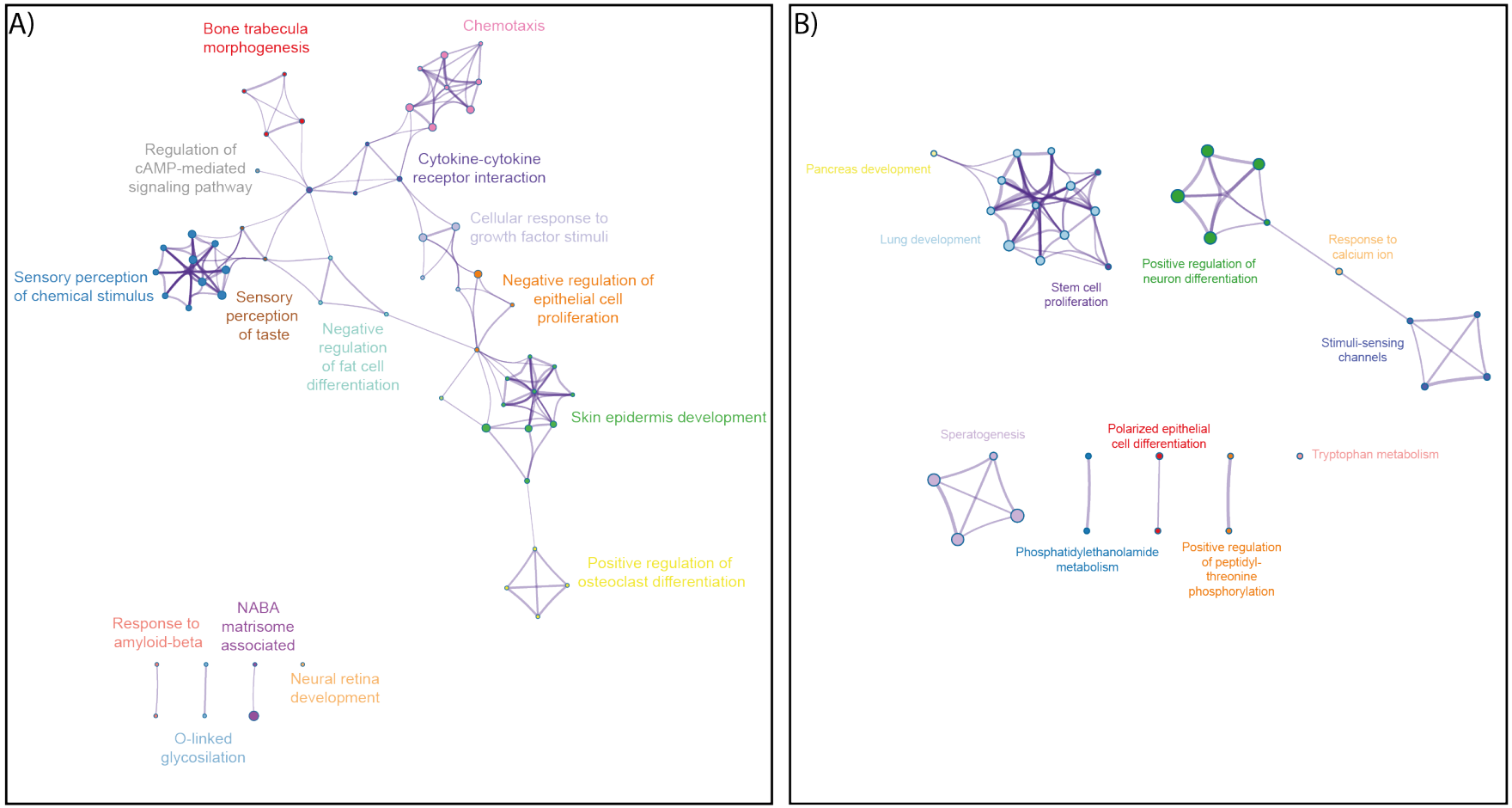

Figure 3.26: Metascape analysis in the follow-up period.

Enrichment networks generated with the software Metascape showing enriched clusters of pathways for the downregulated (**A**) and upregulated (**B**) gene lists outputted from the comparison ΔD85. Each node represents a pathway and terms showing a Kappa similarity score > 0.3 are connected by edges. Clusters are labelled and highlighted using different colours.

Given the identification of interesting pathways/processes suggesting an alteration in neuronal development/differentiation, neurotransmission and axonogenesis identified from both the GO and Metascape enrichment analyses at D85, transcripts included in all these processes were investigated in detail. Twenty-five unique RefSeq terms were reported amongst the CNS-related pathways, nine of which had a decrease expression while 16 showed were increased (**Figure 3.28**). Interestingly, several transcription factors involved in neurogenesis and neuronal development were amongst these altered transcripts. Moreover, transcripts associated with axonogenesis and regulation of neuronal branching (COBL, SLC25A12 and FEZ1) showed an increased expression after the end of ld-IL-2 treatment. However, downregulation of nerve growth factor (NGF) was also reported. This is a crucial factor which regulates the survival, proliferation and differentiation of neurons and its reduced expression might have detrimental consequences.

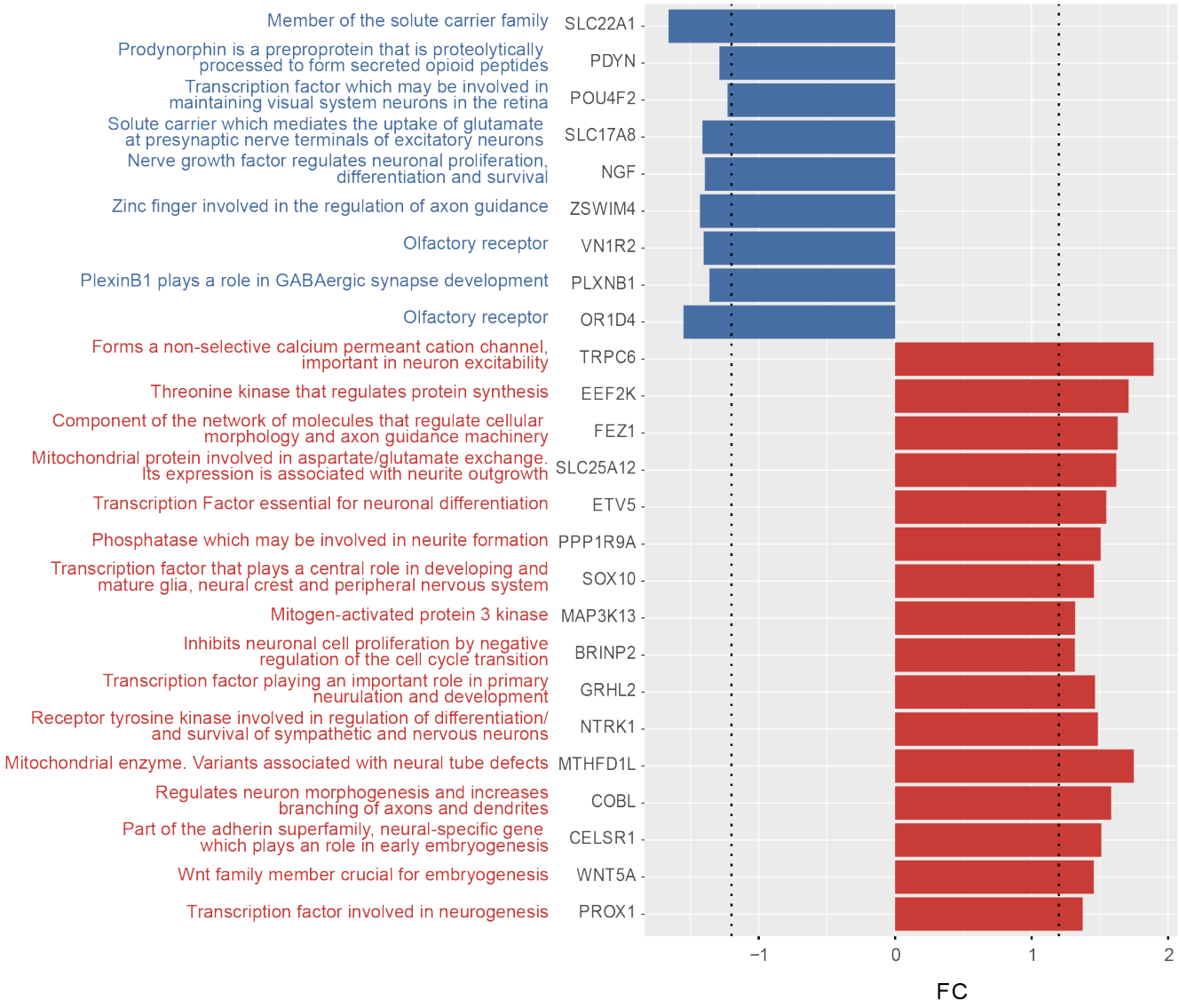

Figure 3.27: ΔD85 Transcripts included in CNS-related pathways

In this plot, all the transcripts included in the different CNS-related processes and pathways identified to be altered at D85 are reported. In particular, their fold change (FC) is displayed on the X-axis while the gene symbol is reported on the Y-axis. Moreover, a short description of each protein function is reported as well (source: GeneCards.org). Terms showing an increased expression are reported in red and decreased genes in blue. Two dotted lines are also displayed which indicate the FC cut-off set ($1.2 \leq FC \leq -1.2|$).

3.6 Microarray validation

Microarray data validation was performed through qRT-PCR. Four key Treg and immune suppression markers (*FOXP3*, *IL2RA*, *CTLA4*, *IKZF2*) were chosen and samples from all 2MIU-IL-2-treated and placebo patients across all time points were screened. In line with microarray data, qRT-PCRs showed a time-dependent increase in the mRNA levels of these markers during the administration period which peaked at D64 (**Figure 3.29**). This suggested an induction of immune suppression over time throughout the trial, with the maximum effect visible following the third treatment cycle. At D85, consistently with microarray gene expression data, this upregulation was no longer sustained and transcripts showed levels more comparable to the baseline. In contrast, no significant alterations were reported longitudinally within the placebo group. Notably, a considerable variability in the expression of the four markers was registered amongst 2MIU-IL-2-treated patients. This suggested the existence of inter-individual variations in the response of ALS patients to the drug. This finding is in line with flow-cytometry data (Camu et al., 2020) showing a wide range of Treg count increases during the administration period (standard deviation of Treg cells measured at D8=101.7 and at D64=144.8). Moreover, to further validate agreement between microarray and qRT-PCR data, expression values retrieved with the two techniques were correlated (Pearson's correlation). Significant positive correlations were reported for all the four markers (IL2RA R=0.547 and P-value=1.6E-08; FOXP3 R=0.477 and P-value=1.1E-06; CTLA4 R=0.42 and P-value=2.4E-05; IKZF2 R=0.358 and P-value=3.5E-04).

A)

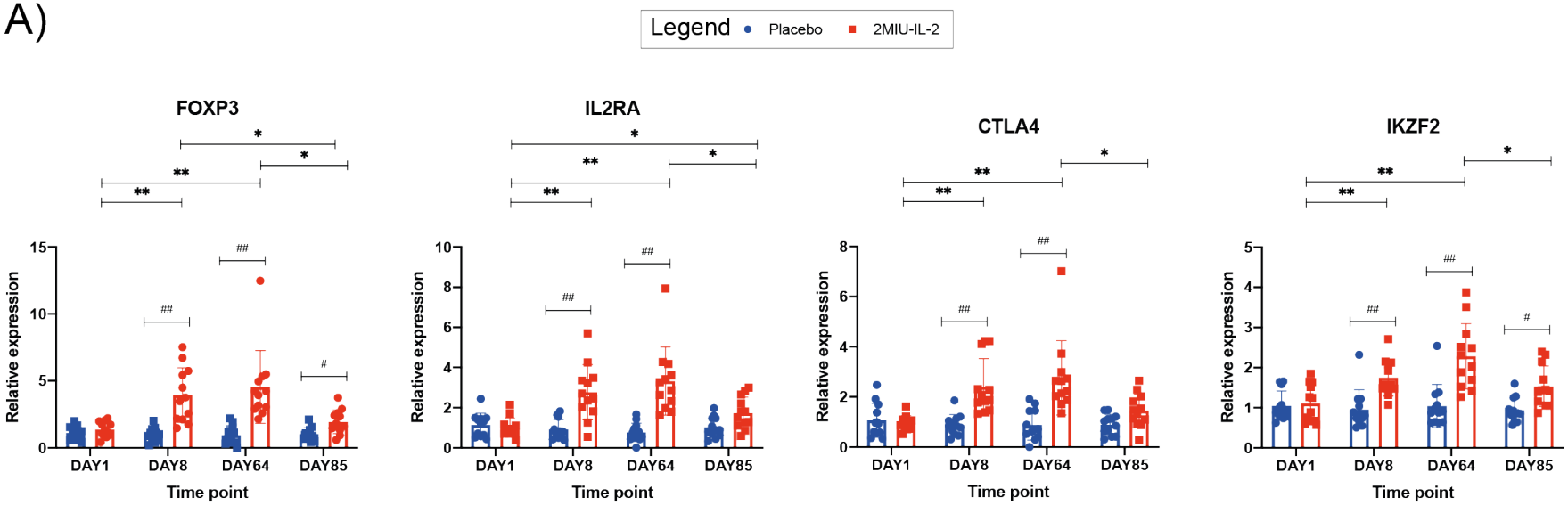
Legend
Placebo
2MIU-IL-2
FOXP3
IL2RA
CTLA4
IKZF2
Relative expression
Time point
DAY1
DAY8
DAY64
DAY85

B)

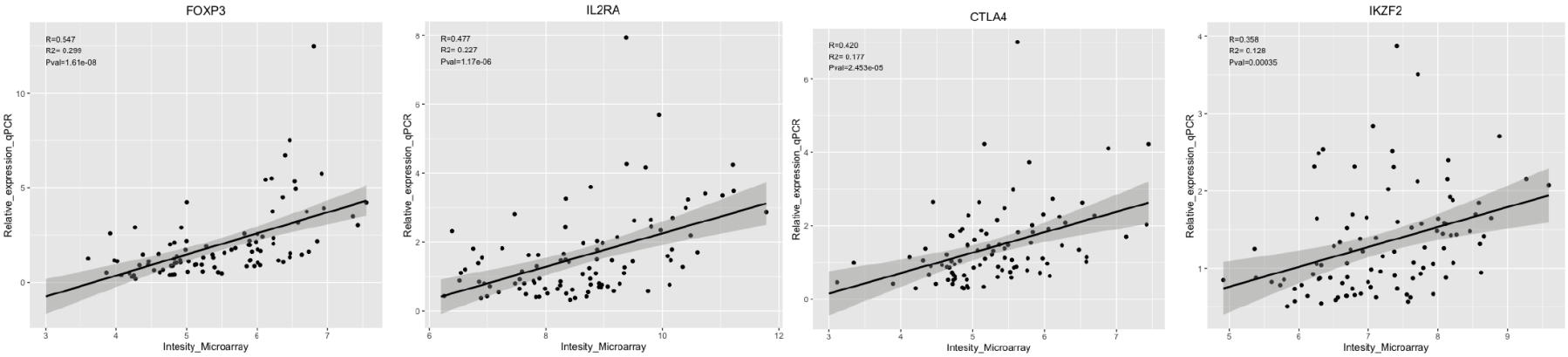
FOXP3
R=0.547
R2= 0.299
Pval=1.61e-08
IL2RA
R=0.477
R2= 0.227
Pval=1.17e-06
CTLA4
R=0.420
R2= 0.177
Pval=2.453e-05
IKZF2
R=0.358
R2= 0.128
Pval=0.00035
Relative_expression_qPCR
Intesity_Microarray

Figure 3.28: Microarray validation

(**A**) Graphs showing expression of *FOXP3*, *IL2RA*, *CTLA4* and *IKZF2* in 2MIU-IL-2 treated (in red) and placebo (in blue) patients at the 4 different time points. Data were generated through qRT-PCR. A time-dependent activation of these markers is reported in the ld-IL-2 group. Box plots display mean $\pm$ SD (technical replicates=3). A two-way ANOVA with either Sidak (for comparisons between different treatment regimens, significant differences indicated with *) or Tukey (for comparisons between time points within the same treatment type, significant differences indicated with #) correction for multiple comparisons was conducted. * or #: Adjusted p-value<0.05, ** or ##: Adjusted p-value<0.01. (**B**) Plots showing correlation between SST-RMA-normalized microarray intensity values and qRT-PCR relative expression. Regression lines (black) and their regression confidence bands (grey) are also shown. Each dot represents a sample belonging to a patient at a certain time point.

In conclusion, microarray gene expression data were validated as they were in line with qRT-PCR findings. Nonetheless, a considerable variation was reported amongst the 2MIU-IL2-treated patients in the level of upregulation of the four Treg markers. Further analysis and discussion relating to these variations is provided in the next chapter.

3.7 Discussion

The overall aim of the work described in this chapter was to generate gene expression profiles from participants recruited into the IMODALS clinical trial to evaluate transcriptomic changes at selected time points and longitudinally throughout the trial. Moreover, differences between the two treatment regimens (1MIU and 2 MIU-IL2) were assessed. A summary of the main results obtained from this section of the study is provided below:

1) Total RNA was extracted from white blood cells at different time points (D1, D8, D64 and D85) and used to generate microarray gene expression profiles. Overall good quality RNA was obtained and microarrays were produced for all the samples except for 68WKU83 (patient C01P011 at D8) whose RNA was degraded. Nonetheless, QC analysis was successful for the remaining 107 microarray gene expression profiles, therefore data quality was ascertained.

2) The first comparative analysis performed focused on studying patients' transcriptional reaction following three administration cycles. Hence, data at D64 were analysed, the time at which the response to ld-IL-2 was hypothesized to have reached a peak. Evidence of different transcriptional status between the three investigated groups (1MIU, 2MIU-IL2 and placebo) was provided in a PCA, where a clear spatial separation was visible. Gene expression and gene enrichment analyses were performed and the higher dosage revealed a broader degree of immune regulation. In addition, dose-dependency was identified for the majority (approximately 70%) of the commonly differentially expressed genes.

3) Longitudinal gene expression analyses were performed in order to assess transcriptional changes occurring throughout the administration period. Specifically, two comparisons were produced, namely ΔD8 and ΔD64, so that 2MIU-IL-2 patients' transcriptomes at specific time points was compared to their baseline levels and normalised to the same comparison

in the placebo group. These comparisons were analysed alongside to highlight similarities and differences in gene expression changes associated with the different stages of the trial. Whilst a broad immune suppression was found at the early trial time point, evidence of the expansion of the Treg population and activation of immune regulative processes was predominantly reported at D64.

4) Transcriptional changes during the follow-up period were also investigated. Similarly to the previous longitudinal analyses, the gene expression profiles of 2MIU-IL-2 treated patients at D85 (24 days after the last injection) were compared to the baseline and normalised to the placebo group. The ld-IL-2-induced transcriptional variations reported during the course of the trial were not sustained following the end of the ld-IL-2 treatment. Nonetheless, some interesting CNS-related pathways were found to be altered at this time point.

5) Lastly, microarray validation was also carried out through a qRT-PCR screening of four Treg markers (*FOXP3*, *IL2RA*, *CTLA4* and *IKZF2*). Significant and positive correlations were reported for all the investigated transcripts between microarray and qRT-PCR data.

The initial analysis of microarray gene expression data at D64 revealed that the higher drug concentration (2MIU-IL-2) was able to induce a greater degree of transcriptional regulation compared to 1MIU-IL-2. Specifically, an almost double amount of differentially expressed genes (DEGs) was found in the 2MIU_vs_Placebo comparison compared to 1MIU_vs_Placebo. More interestingly, functional and biological processes characteristic of each treatment group were identified following gene enrichment analyses. The unique list of genes differentially expressed in the comparison 1MIU_vs_Placebo was enriched in processes including cholesterol and phospholipid homeostasis, nucleoside catabolism and apoptosis regulation. Only a minor number of immune-related mechanisms were identified in this comparison. In contrast, a more evidence of immune regulation was visible in the list characteristic of 2MIU_vs_Placebo. In particular, genes involved in the regulation of the adaptive immune system were solely enriched in this comparison, suggesting a broader

immune modulation promoted by the higher ld-IL-2 dose. Moreover, genes implicated in cellular processes (including intra-cellular transport, transposition, Ca^{2+} and K^{+} signaling), cell cycle and RNA metabolism were differentially expressed in 2MIU_vs_Placebo. The latter mechanism is particularly interesting in the context of ALS given the RNA dysregulation characteristic of the disease (Butti and Patten, 2018). Specifically, genes involved in RNA (mRNA and tRNA) subcellular transport were particularly enriched in the 2MIU_vs_Placebo dataset. Several pieces of evidence in the literature reported an RNA transport impairment in this disease which is particularly associated with mutation in ALS-causing genes such as TDP-43, FUS and C9orf72 (Coyne et al., 2017).

A considerable proportion of transcripts (1160 of which 375 were RefSeq-annotated) were commonly differentially expressed in both comparisons. Their GO analysis revealed a significant enrichment in processes such as the differentiation, function and migration of the T cell subset and in the regulation of production, secretion and signaling of several cytokines (including IL-10, IL-2, IL-4, IL-7 and IL-15). Additionally, results from the Metascape analysis showed specific evidence of Treg mediated immune-modulation with terms such as: "RUNX1 and FOXP3 control the development of regulatory T lymphocytes", "Immunoregulatory interaction between lymphoid and non-lymphoid cell", "negative regulation of immune system process" and "PID IL2 STAT5 signaling pathway", being enriched. This suggested that both ld-IL-2 doses were able to promote an alteration within the immune system and an upregulation of Treg markers. Nonetheless, 2MIU-IL-2 seemed to induce a more pronounced immune-regulation and, in fact, a dose-dependent expression was identified for the majority (~70%) of the commonly DEGs common to both treatment groups. This is in line with results reported by Camu et al. which showed a dose-dependent increase in the percentage of Tregs in IMODALS participants (Camu et al., 2020). Interestingly, ganglioside, ceramide and lipid metabolism were also reported as commonly altered at the end of both 1MIU and 2MIU IL-2 treatments and the genes included in such processes had increased levels of expression. These mechanisms have been implicated in the pathogenesis of several neurodegenerative diseases, including ALS. In particular, gangliosides and ceramides were suggested to be modulators of disease progression (Moll et al., 2020). Conflicting results have been found and it is still debated whether increased or decreased levels are associate with disease pathogenesis. Nonetheless, recent findings in $SOD1^{G93A}$ mice suggested that the

inhibition of glucosylceramide synthase accelerated disease progression (Dodge et al., 2015). Additionally, mutations in the glycosyltransferase GLT8D1 were associated with a familial form of ALS and caused a reduced enzyme activity (Cooper-Knock et al., 2019). Thus, modification in these processes and increased gene expression can potentially contribute to the beneficial effects of ld-IL-2 in ALS patients although further investigation is needed.
Given the reported dose-dependent trend and cost constrains, further analyses were conducted comparing only 2MIU IL-2 with placebo participants.

Longitudinal transcriptional analyses identified a broad differential expression in the comparison at ΔD8 (2643 significantly DEGs). This can be interpreted as a prompt response of the individual to the newly administered drug during the first treatment cycle. Over the course of the trial though, an adaptation probably occurred and less DEGs were reported at ΔD64. Notably, while most of the genes showed reduced level of expression in ΔD8, more upregulation was reported at the later time point.
GO gene enrichment and IPA® pathway analyses were carried out to identify mechanisms longitudinally altered with the treatment. Both revealed a sharp inhibition of inflammatory pathways after the first administration cycle (ΔD8). In particular, transcripts associated with the function of both innate (neutrophils, eosinophils, macrophages and natural killers) and adaptive immune cells (cytotoxic T cells and B cells) were downregulated at D8. Of importance, evidence of dysregulation in the two branches of the peripheral immune systems is reported in the ALS literature. In particular, neutrophil activation correlates with disease severity, predicts patient survival and increased expression of neutrophil-specific markers was documented in the ALS blood transcriptome compared to healthy controls (Choi et al., 2020, Swindell et al., 2019, McGill, 2020). Moreover, natural killer cell alterations in the peripheral blood, as well as their infiltration in the spinal cord and motor cortex of ALS patients was registered (Gustafson et al., 2017, Garofalo et al., 2020). Although the role of monocytes/macrophages in ALS is still to be elucidated and controversial findings have been reported, recently, total CD14+ monocyte levels were found to be significantly higher and they showed increased M1 activation and pro-inflammatory abilities (McCombe et al., 2020, Jin et al., 2020, Du et al., 2020). Moreover, adaptive immune system cells such as cytotoxic T cells are known to infiltrate the CNS in ALS and contribute to MN loss (Coque et al., 2019, Nardo et al., 2018). NF-kB and cytokine

signalling pathways and diapedesis of leukocytes was also inhibited after the first treatment cycle and this may contribute to the early stage immune-suppression induced by ld-IL-2. Furthermore, cell death mechanisms were reported to be activated at this time point. Although this might be perceived as a detrimental effect, these processes seemed to be limited to leukocytes. However, this process specificity toward leukocytes should be further investigated to exclude possible toxic effects on other cell types. In contrast, pro-survival effects were reported on CNS cells with cell death pathways being downregulated relating to brain and cortical neurons. Taken together these data suggest that the initial suppression of the immune system may have beneficial effects by dampening the widespread inflammation characteristic of ALS. This seems to be a short-term effect given that the downregulation of the majority of the inflammatory pathways was no longer present at D64. However, a robust activation of immune-regulatory processes was observed at this later time point, with evidence of progressive and time-dependent activation of both Tregs and Th2 being provided. Of importance, Th2 share anti-inflammatory and neuroprotective properties with Tregs and both cell types are reduced in ALS patients (Beers et al., 2011a, Zhao et al., 2012). Lymphocyte suppression and apoptosis induction were recorded at D64 which might be due to the inhibitory action of Treg/Th2 on inflammatory cells. We can speculate that this Treg/Th2 activation, if sustained over time through continued ld-IL-2 administrations, could lead to a more evident physiological immune-modulation and possibly to the re-establishment of an immunological homeostasis.

Alongside immunological pathway alterations, ld-IL-2 appeared to affect other biological mechanisms. The "protein ubiquitination pathway" and the "NFR2-mediated oxidative stress response" were altered at D8. Given that these processes are disrupted and implicated in the pathogenesis of ALS, a further downregulation consequent to the drug administration may be detrimental. To investigate on this possibility, transcripts included in these processes were analysed in more detail. Dysregulation in proteostasis is a well-known pathological mechanism of ALS. In particular, alteration in protein folding and the consequent aggregation together with defective protein degradation, have been regularly reported in the ALS literature (Medinas et al., 2017, Malik and Wiedau, 2020). The genes included in the IPA "protein ubiquitination pathway" were mainly coding for subunits of the proteasome, ubiquitination or heat shock proteins. A Metascape analysis revealed a close association between these proteins and MHC class I mediated antigen processing and

presentation. Such a mechanism is crucial for pathogen recognition and the initiation of the adaptive immune response. Therefore, it can be speculated that a downregulation of these transcripts at D8 reflected a prompt suppression of inflammatory processes rather than a detrimental effect. In fact, the ubiquitin-proteasome system has been previously reported in the literature as crucial for the formation of the immune-proteasome and immune cells substantially rely on this mechanism for the production of cytokines and immunoglobulins (Kammerl and Meiners, 2016, Çetin et al., 2021). Nonetheless, further investigations is needed to exclude the downregulation of genes involved in the protein-ubiquitination pathway in CNS cells to rule out the possibility of a further impairment in the proteostasis function.

NFR2 is a transcription factor which promotes the expression of free radical scavengers, anti-oxidants but also anti-inflammatory molecules (Sivandzade et al., 2019). Excessive reactive oxygen species (ROS) generation, oxidative stress and consequently oxidative damage are crucial mechanisms in ALS pathophysiology (Barber and Shaw, 2010). Moreover, dysregulation in NRF2 signalling pathways has been reported in both ALS models and patients' samples and it is now considered a promising therapeutic target for this disease (Johnson and Johnson, 2015, Mead et al., 2013). Therefore, the observed inhibition of NFR2 pathways could potentially represent a detrimental short-term effect of ld-IL-2 given that this suppression was not detected at D64. However, considering the concurrent downregulation of mechanisms involved in the metabolism, synthesis and production of ROS, we can speculate that ld-IL-2 could instead have an anti-oxidant effect dampening the production oxidative species and therefore reducing the need for NRF2-mediated activation of anti-oxidant genes. However, further research is necessary to demonstrate the validity of this hypothesis.

Consistently with previous results, the IPA upstream regulator analysis identified genes with immunological functions as able to recapitulate the overall gene expression changes in the comparison ΔD8. In particular, *TGFB1*, *IFNG* and *TCL1A* appeared to be inhibited with a significant Z-score. Moreover, as expected, *NFE2L2*, also known as *NRF2*, was reported as inhibited at D8. In contrast, the more anti-inflammatory *IL-21* was predicted as activated by IPA in the comparison ΔD64. Additionally, despite not reaching a significant Z-score and obviating the possibility of activity prediction

was not possible, other crucial immune-suppressive genes were identified as upregulated at ΔD64, including *FOXP3* and *GATA3*.

The analysis during the follow-up period revealed that the immune-regulatory effect of ld-IL-2 was no longer preserved at D85 and the expression of Treg markers (*FOXP3*, *IL2RA*, *CTLA4* and *IKZF2*) was comparable to baseline levels. These findings are consistent with results shown by Camu et al. who reported a decrease in the percentage of Treg in patients' blood when treatment ceased (Camu et al., 2020). Nonetheless, 508 transcripts were found to be differentially expressed at this post-treatment time point. Their enrichment analysis revealed no clear alteration in immunological pathways, although some CNS developmental processes were upregulated (neural tube formation, development and closure and positive regulation of neuron differentiation) while axonogenesis and neurotransmitter transport were downregulated. Given the potential importance of these mechanisms in neurodegeneration, transcripts included in these processes were investigated in more detail. Interestingly, transcription factors implicated with neuron differentiation (including *SOX10*, *GRHL2* and *PROX1*) showed an increased expression at D85. Moreover, genes involved in neurite outgrowth and axonogenesis were also upregulated (*COBL*, *SLC25A12* and *FEZ1*). This is consistent with previous findings which proposed IL-2 as a neurotrophic factor able to promote morphological changes in cultured neurons including an increase in neurite length and branching index (Sarder et al., 1993, Shen et al., 2010). Nonetheless, these transcriptional changes need to be validated in neuronal cells to ascertain this possible protective effect. Surprisingly, and in contrast with the above findings, the expression of the nerve grow factor (NGF) was slightly decreased (FC= -1.39). This protein regulates neuronal proliferation and survival and therefore its reduced expression could represent a detrimental effect, if confirmed in MNs.

In line with microarray data, a time-dependent increase in the expression of all of these transcripts measured via qRT-PCR was reported within the 2MIU-treated group, whereas no significant variations were observed in placebo participants. In particular, Treg-specific marker expression peaked at D64 which suggests the existence of a cumulative reaction where residual effects of the first two administration cycles impact on the last one. During the follow-up post-treatment period though, 2MIU-IL-2 effect

was no longer sustained and expression levels were comparable to the baseline. Interestingly, this analysis revealed evidence of inter-individual dissimilarities in terms of individual patient responses to ld-IL-2. This is consistent with data presented by Camu et al. (Camu et al., 2020) and the great variability among participant responses in terms of Treg expansion previously reported in other clinical trials evaluating the effects of ld-IL-2 in other autoimmune disorders (Hartemann et al., 2013, Koreth et al., 2011, Rosenzwajg et al., 2018, He et al., 2020). Further discussion and analysis regarding these inter-individual dissimilarities is provided in the Chapter 4.

Chapter 4 – Results: IMODALS Patient Variability and Predictive Biomarker Identification

The previous chapter provided insights on the transcriptomic differences amongst IMODALS trial participants following treatment with low-dose IL2 (ld-IL-2) at different time points and dissimilarities in drug-mediated Treg stimulation were reported. For this reason, the work describes in this chapter aimed to further investigate these inter-individual differences and to identify proposed predictive biomarkers that, given their level of gene expression at baseline, were able to forecast patient responsiveness to ld-IL-2 following three cycles of treatment. Data shown in this chapter were published together with a selection of the results shown in chapter 3 as part of an original article in the journal *Brain Communications* (Giovannelli et al., 2021) (see **Appendix 1**).

4.1 NanoString Analysis

Previous reported gene expression data suggested the existence of differences in the magnitude of different Treg marker upregulation within patients throughout the trial (see chapter 3). This is consistent with flow-cytometry data (as measured by our collaborators Dr Timothy Tree and Dr Marius Mickunas at King's College London) which suggested variability in the Treg count following 2MIU-IL-2 administration (Camu et al., 2020). Some participants (e.g. C01P021, C01P003) showed a rapid and almost exponential increase in their Treg numbers following drug treatment, whilst other individuals (e.g. C01P036, C01P016) seemed to have expanded their Treg population only mildly at D8 and maintained it at constant level with limited or no further increases at D64 (**Figure 4.1**).

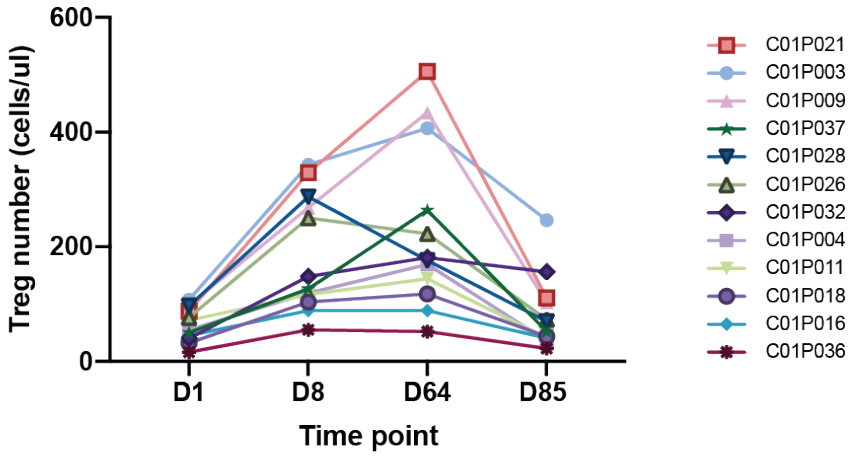

Figure 4.1: Treg Expansion Variations in IMODALS Participants

Graph displaying the number of Tregs per µl of blood of each 2MIU IL-2-treated participant at each time point (Flow-cytometry data). Patients are shown with different colours and their IDs are reported in the legend.

Therefore, classification criteria were proposed and ALS participants were subdivided into low, moderate and high Treg-responders depending on their regulatory T cell counts as measured at D64. Thus, arbitrary criteria were set as: high responders: $Treg_{D64}$ > 250 cells/µl of blood; moderate responders: $Treg_{D64}$ between 250 and 150 cells/µl of blood; low responders: $Treg_{D64}$ < 150 cells/µl of blood (see Methods section, **Table 2.2**). Importantly, no significant differences were reported in terms of age or disease progression (One-way ANOVA statistical analysis with Tukey's multiple comparisons) between these three participant subgroups (**Figure 4.2**). The exclusion of these two factors as possible confounding variables is key for the interpretation of our data.

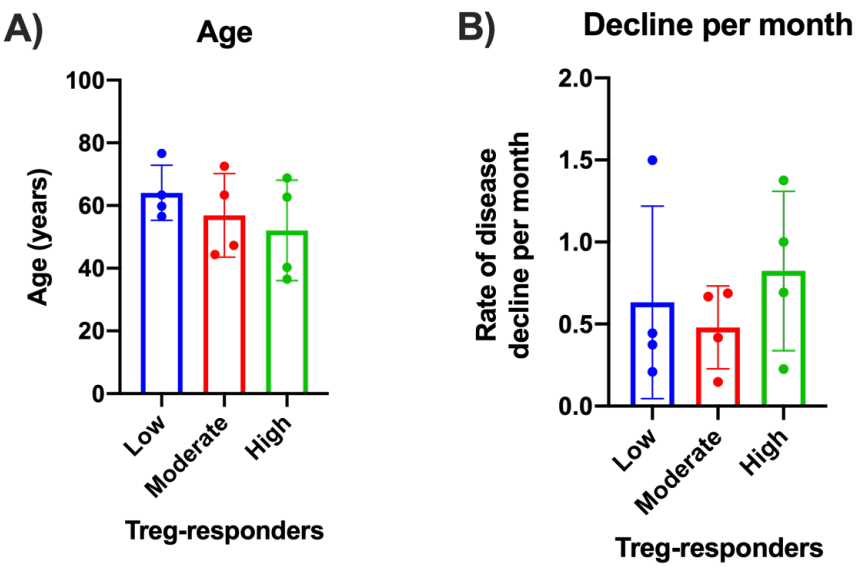

Figure 4.2: Age and Disease Decline in 2MIU-IL2-Treated Patients.

Bar plots showing no significant differences between low, moderate and high Treg-responders in terms of age (**A**) or disease decline per month (as reported in Table 2.2, page 79) based on points of decline and the ALSFRSR (**B**). Graphs display mean ± standard deviation.

The aim of this part of the study was to evaluate the transcriptional response to ld-IL-2 and how this related with the observed differences in Treg counts. In particular, we intended to assess whether these dissimilarities were due to changes in immunological transcriptome of the patient group. For this reason, four high, four low responders and 4 placebo participants were selected and their RNA samples at D1, D8 and D64 were analysed using the NanoString Autoimmune Discovery Panel. This contains a total of 755 transcripts: 740 pro- and anti-inflammatory mediators and 15 housekeeping controls. Notably, data from D85 was not included in this analysis as we aimed to identify transcriptional dissimilarities underlying the differences in the magnitude of Treg expansion during the active treatment period and also because previously reported evidence showed a reduced immune modulatory effect of ld-IL-2 in the follow-up period.

4.1.1 NanoString Quality Control

NanoString gene expression data were analysed using the software nSolver 4.0 in order to assess their quality. For each sample, several quality control (QC) parameters were computed by the software (see section 2.1.7) (**Table 4.1**):

- **Imaging QC**: this metrics indicates the fields of view (FOVs) successfully captured by the instrument. A score of at least 0.75 should be documented in order to considered the data robust. As reported in the table, all the samples passed this QC metric.

- **Binding density QC**: this parameter reports the concentration of barcodes detected by the instrument. The ideal binding density range should be from 0.1 and 2.25. The vast majority of our samples exceeded this range. As reported on the nanoString manual, a plausible explanation of this would be the high input amount of RNA used. In fact, as previously mentioned in section 2.1.7, higher RNA concentrations were used due to prior poor data obtained using the quantities recommended by the company. Consequently, given that more RNA sample was loaded, higher barcode density was reported. However, as indicated by the nanoString user guide, if the binding density is only slightly out of range it does not indicate a problem and it can be ignored. Therefore, we still considered the data to be reliable.

- **Positive control QC**: this score illustrates the correlation between the known concentrations of positive controls included in the panel and the counts measured by the instrument. This value should be equal or greater than 0.9 and the vast majority of our samples passed this threshold. Only four samples showed lower scores. However, given that they were only slightly outside the range (0.86-0.89), they were also considerate acceptable.

- **Limit of detection QC**: this metric indicates whether counts of the positive control POS_E are significantly above the counts of negative controls. If this is at least two standard deviations higher, the sample has passed this QC metric.

As reported in **Table 4.1**, most of the samples did not meet this criterion. However, when closely investigated, the count mean of the all negative controls (NEG_A to NEG_H) is lower the POS_E across all samples (**Figure 4.3A**). Nonetheless, higher counts than expected were recorded for NEG_D and H in all the samples whilst the other controls showed counts close to 0 as anticipated. This is visible in **Figure 4.3B** where the removal of NEG_D and H increased the expression difference between negative controls and POS_E. As reported in the nanoString user manual, these results in one or two negative controls could happen due to cross-hybridization with probe targets in the samples, which is frequent when using high concentrations of RNA as input. In this case, it is advised to closely inspect both positive and negative controls. If positive controls show progressively decreasing concentrations and if only one or two negative controls are markedly different to the expected values, the data is very likely to be robust and reliable. Given that the positive controls from all of our samples showed the anticipated expression pattern with POS_A > POS_B > POS_C > POS_D > POS_E > POS_F (**Figure 4.4**) and, as previously mentioned, only NEG_D and H had higher counts, our data were considered robust.

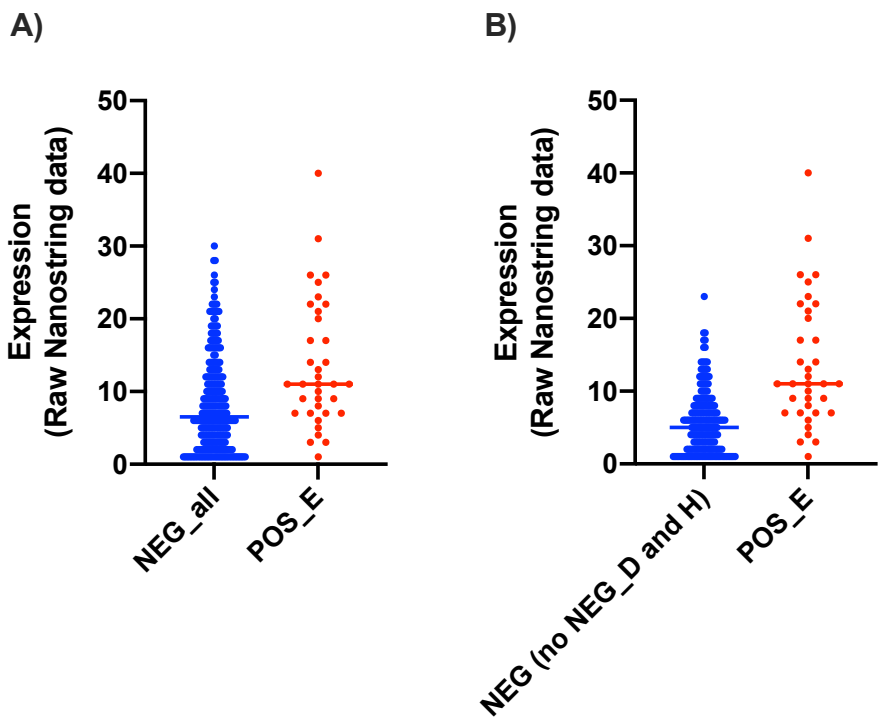

Figure 4.3. Count Differences between Negative Controls and POS_E.

Dot plots showing the raw counts of POS_E and either all the negative controls **(A)** or excluding NEG_D and H **(B)** across all the samples screened. The horizontal line indicates the mean expression. NEG_D and H showed higher raw counts than expected which was probably due to cross-hybridization. Their exclusion increased the differences with POS_E.

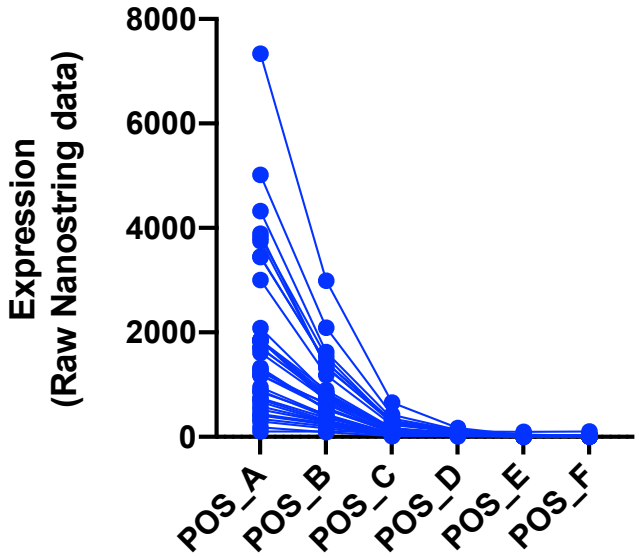

Figure 4.4. NanoString Positive Control Expression.

This graph displays the raw counts of all the positive controls in all the samples. Positive controls belonging to the same sample are connected with lines. POS_A to POS_F showed a decreasing pattern consistent with the standard concentrations described by the manufacturer.

Taken together, these results suggested that the transcriptional data generated with the nanoString platform were of acceptable quality and were therefore used for further gene expression analysis.

Table 4.1: NanoString Data QC summary

Tables 4.1a and 4.1b summarise the quality control scores obtained from the Autoimmune Discovery nanoString panel. Sample characteristics are reported including: patient IDs, visit day, treatment and response type. These were split and run into three different cartridges as indicated in the column "run". Raw QC values are reported for each metric (imaging QC, binding density QC, positive control QC and limit of detection) and scores outside the reference range are reported in red

Table 4.1a

Run	Patient code	Day	Treatment Type	Response Type	Imaging QC	Binding Density QC	Positive Control QC	Limit of detection QC
1	C01P003	1	2MIU	High	0.99	2.71	0.99	20.55
1	C01P003	8	2MIU	High	1	2.38	0.99	26.34
1	C01P003	64	2MIU	High	0.98	1.97	0.99	20.66
1	C01P018	1	2MIU	Low	0.95	3.52	0.86	14.29
1	C01P018	8	2MIU	Low	0.98	3.25	0.94	19.67
1	C01P018	64	2MIU	Low	1	2.28	0.99	25.48
1	C01P021	1	2MIU	High	1	0.18	0.97	5.62
1	C01P021	8	2MIU	High	1	2.55	0.99	19.84
1	C01P021	64	2MIU	High	1	1.64	0.99	23.96
1	C01P022	1	Placebo	NA	0.96	3.18	0.95	15.44
1	C01P022	8	Placebo	NA	0.95	3.31	0.87	22.45
1	C01P022	64	Placebo	NA	1	1.59	0.99	22.27
2	C01P011	1	2MIU	Low	0.98	2.85	0.98	20.71
2	C01P011	8	2MIU	Low	0.99	2.52	0.99	17.58
2	C01P011	64	2MIU	Low	1	2.79	0.98	16.86
2	C01P012	1	Placebo	NA	0.99	2.51	1	17.23
2	C01P012	8	Placebo	NA	0.98	3.14	0.97	26.92
2	C01P012	64	Placebo	NA	0.98	2.87	0.99	19.37
2	C01P009	1	2MIU	High	1	2.65	0.99	23.83
2	C01P009	8	2MIU	High	1	2.88	0.98	24.55
2	C01P009	64	2MIU	High	0.99	2.39	0.98	23.16
2	C01P017	1	Placebo	NA	0.98	3.21	0.94	23.46
2	C01P017	8	Placebo	NA	0.97	3.24	0.95	22.12
2	C01P017	64	Placebo	NA	0.91	3.38	0.95	23.27

Table 4.1b

Run	Patient code	Day	Treatment Type	Response Type	Imaging QC	Binding Density QC	Positive Control QC	Limit of detection QC
3	C01P031	1	Placebo	NA	1	2.28	1	19.43
3	C01P031	8	Placebo	NA	1	2.98	0.95	20.85
3	C01P031	64	Placebo	NA	0.94	3.34	0.89	18.62
3	C01P037	1	2MIU	High	0.99	2.97	0.97	28.22
3	C01P037	8	2MIU	High	0.97	2.93	0.98	22.41
3	C01P037	64	2MIU	High	0.99	3.02	0.97	17.18
3	C01P016	1	2MIU	Low	1	2.61	0.99	17.12
3	C01P016	8	2MIU	Low	0.96	3.38	0.88	15.88
3	C01P016	64	2MIU	Low	1	3.19	0.96	20.27
3	C01P036	1	2MIU	Low	0.98	3.32	0.92	29.64
3	C01P036	8	2MIU	Low	0.99	2.98	0.97	20.96
3	C01P036	64	2MIU	Low	0.97	3.16	0.93	24.55

4.1.2 NanoString Gene Expression Analysis and Validation

Following data generation and normalisation (section 2.1.7), gene expression profiles were analysed with the aim of finding, across different time points (D1, D8, D64), immunological transcripts differentially expressed between patients showing marked dissimilarities in Treg counts at the end of the trial (low, high-Treg responders and placebo).

A heatmap displaying all the 740 transcripts included in the panel was produced in order to gain a general overview of the transcriptional status across patient groups (**Figure 4.5**). An evident difference in gene expression was clearly visible at baseline between high and low responders. At D64, although still quite dissimilar, low responders seemed to start changing their expression status and became more similar to high responders. In contrast, placebo patients showed an opposite trend and their phenotype at D8 was more comparable to low responders at baseline.

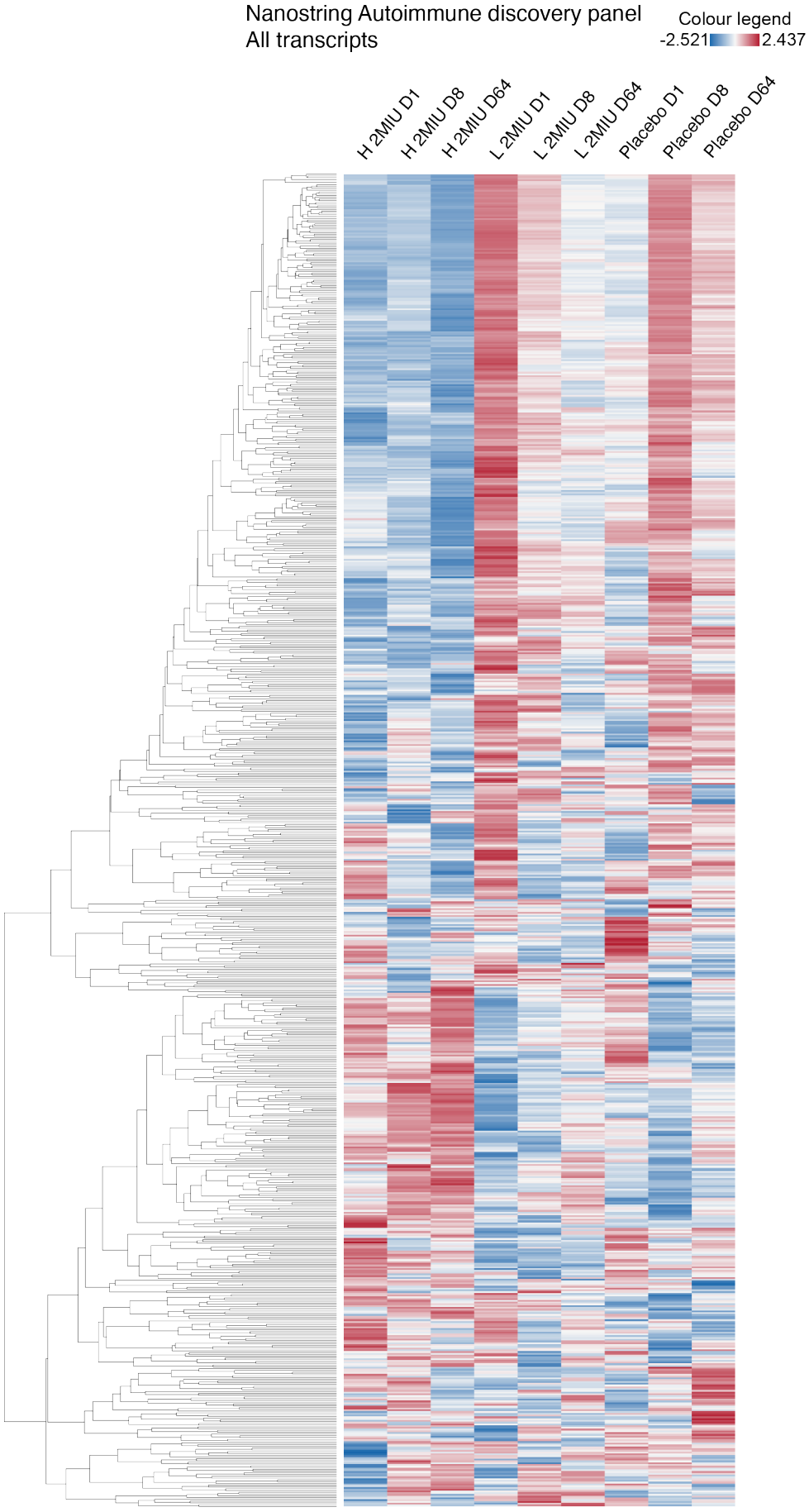
Nanostring Autoimmune discovery panel
All transcripts
Colour legend
-2.521
2.437
H 2MIU D1
H 2MIU D8
H 2MIU D64
L 2MIU D1
L 2MIU D8
L 2MIU D64
Placebo D1
Placebo D8
Placebo D64

Figure 4.5: NanoString Panel Gene Expression Overview

Hierarchically clustered heatmap summarising the expression of the 740 transcripts included in the Autoimmune Discovery nanoString panel. Each gene relative expression across different sample groups (H 2MIU D1, D8, D64= high responders expression across time points; L 2MIU D1, D8, D64= low responders expression across time points and Placebo at D1, D8 and D64) is graphed as z-score. Positive z-scores are colour coded in red and negative in blue.

Subsequently, a principal component analysis (PCA) was performed to assess and visualise transcriptional-driven group separations. In particular, a multi-group comparison (p-value<0.05) was performed using the software Qlucore and a three component PCA was generated (**Figure 4.6**). High-responder samples from D8 and D64 appeared to be spatially distanced from the rest of the samples, whereas, placebo and low-responders were more dispersed and partially overlapped.

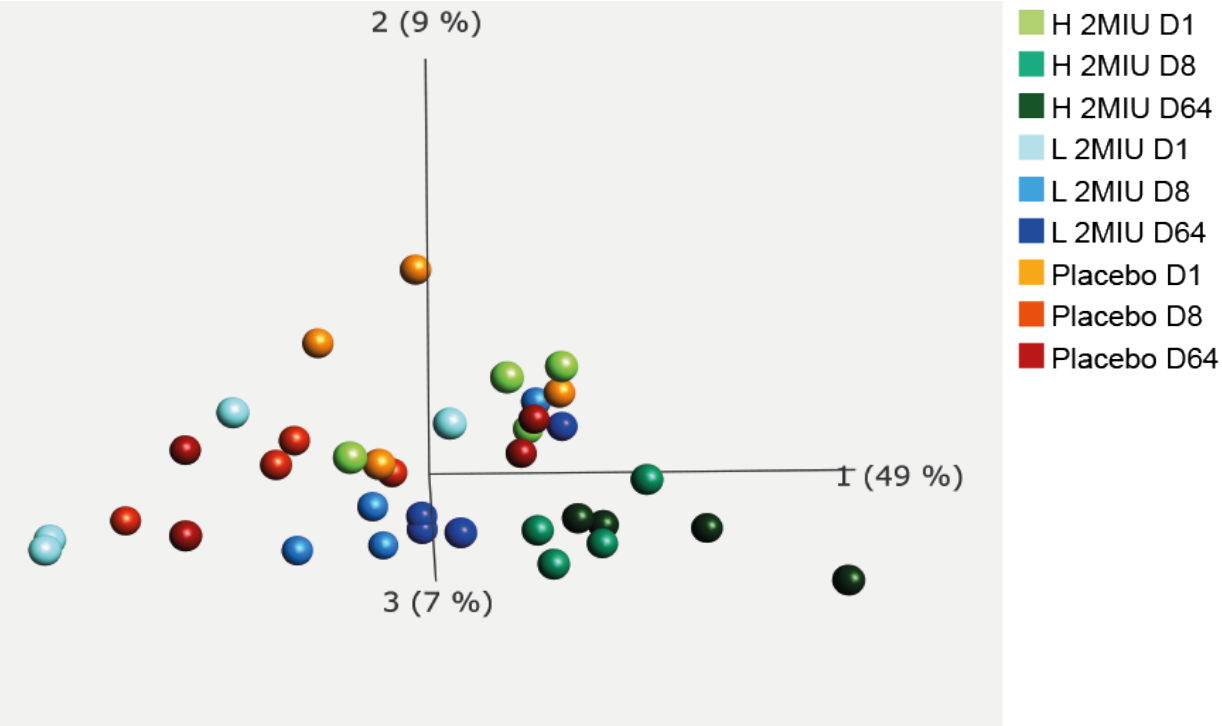

Figure 4.6: Principal Component Analysis of The NanoString Samples

PCA plot summarising expression differences between samples depending on treatment regimen and time point (colour code legend is reported. H 2MIU D1, D8, D64= high-responders at D1, D8 and D64; L 2MIU D1, D8, D64= low-responders at D1, D8 and D64 and Placebo at D1, D8 and D64). This analysis was performed using the software Qlucore and a multi-group comparison statistical test (p-value<0.05).

The Qlucore multi-group comparison revealed a cluster of 81 discriminatory variables or transcripts that were responsible for the PCA spatial group separation. This comprised of a mixture of both pro and anti-inflammatory markers. Interestingly, at baseline, an almost opposite trend was reported between high and low-Treg responders in this selected panel of transcripts (**Figure 4.7**). In particular, a noticeable upregulation was reported in low-Treg responders at D1 in transcripts that were generally downregulated in high-Treg responders. In this latter group, only a minor set of genes showed an expression trend inversion throughout the trial, while the majority

of the transcripts seemed to be progressively up or downregulated during 2MIU-IL-2 administration. In contrast, trend inversions in gene expression were reported in the low responders and, although they started from a very different transcriptional status at baseline compared to high responders, dissimilarities tended to be less evident at the end of the third cycle. Interestingly, at baseline, while patients who responded the most showed low levels of pro-inflammatory mediators, such as TLR1, TLR2, CXCL10, TNFRSF8, TNFRSF10C and IL12A, low-Treg responders expressed these genes considerably more and, concomitantly, their mRNA counts of anti-inflammatory agents, including TIGIT, IL2RA, IDO1, GATA3, IKZF2 and CTLA4, was slightly lower. However, the expression of these latter immune-modulatory mediators seemed to increase in low-Treg responders over the 2MIU-IL-2 administration period, although this was not as pronounced as in high-Treg responsive participants. The placebo group seemed to show a generally stable expression status across all time points although some differences were reported at D8 (**Figure 4.7**).

A complete list of all the transcripts included in the set of eighty-one discriminatory variables is available in **Table 4.2** together with their associated protein functions retrieved from the GeneCard database. Additionally, the normalized raw counts of each of the discriminatory variable for each sample screened is provided in **Appendix 8**.

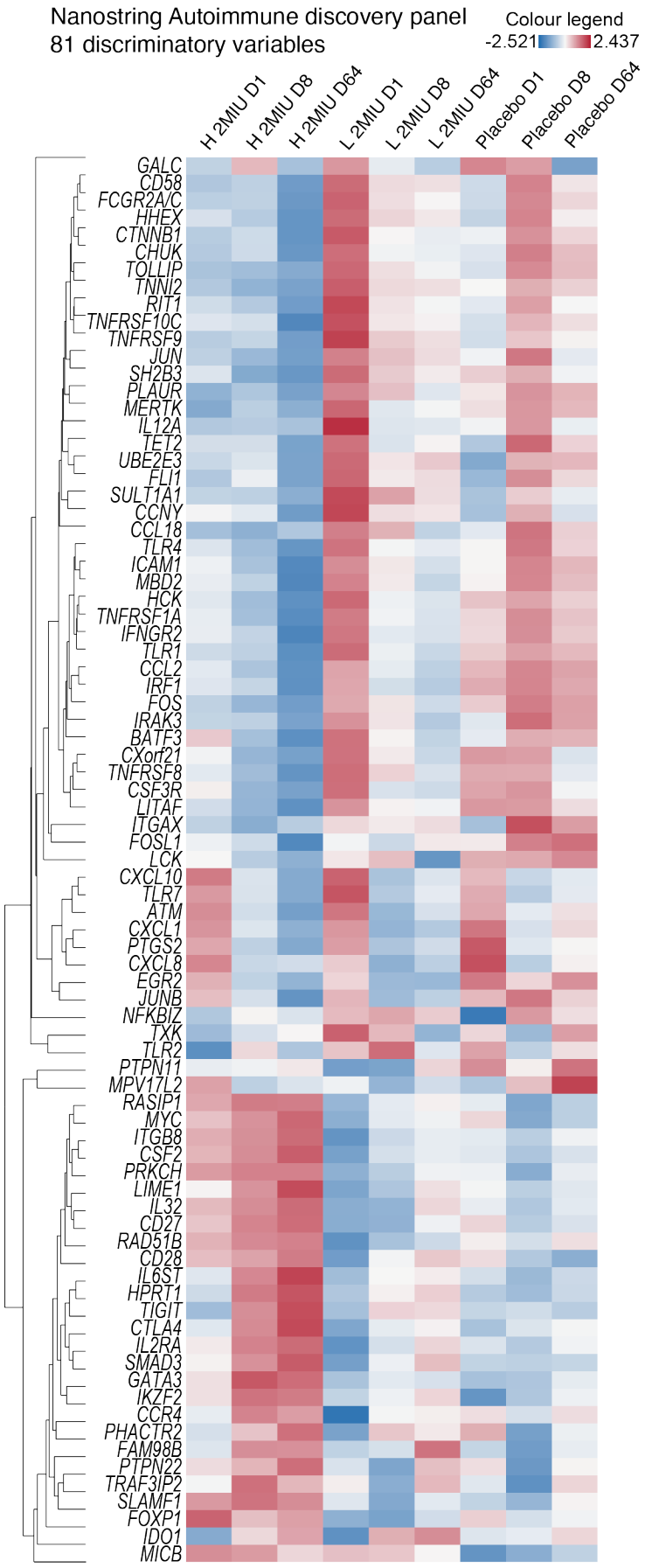
Nanostring Autoimmune discovery panel
81 discriminatory variables
Colour legend
-2.521
2.437
H 2MIU D1
H 2MIU D8
H 2MIU D64
L 2MIU D1
L 2MIU D8
L 2MIU D64
Placebo D1
Placebo D8
Placebo D64
GALC
CD58
FCGR2A/C
HHEX
CTNNB1
CHUK
TOLLIP
TNNI2
RIT1
TNFRSF10C
TNFRSF9
JUN
SH2B3
PLAUR
MERTK
IL12A
TET2
UBE2E3
FLI1
SULT1A1
CCNY
CCL18
TLR4
ICAM1
MBD2
HCK
TNFRSF1A
IFNGR2
TLR1
CCL2
IRF1
FOS
IRAK3
BATF3
CXorf21
TNFRSF8
CSF3R
LITAF
ITGAX
FOSL1
LCK
CXCL10
TLR7
ATM
CXCL1
PTGS2
CXCL8
EGR2
JUNB
NFKBIZ
TXK
TLR2
PTPN11
MPV17L2
RASIP1
MYC
ITGB8
CSF2
PRKCH
LIME1
IL32
CD27
RAD51B
CD28
IL6ST
HPRT1
TIGIT
CTLA4
IL2RA
SMAD3
GATA3
IKZF2
CCR4
PHACTR2
FAM98B
PTPN22
TRAF3IP2
SLAMF1
FOXP1
IDO1
MICB

Figure 4.7: Eighty-one Discriminatory Variables

Hierarchically clustered heatmap displaying differences in the expression of 81 transcripts identified as discriminating variables from the PCA analysis in Chap.4_Figure 3. Gene expression variations across sample groups (H 2MIU D1, D8, D64= high-responders at D1, D8 and D64; L 2MIU D1, D8, D64= low-responders at D1, D8 and D64 and Placebo at D1, D8 and D64) are displayed as z-scores (positive z-scores in red, negative in blue). An opposite expression between high and low-responders is detectable, especially at baseline (D1).

Table 4.2: List of The Eighty-one Discriminatory Transcripts

In this table, all of the 81 discriminating transcripts are listed. In particular, the names of the associated genes are displayed together with their accession numbers (NCBI database) and a brief description of their protein functions (source: https://www.genecards.org/).

Gene name and transcript ID	***Function***
ATM NM_000051.3	Serine/threonine kinase involved in double strand break repair.
BATF3 NM_018664.2	Transcription factor involved in the differentiation of CD8(+) dendritic cells.
CCL18 NM_002988.2	Lymphocyte chemotactic factor.
CCL2 NM_002982.3	Chemoattractant for monocytes and basophils.
CCNY NM_001282854.1	Cyclin Y participates in the regulation of cell division cycle.
CCR4 NM_005508.4	Chemokine (including CCL17, CCL22 and CKLF) receptor.
CD27 NM_001242.4	This receptor is required for generation and long-term maintenance of T cell immunity.
CD28 NM_001243078.1	Protein involved in T-cell proliferation and survival. It also mediates the production of cytokines and the development of Th2.
CD58 NM_001779.2	It binds CD2 and promotes the activation T cells.
CHUK NM_001278.3	This protein inhibits the function of NF-kB.
CSF2 NM_000758.2	Cytokine with stimulatory effects on a variety of immune cells including granulocytes, macrophages, eosinophils and erythrocytes.
CSF3R NM_000760.3	CSF3 receptor. Its activation stimulates the function and differentiation of granulocytes.
CTLA4 NM_005214.3	Important inhibitory receptor expressed on Treg that mediates immune suppression.
CTNNB1 NM_001098210.1	Catenin Beta 1 is involved in cell-cell adhension as it constitutes the adherens junctions.
CXCL1 NM_001511.1	Chemoattractant for neutrophils.
CXCL10 NM_001565.2	Chemokine that attracts monocytes and T cells.
CXCL8 NM_000584.2	Chemokine involved in neutrophil attraction.
CXorf21 NM_025159.2	Uncharacterized protein.
EGR2 NM_000399.3	Early growth factor 2 is a transcription factor involved in myelination.
FAM98B	It promotes arginine methylation.

NM_173611.3	
FCGR2A/C NM_201563.4	This protein is expressed on phagocytic cells and it mediates phagocytosis.
FLI1 NM_001167681.2	Sequence-specific transcriptional activator.
FOS NM_005252.2	Member of the FOS gene family. It interacts with JUN/AP-1 and functions as a transcription factor that regulates a variety of cellular functions.
FOSL1 NM_005438.3	Member of the FOS gene family.
FOXP1 NM_032682.5	Transcriptional repressor that mediates several processes involved in both development and adulthood.
GALC NM_000153.2	This lysosomal protein catalyses the hydrolysis of galactose ester bonds.
GATA3 NM_001002295.1	Transcriptional activator that is fundamental for Th2 differentiation.
HCK NM_002110.2	Protein expressed in haematopoietic cells and that is involved in innate immune response regulation.
HHEX NM_002729.4	Protein involved in haematopoietic differentiation and functions as a transcriptional repressor.
ICAM1 NM_000201.2	Mediates leukocytes trans-endothelial migration.
IDO1 NM_002164.3	Immune suppressive protein secreted by dendritic cells (DC) following the binding of CTLA4 (on Treg) to CD80/86 (on DC).
IFNGR2 NM_005534.3	Subunit of the interferon gamma receptor.
IKZF2 NM_001079526.1	Member of the Ikaros transcription factor family. It is involved in lymphocyte development and it is crucial for Tregs.
IL12A NM_000882.2	Cytokine that stimulates activated T and NK cells.
IL2RA NM_000417.1	IL-2 receptor alpha (also called CD25) involved in the immune regulatory processes mediated by Tregs.
IL32 NM_004221.4	Cytokine that participates in both innate and adaptive immune responses by inducing the production of other cytokines (such as TNF-α and IL8).
IL6ST NM_002184.2	Signal transducer of various cytokines including IL6.
IRAK3 NM_007199.1	Member of the IL1 receptor-associated kinase protein family that negatively regulates TCR signaling.
IRF1 NM_002198.1	Transcriptional regulator involved in both innate and adaptive immune responses.
ITGAX NM_000887.3	Integrin subunit alpha X is a receptor for fibrinogen that is involved in cellular interactions during inflammatory responses.
ITGB8 NM_002214.2	Integrin subunit beta 8 is a receptor for fibrinogen that mediates the release of TGFB1.
JUN NM_002228.3	Transcription factor.
JUNB	Transcription factor activated by primary growth factors.

NM_002229.2	
LCK NM_005356.2	Tyrosine kinase involved in the maturation of T cells.
LIME1 NM_017806.2	Protein involved in the BCR and TCR signaling.
LITAF NM_004862.3	Protein that induces TNF-α expression upon LPS stimulus.
MBD2 NM_003927.3	Binds methylated DNA and induces transcriptional repression.
MERTK NM_006343.2	Receptor tyrosine kinase involved in several physiological processes including in the inhibition of TLRs-mediated innate immune response.
MICB NM_005931.3	Binding to its receptor causes the activation of NKs and T cells.
MPV17L2 NM_032683.2	This protein is essential for the assembly and stability of the mitochondrial ribosome.
MYC NM_002467.3	Non-specific transcription factor.
NFKBIZ NM_001005474.1	Protein that inhibits NFkB activity.
PHACTR2 NM_001100165.1	Phosphatase and active regulator.
PLAUR NM_001005376.1	Urokinase receptor which participates in plasmin formation.
PRKCH NM_006255.3	Member of the PKC (protein kinase C) family.
PTGS2 NM_000963.1	Fundamental enzyme for prostaglandin biosynthesis.
PTPN11 NM_002834.3	Member of the protein tyrosine phosphatase family which regulate a variety of different cellular processes.
PTPN22 NM_012411.5	Member of the protein tyrosine phosphatase family that negatively regulates the T cell receptor (TCR) signaling.
RAD51B NM_002877.5	Mediates the DNA repair processes.
RASIP1 NM_017805.2	Protein that plays a crucial role in vasculogenesis and angiogenesis.
RIT1 NM_006912.4	Ras-related GTPase involved in the regulation of p38 MAPK-dependent signaling cascades.
SH2B3 NM_005475.2	This protein is a negative regulator of cytokine signaling and it is involved in haematopoiesis.
SLAMF1 NM_003037.2	Member of the SLAM receptor family involved in the regulation and interconnection of innate and adaptive immune response.
SMAD3 NM_005902.3	TGFB- induced signal transducer.
SULT1A1 NM_177534.2	Sulphotransferase that catalyses the addition of sulphate on different molecules.
TET2 NM_001127208.2	Enzyme involved in the myelopoiesis.

TIGIT NM_173799.2	TIGIT is produced by a subset of Tregs. It binds CD155 on DCs and it inhibits IL-12 secretion while inducing IL-10 production. Thus, it mediates the suppression of Th1 and Th17 but not Th2.
TLR1 NM_003263.3	Toll-like receptor 1 has a key role in pathogen recognition and innate immunity activation.
TLR2 NM_003264.3	Involved in pathogen recognition and activation of innate immunity in response to bacteria.
TLR4 NM_138554.2	Receptor implicated in signal transduction induced by LPS.
TLR7 NM_016562.3	Toll like receptor that is activated by single-stranded RNA which promotes NF-kB and the inflammatory response.
TNFRSF10C NM_003841.3	Receptor of the cytotoxic ligand TRAIL which protects from TRAIL-induced apoptosis.
TNFRSF1A NM_001065.2	Member of the TNF receptor superfamily. Its binding to TNF-α induces receptor trimerization and activation.
TNFRSF8 NM_152942.2	Member of TNF-α receptor which is expressed on activated T and B cells and promotes inflammation.
TNFRSF9 NM_001561.4	Member of the TNF-receptor superfamily which mediates clonal expansion, survival and development of T cells.
TNNI2 NM_003282.2	Inhibitory subunit of troponin.
TOLLIP NM_019009.2	Protein involves in the IL-1 signaling pathway.
TRAF3IP2 NM_001164281.1	Involved in innate immunity interacting with TRAF protein, IkB and NF-kB.
TXK NM_003328.1	Non-receptor tyrosine kinase involved in regulation of the development, differentiation and function of T cells and NKT cells.
UBE2E3 NM_006357.2	Member of the E2-ubiquitin-conjugating enzyme family.

Subsequently, nanoString gene expression data were correlated with qRT-PCR previously generated (see Chapter 3.5) for data validation. As expected, strong and significant positive correlations were reported for IL2RA (Pearson correlation, R= 0.895, R^2= 0.802, P-value= 1.61E-13), CTLA4 (Pearson correlation, R= 0.890, R^2= 0.793, P-value= 3.5E-13) and IKZF2 (Pearson correlation, R= 0.728, R^2= 0.530, P-value= 4.86E-07) (**Figure 4.10**). This suggested the overall validity and reliability of nanoString transcriptomic data.

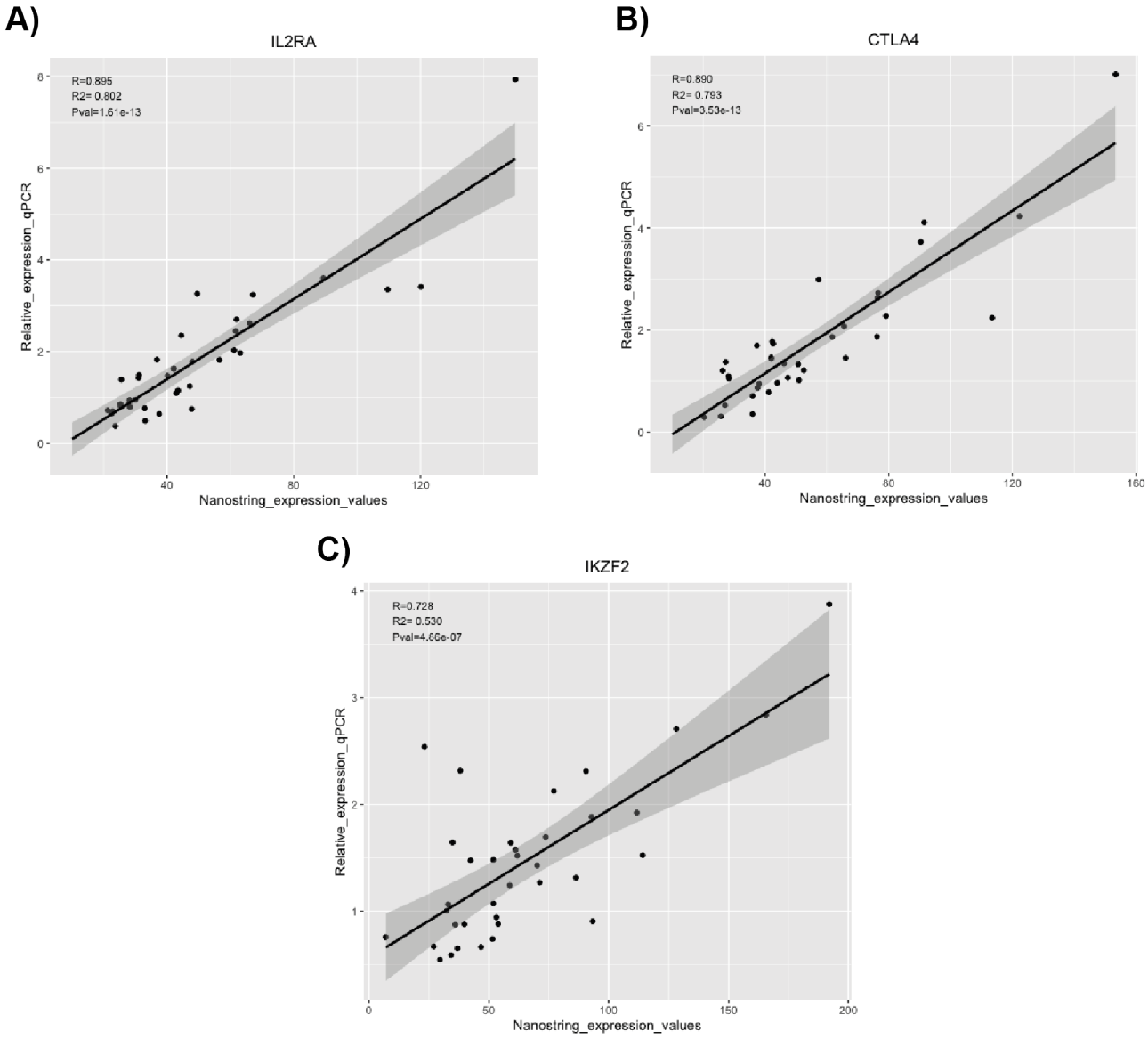

Figure 4.8: Nanostring Data Validation.

Three plots are displayed showing the correlation between nanoString (X-axis) and qRT-PCR (Y-axis) expression data from IL2RA (**A**), CTLA4 (**B**) and IKZF2 (**C**). Positive and very significant correlations were detected suggesting agreement between expression data retrieved from these two techniques. Pearson correlation coefficient (R), R^2 and P-value are displayed in the top left corner of the plot. Each dot represents a sample collected from a patient at a specific time point.

Surprisingly though, FOXP3, the most important transcription factor for Treg functions and differentiation, was not amongst the eighty-one variables accounting for group

separation in the PCA analysis. Moreover, no significant correlation (Pearson correlation, R= -0.031, R^2= 0.0009, P-value= 0.854) was reported between expression data retrieved from qRT-PCR and nanoString (**Figure 4.8**).

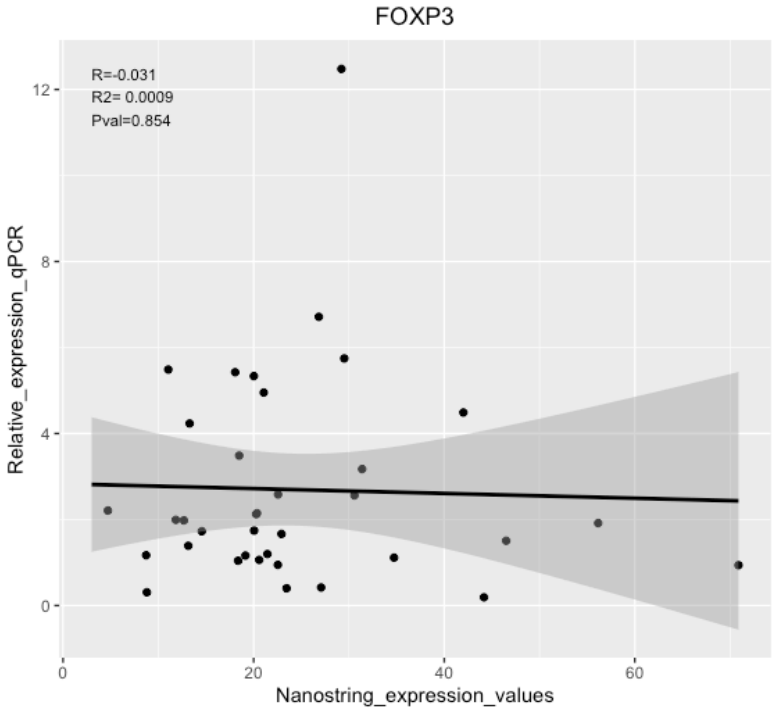

Figure 4.9: Correlation Between qRT-PCR and NanoString FOXP3 Expression Data.

Plot showing the correlation between FOXP3 expression data retrieved from either nanoString or qRT-PCR. As expected, no significant correlation was found due to the different primers able to detect different FOXP3 isoforms (qRT-PCR= NM_001114377, NM_014009 while nanoString = NM_014009 only). Pearson correlation coefficient (R), R^2 and P-value are displayed in the top left corner of the plot. Each dot represents a sample collected from a patient at a specific time point. X-axis: normalised *FOXP3* expression values obtained using the NanoString instrument, Y-axis: normalised *FOXP3* expression values calculated from microarray analysis.

To further investigate this, FOXP3 nanoString mRNA counts were closely inspected and plotted separately (**Figure 4.9**). No significant expression differences in FOXP3 were detectable over time in the different patient groups. This result was in contrast to what was previously reported from our microarray and qRT-PCR gene expression data. However, this could be explained by the different probes used for the different

techniques. In fact, nanoString primers were capable of detecting only one transcript variant (NM_014009) of FOXP3 while Clariom D microarray probes and qRT-PCR primers recognised two isoforms (NM_001114377, NM_014009). The variant NM_014009 encodes for the full length FOXP3 (FOXP3fl) whilst NM_001114377 transcript had a deletion of exon 2 (it lacks amino acids 72-106, also referred to as FOXP3Δ2). While only 20-30% of the total FOXP3 mRNAs are in the NM_014009 (FOXP3fl) isoform, 70% of transcripts are NM_001114377 (FOXP3Δ2) in human $CD4^+$ $CD25^+$ Tregs. Exon 2 contains a nuclear export sequence (NES) which promotes cytoplasmic localization of FOXP3fl and therefore, this isoform is more localised in the cellular cytoplasm compared to FOXP3Δ2 (Mailer, 2018). These results suggested that the isoform FOXP3Δ2 was specifically upregulated following the ld-IL-2 administration in ALS patients, while no significant variation was detected in FOXP3fl.

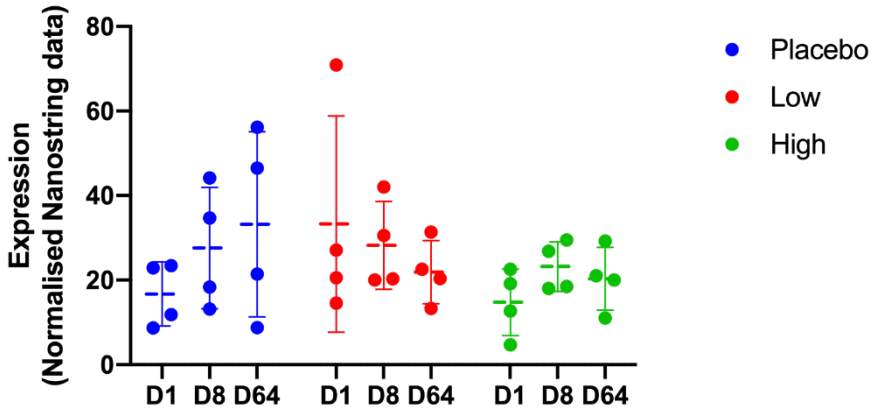

Figure 4.10: Expression of the FOXP3 Isoform NM_014009 Measured through NanoString.

Violin plots showing the expression of FOXP3 (NM_014009) in each patient group. Each dot represents a sample and the mean (horizontal lines) and SD (vertical lines) of each group are also shown. On the x-axis the normalised expression of FOXP3 (NM_014009) is reported for each sample (placebo in blue, low Treg-responders in red and high Treg-responders in green). No significant variations are reported across different patient groups throughout the trial.

4.1.3 NanoString Pathway Scoring Analysis

Following the gene expression analysis, a broader biological investigation was performed in order to identify altered cellular processes characteristic of the different patient groups (placebo, low and high-Treg responders) at specific time points (D1, D8 and D64). This was achieved by carrying out a pathway scoring analysis. This tool is provided by the nCounter Advanced Analysis 2.0 software (https://www.nanostring.com/products/analysis-solutions/ncounter-advanced-analysis-software) and it allows the summarization of the changes at the gene expression level by grouping genes into functionally and biologically related groups. Subsequently, a score is computed reflecting the level of activation (the majority of the genes included in a process showed increased expression and therefore a positive score was assigned to the pathway) or inhibition (negative scores) of a certain pathway.

Transcripts included in the Autoimmune Discovery nanoString panel are annotated as involved in fifty-five inflammatory pathways known to be involved in the onset of several autoimmune disorders. The pathway scoring analysis identified a marked inhibitory trend throughout the trial of nearly all of these pro-inflammatory processes. Interestingly, this tendency was reported for both high and low-Treg responders (**Figure 4.11**). However, baseline scores of these processes were considerably different between the two groups. In fact, patients who showed less Treg expansion at the end of the treatment tended to exhibit higher positive scores in these inflammatory pathways at D1. In contrast, high-Treg responders exhibited lower baseline scores. These results suggested that a very different immunological state was characteristic of the two Treg responder groups prior to drug administration with the lowest responsive patients showing a more inflammatory prone phenotype. Therefore, this might have had a significant influence on participant Treg reaction to 2MIU-IL-2. Placebo patients showed positive scores which indicated activation of the inflammatory pathways throughout the trial. While D1 and D64 scores were comparable, a further increase was reported at D8. The relevance of this surge is still to be understood.

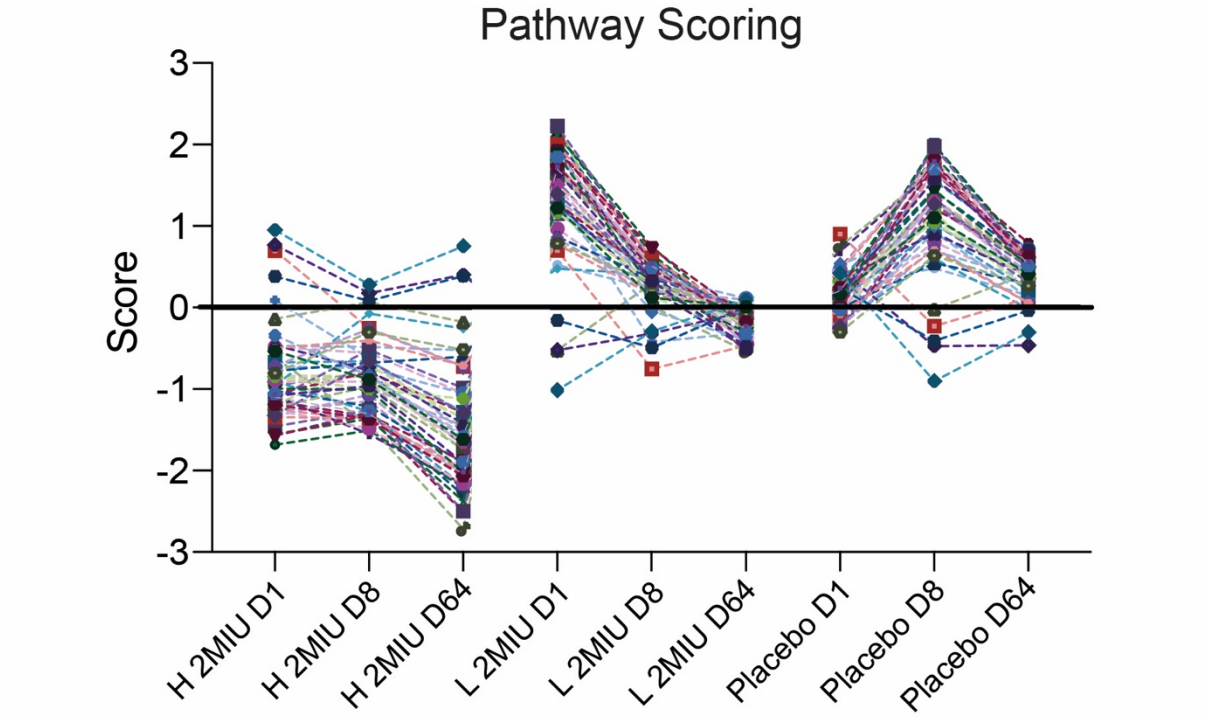

Legend

- Antigen processing and presentation
- B cell receptor signaling pathway
- Cell adhesion molecules (CAMs)
- Cell growth and death
- Cellular community
- Chemokine signaling pathway
- Choline metabolism in cancer
- Complement and coagulation cascades
- Development
- Digestive system
- Endocrine and metabolic diseases
- Endocrine system
- Epstein-Barr virus infection
- Epithelial cell signaling in H. pylori infection
- Fc epsilon RI signaling pathway
- Genetic Information Processing
- HTLV-I infection
- Hematopoietic cell lineage
- Herpes simplex infection
- Infectious diseases.CL. Parasitic
- Inflammatory bowel disease (IBD)
- Influenza A
- Intestinal immune network for IgA production
- Jak-STAT signaling pathway
- Leukocyte transendothelial migration
- MAPK signaling pathway
- Measles
- Metabolism
- MicroRNAs in cancer
- NF-kappa B signaling pathway
- Natural killer cell mediated cytotoxicity
- Nervous system
- Neuroactive ligand-receptor interaction
- Neurodegenerative diseases
- PI3K-Akt signaling pathway
- Pathways in cancer
- Pertussis
- Phosphatidylinositol signaling system
- Proteoglycans in cancer
- RIG-I-like receptor signaling pathway
- Rap1 signaling pathway
- Ras signaling pathway
- Regulation of actin cytoskeleton
- Sensory system
- TGF-beta signaling pathway
- TNF signaling pathway
- Toll-like receptor signaling pathway
- Transcriptional misregulation in cancer
- Transport and catabolism
- Tuberculosis

Figure 4.11: Longitudinal Pathway Scoring Analysis.

Graph showing results from pathway scoring analysis performed using Advanced Analysis nSolver software. Pathway scores are plotted as a function of the different treatment type and time points (H 2MIU D1, D8, D64= high-Treg-responders at D1, D8 and D64; L 2MIU D1, D8, D64= low-Treg-responders at D1, D8 and D64 and Placebo at D1, D8 and D64). Positive scores suggest activation of a pathway whilst negative scores indicates inhibition. An evident downregulation of several pro-inflammatory pathways is reported in both high and low-Treg-responders.

To gain a better understanding of each patient pathway scores in a panel of key inflammatory pathways, ten biological processes were selected and plotted separately: antigen processing and presentation, B cell receptor signaling pathway, chemokine signaling pathway, JAK-STAT signaling pathway, MAPK signaling pathway, natural killer cell mediated cytotoxicity, NF-kB signaling pathway, TNF signaling pathway, PI3K-Akt signaling pathway and Toll-like receptor signaling pathway (**Figure 4.12**). These were chosen as they are involved in the general inflammation process and are not specific to a particular inflammatory disease. All the pathways showed a reduction in their score over time in both high and low-Treg responders while an increase was observed within the placebo participants. Interestingly, the high-Treg responders exhibited tighter and less dispersed scores whilst both low responders and placebo were more variable. In particular, two low-Treg responders – C01P018 and C01P36 showed very high scores in all the pathways. Interestingly, C01P036 was the participant showing lowest value of Treg count at the end of the administration period (52.22 cells/ul of blood). However, both patients showed a sharp reduction in the pathway scores following the end of the first (D8) and third (D64) treatment cycles which was consistent with a drug-induced immune suppression.

Figure 4.12a

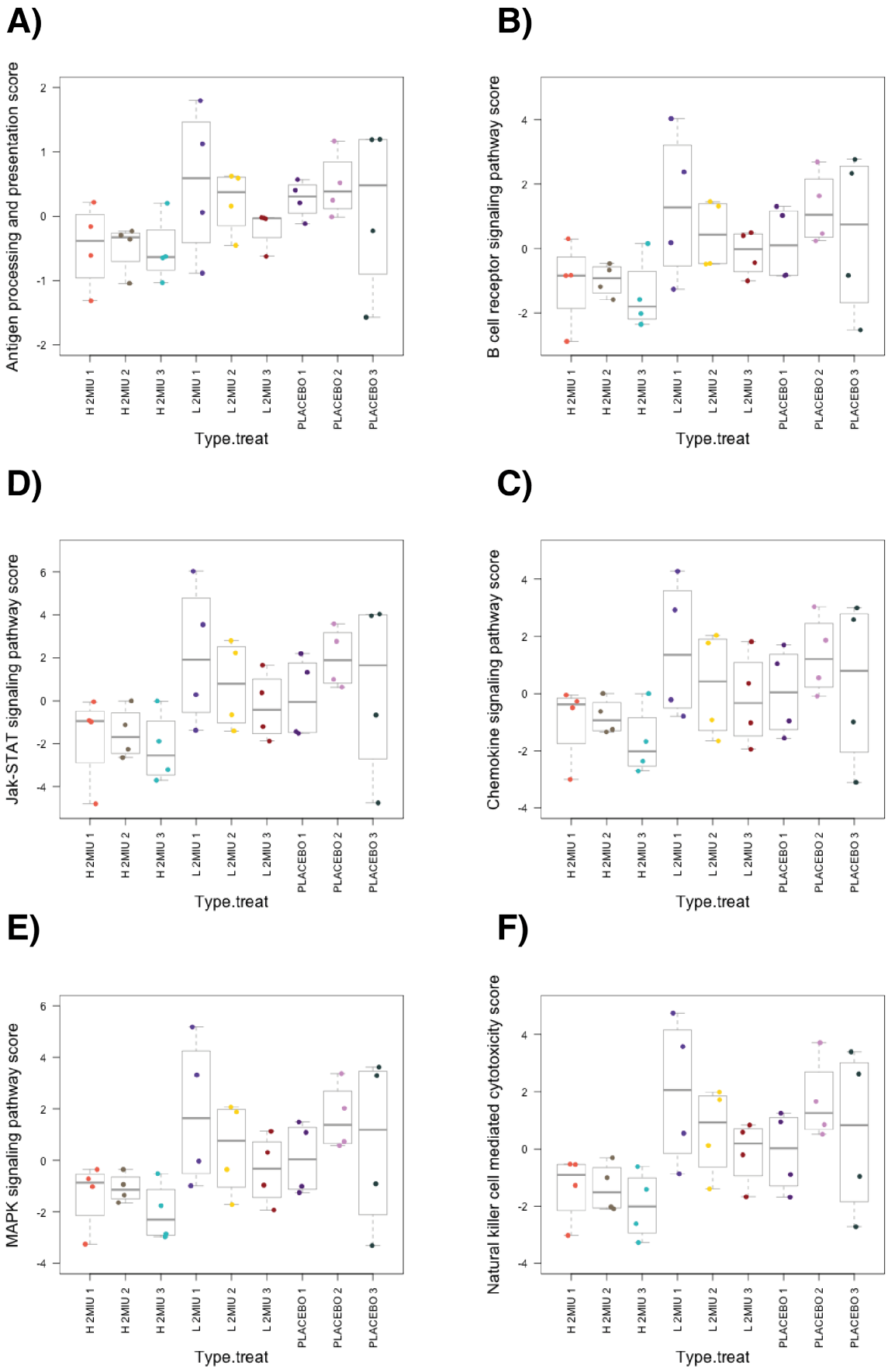
A)
Antigen processing and presentation score
B)
B cell receptor signaling pathway score
D)
Jak-STAT signaling pathway score
C)
Chemokine signaling pathway score
E)
MAPK signaling pathway score
F)
Natural killer cell mediated cytotoxicity score
H 2MIU 1
H 2MIU 2
H 2MIU 3
L 2MIU 1
L 2MIU 2
L 2MIU 3
PLACEBO 1
PLACEBO 2
PLACEBO 3
Type.treat

Figure 4.12b

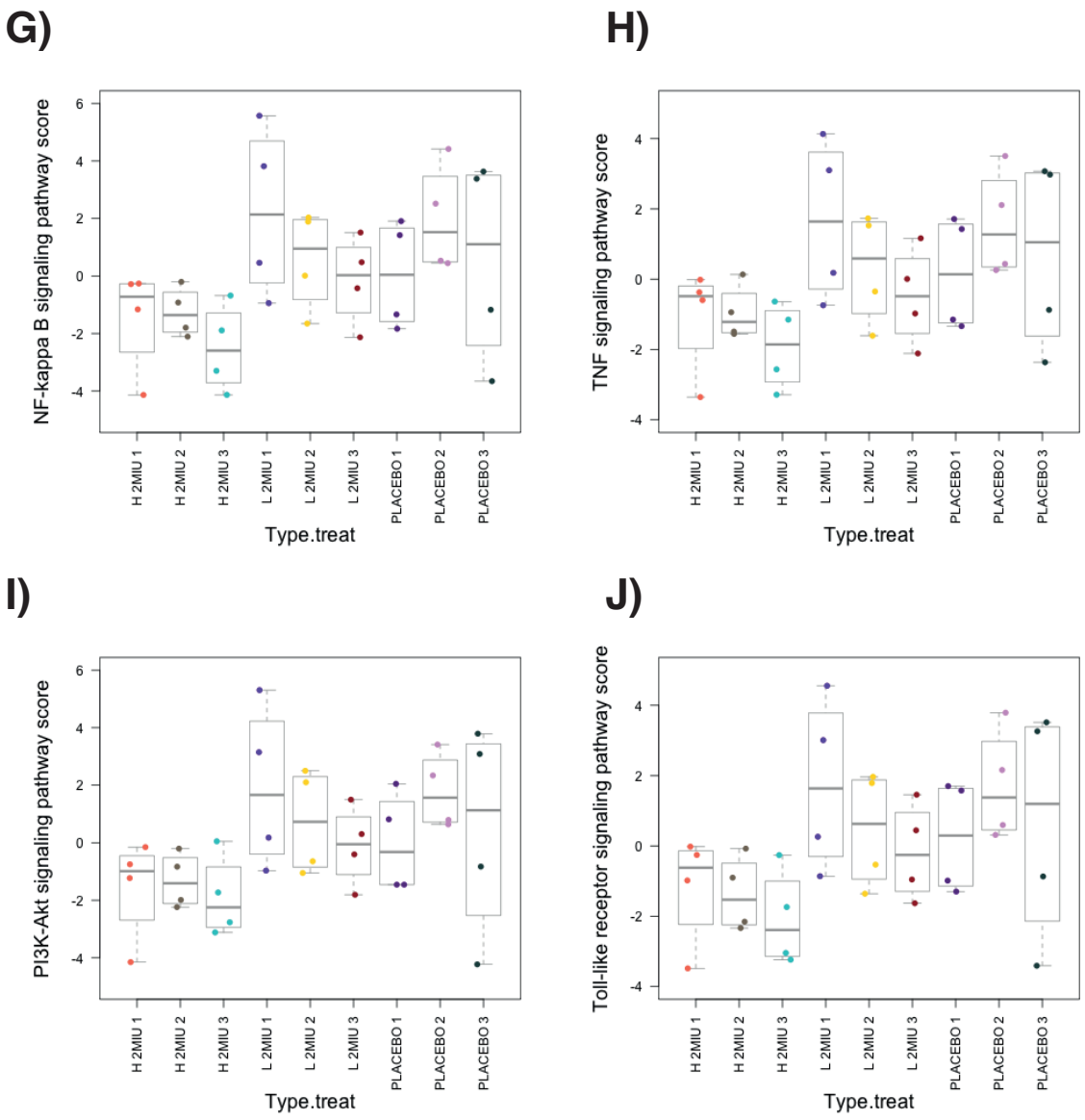
G)
NF-kappa B signaling pathway score
H)
TNF signaling pathway score
I)
PI3K-Akt signaling pathway score
J)
Toll-like receptor signaling pathway score
H 2MIU 1
H 2MIU 2
H 2MIU 3
L 2MIU 1
L 2MIU 2
L 2MIU 3
PLACEBO 1
PLACEBO 2
PLACEBO 3
Type.treat

Figure 4.12: Longitudinal Inflammatory Pathway Scoring.

Box and whisker plots displaying pathway scores for a selection of ten inflammatory processes (Figure 4.12a: A-F: antigen processing and presentation, B cell receptor signaling pathway, chemokine signaling pathway, JAK-STAT signaling pathway, MAPK signaling pathway, natural killer cell mediated cytotoxicity; Figure 4.12b: G-J: NF-kB signaling pathway, TNF signaling pathway, PI3K-Akt signaling pathway, Toll-like receptor signaling pathway). Each dot represents a trial participant while the median values is reported as a thick horizontal line. A time-dependent reduction in the scores of these inflammatory pathways was reported in both low and high-Treg responders whilst an increase was evident within the placebo group. Legend: H 2MIU 1, 2, 3= high-Treg-responders at D1, D8 and D64; L 2MIU 1, 2, 3= low-Treg-responders at D1, D8 and D64; Placebo 1, 2, 3= placebo patients at D1, D8 and D64.

Amongst the pathways investigated with the scoring analysis, one was particularly interesting in the context of ALS as it summarises processes involved in neurodegenerative diseases. For this reason, this was plotted separately to visualise each patient score (**Figure 4.13**). Similar to the pathways reported above, both high and low-Treg responders showed a marked time-dependent decrease in this score. In contrast, an increase was evident within the placebo group. Considering that for this analysis the Autoimmune Discovery panel was used, these results suggested that inflammatory pathways participating in neurodegeneration were progressively inhibited over time as a result of the 2MIU-IL-2 administration.

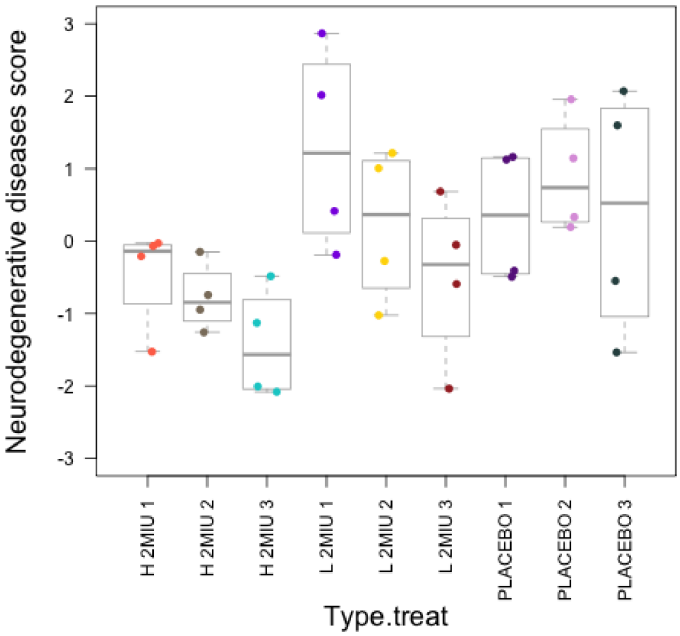

Figure 4.13: Longitudinal Neurodegenerative Disease Pathway Scoring.

Box and whisker plot showing patient scores of the pathway called "neurodegenerative diseases". Each dot represents a trial participant while the median value is reported as a thick horizontal line. A decrease in the median score was visible over time in both low and high-Treg responders whilst the placebo group showed a mild increase. Legend: H 2MIU 1, 2, 3= high-Treg-responders at D1, D8 and D64; L 2MIU 1, 2, 3= low-Treg-responders at D1, D8 and D64; Placebo 1, 2, 3= placebo patients at D1, D8 and D64.

Taken together, the results from the nanoString gene expression analysis suggested that immunological difference were evident prior to drug administration. In particular, low-Treg responders showed a more inflammatory prone phenotype at recruitment which might have had a significant influence on their ability to react to the 2MIU-IL-2 administration. Nonetheless, an inhibition of these pro-inflammatory processes was evident over time both in the high and in the low-Treg responders.

4.2 Predictive Biomarker Analysis

Given the reported dissimilarities between Treg responder groups, which were particularly pronounced at time of recruitment, the work described in this chapter also aimed to identify predictive biomarkers of the outcome of the trial. In particular, the final objective was to identify a small number of transcripts that could be used to build a predictive model in a way that their gene expression at D1 would be able to forecast target engagement at the end of the three cycles of treatment. This reflected the degree of IL2-receptor stimulation on Treg and therefore the magnitude of their cellular expansion following three cycles of 2MIU-IL-2 administration.

4.2.1 Preliminary Screening

NanoString gene expression analysis revealed a marked transcriptional difference between high and low-Treg responders, which was particularly evident at baseline (D1). Therefore, with the aim of finding predictive biomarkers, correlation analyses were carried out. In particular, a preliminary screen was conducted by correlating the expression of all the targets included into the Autoimmune Discovery nanoString panel at D1 with the Treg counts at D64 or with the expression of *IL2RA* at D64 (nanoString data). *IL2RA* was chosen as a second independent variable because it is a marker of Tregs and both our longitudinal microarray analysis and qRT-PCR validation indicated a time-dependent increase in this transcripts which reached a peak at D64, suggesting an expansion in the Treg population. Moreover, IL2RA was also selected because of the direct action of IL-2 on its protein synthesis, as several pieces of evidence in the literature suggested an increased expression of this receptor subunit after the cytokine administration (reviewed in (Malek and Castro, 2010)). Subsequently, only transcripts showing significant correlation with both of the measurements at D64 were selected for further investigation. The decision of focusing on the significant and commonly correlated genes was made to identify potentially more robust biomarker candidates.

Fifty transcripts showed a significant (p-value<0.05) correlation with the Treg count at D64 while 72 were significantly correlated with *IL2RA* expression at D64. We then

ranked these transcripts by their p-value with rank=1 indicating the transcripts showing the lowest p-values. The comparison of the two lists identified 35 transcripts to be commonly and significantly correlated with the two chosen variables measured at D64. Lastly, a combined score was computed by adding the two ranks calculated for the Treg and *IL2RA* correlations. A table summarising R^2, p-value and rank for each correlation and combined scores is reported in **Table 4.2**. The top five transcripts showing the best combined scores were *BTLA*, *SBNO2*, *TRAF2*, *CD27* and *BLNK* which were selected as proposed biomarker candidates to be further investigated. Importantly, *TLR9* was also included as, despite being the twelfth term for combined score, it was the transcript showing the best correlation with *IL2RA* at D64 (rank=1). Unfortunately, due to time and cost constraints, the remaining 29 transcripts, which commonly significantly correlated, were not analysed further.

Table 4.2: Preliminary Biomarker screening results.

This table illustrates the list of 35 transcripts for which expression at D1 significantly correlated with both Treg count and IL2RA expression (nanoString data) measured at D64. For each term, R^2, p-value and rank are reported for each correlation analysis and the combined score is also shown.

	Correlation with Treg count at D64			Correlation with IL2RA expression at D64			
	R^2	Pval	Rank	R2	Pval	Rank	Combined_score
BTLA	0.829	0.002	1	0.808	0.002	2	3
SBNO2	0.736	0.006	5	0.762	0.005	5	10
TRAF2	0.691	0.010	9	0.785	0.003	3	12
CD27	0.794	0.003	2	0.656	0.015	13	15
BLNK	0.705	0.009	6	0.651	0.015	15	21
AFF3	0.644	0.017	14	0.676	0.012	10	24
SOX8	0.641	0.017	15	0.665	0.014	11	26
RASIP1	0.783	0.003	3	0.607	0.023	25	28
LCK	0.646	0.016	12	0.633	0.018	17	29
MPV17L2	0.704	0.009	7	0.619	0.021	22	29
RABEP2	0.559	0.033	27	0.783	0.004	4	31
TLR9	0.554	0.034	31	0.821	0.002	1	32
DLD	0.580	0.028	21	0.656	0.015	12	33
GMPPB	0.591	0.026	19	0.655	0.015	14	33
FKBP5	0.556	0.034	29	0.728	0.007	6	35
ZC2HC1A	0.675	0.012	10	0.586	0.027	32	42
UCN	0.338	0.131	17	0.605	0.023	27	44
PHRF1	0.503	0.049	49	0.716	0.008	7	56
TNFSF8	0.547	0.036	33	0.611	0.022	23	56
MYC	0.569	0.031	25	0.581	0.028	33	58
SPHK2	0.742	0.006	4	0.541	0.037	54	58
ADA	0.590	0.026	20	0.568	0.031	41	61
FADS3	0.502	0.049	50	0.625	0.020	21	71
TRAF3IP2	0.543	0.037	35	0.571	0.030	38	73
TNFAIP6	0.523	0.043	41	0.576	0.029	36	77
SPRY4	0.569	0.031	26	0.542	0.037	53	79
UBASH3A	0.510	0.047	44	0.577	0.029	35	79
IL6ST	0.698	0.010	8	0.501	0.049	72	80
CD48	0.645	0.016	13	0.511	0.046	68	81
TMBIM1	0.524	0.042	40	0.559	0.033	45	85
RUNX1	0.537	0.039	37	0.551	0.035	50	87
PROCR	0.545	0.036	34	0.536	0.039	61	95
CXCL9	0.555	0.034	30	0.520	0.043	66	96
WDFY4	0.513	0.046	42	0.541	0.038	56	98
IRF8	0.524	0.042	38	0.521	0.043	65	103

4.2.2 qRT-PCR Validation and Correlation

Given that the NanoString analysis was performed only on a selection of the trial participants (four high, four low-Treg responders and four placebo), the preliminary screening involved only eight out of twelve 2MIU-IL-2 treated patients. Therefore, qRT-PCRs were conducted to obtain baseline expression values of the six gene candidates (*BLNK*, *BTLA*, *CD27*, *SBNO2*, *TLR9* ,*TRAF2*) from all 12 2MIU-IL-2 treated patients in order to confirm the validity of the proposed biomarkers. These data were correlated with the Treg counts at D64. Importantly, *IL2RA* was not used as a second dependent variable at this stage. Although this was useful in the previous analysis to identify more robust candidates, the outcome we finally aimed to forecast was the number of Tregs at D64. Such a model with this predictive capability would allow the stratification of patients and the identification of the more Treg-responsive individuals who would benefit the most from treatment with ld-IL-2.

Correlation plots were generated for each of the six biomarker candidates (**Figure 4.14**) and a summary of the scores obtained from the Pearson correlations are provided in **Table 4.3**. While, *BLNK*, *BTLA*, *SBNO2* and *TRAF2* did not show any significant relationship (**Figure 4.14C-F**), a strong negative and significant correlation was observed in the case of *TLR9* (R= -0.809, R^2= 0.654, p-value=0.0014) (**Figure 4.14A**). A milder positive correlation was reported for *CD27* although it did not reach statistical significance (R= 0.416, R^2= 0.173, p-value=0.179). Nonetheless, for both TLR9 and CD27, gene expression was able to clearly separate the three groups of drug-responders. When visually inspected, *CD27* showed an interesting trend and its scores were probably influenced by the patient C01P032 (**Figure 4.14B**). This was a moderate-Treg responder, the most variable class which is therefore more difficult to predict. In this case, patient C01P032 could be considered as having an outlier trend and its removal would increase the correlation scores (R= 0.764, R^2= 0.583, p-value=0.006). Nonetheless, given the particularly small sample size, the exclusion of a patient could excessively influence the predictive analysis. For this reason, a decision was made not remove it from further analyses. However, both the linear models using either TLR9 or CD27 showed good root mean squared errors ($RMSE_{TLR9}$=81.4, $RMSE_{CD27}$=126.0). This metric is a measure of the standard deviation

of the residuals that indicate the prediction error (this was computed as the difference between predicted and the actual outcome). RMSE is a scale-dependent variable, which means that it needs to be interpreted in the context of the range of values assumed by the dependent variable (Treg count at D64). As mentioned before, its standard deviation was quite high (SD_{Treg_D64}=144.8) and given that RMSE of both the single linear regressions were less than the SD_{Treg_D64}, this suggested that the two models tended to estimate the outcome better than a random model.

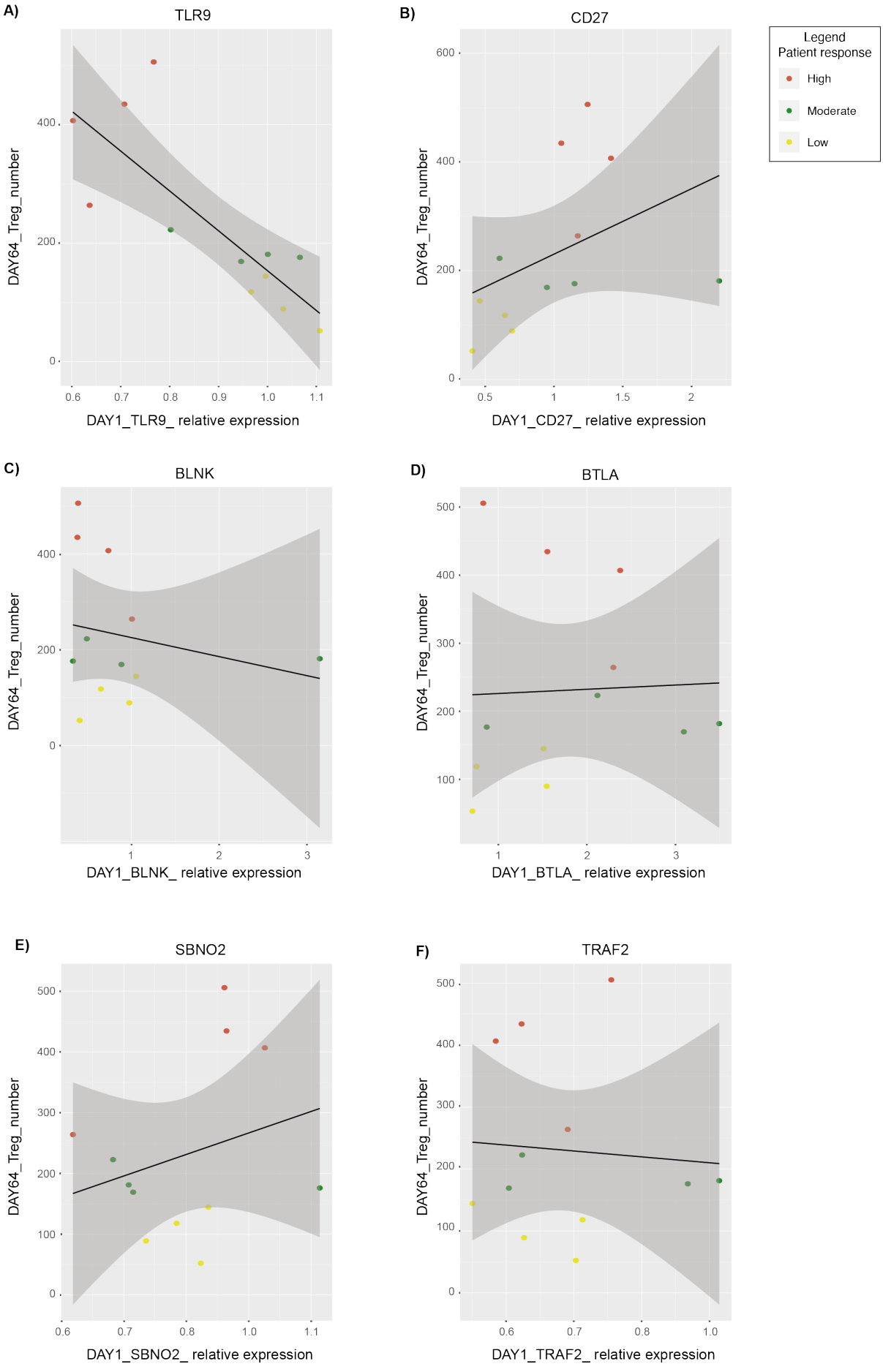
A)
TLR9
DAY64_Treg_number
DAY1_TLR9_ relative expression
B)
CD27
DAY64_Treg_number
DAY1_CD27_ relative expression
Legend
Patient response
High
Moderate
Low
C)
BLNK
DAY64_Treg_number
DAY1_BLNK_ relative expression
D)
BTLA
DAY64_Treg_number
DAY1_BTLA_ relative expression
E)
SBNO2
DAY64_Treg_number
DAY1_SBNO2_ relative expression
F)
TRAF2
DAY64_Treg_number
DAY1_TRAF2_ relative expression

Figure 4.14: Biomarker Candidates' Correlation Plots.

Linear regression plots showing the correlation between the expression of *TLR9* (**A**), *CD27* (**B**), *BLNK* (**C**), *BTLA* (**D**), *SBNO2* (**E**) and *TRAF2* (**F**) at the baseline (D1) and the Treg number at D64 for each 2MIU-IL-2 treated patient. Each dot represents a trial participant (average expression values computed from three qRT-PCR experiments, N=3) and they are colour-coded depending on their Treg-response type: high (orange), moderate (green) and low (yellow). A regression line (black) and its regression confidence bands (grey) are also shown. A strong linear and negative correlation was found for *TLR9* (**A**: R= -0.809, R^2= 0.654, p-value=0.0014) while a mild, positive relationship was reported for *CD27* (**B**: R= 0.416, R^2= 0.173, p-value=0.179) although it did not reach statistical significance. No evident or significant trend was reported for the rest of the biomarker candidates (*BLNK*, *BTLA*, *SBNO2* and *TRAF2*).

Table 4.3: Biomarker Candidates' Correlation Scores

This table displays the correlation scores (Pearson' correlation) and associated p-values (T-test statistics) computed for each biomarker candidate. A significant correlation was found only for TLR9 although interesting scores and a trend was reported for CD27.

ID	R	R^2	P-value
TLR9	-0.809	0.654	0.0014
CD27	0.416	0.173	0.17
SBNO2	0.273	0.074	0.38
BLNK	-0.209	0.043	0.51
BTLA	0.039	0.0016	0.9
TRAF2	0.023	0.0005	0.9

4.2.3 Multiple Linear Model

Given the intriguing results obtained from the single linear models, expression data from TLR9 and CD27 at D1 were combined and used as variables to create a more robust multiple linear regression model (**Figure 4.15**). Patient C01P032, the same mild responder mentioned in the previous analysis, increased variability and was spatially distanced from the rest of the mild-Treg responders. Despite this, the model plot showed an evident separation of the three Treg-responders subgroups with the high and low responders being clearly clustered and spatially separated. The multiple model performed better that the aforementioned single linear models and its metrics were encouraging (R^2= 0.694, Adjusted R^2= 0.626, p-value= 0.005). In particular, the coefficient of determination (R^2) and the fitting root mean squared error (RMSE) obtained with this last model were better than those retrieved from the one using TLR9 as the only independent variable ($R^2_{multiple}$=0.694 $RMSE_{multiple}$=76.7, R^2_{TLR9}=0.654, $RMSE_{TLR9}$=81.4). This suggested a greater prediction ability of the multiple linear model.

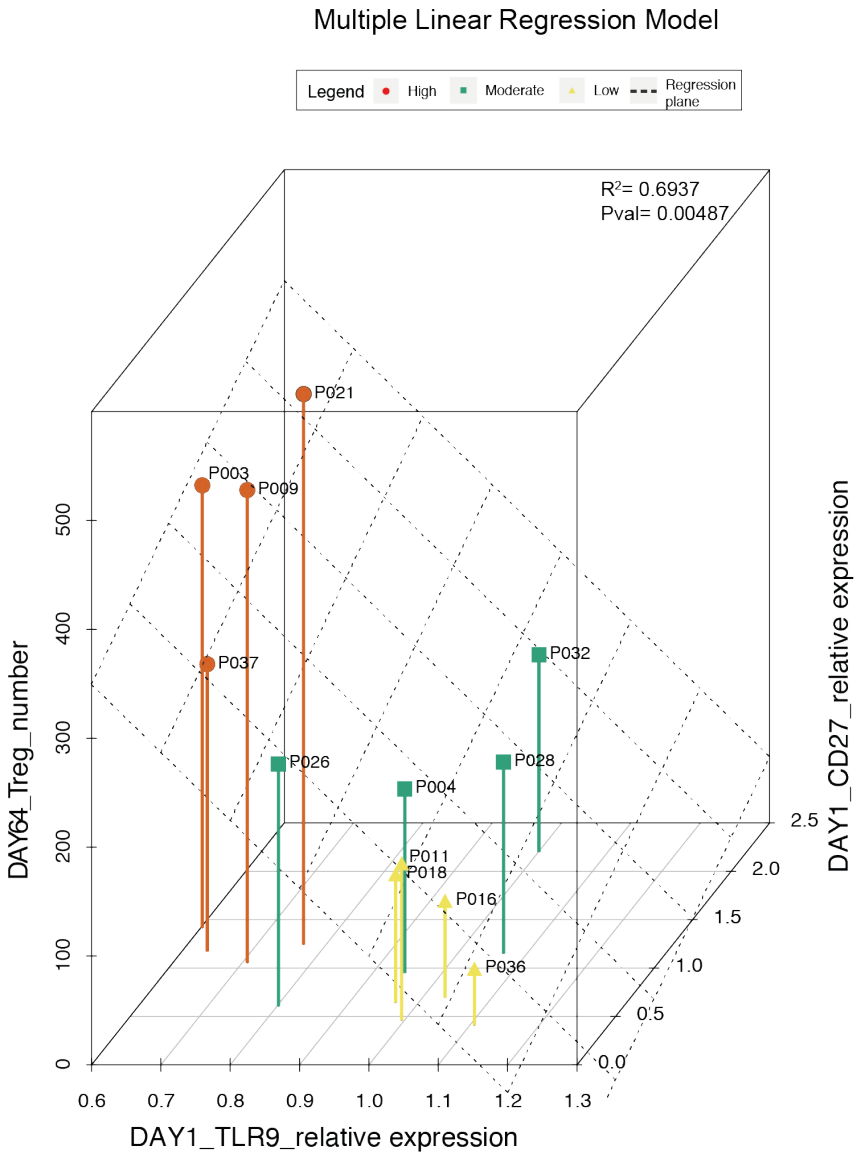

Figure 4.15: Multiple Linear Regression Model.

This 3D plot displays the multiple linear regression model obtained using the expression of both TLR9 and CD27 at D1 as predictors of the response variable (number of Tregs at D64). A model with intriguing scores was obtained (R^2= 0.6937and p-value= 0.00487). Each dot represents a patient and they are colour-coded depending on their Treg-response type: high (orange dots), moderate (green squares) and low (yellow triangles). The regression plane is also displayed in black dotted lines. X-axis: the relative expression of TLR9 at D1; Y-axis: Treg counts at D64; Z-axis: the relative expression of CD27 at D1.

Therefore, the computed multiple model formula (**Formula 4.1**) could be used to predict the Treg count after three cycles of 2MIU-IL-2 treatment in random ALS patients knowing their levels of CD27 and TLR9 expression at baseline.

$$\text{Treg number D64} = 724.57 + (59.49 * \text{CD27}) + (-625.00 * \text{TLR9})$$

Formula 4.1: Multiple linear model equation which would be able to predict Treg levels and thus patients' Treg-response to 2MIU-IL-2 administration given their measured level of TLR9 and CD27 expression at time of recruitment.

Moreover, the performance of the model was visually inspected by correlating the experimentally measured values, or observed Treg counts at D64, with the predicted ones (**Figure 4.16**). As expected, a strong positive correlation was reported (R= 0.833, R^2= 0.693, p-value= 0.0007) suggesting the robustness of the model.

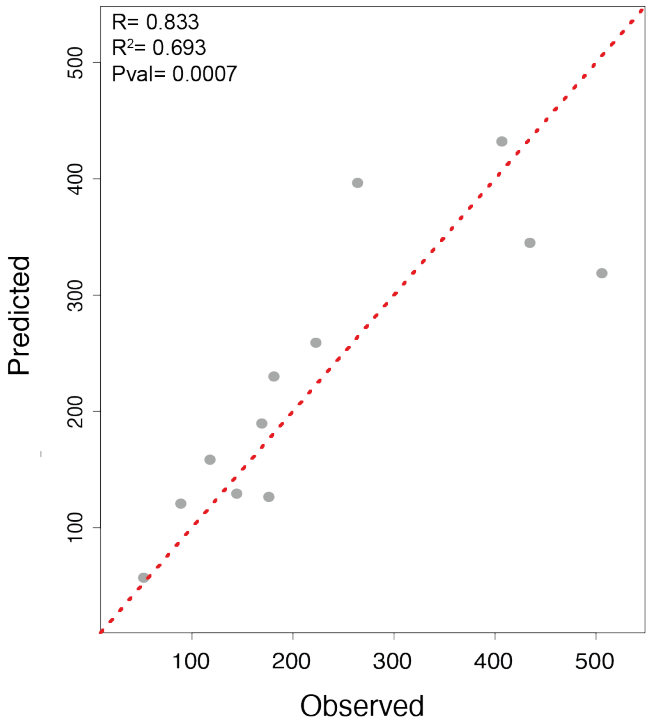

Figure 4.16: Model Predicted vs Observed Treg Values

Plot showing the correlation between flow-cytometry-measured Treg counts (observed) and the Treg numbers predicted using the multiple linear model (predicted). Correlation metrics (R= 0.833, R^2= 0.693, p-value= 0.0007) suggest an acceptable predictive model. Each dot represents a sample and a red dotted regression line is also shown.

Subsequently, tests were conducted in order to verify that the linear model assumptions (linearity, normality, homoscedasticity and independence; section 2.1.8) were met. This validation is crucial as, if these were not satisfied, the model would be impossible to interpret and to use. A summary of the scores obtained from these analyses is provided in **Table 4.4**. The first two tests aimed to confirm the linearity assumption. In fact, in the Global Statistics, the null hypothesis presumed a linear relationship between the two predictors and the outcome variable. This was not rejected (p-value>0.05) and therefore the linearity assumption was verified. The link function instead validated whether the dependent variables were continuous (and therefore a linear model can be used) and not categorical which would require the employ of other models (such as logistic regression). The obtained results were consistent with continuous variables as the null hypothesis (=variables are continuous) was not rejected (p-value>0.05). Skewness and Kurtosis are two tests that are useful to assess the normality of a given data set. The statistical hypotheses underlying these tests was that the distribution of the data was not symmetrical (normally distributed) but positively or negatively skewed or tailed. Scores obtained from both these tests suggested that the data followed a normal distribution and therefore this assumption was also acceptable. Lastly, a heteroscedasticity test was performed to verify that the residual variance is constant. This hypothesized homoscedasticity and, given that the null hypothesis was not rejected, this linear model assumption was also confirmed.

Table 4.4: Linearity Assumption Tests

This table summarises the results obtained from the statistical tests used to verify the linear model assumptions. These were performed using the gvmla() function in R (see chapter 2). For each test, the outputted value and p-value is reported together with the final decision on whether an assumption was met or not.

Statistical test name	Value	P-value	Decision
Global Statistics	3.3473	0.5015	Assumption acceptable
Link Function	0.5375	0.4635	Assumption acceptable
Skewness	1.5319	0.2158	Assumption acceptable
Kurtosis	0.3788	0.5382	Assumption acceptable
Heteroscedasticity	0.8991	0.3430	Assumption acceptable

To further validate the linear model assumptions and to graphically evaluate data, diagnostic plots were generated (**Figure 4.17**). The first graph called residual vs fitted was used to check the linear assumption. Dispersed data around the horizontal line without showing a clear pattern suggested a linear relationship between predictors and the outcome variable (**Figure 4.17A**). The Q-Q plot, shown in **Figure 4.17B**, was useful to inspect the normal distribution of the residuals. Data showing such a distribution should follow the red straight line. The majority of our samples were close to the reference line although some seemed to deviate slightly. However, they were all inside the standard error lines (dashed red lines) and therefore residuals were assumed to be normally distributed. The scale-location plot (**Figure 4.17C**) was generated to assess the homogeneity of the residual variance. Data seemed to be dispersed without a clear pattern which was consistent with a homoscedasticity. Lastly, the residual vs leverage plot was produced in order to depict samples with the greatest influence on the model. In fact, the leverage is an indicator of the impact of each data point as it iteratively removes one value and calculates the difference between the resulting model and the original one. Therefore, the larger the leverage, the more impactful is that data point on the model. Cook's distance was also shown and this score was computed as a combination of residual size and leverage. Data points outside the Cook's distance can be considered influential. **Figure 4.17D**

suggested that most of the data had a very mild impact on the model (leverage around 0.2). However, one data point seemed to be influential as it was beyond the Cook's distance. As expected, this value belonged to patient C01P032, the mild Treg-responder who seemed to have an outlier trend and for which removal would increase model performance. Nonetheless, as previously discussed, given the small patient size, it was not removed.

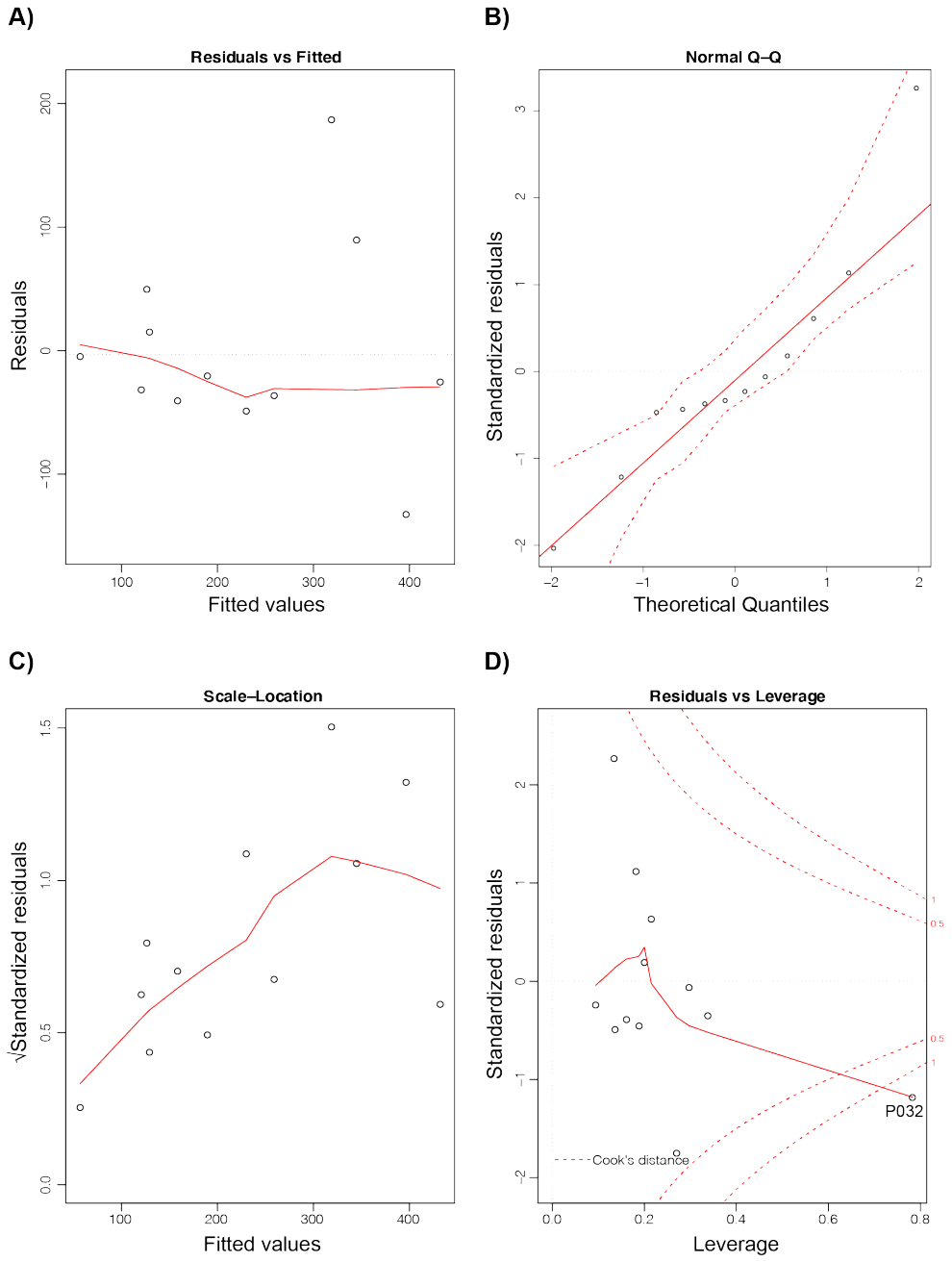

Figure 4.17: Diagnostic Plots.

This figure shows four diagnostic plots produced to visually inspect data and to verify if the linear assumption was met in the multiple linear regression model. These were generated using the plot() function in the basic R package **A)** Residual vs fitted plot is useful to check the linearity assumption. **B)** Q-Q plot is produced to visually assess the normal distribution of the data residuals. **C)** Scale-location plot allows the examination of data homoscedasticity. **D)** Residual vs Leverage plot helps with the identification of influential data points.

In addition, given that the proposed predictive biomarker model was a multiple linear regression model and therefore two predictors were used to forecast the outcome variable, a collinearity check was performed. This is the phenomenon by which two independent variables are correlated to each other. Ideally, no collinearity should be detected as this would impact the reliability of model. In fact, the information provided by the two predictive variables would be redundant which potentially leads to over-fitting (Bruce, 2017). Collinearity was assessed by computing the variance inflation factor (VIF). This calculates how the variance of the regression coefficients increases due to a correlation between the two or more predictors. A VIF value greater than 5 or 10 is generally accepted as in indicator of collinearity (Surles, 2007). The calculated VIF value indicated no cross correlation between TLR9 and CD27 in the proposed model (VIF= 1.084).

Altogether, both the results from the tests assessing the linear model assumptions and the collinearity check suggested that our multiple linear regression model was reliable.

Finally, a leave one out cross validation (LOOCV) was performed. This is an unbiased estimate of how the model fitted to the training data set would perform on new unseen data. The computed LOOCV metric was encouraging ($RMSE_{LOOCV}$= 84.28). Although these might be interpreted as a high score, as mentioned before, RMSE is scale-dependent measurement and therefore needs to be interpreted in the context of the range of values assumed by the dependent variable (Treg count at D64, SD_{Treg_D64}=144.8). The LOOCV RMSE was less than the SD of Treg counts at D64 and it was also close to the RMSE of the model ($RMSE_{multiple}$=76.7). Therefore, we concluded that the model was sufficiently robust when predicting new sets of data.

4.3 Discussion

The aim of the work described in this result chapter was to investigate on the inter-individual dissimilarities in patient Treg expansion following 2MIU-IL-2 treatment and how this correlated with their transcriptomic profile. In particular, immunological gene expression variations were evaluated through the use of the nanoString platform and the Autoimmune Discovery panel.

Given the considerable variations reported by Camu and colleagues (Camu et al., 2020) in terms of the Treg increase at the end of the trial, in this section of the study, patients were arbitrarily classified into high, moderate and low Treg-responders depending on the number of Tregs reported at D64 (high responders: $Treg_{D64}$ > 250 cells/ul of blood; moderate responders: $Treg_{D64}$ between 250 and 150 cells/ul of blood; low responders: $Treg_{D64}$ < 150 cells/ul of blood). Importantly, no significant changes were detected in these three groups in terms of age or disease decline per month. This is of crucial importance as immunological changes have been previously associated with the aging process (Montecino-Rodriguez et al., 2013) and a faster disease decline could have accounted for any reported transcriptional variability. Therefore, the exclusion of these two factors as possible confounding variables is key for the interpretation of our data.

A summary of the key findings reported in this chapter is provided below:

1) RNA samples from D1, D8 and D64 from four high, four low Treg-responders and four placebo were screened through nanoString to investigate the immunological transcriptomic changes that could account for the observed Treg dissimilarities throughout the course of the trial. Following the generation of nanoString gene expression profiles, quality controls were performed and the all the samples was considerate of acceptable quality to be included in the subsequent data analyses. A general overview of the expression of all the transcripts included into the panel across the different samples suggested a significant difference between high and low Treg-responders which was particularly evident at the baseline (D1). The subsequent multigroup comparison performed using the software Qlucore allowed the identification of 81 genes

being significantly differentially expressed and able to spatially separate the groups in a PCA plot. Moreover, a pathway scoring analysis revealed a more inflammatory-prone phenotype in the low compared to the high Treg-responders at time of recruitment.

2) Given the evident transcriptional dissimilarities reported between low and high Treg-responders at D1, the second objective of this study section was to identify a small number of transcripts whose expression at time of recruitment would be able to predict patient Treg-responsiveness (measured as number of Tregs at D64) at the end of the three administration cycles.
   A preliminary screening analysis was conducted by correlating the expression of all the transcripts included in the Autoimmune Discovery panel with either the Treg levels measured at D64 by flow cytometry (Camu et al 2020) or the *IL2RA* expression at D64 (nanoString data). Six promising biomarker candidates were selected (*BTLA*, *SBNO2*, *TRAF2*, *CD27*, *BLNK* and *TLR9*) and further investigated through qRT-PCR to obtain a complete expression dataset from all the 12 2MIU-IL-2 treated patients (given that nanoString analysis was only conducted on a selection of eight patients: four high and four low Treg-responders). The analysis of the full dataset revealed only one significant and strong negative correlation between *TLR9* expression at baseline and Treg numbers at D64 ($R= -0.809$, $R^2= 0.654$, p-value=0.0014). Although it did not reach statistical significance, *CD27* baseline expression showed a trend toward a correlation with Treg levels at D64 ($R= 0.416$, $R^2= 0.173$, p-value=0.179). Given the results obtained with the single linear models, *CD27* and *TLR9* expression data were combined and used to build a multiple linear regression model. Interestingly, this latter and more complex model appeared to perform better than the two single analyses and its metrics were particularly encouraging ($R^2= 0.694$, Adjusted $R^2= 0.626$, p-value= 0.005). Of importance, tests were carried out in order to ascertain the linear model assumptions and a leave one out cross validation (LOOCV) was performed to validate the robustness of our model when predicting new sets of data.

The performed nanoString analysis allowed the identification of a cluster of 81 genes showing an almost opposite expression between high and low Treg-responders at

time of recruitment. In particular, although this included genes encoding for both pro- and anti-inflammatory agents, it is interesting to note that the level of some pro-inflammatory mediator expression was higher in low compared to high Treg-responders at D1. This included some toll-like receptors (*TLR1* and *TLR2*), which have been previously reported to be elevated in ALS and in other neurodegenerative disorders (Casula et al., 2011, Azam et al., 2019); some members of the tumour necrosis factor superfamily (*TNFRSF8* and *TNFRSF10C*), a class of TNFα known to be implicated in the disease pathogenesis (Guidotti et al., 2021); and a chemokine ligand (*CXCL10*), whose levels of expression were previously shown to be negatively correlated with rate of ALS progression (Tateishi et al., 2010). In contrast, an opposite pattern was evident for some anti-inflammatory agents (including *TIGIT*, *IL2RA*, *IDO1*, *GATA3*, *IKZF2* and *CTLA4*), whose importance for Treg and immune suppression has been discussed in previous sections. These results suggested that less responsive individuals to ld-IL-2 were characterised by a more inflammatory prone phenotype at time of recruitment and therefore their reaction to the treatment appeared to be milder. This result is completely novel to the ld-IL-2 research, however, dissimilarities in the baseline immune transcriptional status might explain the previously reported inter-individual differences in other clinical trials investigating low levels of this cytokine as a treatment for different autoimmune disorders (Koreth et al., 2011, Koreth et al., 2016, Rosenzwajg et al., 2020, He et al., 2020). Nonetheless, it is important to notice that low vs high Treg-responders dissimilarities tended to became less evident over time during the administration period, as ALS patients who responded less appeared to have a more similar transcriptional phenotype to the high responders at D8 or D64. Placebo patients were instead characterised by less evident variations throughout the trial and, interestingly, their gene expression was more similar to the low Treg-responders at D1.

Consistently, the pathway scoring analysis showed that less responsive patients generally had increased baseline levels of activation of pro-inflammatory pathways compared to high Treg-responders. Nonetheless, a steep inhibition of nearly all these processes was reported in all the screened patients treated with the cytokine throughout the administration period regardless of their Treg responsiveness. More interestingly, some pathways appeared to have a greater degree of inhibition following 2MIU-IL-2 treatment in low compared to high Treg-responders. Therefore, we could speculate that, despite having a more inflammatory-prone transcriptome at the

beginning of the trial, the ld-IL-2-mediated expansion of the Treg population in low responders, although mild, was able to promote a continuous downregulation of pro-inflammatory pathways. In line with this, when closely investigated, ten processes involved in general inflammation (antigen processing and presentation, B cell receptor signaling pathway, chemokine signaling pathway, JAK-STAT signaling pathway, MAPK signaling pathway, natural killer cell mediated cytotoxicity, NF-kB signaling pathway, TNF signaling pathway, PI3K-Akt signaling pathway and Toll-like receptor signaling pathway) appeared to be downregulated both in the high as well as in the low Treg-responders over time whilst being upregulated in the placebo group. Two low responders (C01P018 and C01P36) appeared to be particularly inflammatory prone at the baseline and their pathway scores increased the variability of that group score. Interestingly, patient C01P036 was the participant showing the lowest Treg number at D64 (52.22 cells/ul of blood). Nonetheless, the variability seemed to be less evident over time suggesting that even this extremely low responder was able to downregulate these inflammatory pathways following 2MIU-IL-2 administration. Intriguingly, both high and low Treg-responders appeared to downregulate genes included in the pathway called "Neurodegenerative disease" and therefore progressively reduced scores were registered in both treated groups. In contrast, increased scores were reported over time in the placebo group. Despite this very interesting result, it is important to stress that the genes included in the Autoimmune Discovery nanoString panel are known to have a crucial role in the immune system and in the onset of autoimmune disorders. Therefore, inferring a reduced neurodegeneration or a decrease in disease progression would represent an over interpretation of the results. However, this evidence might suggest that the inflammatory pathways underlying and participating in neurodegenerative processes were mitigated following treatment administration.

Similarly to microarray data, nanoString results were validated by correlating the expression levels of the four key Treg transcripts (*FOXP3*, *IL2RA*, *CTLA4* and *IKZF2*) measured by qRT-PCR with those retrieved from the nanoString analysis. Strong, positive and very significant correlations were found for *IL2RA*, *CTLA4* and *IKZF2* which supported the validity and reliably of the nanoString gene expression profiles. However, surprisingly, no significant correlation was recorded for *FOXP3*. Consistently with this, *FOXP3* was not amongst the aforementioned 81 discriminatory variables.

This apparent paradoxical result can be explained by the different variants recognized by the qRT-PCR probes and the ones included in the nanoString panel. In fact, whilst qRT-PCR allowed the detection of two splicing isoforms (NM_001114377, NM_014009), only the variant NM_014009 was identified by the Autoimmune Discovery panel. This latter variant encodes for the full length *FOXP3* (*FOXP3*fl), which constitutes only 20-30% of the total *FOXP3* mRNAs, whilst 70% of the transcripts are NM_001114377, which is the result of exon 2 skipping (FOXP3Δ2) (Mailer, 2018). A recent review described specific functions associated with the different variants and their impact in health and disease (Mailer, 2018). Exon 2 seemed to be crucial for the inflammatory Th17 as it interacted with transcription factors (such as RORα and RORγt), which are responsible for their differentiation (Zhou et al., 2008, Mailer, 2018). This exon harbours a nuclear export sequence (NES) which promotes the relocalization of the protein from the nucleus to the cytoplasm. Interestingly, predominant localization of FOXP3 in the nucleus has been reported to be mainly associated with $CD4^{+}CD25^{+}$ Tregs (Magg et al., 2012). In addition, increased FOXP3fl levels were linked with several autoimmune and inflammatory disease such as psoriasis, rheumatic arthritis and inflammatory bowel disease (Mailer, 2018). Moreover, in a recent report, immunodysregulation polyendocrinopathy enteropathy X-linked syndrome (IPEX), a disease characterized by mutations in FOXP3 and autoimmunity, FOXP3Δ2 was found to support Treg development and mitigate IPEX symptoms (Frith et al., 2019). Taken together, this body of evidence suggests a crucial importance of FOXP3Δ2 for Tregs. Therefore, our data indicating a preferential increase in the expression in this splice variant, and not FOXP3fl, is probably consistent with augmented suppressive capacity of ALS Tregs following 2MIU-IL-2 treatment. PCR validation of these results is currently planned to be conducted by Mariam Alajmi, an MSc student in Prof Janine Kirby's laboratory.

Lastly, following a biomarker screening, a predictive multiple linear regression model was generated able to forecast the level of Treg expansion in ALS patients given their baseline expression of two gene: *TLR9* and *CD27*. Specifically, patients showing higher levels of *TLR9* and lower levels of CD27 were more likely found to respond more to the 2MIU-IL-2 treatment. Toll-like receptors (TLR) are a class of pattern recognition receptors implicated in pathogen identification and immune-response initiation. TLR9 is localized on the endoplasmic reticulum and recognizes

unmethylated CpG motifs, characteristic of bacterial and viral DNA. Dysregulation of *TLR9* signaling has been associated with several autoimmune but also neurodegenerative diseases (Fiebich et al., 2018, Marongiu et al., 2019). Interestingly, increased *TLR9* expression was reported in the spinal cord of $SOD1^{G93A}$ transgenic mice (Letiembre et al., 2009). Moreover, mice lacking of SMCR8, a protein which interacts with C9ORF72 to regulate autophagy and lysosomal function, had disrupted TLR3, TLR7 and TLR9 signaling which resulted in widespread inflammation (McAlpine et al., 2018). CD27 is a member of the tumor necrosis factor receptor family. It is expressed on a variety of immune cells including $CD4^+$, $CD8^+$ T cells, B cells and NKs. The binding of its ligand CD70 leads to the activation of these cells and an inflammatory response. However, CD27-CD70 was found to play a key role in Treg generation in the thymus and genetic ablation of either protein lead to a reduced number of thymic Tregs (Coquet et al., 2013). Moreover, CD27-deficiency caused reduction in the frequency of Tregs (Winkels et al., 2017, Claus et al., 2012). Interestingly, a recent study reported CD27 as one of the downregulated transcripts solely differentially expressed in rapidly progressive patient monocytes (Zhao et al., 2017). Collectively these data highlight the great potential of this predictive model for future ALS clinical treatments with ld-IL-2. If validate in a larger cohort, these transcripts could serve both as biomarkers of target engagement, to monitor the efficacy of the drug administration in each affected individuals, and as a crucial tool for patient stratification. Importantly, there is an urgent need for such tools in ALS clinical research, as currently no effective biomarkers have been identified despite a thorough investigation over the past 20 years (Bakkar et al., 2015, Verber et al., 2019). If proven valuable after appropriate validation steps, our model could be used for future precision medicine approaches, which would allow the stratification of ALS individuals to enrich for patients who are more likely to respond to ld-IL-2.

In conclusion, results presented in chapter 3 and 4 highlight the molecular effects of ld-IL-2 as a treatment for ALS. Data are consistent with a dose-dependent IL-2 effect on gene expression, with increased transcripts showing a greater level of upregulation, and similarly, decreased DEGs being more downregulated following the higher dose administration of IL-2. This is in line with a greater degree of Treg marker upregulation and a more evident Treg expansion, as measured by flow cytometry (Camu et al., 2020), in the 2MIU-IL-2-treated group compared to 1MIU. For this reason, this was

proposed as ideal treatment dosage for ALS and further clinical investigation are currently being conducted investigating only the effects of 2MIU-IL-2 in a larger phase III trial (MIROCALS, see chapter 6 for trial description). Blood longitudinal transcriptomic analysis revealed evidence of reduced inflammation as early as after the first injection cycle, although Treg markers upregulation reached a peak only following the third cycle, suggesting a cumulative effects of repeated 2MIU-IL-2 administrations. Gene expression analyses also suggested the presence of inter-individual dissimilarities in patient reaction to 2MIU-IL-2 due to different inflammatory transcriptional phenotypes at recruitment. In this respect, the generated predictive model is of crucial importance as, if validate, would allow ALS patient stratification and it could be used as biomarker of target engagement in clinical trial settings.

Chapter 5 – Results: The Effects of IL-2 on CNS Cells

Considering the promising effects of ld-IL-2 reported in the peripheral blood of the IMODALS participants, and also taking into account that this cytokine is able to cross the blood brain barrier, the overall aim of the work described in this chapter was to characterize the effect of IL-2 on central nervous system (CNS) cells. Specifically, the first objective was to evaluate the transcriptional response of this cytokine on induced neuronal progenitor cell (iNPC)-derived astrocytes reprogrammed from ALS or healthy control fibroblasts (iAstrocytes) using the Oxford Nanopore cDNA sequencing technique. Additionally, normal murine MNs were co-cultured with iAstrocytes in the presence of IL-2 to establish whether this cytokine reduces ALS iAstrocyte-induced toxicity, though increasing MN viability and axon arborization. To our knowledge, this was the first time that the molecular effects of IL-2 were investigated on astrocytes or MNs. Results reported in this last chapter were collected over the period from June 2020 to July 2021. Due to several Covid-19 related impediments (such as: reduced working hours, limited laboratory occupancy and delays in the arrival of consumable deliveries), some data are still preliminary although the aim is to complete data collection following the completion of the PhD.

5.1 Treatment Optimization

Given the novelty of this type of work involving IL-2 and CNS cells, the first objective was to optimize the treatment settings. Specifically, this cytokine was administered at different concentrations and with different incubation times to test for the best combination that allowed the most evident reaction. The experiments were conducted on nine iNPC-derived astrocytes reprogrammed from the fibroblasts of: three sporadic ALS (sALS) (namely P009, P12 and P17), three ALS patients carrying a *C9orf72* mutation (P78, P183 and P201) and three age-matched controls (155, 161 and AG). Importantly, these fibroblasts were not biopsied from patients included into the IMODALS trial but these cells were available in our Department and they are routinely used by Dr Laura Ferraiuolo and her team.

Firstly, the expression of the IL-2 receptor subunits (*IL2RA*, *IL2RB* and *IL2RG*) was assessed through qRT-PCR in untreated ALS and in healthy control iAstrocytes to ascertain their presence on these cells under basal conditions. This is of crucial importance as the lack of the receptor would preclude any molecular effect of the cytokine. Results from *IL2RA* revealed that the expression of this subunit was extremely low (threshold cycle (Ct) > 32) in all the investigated iAstrocyte lines (**Figure 5.1**). This was particularly evident in two experimental replicates of two sALS iAstrocytes (P009 and P12), in which expression was probably below the sensitivity of the instrument.

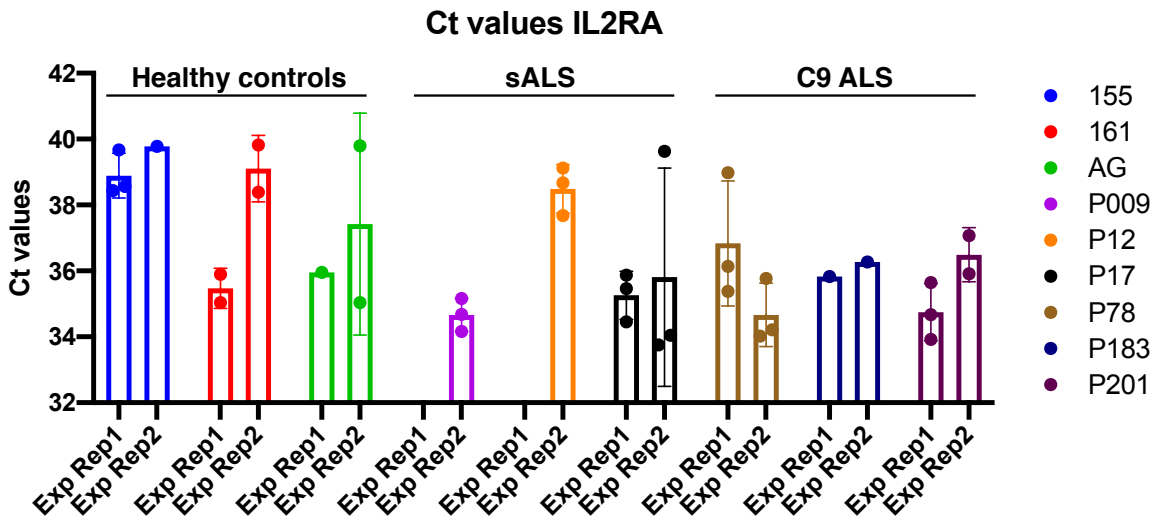

Figure 5.1: Basal IL2RA Level of Expression in iAstrocytes

This bar graph show the level of *IL2RA* expression in the iAstrocytes reprogrammed from healthy controls (155, 161and AG), sALS (P009, P12 and P17) and C9 ALS (P78, P183 and P201). In particular, on the X-axis, two experimental replicates (indicated in the graph as Exp Rep 1 or 2, N=2) for each line are displayed alongside each other whilst on the Y-axis raw Ct (threshold cycle) values are reported. Each dot represent a technical replicate (three technical replicates were performed for each line but often no Ct value was detected by the qRT-PCR instrument, therefore in several occasions less than three dots are displayed for one experimental replicate). This suggests that IL2RA expression is very low in this cells. Data are reported as mean ± SD. A colour legend indicates the different iAstrocyte lines.

Subsequently, the expression of *IL2RB* and *IL2RG* were investigated. Both the ΔCt value, which is the difference between the threshold cycle of the gene of interest and the reference housekeeping gene (GAPDH), and the relative expression value (normalized on the average ΔCt of the healthy controls) were plotted in **Figure 5.2A** and **5.2B-C**, respectively. These data suggested that the other two subunits of IL-2 receptor were expressed in all the iAstrocyte lines. However, elevated levels of *IL2RB* were reported in P12 and P78 lines whereas *IL2RG* expression was increased in P201. Importantly, a qualitative analysis was conducted here as only two experimental replicates were performed, statistical analysis is pending and will be performed in the future following the collection of the third replicate. This will assess any significant difference between astrocyte lines in the subunit expression.

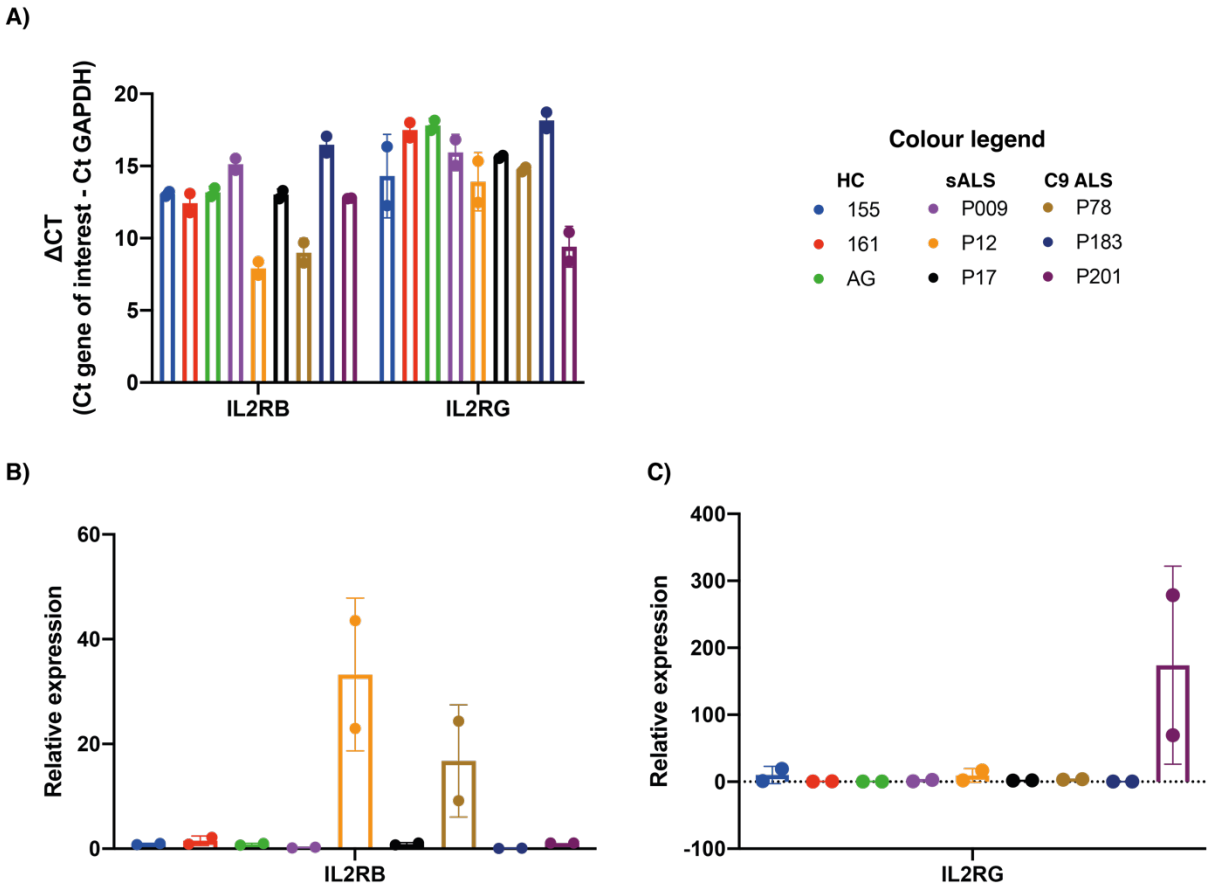

Figure 5.2: Basal IL2RB and IL2RB Level of Expression in iAstrocytes

In these figures, the basal level of expression of *IL2RB* and *IL2RG* are reported. (**A**) A bar graph shows the ΔCt (difference between the threshold cycle of the gene of interest and the reference housekeeping gene GAPDH) of *IL2RB* and *IL2RG* across all the samples. Each dot represents the mean ΔCt from three technical replicates. Two experimental replicates (N=2) are reported for each iAstrocyte line. Moreover, two plots show the relative expression of *IL2RB* (**B**) and *IL2RG* (**C**) (data normalized on the average ΔCt value of the healthy controls). Each dot represents the mean relative expression from three technical replicates. Two experimental replicates (N=2) are reported for each iAstrocyte line. Data are reported as mean ± SD. A colour legend is also shown.

Taken together, these data suggest that iAstrocytes predominantly expressed an IL-2 receptor which is only made of the subunits IL2RB and IL2RG. This is consistent with an intermediate affinity IL-2 receptor. In fact, as review by Spolski and colleagues and as mention in the introduction, three receptor classes have been reported in the literature: the low affinity (with a constant of dissociation Kd ~10^{-8} M) receptor, which

only consists of the subunit IL2RA; the intermediate affinity (Kd ~10^{-9} M), which contains IL2RB and IL2RG subunits; or the high affinity (Kd ~10^{-11} M) receptor made of IL2RA, IL-2RB and IL2RG (Spolski et al., 2018) (see **Figure 1.5**). Therefore, given the constant of dissociation of the intermediate affinity receptor, iAstrocytes were hypothesized to react to nanomolar concentrations of the cytokine.

Therefore, a decision was made to test for different nanomolar concentrations of IL-2 and different incubation periods to find the optimal treatment combination. Various settings were tested and samples analysed through qRT-PCR. In particular, the expression of *IL2RB* was measured as several pieces of evidence suggest that it is induced following IL-2 treatment (as reviewed by (Spolski et al., 2018). Additionally, three other genes (MYB proto-oncogene, cyclin D2 or CCND2 and caspase-3 or CASP3), the expression of which was previously reported to be increased following the exposure to this cytokine (Beadling and Smith, 2002, Kovanen et al., 2005), were also investigated. Importantly, transcriptomic data published in these papers were obtained from both human peripheral blood mononuclear cells and T cells and these genes appeared to be commonly differentially expressed upon IL-2 receptor stimulation. However, to our knowledge, no similar studies were previously conducted on astrocytes. Therefore, an additional aim was to investigate whether these genes were also induced in iAstrocytes as a result of a common regulative effect promoted by the cytokine.

Firstly, two different incubation periods (1 hr or 4 hrs) and two IL-2 doses (10 and 100nM) were tested as an initial trial involving only two iAstrocyte lines per group (**Figure 5.3**). Although a trend toward an increase was reported over time in several lines, a significant increase in *CASP3* and *CCND2* was reported exclusively in the P78 line following exposure to 10nM IL-2 for 1 hr. Generally, high standard deviations were reported. Interestingly, most of the lines exposed to the control condition (1:1000, phosphate-buffered saline (PBS) + 5% glucose solution) for 4 hrs showed higher levels of expression of the four transcripts compared to the 1hr counterpart.

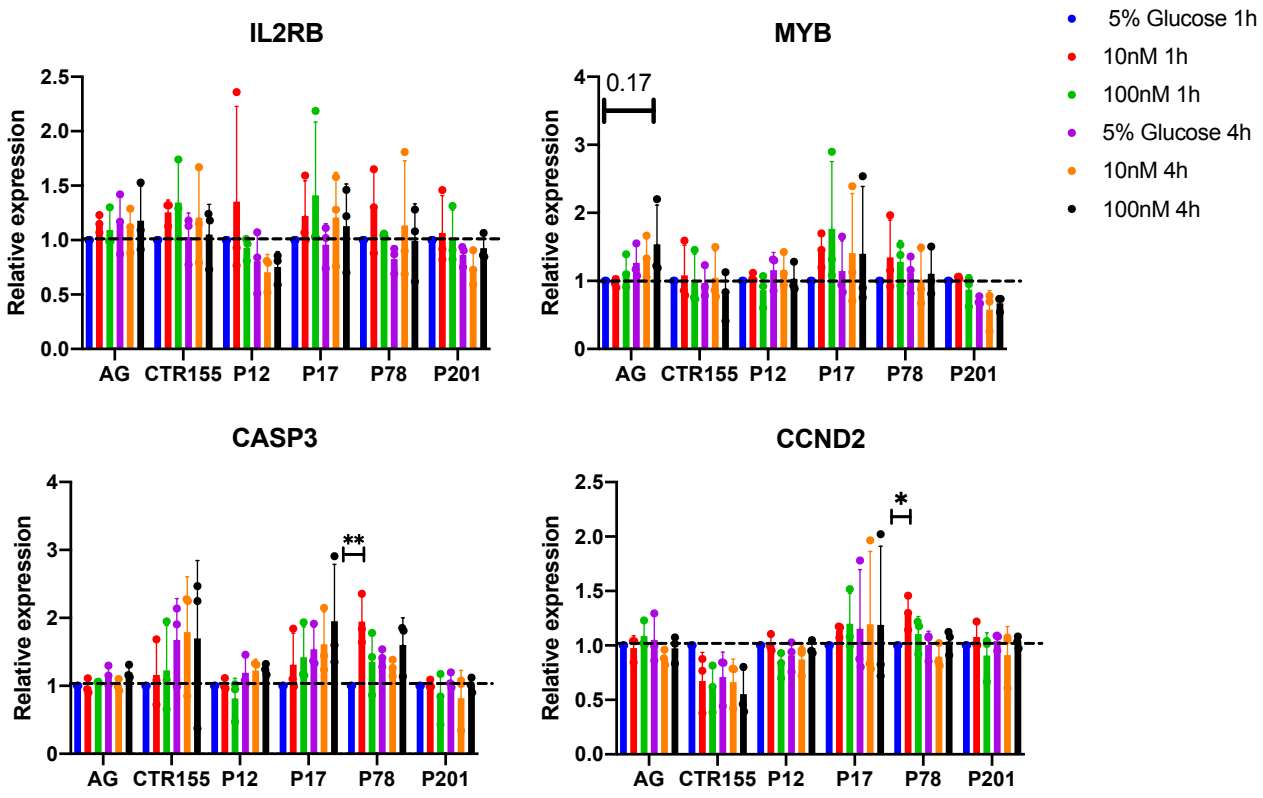

Figure 5.3: The Effect of IL-2 (10 or 100nM) for 1 or 4 Hours on iAstrocytes

Levels of expression of *IL2RB*, *MYB*, *CASP3* and *CCND2* following either 10 or 100nM IL-2 treatment for 1 or 4 hours are displayed in this figure. No significant increases are reported except for *CASP3* and *CCND2* in P78. Interestingly, higher expression levels are visible after 4hrs in samples exposed to the control condition (1:1000, 5% PBS + glucose solution). This preliminary analysis was performed on a selection of 6 out of 9 iAstrocytes (2 healthy controls: AG and 155, 2 sALS: P12, P17 and 2 C9 ALS: P78 and P201). A colour legend indicating the different treatment settings is shown on the right hand side of the figure. Each dot represents the mean relative expression from three technical replicates. Three experimental replicates (N=3) are reported for each iAstrocyte line. Expression data of each gene in each iAstrocyte line were normalized to GAPDH and to the control condition at 1hr (1:1000, 5% PBS + glucose solution). Mean ± SD are displayed. One-way ANOVA with Tukey's correction for multiple comparisons was performed (* : Adjusted p-value < 0.05; ** : Adjusted p-value < 0.01).

To investigate this further, a literature review was carried out. Intriguingly, a recent study suggested that the foetal bovine serum (FBS), included in the culture medium of human induced pluripotent stem cell-derived astrocytes, was capable of inducing transcriptional changes that were comparable to those promoted by a treatment with TNF-α. In fact, cells similarly acquired a reactive and inflammatory phenotype with either FBS or TNF-α (Perriot et al., 2018). This is in line with other studies in the literature that investigated the effect of several cytokines (although not IL-2) in astrocytes, which were treated in either reduced or in serum-free medium (summarised in **Table 5.1**). This is interesting considering that data reported in **Figure 5.3** were obtained using medium containing 10% FBS. Nonetheless, contradictory methods are reported in the literature as other research groups used higher FBS concentration (10%) in their medium when treating cells with different cytokines (**Table 5.1**). Given this body of evidence, FBS was hypothesized as impactful on gene expression levels of *IL2RB*, *MYB*, *CASP3* and *CCND2* and able to mask the effect of the IL-2 treatment. This was particularly when assessing the longest exposure time (4 hrs).

Table 5.1: Experimental Settings in Previous Studies Testing Cytokines in Astrocytes

This table summarises the evidence from the literature regarding treatment settings when investigating cytokine effects on astrocytes. Author and date of the study is reported in the first column while the complete citation is available in the bibliography. For each paper, the type of astrocyte and cytokine used are reported together with chosen experimental settings (i.e dose, treatment time and medium ingredients). Particular attention was given to the chosen FBS concentrations which are reported in bold.

Paper	Cell type used	Cytokine tested	Dose of cytokine tested	Ingredients of media used during cytokine treatments	Cytokine incubation time
(Thelin et al., 2020)	iPSC-derived astrocytes	IL-1b, IL-4, IL-6, IL-10, TNF-a	1-10,000 pg/ml 100-1,000,000 pg/mml (IL6)	- DMEM/F12 Glutamax - Neurobasal - L-glutamine - N2 supplement - non-essential amino acids - B27 supplement - β-mercaptoethanol - insulin - **serum-free**	1-24-48-72 hours
(Burmeister et al., 2019a)	Murine primary astrocytes	IL-20	1-10-30-100 ng/ml	- DMEM - penicillin/streptomycin - **5% FBS**	30 min, 2 and 4 hours
(Santos et al., 2017)	iPSC-derived astrocytes	IL-1b	10ng/ml	- DMEM/F12 Glutamax - N2 supplement - B27 supplement - **10% FBS**	5 hours
(Tarassishin et al., 2014)	Mouse and human astrocytes	IL-1b	10 ng/ml	- DMEM - antibiotics - **0.5% FBS**	6 and 22 hours
(Wang et al., 2014)	Primary cultured astrocytes	IL-1b	0.02 to 2 ng/ml	- DMEM - 5 µg/ml bovine insulin - 0.6% glucose - **10% FBS**	6h and 24h
(Norden et al., 2014)	Murine primary astrocytes	Activated with LPS (1h) and then IL-10 (3 hours)	10 ng/ml	Unclear astrocyte medium ingredients, however, before treatment, cells were washed with **serum-free** medium	3 hours
(Jang et al., 2013)	Murine primary astrocytes	IL-4 and IL-10	10 ng/ml	- DMEM - 100 U/ml penicillin - 100 µg/ml streptomycin - **10% FBS**	8 hours and 24 hours
(Semple et al., 2010)	Murine primary astrocytes WT and CCL2-/-	IL-1b	10 ng/ml	- DMEM **- 1% FBS** medium	2-4-8-16-24 hours
(Ma et al., 2010)	Murine primary astrocytes	IL-6/R (IL-6 + sIL-6R), IL-17, IL-6R + IL-17	10 ng/ml and 25 ng/ml	-DMEM - glucose (6 g/l)/glutamine (2 mM) - non essential amino acid (0.1 mM) - 0.1% gentamicin -**serum free**	2-4-8-24 hours
(Dong et al., 1999)	Rat primary astrocytes	IFN-γ	250 U/ml	-DMEM - glucose (6 g/l)/glutamine (2 mM) - non essential amino acid (0.1 mM) - 0.1% gentamicin -**serum free**	1-2-12 hours

Therefore, to test this hypothesis, the experiment was repeated such that iAstrocytes were only cultured in medium containing 10% FBS during their differentiation (until D5), whilst the treatment (at D6) was performed in 1% FBS medium. As more encouraging results were registered with 10nM IL-2, we decided to focus on this concentration to perform a preliminary evaluation of this treatment in 1% FBS medium for 1 or 4 hrs (**Figure 5.4**). While no variation was reported amongst the healthy controls, results showed a trend toward an increased expression of the investigated genes in both C9 and sALS iAstrocytes. This was particularly evident for *MYB* and *CCND2* following 4 hrs of IL-2 exposure although the data did not reach statistical significance. However, it is important to notice that we used a very stringent type of statistical test (Two-way ANOVA with Tukey's multiple comparison correction), which is affected by the small number of replicates.

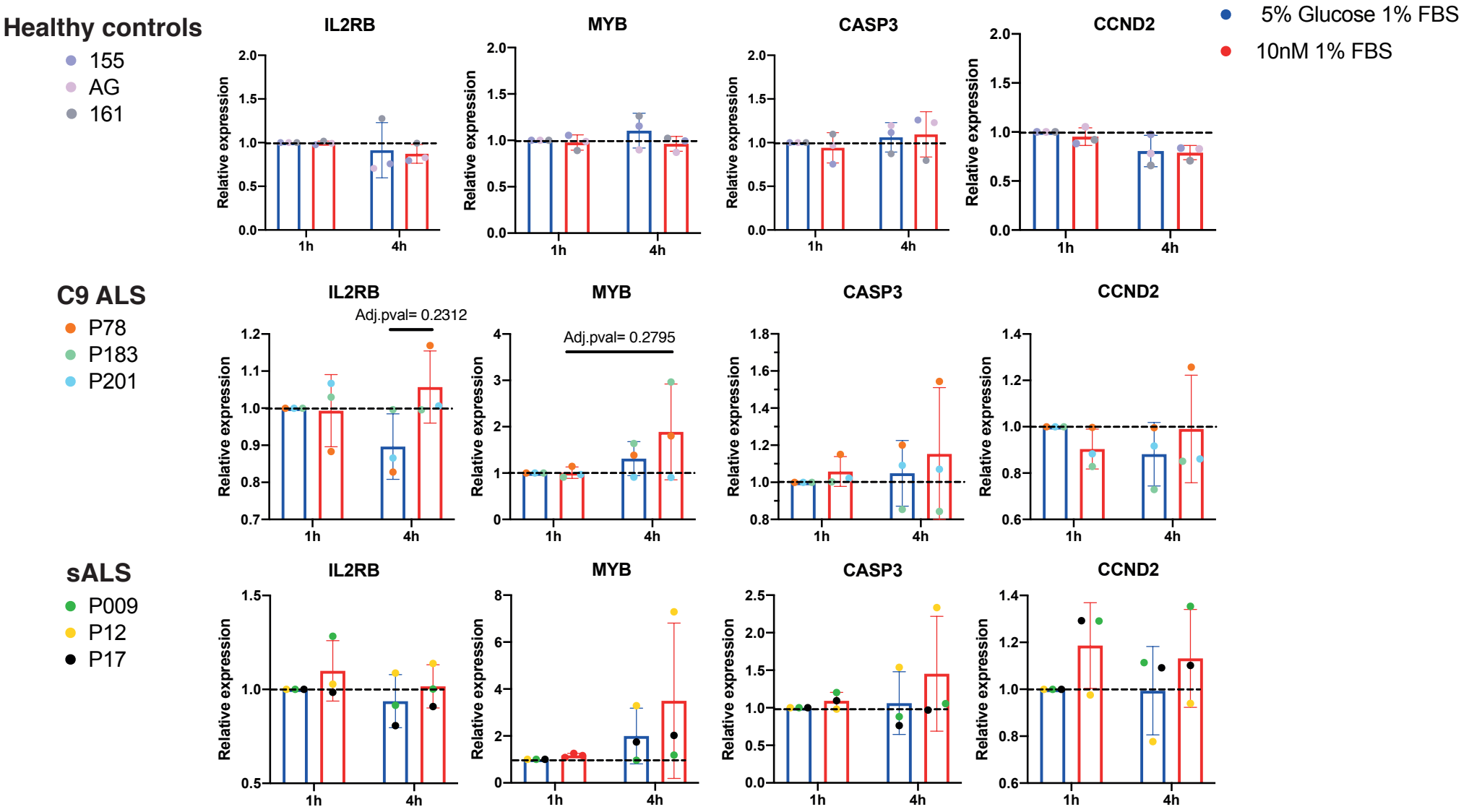
Healthy controls
155
AG
161
C9 ALS
P78
P183
P201
sALS
P009
P12
P17
5% Glucose 1% FBS
10nM 1% FBS
IL2RB
MYB
CASP3
CCND2
Relative expression
1h
4h
Adj.pval= 0.2312
Adj.pval= 0.2795

Figure 5.4: The Effect of IL-2 (10nM in 1% FBS medium) for 1 or 4 Hours on iAstrocytes.

This figure summarises the changes in the expression of *IL2RB*, *MYB*, *CASP3* and *CCND2* following the exposure to 10nM IL-2 in 1% FBS medium for 1 or 4 hours. No differences are reported amongst the healthy control (155, 161 and AG) lines while both C9 (P78, P183 and P201) and sALS (P009, P12 and P17) iAstrocytes show a trend toward an increased expression, although they do not reach statistical significance. Each dot represents the mean relative expression from three technical replicates. One experimental replicate (N=1) and three biological replicates are reported for each iAstrocyte line. Expression data of each gene in each iAstrocyte line were normalized to GAPDH and to the control condition at 1hr (1:1000, 5% PBS + glucose solution). Mean ± SD are graphed. Two-way ANOVA with Tukey's correction for multiple comparisons was performed.

To increase the statistical power of the analysis, all the ALS iAstrocyte samples following 4 hr treatment were grouped together and analysed regardless of their genetic background (**Figure 5.5**). A significant (p-value < 0.05, Two-tailed unpaired T test) increase was reported for *IL2RB*, *MYB* and *CASP3*. High variability was reported, which was particularly evident for the expression of *CCND2*.

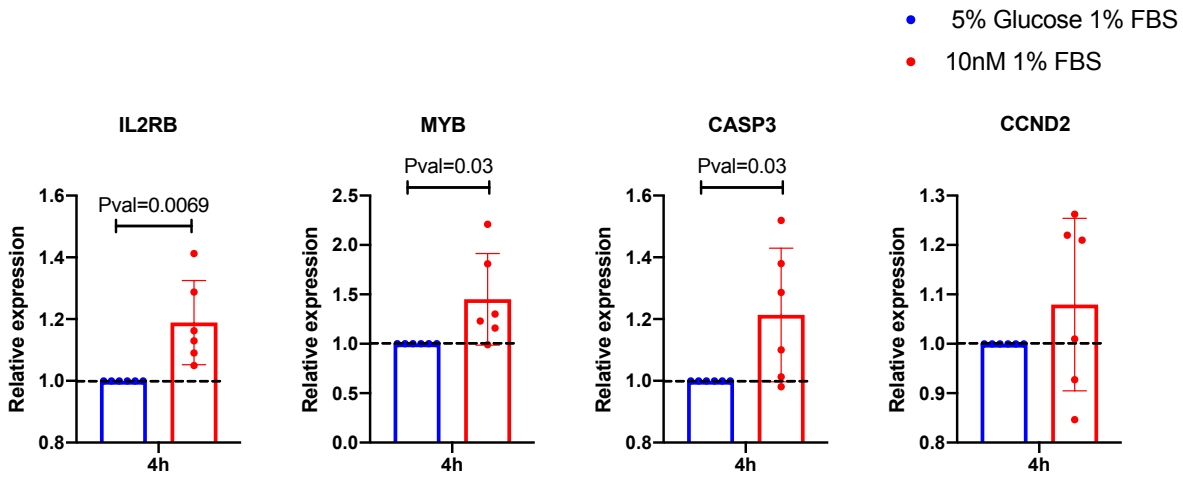

Figure 5.5: Effect of IL-2 (10nM in 1% FBS Medium) for 4 hrs on iAstrocytes.

In this figure, the expression data from the 3 C9 (P78, P183 and P201) and 3 sALS (P009, P12 and P17) iAstrocytes were plotted together to increase the statistical power of the analysis. Each dot represents the mean relative expression from three technical replicates. One experimental replicate (N=1) is reported for each of the 6 iAstrocyte lines. Expression data of each gene in each iAstrocyte line were normalized to GAPDH and to the control condition at 4 hr (1:1000, 5% PBS + glucose solution). Mean ± SD are graphed. Two-tailed unpaired T-test was performed.

Taken together, these data suggested that reduced FBS levels increased the detectability of gene expression changes in iAstrocytes. Moreover, the most evident reaction was obtained following 4 hr treatment with IL-2. In particular, 10nM seemed to be the most promising concentration. However, to validate this hypothesis, experiments were performed by treating cells with a range of different IL-2 concentrations (1, 5, 10, 50, 100nM) (**Figure 5.6**). A steady increase in the expression of all the four genes, which peaked with 10nM IL-2, was reported in most of the ALS iAstrocyte lines, particularly in C9 ALS cells. However, the level of expression tended to be decreased with higher IL-2 doses (50 and 100nM). Consistent with previous findings, *MYB* and *CASP3* appeared to be the major induced transcripts although the MYB increase in C9 ALS iAstrocyte was the only one to reach statistical significance

(Two-way ANOVA with Tukey's multiple comparison correction). However, when all ALS patient derived iAstrocytes were plotted together (both C9 and sALS lines), significant increases in expression were detected for both *CASP3* and *MYB* (**Figure 5.6D**). Generally, some changes were also reported in the healthy controls whilst a sharp, but more variable, peak in *MYB* expression was registered with 10nM IL-2.

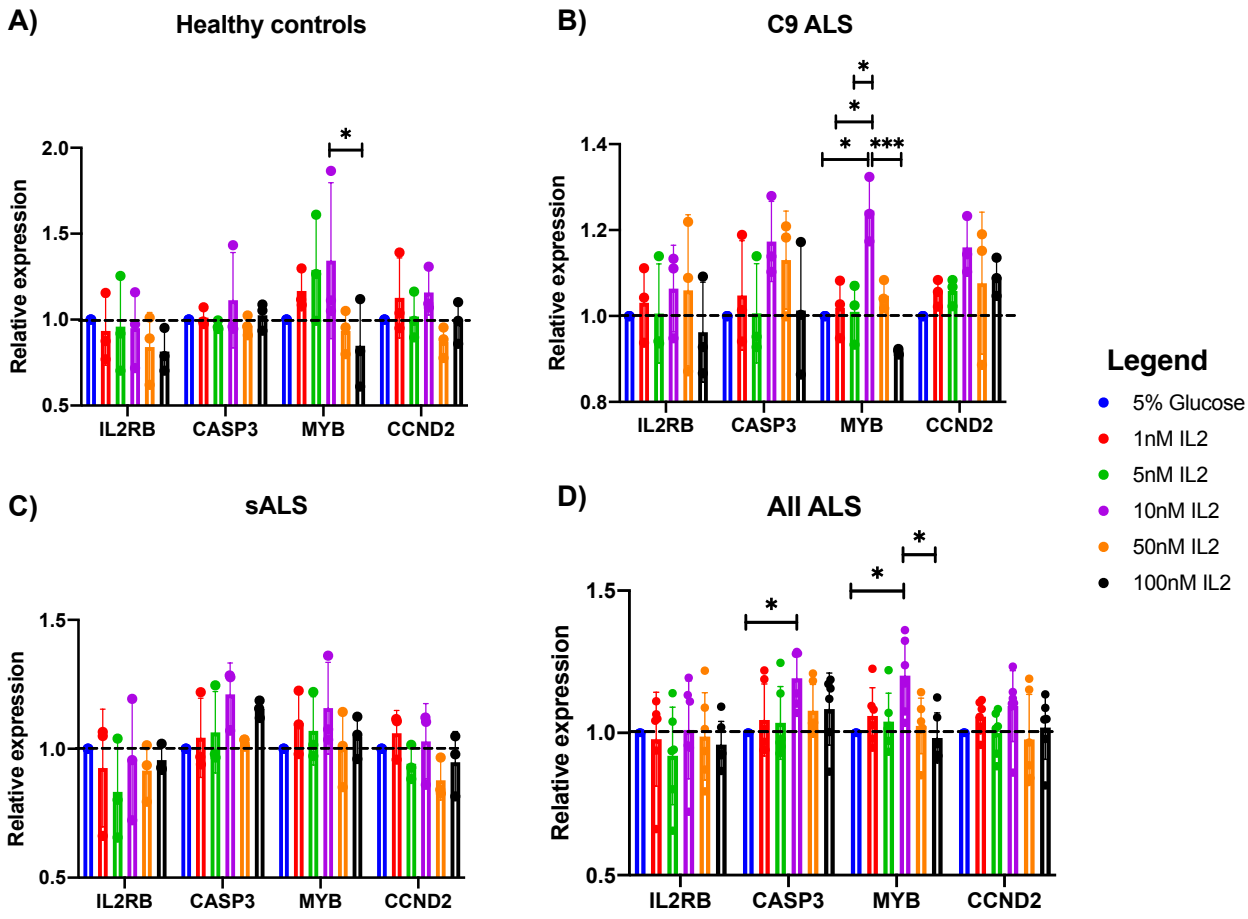

Figure 5.6: IL-2 Dose-Dependency in iAstrocytes.

This figure summarises gene expression changes of the four genes following treatment with different concentration of IL-2 (1, 5, 10, 50 and 100nM) for 4 hrs in 1% FBS medium. Results from three biological replicates of (**A**) healthy controls (155, 161 and AG), (**B**) C9 ALS (P78, P183 and P201), (**C**) sALS (P009, P12 and P17) or all the ALS iAstrocytes together (P78, P183, P201, P009, P12 and P17) are displayed. Each dot represents the mean relative expression from three technical replicates. One experimental replicate (N=1) is reported for each iAstrocyte line. Expression data of each gene in each iAstrocyte line were normalized to GAPDH and to the control condition (1:1000, 5% PBS + glucose solution). Mean ± SD are graphed. Two-way ANOVA with Tukey's correction for multiple comparisons was performed (* : Adjusted p-value < 0.05; ** : Adjusted p-value < 0.01).

Taken together, these data suggested that the optimal treatment settings for iAstrocytes were 10nM IL-2 in 1% FBS medium for 4 hr. Although statistical significance was reported in limited number of cases, this decision was further supported by the fact that these cells predominantly express the intermediate affinity receptor, whose constant of dissociation is ~10^{-9} M. Therefore, it was proposed to use 10nM as the most suitable concentration at which iAstrocytes would illicit a response to treatment. Additionally, as previously reported in the literature (Santos et al., 2017, Tarassishin et al., 2014, Wang et al., 2014, Norden et al., 2014, Jang et al., 2013, Semple et al., 2010, Ma et al., 2010, Burmeister et al., 2019a, Dong et al., 1999), short incubation periods seemed to be ideal to study gene expression changes in astrocytes and, in line with this, 4hr was chosen as treatment time length. Moreover, as summarised in **Table 5.1**, reduced levels of FBS were repeatedly used in different studies to test the effect of interleukins on astrocytes (Perriot et al., 2018, Tarassishin et al., 2014, Norden et al., 2014, Semple et al., 2010, Burmeister et al., 2019a, Dong et al., 1999) as higher concentrations seemed to promote a reactive and inflammatory transcriptional phenotype (Perriot et al., 2018).

5.2 Cytotoxicity Assays

As previously discussed, *CASP3* has been reported in the literature as an IL-2 induced transcript. Consistently with this, increased expression was reported in our iAstrocyte lines following IL-2 treatment (**Figure 5.7**). Caspases are a well-defined class of proteases that are crucial mediators of apoptosis. Given this, an investigation was performed in order to exclude any possible cell death induction following 4 hr treatment with IL-2. To this end, lactate dehydrogenase (LDH) cytotoxicity assays, which are colorimetric assays that allow the measurement of damaged cells in culture, were carried out (see section 2.2.3).

Following 4 hrs of 10nM IL-2 treatment in 1% FBS medium, LDH assays were performed (**Figure 5.7**). Low percentages of cell damage were observed (approximately 2-4%) and, importantly, no significant (two-tailed unpaired T test) increase in cytotoxicity was reported following IL-2 treatment in either healthy controls, C9 or sALS iAstrocytes compared to the control condition (1:1000, PBS + 5% glucose solution for 4 hrs). Interestingly, a significant difference was reported only for the control line 161. However, data indicated a decrease in the levels of damaged cells following IL-2 treatment. A similar trend was reported for patients P78 and P201 although statistical significance was not reached.

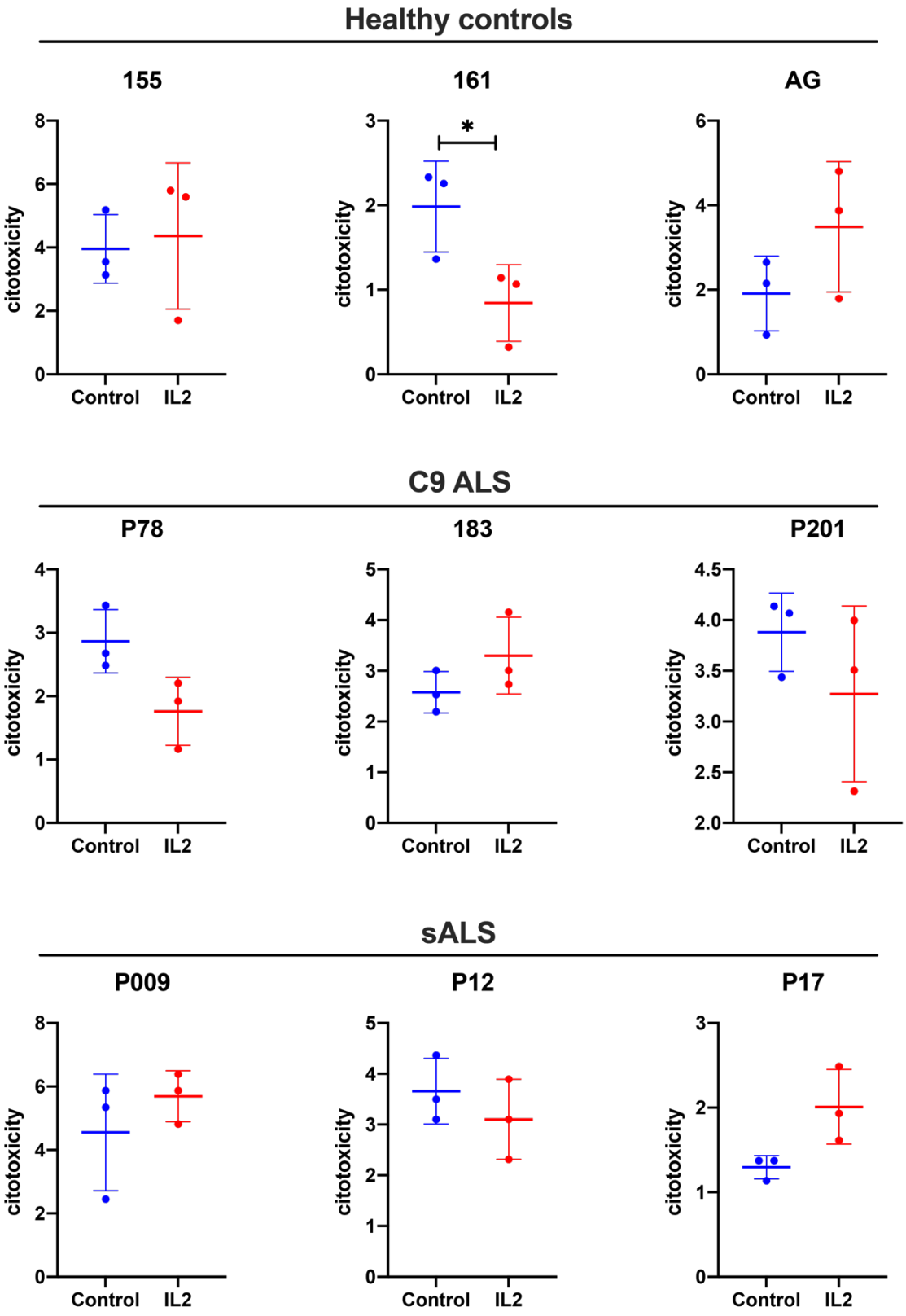
Healthy controls
155
161
AG
citotoxicity
Control
IL2
*
C9 ALS
P78
183
P201
sALS
P009
P12
P17

Figure 5.7: LDH Cytotoxicity Assays.

Scatter plots showing the percentage of cytotoxicity following control (1:1000, PBS + 5% glucose solution) or IL-2 (10nM, 4 hrs in 1% FBS medium) treatments are reported. All the 9 iAstrocyte lines were screened (healthy controls: 155, 161 and AG; C9 ALS: P78, P183 and P201; sALS: P009, P12 and P17). No significant variations (two-tailed unpaired T tests) were reported between IL-2 treated and control (spontaneous LDH release in untreated astrocytes) samples. Each dot represents a technical replicate and mean ± SD are graphed.

Taken together, these data showed that no cytotoxicity was associated with the optimized IL-2 treatment in iAstrocytes and therefore, this was considered safe for iAstrocytes.

5.3 iNPC-derived Astrocytes Transcriptional Profile

To investigate the molecular effects of IL-2 on iAstrocytes, RNA samples from 3 healthy controls (155, 161 and AG), 3 ALS patients carrying a C9orf72 mutation (P78, P183 and P201) and 3 sALS (P009, P12 and P17)-derived astrocytes were transcriptionally profiled using the Oxford Nanopore cDNA sequencing technique. Results from the quality control, differential expression and gene enrichment analyses are described in the next paragraphs.

5.3.1 RNA Samples and Sequencing Quality Control

Following 4 hr exposure to either 10nM IL-2 or PBS + 5% glucose solution in media containing 1% FBS, cells were harvested and RNA extracted, which was then used for library preparation. RNA sample characteristics are summarised in **Table 5.2**. Overall, good quantity and quality scores were obtained and extremely high RIN (RNA integrity number) numbers were observed. Therefore, the quality of the RNA samples was ascertained. In particular, RNA integrity is of crucial importance for the Oxford nanopore technique to allow long-read sequencing.

Table 5.2: Astrocytic RNA Sample Quality.

RNA sample characteristics are summarised in this table. For each RNA sample, cell details (iAstrocyte line name, ALS and treatment types) are reported together with RNA concentration, 260:280 ratio and RIN value.

Sample name	Astrocyte line	ALS type	Treatment type	Concentration (ng/ul)	260/280 ratio	RIN
155 G	155	NA	PBS + 5% glucose	98	2.11	9.7
155 IL2	155	NA	IL2 (10nM)	106.9	2.12	9.9
AG G	AG	NA	PBS + 5% glucose	239.5	2.14	10
AG IL2	AG	NA	IL2 (10nM)	163.7	2.14	10
161 G	161	NA	PBS + 5% glucose	314.3	2.11	10
161 IL2	161	NA	IL2 (10nM)	303.9	2.11	10
P78 G	P78	C9 ALS	PBS + 5% glucose	75.6	2.06	10
P78 IL2	P78	C9 ALS	IL2 (10nM)	128.9	2.07	10
P183 G	P183	C9 ALS	PBS + 5% glucose	287.1	2.12	10
P183 IL2	P183	C9 ALS	IL2 (10nM)	282.6	2.12	10
P201 G	P201	C9 ALS	PBS + 5% glucose	169.4	2.15	10
P201 IL2	P201	C9 ALS	IL2 (10nM)	142.9	2.14	10
P009 G	P009	sALS	PBS + 5% glucose	122.5	2.12	10
P009 IL2	P009	sALS	IL2 (10nM)	151.4	2.13	10
P12 G	P12	sALS	PBS + 5% glucose	182.5	2.15	10
P12 IL2	P12	sALS	IL2 (10nM)	203.1	2.11	10
P17 G	P17	sALS	PBS + 5% glucose	98	2.1	10
P17 IL2	P17	sALS	IL2 (10nM)	89.7	2.11	10

Following library preparation and sequencing by Matt Wyles, a QC analysis was also performed to assess the quality of the sequencing process. This was conducted using the MultiQC software by Matt Parker and a general summary of the obtained scores can be found in **Table 5.3**. A considerably high number of mapped reads were obtained (average = 27 millions). This yield was greater than the typical number of reads reported on the Oxford Nanopore guide (generally 7-12 millions, https://nanoporetech.com/). Additionally, both the percentage of the total reads that were mapped onto the human genome and the proportion of sequences being assigned to a known gene were very high (81.9 and 83.0% on average respectively). The mean sequence length was greater that 400 bp for all the samples (525 bp on average), which suggested that the majority of the reads were from full-length transcripts. Moreover, the average percentage of GC bases was around 45% which is consistent with human samples.

Table 5.3: Summary of MultiQC scores.

This table summarises, for each astrocyte sample, the quality of the reads obtained using Oxford Nanopore cDNA sequencing. In particular, for each sample, the millions of sequenced reads, the percentage of mapped reads and their proportion of assignment to the genome are reported. Moreover, the average sequence length and percentage of GC bases are also included. These scores were retrieved from the software MultiQC and were useful to inspect the quality and assess the yield of the sequencing process.

Sample	Mapped reads (Millions)	% Mapped reads	% Assigned reads	Avg sequence length	Avg %GC
155_G	22.3	73.70%	76.90%	429 bp	45%
155_IL2	17.7	80.00%	81.60%	544 bp	46%
AG_G	14.3	61.00%	70.20%	473 bp	45%
AG_IL2	26.4	72.70%	77.20%	486 bp	45%
161_G	40.4	86.60%	87.40%	593 bp	46%
161_IL2	39.2	87.50%	87.30%	546 bp	46%
P78_G	30.1	85.50%	84.90%	545 bp	46%
P78_IL2	29.2	84.10%	83.90%	512 bp	45%
P183_G	30.1	85.50%	84.90%	545 bp	46%
P183_IL2	29.2	84.10%	83.90%	512 bp	45%
P201_G	40.4	86.60%	87.40%	593 bp	46%
P201_IL2	39.2	87.50%	87.30%	546 bp	46%
P009_G	35.4	86.80%	87.20%	540 bp	46%
P009_IL2	10.3	87.70%	87.50%	571 bp	46%
P12_G	35.4	86.80%	87.20%	540 bp	46%
P12_IL2	26.4	72.70%	77.20%	486 bp	45%
P17_G	16	83.10%	81.50%	501 bp	45%
P17_IL2	10.4	83.00%	81.40%	480 bp	45%

Additional quality control was performed by generating diagnostic plots using the software MultiQC (**Figure 5.8**). As previously mentioned, all the samples were characterized by a good proportion of assigned reads (~80%) and a limited numbers of unassigned ones (~20%) (**Figure 5.8A**). As expected, the sequence length graphs showed that all of the generated libraries had a similar distribution with a peak at around 500 bp (**Figure 5.8B**). The sample obtained from the iAstrocyte line 161 treated with PBS + 5% glucose solution (161_G) showed a considerably higher proportion of reads having 500 bp length. Nonetheless, this result was not considered problematic as 161_G showed a distribution of sequence lengths similar to all the rest of the samples and, for the purpose of differential expression analysis, the difference in library sizes were addressed using DESeq2 median of ratios normalization method (as described in the method section 2.2.5). The per sequence GC graph showed the average content of guanosine and cytosine residues (in percentage) across the sequences in a sample. A library passing this QC metric should have a roughly normal distribution of these bases with a peak corresponding to the overall GC content of the analysed organism (human ~ 42-45%). As reported in **Figure 5.8C** the majority of the samples met this criterion showing a Gaussian distribution of the percentage of GC content. However, samples obtained from astrocytes AG (healthy control) treated with PBS + 5% glucose solution and P12 (sALS) treated with IL-2 showed an additional peak at around 35%. This might indicate either a contamination in the library preparation process or an enrichment for A/T rich sequences and therefore this was taken into consideration as a possible limitation of the study. Lastly, the quality of a given base call was assessed by measuring the Phred quality score. This indicated the probability of a base being correctly recognised. Usually values above 20 (which is equal to a 99% accuracy and therefore to a probability of an incorrect base call of 1% as this is calculated as: $10^{-(\text{Phred score}/10)}$) are generally accepted as good quality scores. The per sequence quality score plot displays the distribution of the mean quality scores all the bases of each sequence in a sample. Gaussian distribution of the scores showed peaks corresponding to a Phred scores of around 23 for all the samples which indicated a good level of sequencing accuracy for the majority of the reads (**Figure 5.8D**).

These results are consistent with acceptable good quality sequencing and data were subsequently used for gene expression analysis.

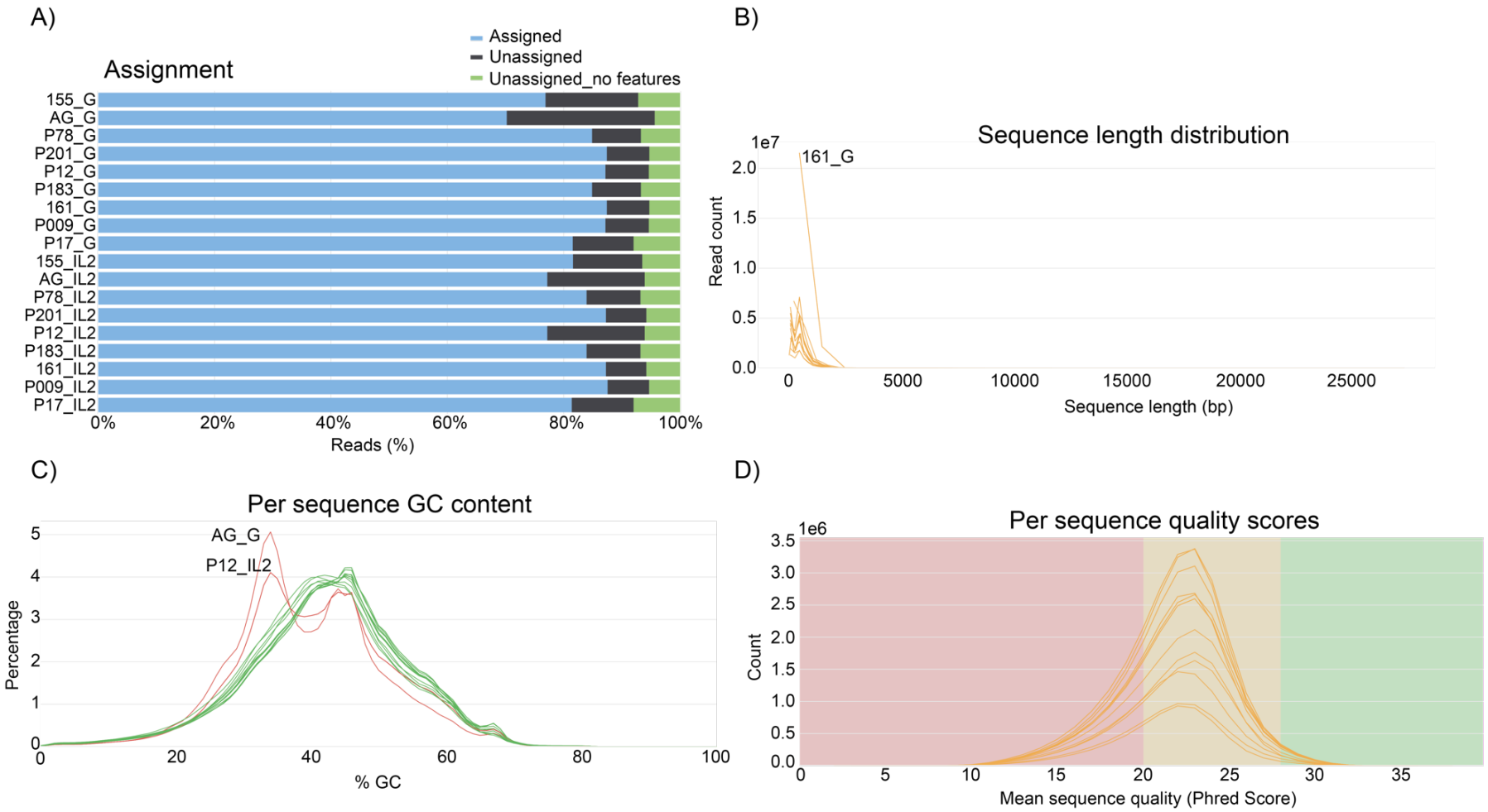
A)
Assignment
Assigned
Unassigned
Unassigned_no features
155_G
AG_G
P78_G
P201_G
P12_G
P183_G
161_G
P009_G
P17_G
155_IL2
AG_IL2
P78_IL2
P201_IL2
P12_IL2
P183_IL2
161_IL2
P009_IL2
P17_IL2
0%
20%
40%
60%
80%
100%
Reads (%)
B)
Sequence length distribution
1e7
161_G
Read count
Sequence length (bp)
C)
Per sequence GC content
AG_G
P12_IL2
Percentage
% GC
D)
Per sequence quality scores
1e6
Count
Mean sequence quality (Phred Score)

Figure 5.8: iAstrocyte cDNA Sequencing QC Plots.

In this figure, quality controls diagnostic plots are displayed. (**A**) The assignment graph shows the proportion of reads being assigned to a specific gene compared to unassigned ones. As expected, the majority of the reads were assigned. X-axis: percentage of reads, Y-axis: sample names. (**B**) The distribution of the read length is shown in this plot. All the samples show a peak at 500bp which indicated that most of the reads were from full-length transcripts. X-axis: sequence length reported in base pairs, Y-axis: the read counts. (**C**) This graph shows the percentage of GC content per sequence in a sample. The majority of libraries showed a normal distribution with a peak at 42%, which is consistent with the human transcriptome, however two samples had an additional peak at around 35%. X-axis: percentage of GC content, Y-axis: percentage of sequences. (**D**) The per sequence quality (or Phred) score is displayed. Most of the reads from all the samples had a good quality score of approximately 23. X-axis: mean quality score per sequence, Y-axis: number of read counts.

Although not strictly considered a quality control metric, a principal component analysis (PCA) was also carried out to summarise and visually inspect differences and similarities amongst transcriptional profiles of sequenced samples. The PCA plot revealed a clear separation between samples 161 (healthy control) and P201 (C9 ALS) - regardless of their treatment type - and all the rest of the samples along the first principal component, which account for most of the variance within the data (**Figure 5.9**). This suggested a substantial difference in their transcriptomes compared to the other samples possibly indicating an outlier trend of these two iAstrocyte lines.

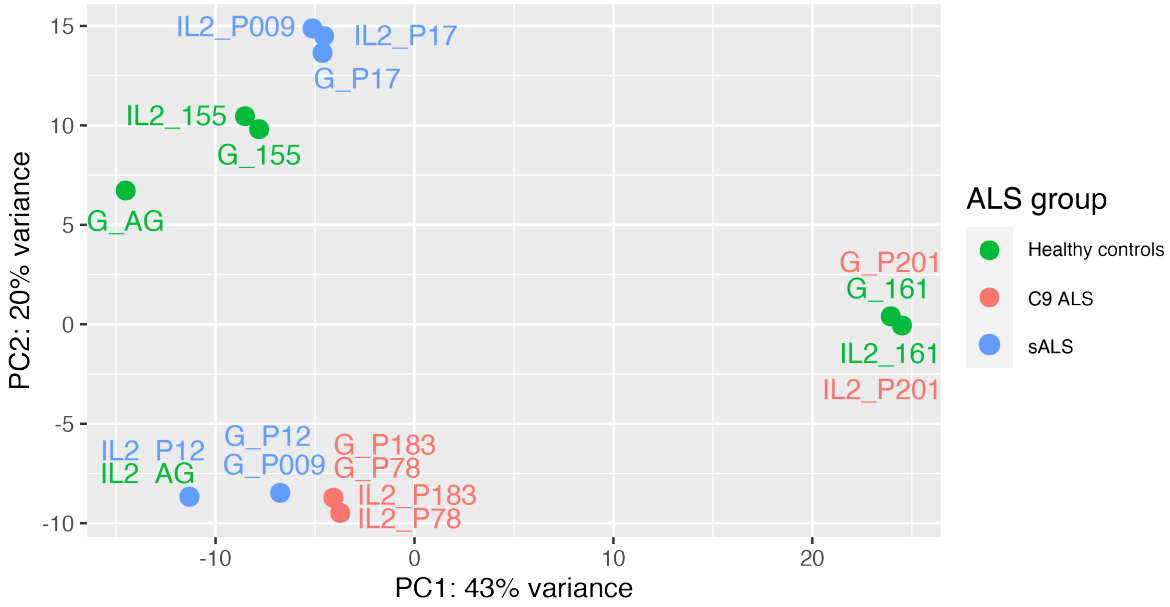

Figure 5.9: Principal Component Analysis of iAstrocyte Sequencing Data

Cartesian plot displaying principal component analysis of the Oxford nanopore sequencing data. Samples are colored by ALS group type (healthy controls in green, C9 ALS in red and sALS in blue), while iAstrocyte line names are reported in the plot next to each dot (the name of the line is accompanied by either G or IL2 to indicate the treatment type: either PBS + 5% glucose or IL-2, respectively). Importantly, although 18 samples were screened, only 12 dots were displayed in this plot. This is because some of the samples were so similar that the PCA assigned the same PC1 and PC2 scores. In such cases, the names of the overlapping samples are written close each other and next to their common dot (e.g. samples G_P201 and G_161).

To further investigate on the reason why 161 and P201 were plotted distantly in the PCA, different sources of variation were investigated. First of all, the possibility of batch effects was explored (**Figure 5.10**) as RNA was extracted at different times and, as reported in the methods (section 2.2.4), samples were divided and processed in two batches for library preparation. However, no clear batch effect was identified for both processes. In fact, although cell line 161 was the only one whose RNA was extracted on 5th February and therefore, difference in the extraction process could have explained the spatial separation, the RNA of line P201 was produced on the same day as AG samples, which were displayed on the left-hand side of the graph together with the rest of the samples. This suggested that no batch effect was reported in terms of RNA extraction (**Figure 5.10A**). Similarly, differences in the sequencing library preparation did not result in a batch effect as 161 and P201 belonged to separate batches (**Figure 5.10B**).

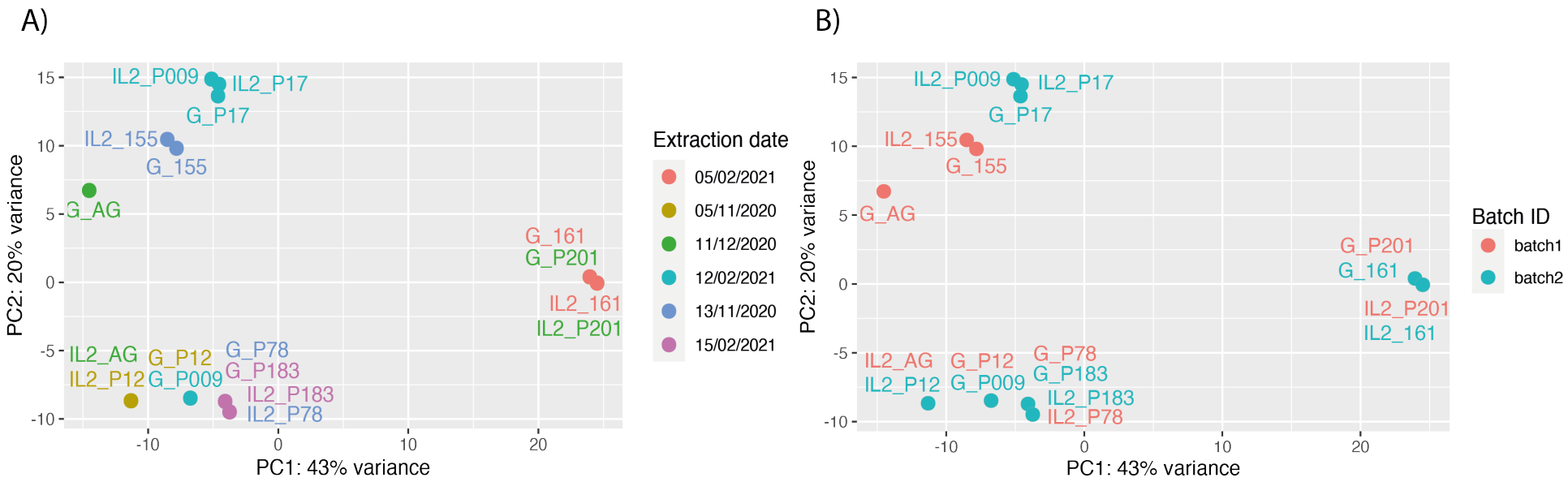

Figure 5.10: Principal Component Analysis – Investigation of Potential Batch Effect.

In these images the PCA plot is colored by either the RNA extraction date (**A**) or the library preparation ID (**B**) to investigate on possible batch effects. Nonetheless, RNA from 161 and P201 were extracted at different times and their libraries were not processed on the same days and therefore, no clear technical problems could have accounted for this spatial separation.

Additionally, some confounders were investigated as possible causes of the 161 and P201 spatial separation (**Figure 5.11**). These included gender and age of the patients and healthy controls at which their skin biopsy was taken and the number of passages at which the iNPCs were kept in culture before starting the differentiation to astrocytes. However, 161 and P201 were from a male and a female donor respectively and therefore no clear gender difference was identified (**Figure 5.11A**). Although 161 was the youngest healthy control (31 years of age), P201 was one of the oldest samples (66 years of age) and therefore, the spatial distance could not be explained as the result of a different age cluster with a dissimilar transcriptional profile (**Figure 5.11B**). Interestingly, P201 was the sample cultured for the highest number of passages (24 passages) and, similarly, 161 was the one kept longer in culture (19 passages) amongst the healthy controls (**Figure 5.11C**). However, it is unlikely that this was the source of the separation as other samples, such as P12 and P17, were also maintained in culture for a high number of passages (21 and 19 respectively) but these were on the left -hand side of the PCA plot.

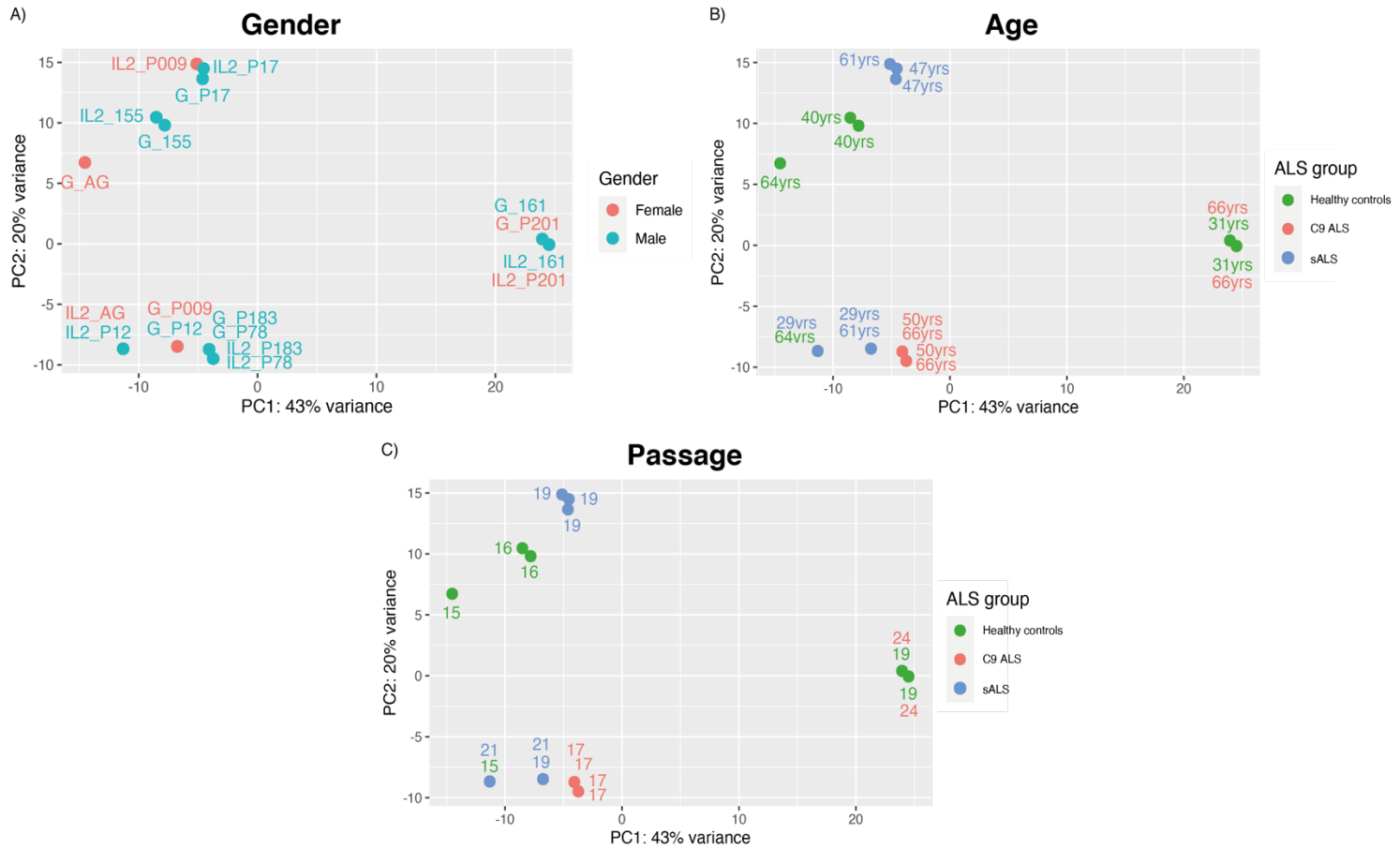

Figure 5.11: Principal Component Analysis– Investigation of Possible Confounders.

To investigate for possible confounders, in these images, the PCA was coloured by gender type (**A**) or samples were named by age (**B**) or passage number (**C**) at which iNPCs were kept in culture before being differentiated to astrocytes. No clear association of gender, age and passage was identified and able to explain 161 and P201 separation.

Moreover, to further validate the spatial separation of 161 and P201, data were also analysed using multidimensional scaling (MDS), another dimensionality reduction technique (extensively described in chapter 3) (**Figure 5.12A**). In agreement with the PCA analysis, MDS also revealed a spatial separation of 161 and P201. Upon the removal of these samples (**Figure 5.12B**), as expected, three groups were clearly recognized with the healthy controls and the two ALS groups being separated. Moreover, lesser differences were reported between samples treated with IL-2 or with the control condition (PBS + 5% glucose solution), as the major source of variation was anticipated to be the disease condition.

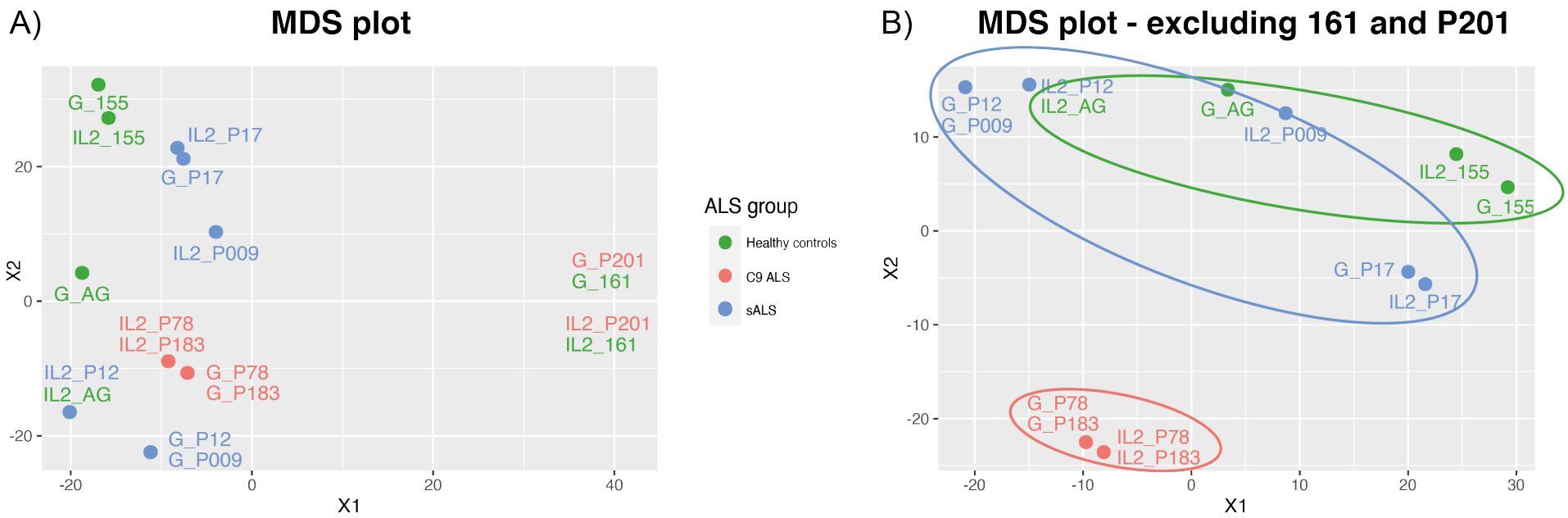

Figure 5.12: Multidimensional Scaling Plots

Two multidimensional scaling (MDS) plots, either including all samples (**A**) or excluding 161 and P201 (**B**), are shown. Samples are colour coded by ALS group type (healthy controls in green, C9 ALS in red and sALS in blue). Similarly, to the PCA plot 161 and P201 (regardless of their treatment type) were spatially distanced. Their removal allows the identification of the three disease-associated groups: healthy controls, C9 ALS and sALS (highlighted with coloured circles).

Despite these results suggesting 161 and P201 as possible outliers, a decision was made not to exclude those samples from our subsequent differential expression analysis. In fact, the removal of 4 out of 18 samples would have probably excessively biased the analysis and would have increased the number of falsely differentially expressed genes detected. Additionally, when data were analysed by creating a correlation heatmap (**Figure 5.13**), although 161 and P201 appeared to be less correlated compared to the rest of the samples, their coefficients were ≥ 0.99. This extremely high score did not justify their classification as outliers and therefore their exclusion from any further differential expression analysis. Nonetheless, we recognized this as a limitation of our study and, in light of a future publication, we aim to sequence other samples in order to be able to validate these as outliers and, if confirmed, to exclude them and re-run the differential expression analysis.

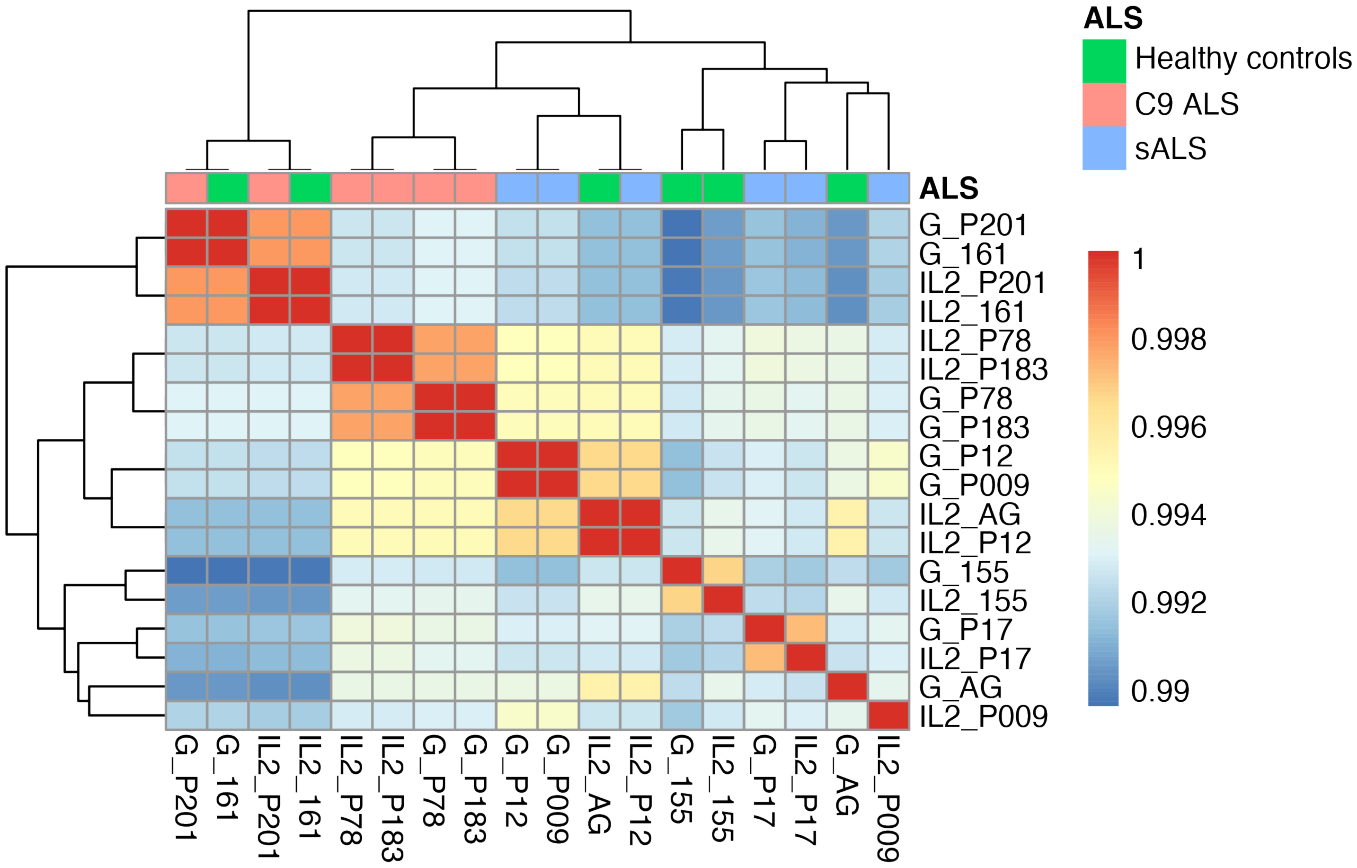

Figure 5.13: Gene Expression Correlation Heatmap to Detect Outliers.

Hierarchically clustered heatmap displaying the correlation scores between the gene expression profile of a sample with all the other samples. As expected, 161 and P201 correlated with each other whilst being more different from the rest of the samples. Nonetheless, the lowest correlation coefficient computed was = 0.99 and therefore this does not justify the exclusion of 161 and P201 from any subsequent analysis. To allow easier interpretation ALS group types are also reported in different colours (healthy controls in green, C9 ALS in red and sALS in blue).

5.3.2 Differential Expression Analysis

Following quality control analysis, Oxford Nanopore sequencing data was used to perform differential gene expression analyses in order to assess the effect of IL-2 on these cells. In particular, three analyses were carried out, one for each iAstrocyte group (healthy controls, C9 ALS and sALS), in which treated samples were compared to the control condition (PBS + 5% glucose solution). These will be subsequently referred to in the text as HC_IL2vsG for the healthy controls, C9_IL2vsG for the C9 ALS and SALS_IL2vsG for the sALS samples.

The comparison HC_IL2vsG retrieved 83 genes as significantly differentially expressed ($log_2FC \leq -0.58$ or ≥ 0.58 which is equal to $1.5 \leq FC \leq -1.5$ and p-value <0.05) of which 41 were decreased and 42 increased (full list reported in **Appendix 9**). Interestingly, of these 83 genes (annotated using Ensembl transcript IDs), only 53 were also annotated as having an official gene symbol. The number of significantly ($1.5 \leq FC \leq -1.5$ and p-value <0.05) differentially expressed genes promoted by IL-2 increased in ALS patient-derived astrocytes. In fact, 183 DEGs were identified in SALS_IL2vsG (59 decreased and 124 increased, **Appendix 10**), whilst 456 were identified in the C9_IL2vsG comparison (230 decreased and 226 increased, **Appendix 11**). Therefore, the C9 ALS patients seemed to be the most responsive group, with the greatest observed transcriptional variation promoted by IL-2. Similarly to the healthy controls, the proportion of genes being also annotated with a gene symbol was reduced to 116 for SALS_IL2vsG and to 276 for C9_IL2vsG. These results are summarized in three volcano plots displayed in **Figure 5.14**.

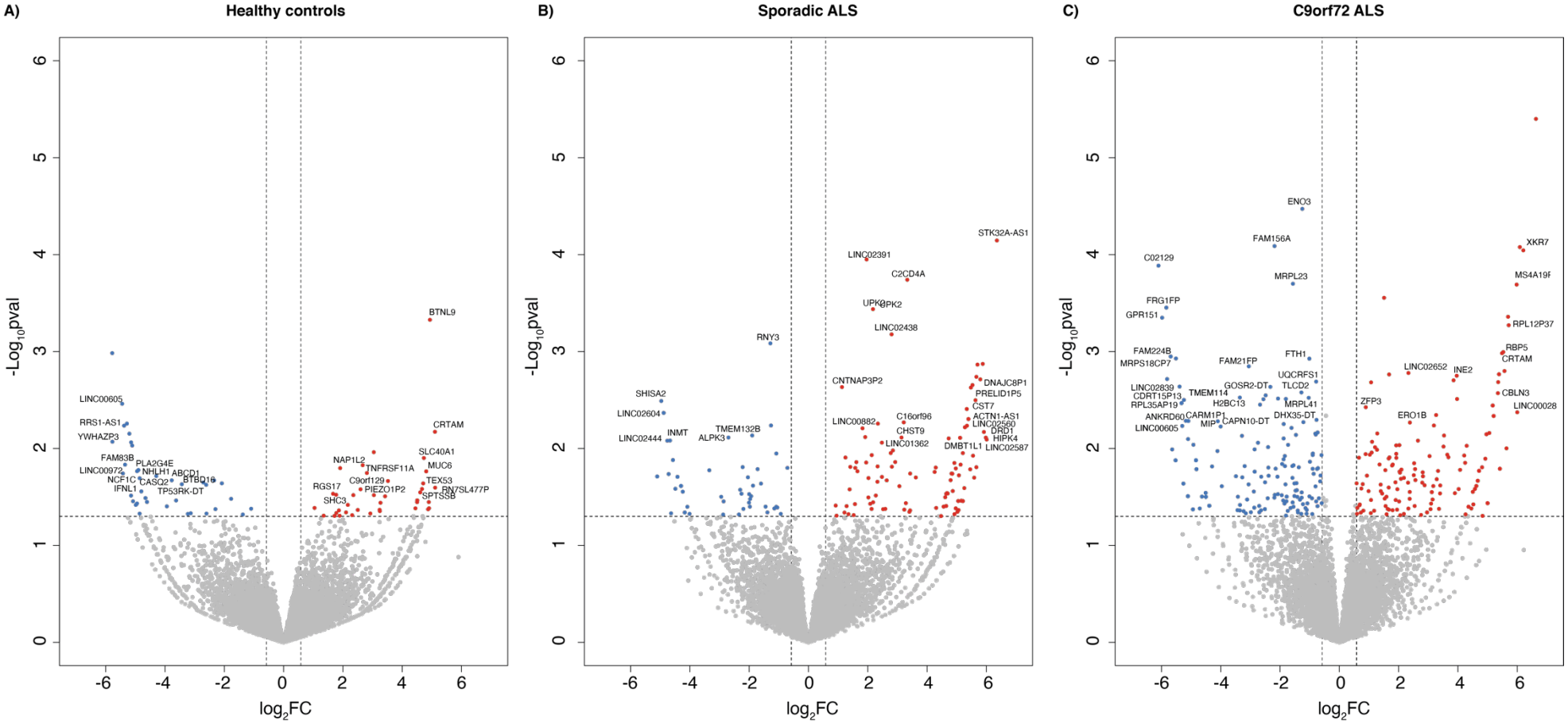
A)
Healthy controls
B)
Sporadic ALS
C)
C9orf72 ALS
-Log10pval
log2FC
BTNL9
LINC00605
RRS1-AS1
YWHAZP3
CRTAM
FAM83B
PLA2G4E
LINC00972
NHLH1
ABCD1
NCF1C
CASQ2
BTBD16
IFNL1
TP53RK-DT
NAP1L2
TNFRSF11A
SLC40A1
MUC6
C9orf129
PIEZO1P2
TEX53
RGS17
SHC3
RN7SL477P
SPTSSB
STK32A-AS1
LINC02391
C2CD4A
UPK3BPK2
LINC02438
RNY3
SHISA2
LINC02604
INMT
LINC02444
TMEM132B
ALPK3
CNTNAP3P2
DNAJC8P1
PRELID1P5
CST7
ACTN1-AS1
LINC02560
DRD1
HIPK4
LINC02587
LINC00882
C16orf96
CHST9
LINC01362
DMBT1L1
ENO3
FAM156A
C02129
MRPL23
XKR7
MS4A19P
FRG1FP
GPR151
RPL12P37
FAM224B
MRPS18CP7
FAM21FP
FTH1
RBP5
CRTAM
LINC02652
INE2
UQCRFS1
TLCD2
LINC02839
GOSR2-DT
CDRT15P13
TMEM114
RPL35AP19
H2BC13
MRPL41
CBLN3
LINC00028
ZFP3
ERO1B
ANKRD60
CARM1P1
DHX35-DT
LINC00605
MIP
CAPN10-DT

Figure 5.14: Differentially Expressed Genes Following IL-2 Treatment in iAstrocytes.

Volcano plots displaying DEGs resulting from the comparisons HC_IL2vsG (**A**), SALS_IL2vsG (**B**) and C9_IL2vsG (**C**). DEGs are plotted and colour-coded depending on their logarithmic fold change (log_2FC) and their significance levels (-Log10 p-value): non-significant transcripts are reported in grey, significant and with $log_2FC \leq -0.58$ in blue and significant and with $log_2FC \geq 0.58$ in red. Three black lines are also shown: the horizontal one indicates the p-value threshold (-Log10 p-value=1.3) and two vertical dotted lines mark the FC cut-offs ($log_2FC \leq -0.58$ or ≥ 0.58 which is equal to $1.5 \leq FC \leq -1.5$). Official gene symbols are displayed for some of the top differentially expressed genes (notably, some of the top DEGs are not named as these were not annotated with any official gene symbol, whilst only Ensembl transcript ID was available). A greater number of DEGs was retrieved in ALS patients compared to healthy controls following IL-2 treatment. This was particularly evident in C9orf72 ALS. (Wald statistics was conducted by DESeq2 to find significant DEGs).

Subsequently, DEGs from the three comparisons were analysed to find any genes whose expression was commonly altered as a result of the IL-2 treatment. However, no terms were found as differentially expressed in common in the three groups (healthy controls, C9 ALS and sALS) (**Figure 5.15**). Additionally, only 10 genes were altered in both sporadic and C9orf72 ALS patient-derived astrocytes. Amongst those, one stimulated by retinoic acid 8 (STRA8) was increased in both ALS groups following IL-2 treatment. This is intriguing considering that multiple studies have linked retinoids to ALS (Riancho et al., 2016). An even more limited number of terms was found as commonly expressed between healthy controls and C9 ALS and between healthy controls and sALS. Interestingly, cytotoxic and regulatory T cell molecule (CRTAM) was found to be upregulated in both healthy control and C9 ALS patients following IL-2 treatment. This protein mediates the activation and differentiation of several T cell subsets. A complete list of these commonly differentially expressed genes is provided in **Table 5.4**. Altogether these results suggested that IL-2 was able to promote transcriptional variations that were unique and characteristic of each of the three different subgroups.

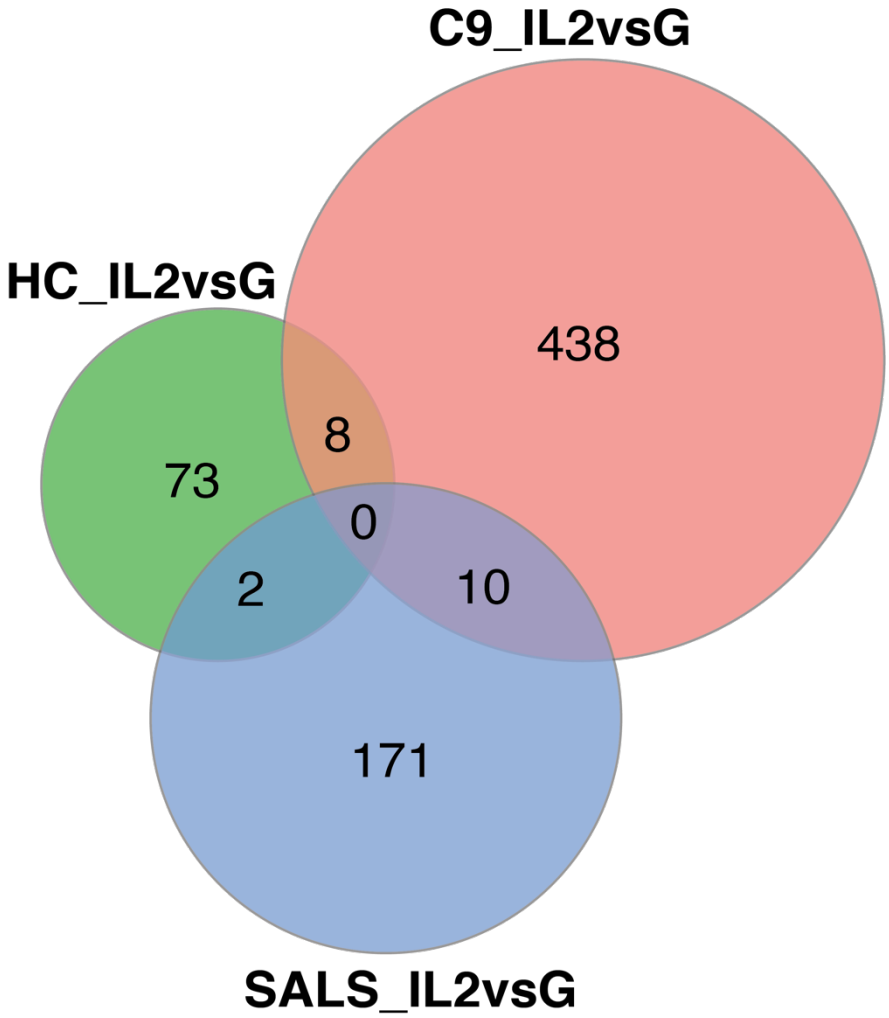

.

Figure 5.15: Commonly Differentially Expressed Genes in iAstrocytes Following IL-2 Treatment.

Venn Diagram displaying common DEGs between the three groups following IL-2 treatment. A very limited number of genes appeared to be in common which suggested that this cytokine is able to promote characteristic transcriptional alteration in each of the groups

Table 5.4: List of Common Differentially Expressed Genes.

In this table, genes commonly differentially expressed in the three analyses (HC_IL2vsG, C9_ IL2vsG and sALS_ IL2vsG) are listed. For each gene, both Ensemble ID and gene symbol are displayed (where no gene symbol was available, the symbol "-" was used) together with log_2FC and p-value of each of the three comparisons ("NA" is shown if a gene was not significantly differentially expressed in a comparison).

Ensembl ID	Gene Symbol	HC_IL2vsG log2FC	HC_IL2vsG pvalue	C9_lvsG log2FC	C9_IL2vsG pvalue	sALS_IL2vsG log2FC	sALS_IL2vsG pvalue
ENSG00000279026	-	-5.781	0.001	-4.502	0.032	NA	NA
ENSG00000251533	LINC00605	-5.446	0.003	-5.300	0.006	NA	NA
ENSG00000241754	-	-5.287	0.006	-4.709	0.042	NA	NA
ENSG00000206228	HNRNPA1P4	-4.946	0.037	-4.502	0.032	NA	NA
ENSG00000171786	NHLH1	-4.857	0.020	-4.820	0.016	NA	NA
ENSG00000261204	-	2.105	0.046	2.376	0.028	NA	NA
ENSG00000184956	MUC6	4.811	0.017	4.670	0.022	NA	NA
ENSG00000109943	CRTAM	5.106	0.007	5.487	0.001	NA	NA
ENSG00000234155	LINC02535	-4.609	0.036	NA	NA	-4.717	0.018
ENSG00000246316	-	-2.602	0.047	NA	NA	5.665	0.002
ENSG00000235052	-	NA	NA	-4.820	0.016	4.849	0.018
ENSG00000267676	THA1P	NA	NA	-2.744	0.009	2.332	0.015
ENSG00000283141	LINC02666	NA	NA	-2.506	0.022	-4.300	0.024
ENSG00000268307	LINC02560	NA	NA	-2.192	0.032	5.279	0.006
ENSG00000249572	-	NA	NA	-0.898	0.012	1.247	0.012
ENSG00000201098	RNY1	NA	NA	0.583	0.023	-1.084	0.011
ENSG00000180730	SHISA2	NA	NA	1.068	0.034	-4.965	0.003
ENSG00000258123	LINC02444	NA	NA	4.359	0.040	-4.671	0.008
ENSG00000272040	-	NA	NA	5.206	0.005	5.879	0.001
ENSG00000146857	STRA8	NA	NA	5.416	0.016	5.132	0.015

5.3.3 Gene Enrichment Analysis

Following differential expression analysis, gene enrichment was performed with the aim of discovering pathways and biological processes which were modified in response to the IL-2 treatment. Two different analyses were carried out: the first one using the software Enrichr and REVIGO, which focused on altered GO biological processes (GO BP), and the second one was performed utilising Ingenuity Pathway Analysis (IPA). Results obtained using these different methods are discussed in the following paragraphs.

Lists of upregulated and downregulated genes from the three comparisons were imported separately into Enrichr, GO analyses were carried out and similar terms were summarised by REVIGO (semantic similarity cut off= 0.5).

For the comparison HC_IL2vsG, a total of 76 increased and 100 decreased GO BPs were found to be significantly (p-value <0.05) enriched which were summarised into 30 and 35 clusters by REVIGO, respectively. These are displayed in **Figure 5.16** and further grouped into master categories which are marked in the image by using different colours. Several processes involved in the CNS homeostasis were documented to be altered (both increased and decreased) with the treatment. In particular, several terms linked to the myelination and axonogenesis processes appeared to be upregulated, suggesting a possible protective central effect of the interleukin on healthy control astrocytes. Additionally, a multitude of immune-related GO BPs were reported to be both increased and decreased. This indicates that IL-2, at this range of treatment doses, does not induce a consistent immune stimulation or suppression but, in turns, alters the expression immunological genes in a characteristic way. Several processes involved in ion homeostasis were also altered (the majority of which were downregulated, particularly those involving K ions) together with pathways implicated in the fatty acid metabolism and in mitochondrial homeostasis. In addition, different mechanisms responsible for the regulation of oxidative stress were also downregulated ("negative regulation of hydrogen peroxide-induced cell death", "regulation of response to oxidative stress", "regulation of cellular response to oxidative stress", "regulation of reactive oxygen species biosynthetic

process"), potentially reflecting a reduction in the ROS biosynthesis in response to the treatment. This is consistent with the results found in the IMODALS trial participants, which also indicated a decrease in the production of ROS species and in NRF2 pathway activation.

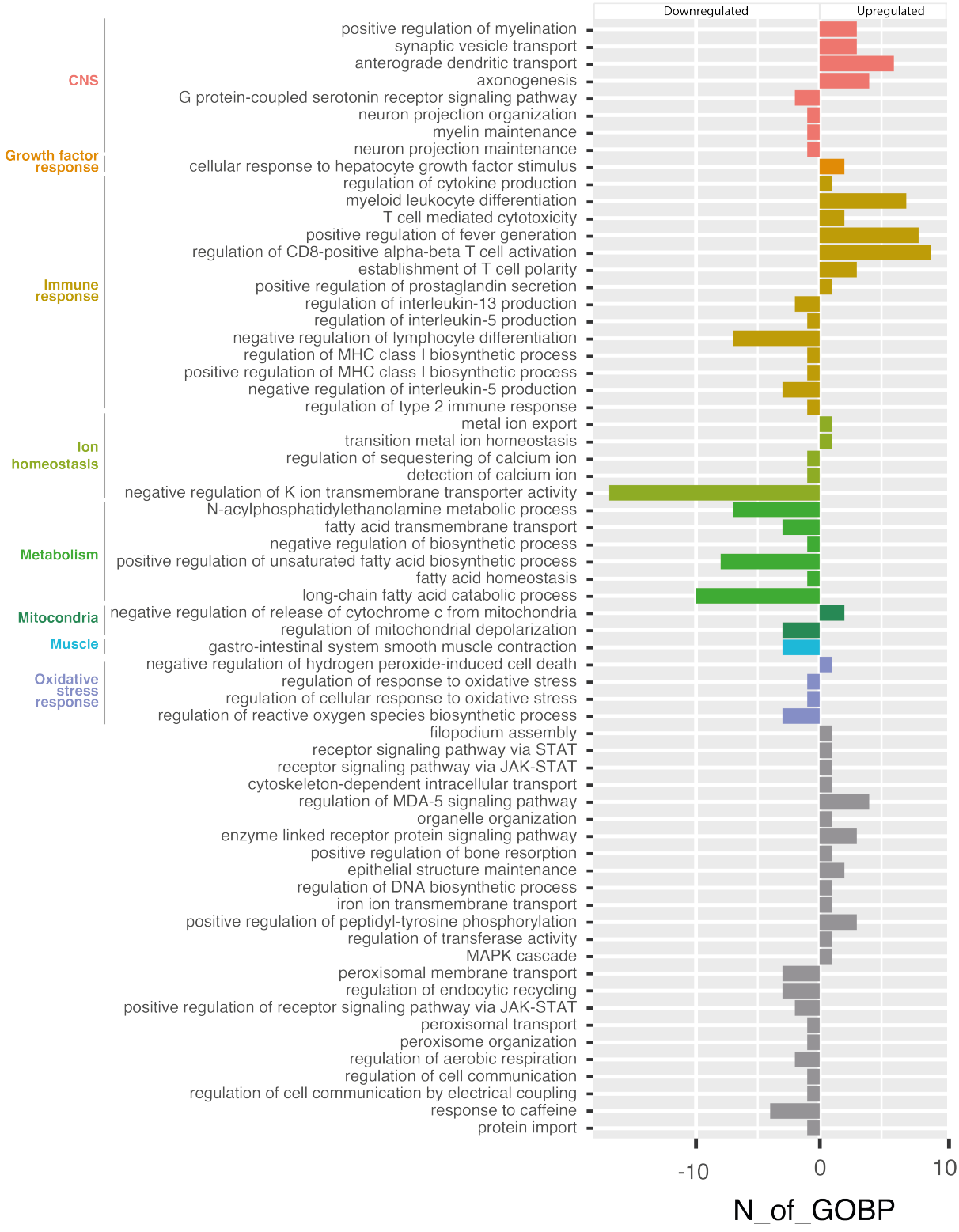

Figure 5.16: Enriched GO BPs in Healthy Controls iAstrocytes Following IL-2 Treatment.

In this image, the enriched and REVIGO clustered GO BPs from the comparison HC_IL2vsG are displayed. Per each cluster representative (the name of which is reported on the Y-axis), the number of biological processes included in that cluster is shown. To clearly visualise the directionality of the altered processes (either increase or decrease), positive values of GO BPs were used to indicate upregulation whilst negative for downregulation. The terms are also manually grouped into master categories as indicated by the different colours.

The Enrichr analysis of the DEGs resulted from the comparison SALS_IL2vsG retrieved 106 upregulated and 70 downregulated significantly (p-value <0.05) enriched GO BPs. These were summarised into 61 increased and 43 decreased REVIGO clusters respectively (**Figure 5.17**). Consistent with the healthy control astrocytes, sALS patient-derived cells also showed an extensive alteration of CNS-related processes in response to IL-2 administration. In fact, myelination pathways were increased whilst GO BPs involved in dendritic spine and axonogenesis were both up and downregulated. Processes implicated in the nerve growth factor response appeared to be decreased, which might constitute a detrimental effect. However, pathways involved in the signalling of neurotrophins, a class of growth factor implicated in neuronal survival and development, were upregulated. Additionally, a substantial increase in catecholamine neurotransmission was reported. In line with healthy control results, mixed alterations of immune-related processes were reported together with changes in ion homeostasis pathways. In addition to modifications in metabolic mechanisms involving lipids (triglycerides), the metabolism of amines and glucose also appeared to be affected. In particular, the process of gluconeogenesis seemed to be increased whilst glycogen biosynthesis was reduced. This is of particular importance for astrocytes, which are pivotal for providing neurons with the necessary energy sources. As mentioned in the introduction, decreased glycogen mobilization and degradation to glucose has been reported in ALS, together with an increment in glycogen levels. Therefore, these alterations induced by IL-2 may be protective and may be able to alleviate the impaired glucose metabolism in astrocytes. Processes linked to the cellular response to retinoic acid were also increased in response to the

treatment. Interestingly and consistently with healthy control data, GO BPs involved in the regulation of oxidative stress response were enriched in sALS patient-derived astrocytes following IL-2 treatment. However, these ROS regulative processes appeared to be increased rather than decreased as in the healthy controls.

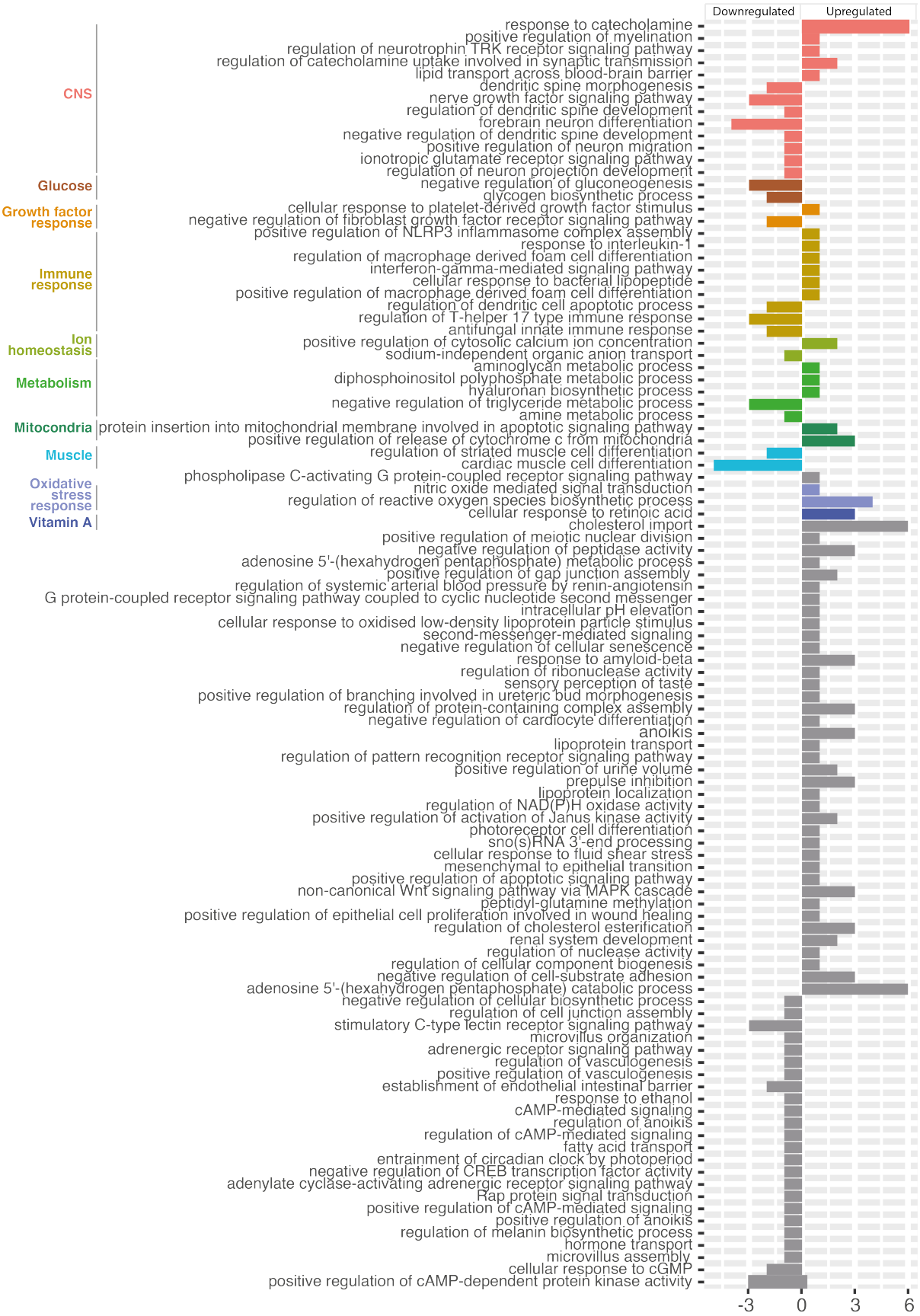
Downregulated
Upregulated
CNS
Glucose
Growth factor response
Immune response
Ion homeostasis
Metabolism
Mitocondria
Muscle
Oxidative stress response
Vitamin A
response to catecholamine
positive regulation of myelination
regulation of neurotrophin TRK receptor signaling pathway
regulation of catecholamine uptake involved in synaptic transmission
lipid transport across blood-brain barrier
dendritic spine morphogenesis
nerve growth factor signaling pathway
regulation of dendritic spine development
forebrain neuron differentiation
negative regulation of dendritic spine development
positive regulation of neuron migration
ionotropic glutamate receptor signaling pathway
regulation of neuron projection development
negative regulation of gluconeogenesis
glycogen biosynthetic process
cellular response to platelet-derived growth factor stimulus
negative regulation of fibroblast growth factor receptor signaling pathway
positive regulation of NLRP3 inflammasome complex assembly
response to interleukin-1
regulation of macrophage derived foam cell differentiation
interferon-gamma-mediated signaling pathway
cellular response to bacterial lipopeptide
positive regulation of macrophage derived foam cell differentiation
regulation of dendritic cell apoptotic process
regulation of T-helper 17 type immune response
antifungal innate immune response
positive regulation of cytosolic calcium ion concentration
sodium-independent organic anion transport
aminoglycan metabolic process
diphosphoinositol polyphosphate metabolic process
hyaluronan biosynthetic process
negative regulation of triglyceride metabolic process
amine metabolic process
protein insertion into mitochondrial membrane involved in apoptotic signaling pathway
positive regulation of release of cytochrome c from mitochondria
regulation of striated muscle cell differentiation
cardiac muscle cell differentiation
phospholipase C-activating G protein-coupled receptor signaling pathway
nitric oxide mediated signal transduction
regulation of reactive oxygen species biosynthetic process
cellular response to retinoic acid
cholesterol import
positive regulation of meiotic nuclear division
negative regulation of peptidase activity
adenosine 5'-(hexahydrogen pentaphosphate) metabolic process
positive regulation of gap junction assembly
regulation of systemic arterial blood pressure by renin-angiotensin
G protein-coupled receptor signaling pathway coupled to cyclic nucleotide second messenger
intracellular pH elevation
cellular response to oxidised low-density lipoprotein particle stimulus
second-messenger-mediated signaling
negative regulation of cellular senescence
response to amyloid-beta
regulation of ribonuclease activity
sensory perception of taste
positive regulation of branching involved in ureteric bud morphogenesis
regulation of protein-containing complex assembly
negative regulation of cardiocyte differentiation
anoikis
lipoprotein transport
regulation of pattern recognition receptor signaling pathway
positive regulation of urine volume
prepulse inhibition
lipoprotein localization
regulation of NAD(P)H oxidase activity
positive regulation of activation of Janus kinase activity
photoreceptor cell differentiation
sno(s)RNA 3'-end processing
cellular response to fluid shear stress
mesenchymal to epithelial transition
positive regulation of apoptotic signaling pathway
non-canonical Wnt signaling pathway via MAPK cascade
peptidyl-glutamine methylation
positive regulation of epithelial cell proliferation involved in wound healing
regulation of cholesterol esterification
renal system development
regulation of nuclease activity
regulation of cellular component biogenesis
negative regulation of cell-substrate adhesion
adenosine 5'-(hexahydrogen pentaphosphate) catabolic process
negative regulation of cellular biosynthetic process
regulation of cell junction assembly
stimulatory C-type lectin receptor signaling pathway
microvillus organization
adrenergic receptor signaling pathway
regulation of vasculogenesis
positive regulation of vasculogenesis
establishment of endothelial intestinal barrier
response to ethanol
cAMP-mediated signaling
regulation of anoikis
regulation of cAMP-mediated signaling
fatty acid transport
entrainment of circadian clock by photoperiod
negative regulation of CREB transcription factor activity
adenylate cyclase-activating adrenergic receptor signaling pathway
Rap protein signal transduction
positive regulation of cAMP-mediated signaling
positive regulation of anoikis
regulation of melanin biosynthetic process
hormone transport
microvillus assembly
cellular response to cGMP
positive regulation of cAMP-dependent protein kinase activity
-3
0
3
6

Figure 5.17: Enriched GO BPs in sALS iAstrocytes Following IL-2 Treatment.

In this image, the enriched and REVIGO clustered GO BPs from the comparison SALS_IL2vsG are displayed. Per each cluster representative (the name of which is reported on the Y-axis), the number of biological processes included in that cluster is shown. To clearly visualise the directionality of the altered processes (either increase or decrease), positive values of GO BPs were used to indicate upregulation whilst negative for downregulation. The terms are also grouped manually grouped into master categories as indicated by the different colours.

Lastly, the Enrichr analysis of the comparison C9_IL2vsG identified 73 upregulated and 36 downregulated significant (p-value <0.05) GO BPs, which were summarised into 30 increased and 30 decreased REVIGO clusters (**Figure 5.18**). Interestingly, despite the fact that this comparison retrieved the highest number of DEGs (456), these were enriched into a smaller number of biological processes in the GO analysis compared to the healthy controls and sALS. This was probably because a large proportion of DEGs were long intergenic non protein coding (LINC) RNAs and because the software Enrichr did not have ontology information for a multitude of C9_IL2vsG differentially expressed genes. Therefore, data were also subsequently analysed using a different enrichment software (IPA, see following paragraphs) to ensure an exhaustive pathway analysis. In line with previous results from both healthy controls and sALS astrocytes, a significant alteration in CNS processes was reported. In particular, axonogenesis and myelination pathways seemed to be consistently increased in all the three comparisons. However, C9_IL2vsG also revealed an increment in synaptic and dendritic transport. Additionally, as per previous results, mixed up and downregulation of immune-related and ion homeostatic pathways were reported. Metabolic processes also seemed to be consistently impacted by the treatment although phospholipids and monocarboxylic acids appeared to be the principal targets in IL-2-treated C9 ALS astrocytes. Interestingly and as observed in healthy controls, negative regulation of cell death processes involving ROS and mitochondria were increased and therefore the treatment seemed to induce an important reduction in these toxic pathways.

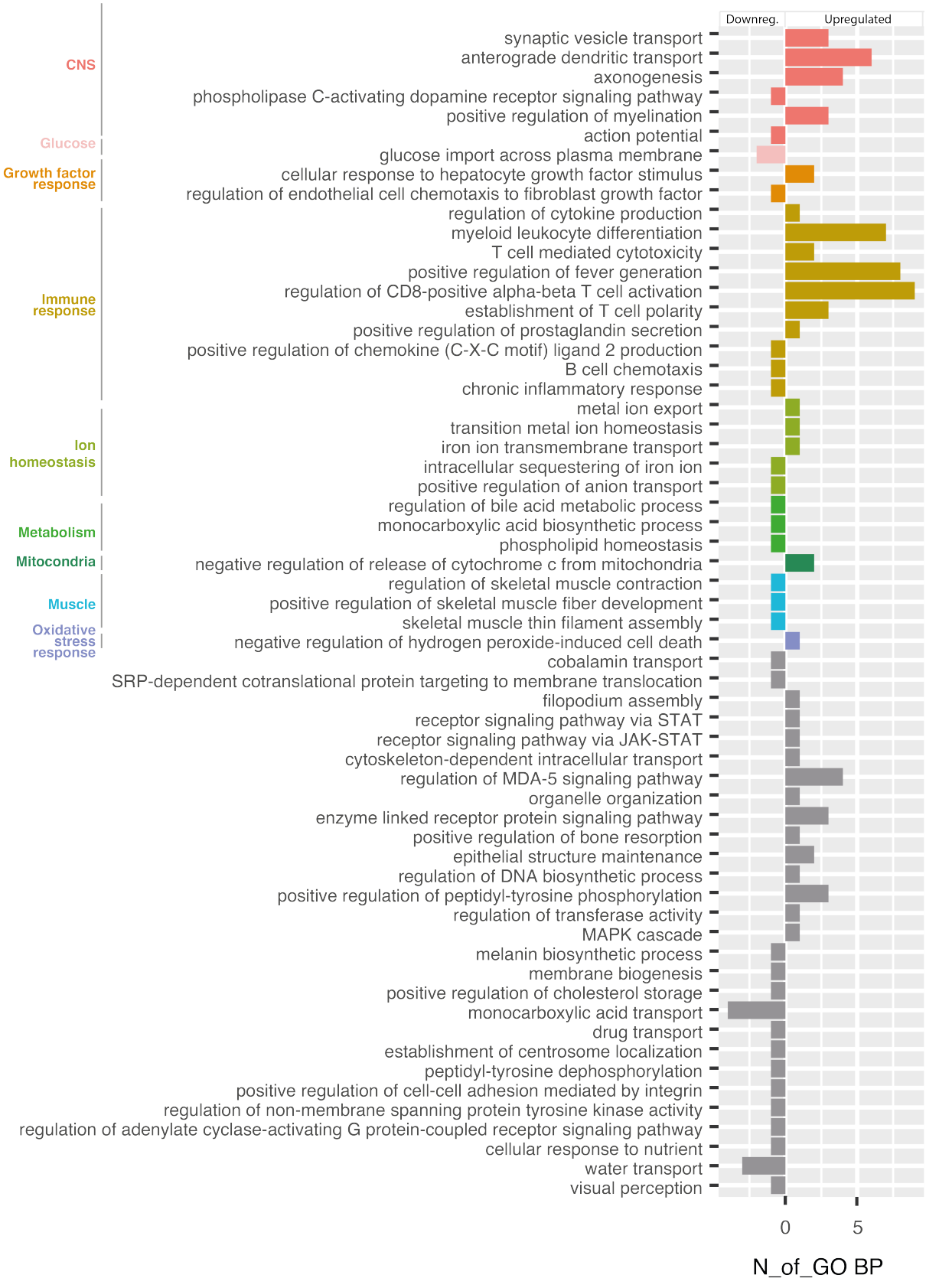
Downreg.
Upregulated
CNS
Glucose
Growth factor response
Immune response
Ion homeostasis
Metabolism
Mitocondria
Muscle
Oxidative stress response
synaptic vesicle transport
anterograde dendritic transport
axonogenesis
phospholipase C-activating dopamine receptor signaling pathway
positive regulation of myelination
action potential
glucose import across plasma membrane
cellular response to hepatocyte growth factor stimulus
regulation of endothelial cell chemotaxis to fibroblast growth factor
regulation of cytokine production
myeloid leukocyte differentiation
T cell mediated cytotoxicity
positive regulation of fever generation
regulation of CD8-positive alpha-beta T cell activation
establishment of T cell polarity
positive regulation of prostaglandin secretion
positive regulation of chemokine (C-X-C motif) ligand 2 production
B cell chemotaxis
chronic inflammatory response
metal ion export
transition metal ion homeostasis
iron ion transmembrane transport
intracellular sequestering of iron ion
positive regulation of anion transport
regulation of bile acid metabolic process
monocarboxylic acid biosynthetic process
phospholipid homeostasis
negative regulation of release of cytochrome c from mitochondria
regulation of skeletal muscle contraction
positive regulation of skeletal muscle fiber development
skeletal muscle thin filament assembly
negative regulation of hydrogen peroxide-induced cell death
cobalamin transport
SRP-dependent cotranslational protein targeting to membrane translocation
filopodium assembly
receptor signaling pathway via STAT
receptor signaling pathway via JAK-STAT
cytoskeleton-dependent intracellular transport
regulation of MDA-5 signaling pathway
organelle organization
enzyme linked receptor protein signaling pathway
positive regulation of bone resorption
epithelial structure maintenance
regulation of DNA biosynthetic process
positive regulation of peptidyl-tyrosine phosphorylation
regulation of transferase activity
MAPK cascade
melanin biosynthetic process
membrane biogenesis
positive regulation of cholesterol storage
monocarboxylic acid transport
drug transport
establishment of centrosome localization
peptidyl-tyrosine dephosphorylation
positive regulation of cell-cell adhesion mediated by integrin
regulation of non-membrane spanning protein tyrosine kinase activity
regulation of adenylate cyclase-activating G protein-coupled receptor signaling pathway
cellular response to nutrient
water transport
visual perception
0
5
N_of_GO BP

Figure 5.18: Enriched GO BPs in C9-ALS iAstrocytes Following IL-2 Treatment.

In this image, the enriched and REVIGO clustered GO BPs from the comparison C9_IL2vsG are displayed. Per each cluster representative (the name of which is reported on the Y-axis), the number of biological processes included in that cluster is shown. To clearly visualise the directionality of the altered processes (either increase or decrease), positive values of GO BPs were used to indicate upregulation whilst negative for downregulation. The terms are also manually grouped into master categories as indicated by the different colours.

A subsequent gene enrichment analysis was performed using the software IPA to retrieve significantly altered pathways following the IL-2 treatment. Similarly to what was previously done for microarray gene expression data, two different IPA tools were used, namely: canonical pathway, which allowed the identification of enriched pathways included in the Ingenuity Knowledge Base®, and the "diseases and functions" tab, which highlighted disease-characteristic mechanisms and biological functions within the data sets. Interesting enriched pathways resulted from the IPA canonical pathway analyses (**Figure 5.19**). In healthy controls, 13 terms were enriched (**Figure 5.19A**). In particular, the IL-2 treatment seemed to induce modification in the STAT3 pathway, which was the most significantly altered pathway although no activation or inhibition (Z-score=0) was predicted. This suggested a mixed phenotype with both increased and decreased genes being included in this process. However this pathway enrichment is interesting as STAT3 is known to be crucial for a multitude of astrocytic functions including differentiation (Hong and Song, 2014), proliferation (Tsuda et al., 2011) and reactivity (Ceyzériat et al., 2016). Intriguingly, the pathway "CREB signaling in neurons" appeared to be activated in the IL-2 treated healthy control astrocytes. The cyclic AMP response element binding protein (CREB) signalling is known to exert a key and neuroprotective role in both neurons and astrocytes (Pardo et al., 2017).

In sALS astrocytes, 12 canonical pathways appeared to be enriched although their significance level (p-value of enrichment) is generally reduced compared to healthy controls (**Figure 5.19B**). Nonetheless, it is worth noting that a neuroprotective pathway

involved in a neurodegenerative disease (“Neuroprotective Role of THOP1 in Alzheimer's disease”) was enriched in these astrocytes, which suggested a possible beneficial effect of IL-2 treatment on these cells. Interestingly, both heathy controls and sALS canonical pathway analysis revealed evidence of alterations of immune-related pathways ("Role of osteoblasts, osteoclasts and chondrocytes in rheumatoid arthritis" was enriched in both while "CCR3 signaling in eosinophils" and "Role of WNT/GSK-3b signaling in the pathogenesis of Influenza" were altered in healthy controls and sALS respectively). This suggested an effect of the interleukin on the transcription of immunological genes, which are expressed in immune cells but also astrocytes.

The IPA canonical pathway analysis of the C9 ALS astrocyte returned 14 terms as significantly enriched (**Figure 5.19C**). The top scoring one was the "Gustation pathway", which was inhibited and whose importance in ALS is uncertain. However, despite their Z-scores =0, interesting alterations in the retinol (also known as vitamin A) and retinoate biosynthesis were reported. This is consistent with other results from the Enrich and REVIGO analyses, where vitamin A processes were enriched, although these were not reported in C9 ALS astrocytes. These data suggested an IL-2-driven modification in vitamin A metabolism, a potentially interesting results as this molecule is known to impact on crucial mechanisms in ALS-related pathogenesis including neuronal differentiation, cellular proteostasis and antioxidant defence. Additionally, some pathways involved in synaptic stimulation and neuronal transmission were altered in response to IL-2 in C9 ALS astrocytes. These included "Synaptic long-term depression" and "GABA receptor signalling". Consistently with Enrichr and REVIGO analysis, the metabolism of lipids appeared to be impacted by the treatment (with the term "triacylglycerol degradation" being significantly enriched in IPA's canonical pathway analysis).

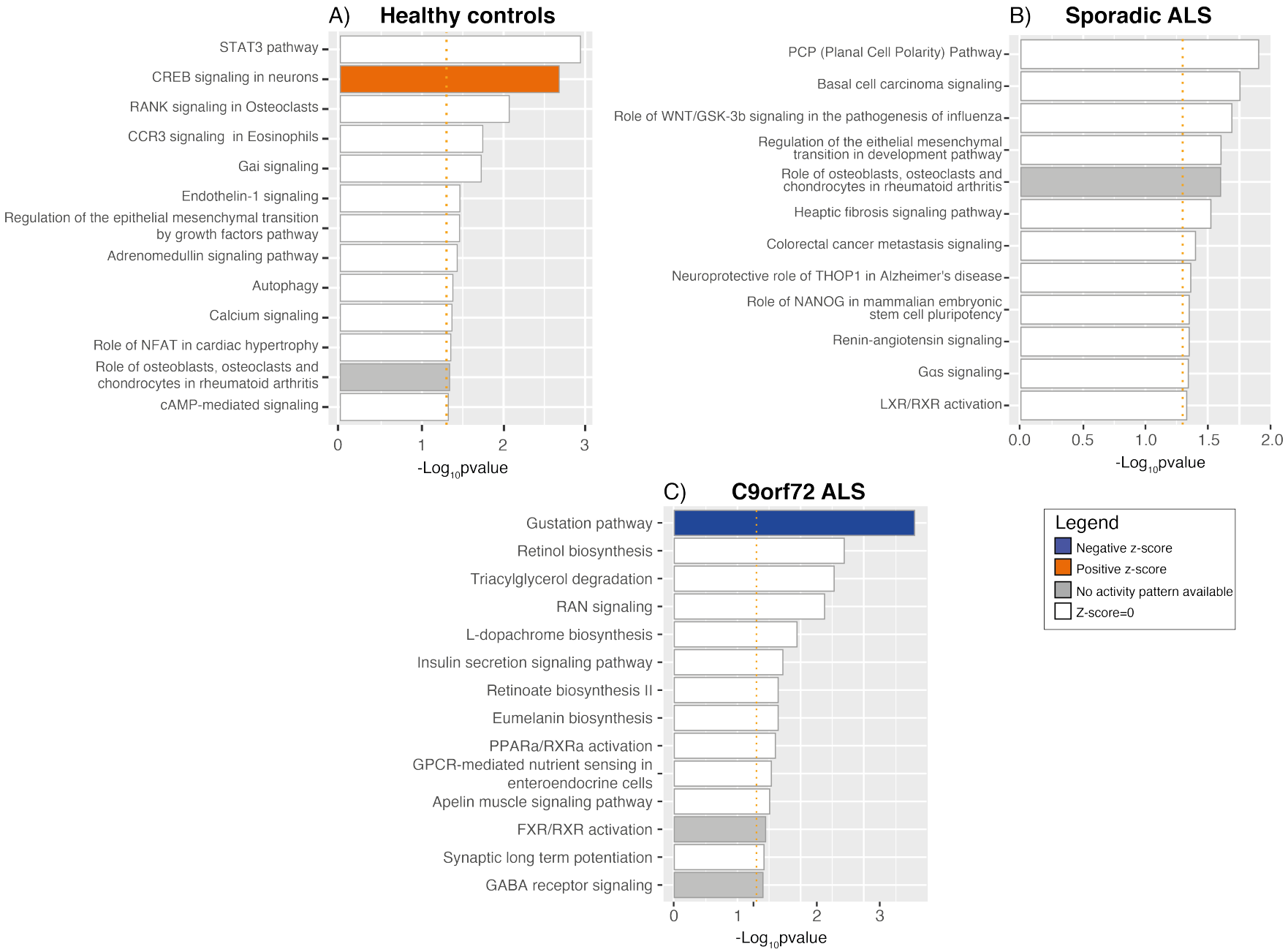
A) Healthy controls
STAT3 pathway
CREB signaling in neurons
RANK signaling in Osteoclasts
CCR3 signaling in Eosinophils
Gai signaling
Endothelin-1 signaling
Regulation of the epithelial mesenchymal transition by growth factors pathway
Adrenomedullin signaling pathway
Autophagy
Calcium signaling
Role of NFAT in cardiac hypertrophy
Role of osteoblasts, osteoclasts and chondrocytes in rheumatoid arthritis
cAMP-mediated signaling
0
1
2
3
-Log10pvalue
B) Sporadic ALS
PCP (Planal Cell Polarity) Pathway
Basal cell carcinoma signaling
Role of WNT/GSK-3b signaling in the pathogenesis of influenza
Regulation of the eithelial mesenchymal transition in development pathway
Role of osteoblasts, osteoclasts and chondrocytes in rheumatoid arthritis
Heaptic fibrosis signaling pathway
Colorectal cancer metastasis signaling
Neuroprotective role of THOP1 in Alzheimer's disease
Role of NANOG in mammalian embryonic stem cell pluripotency
Renin-angiotensin signaling
Gαs signaling
LXR/RXR activation
0.0
0.5
1.0
1.5
2.0
-Log10pvalue
C) C9orf72 ALS
Gustation pathway
Retinol biosynthesis
Triacylglycerol degradation
RAN signaling
L-dopachrome biosynthesis
Insulin secretion signaling pathway
Retinoate biosynthesis II
Eumelanin biosynthesis
PPARa/RXRa activation
GPCR-mediated nutrient sensing in enteroendocrine cells
Apelin muscle signaling pathway
FXR/RXR activation
Synaptic long term potentiation
GABA receptor signaling
0
1
2
3
-Log10pvalue
Legend
Negative z-score
Positive z-score
No activity pattern available
Z-score=0

Figure 5.19: Enriched IPA Canonical Pathways in iAstrocytes Following IL-2 Treatment.

Bar plots displaying IPA canonical pathway analysis retrieved from HC_IL2vsG (**A**), SALS_IL2vsG (**B**) and C9_IL2vsG (**C**) gene lists. Activated (z-score>0, in orange) or inhibited pathways (z-score<0, in blue) are shown. Significant pathways but with z-score equal to 0 (in white) or with no activation prediction available in the software (in grey) are also reported. A significance threshold is displayed as a dotted orange line ($-Log_{10}$ p-value=1.3).

Subsequently, the IPA tool called diseases and functions revealed a large number of processes being impacted by the IL-2 treatment. To gain a clear interpretation of these results, data reported in the following paragraphs only shows diseases and functions with computed positive or negative Z-scores, which indicate processes being activated or inhibited with the treatment. Interestingly, in the case of the healthy control astrocytes (**Figure 5.20**), genes involved in the proliferation of immune cells and T lymphocytes appeared to be markedly inhibited whilst more general terms like "quantity of cells" and "cell viability of tumour cell lines" were activated with the IL-2 treatment. Additionally, the process "quantity of neurons", which is particularly interesting in the context of ALS, also appeared to show a positive Z-score. These findings suggested a general increase in the survival of these cells and it would be interesting to validate the possible impact of IL-2 on neuron quantity. Nonetheless, although genes implicated in the proliferation of immune cells were inhibited, the term "leukopoiesis" was activated. This is consistent with the immune modulatory effect of the cytokine, which promotes a reorganization within the immune system rather than a general suppression. Lastly, the increase reported in the term "quantity of metal" suggested an impact of IL-2 on ion and metal homeostasis, which is in line with the Enrichr and REVIGO results.

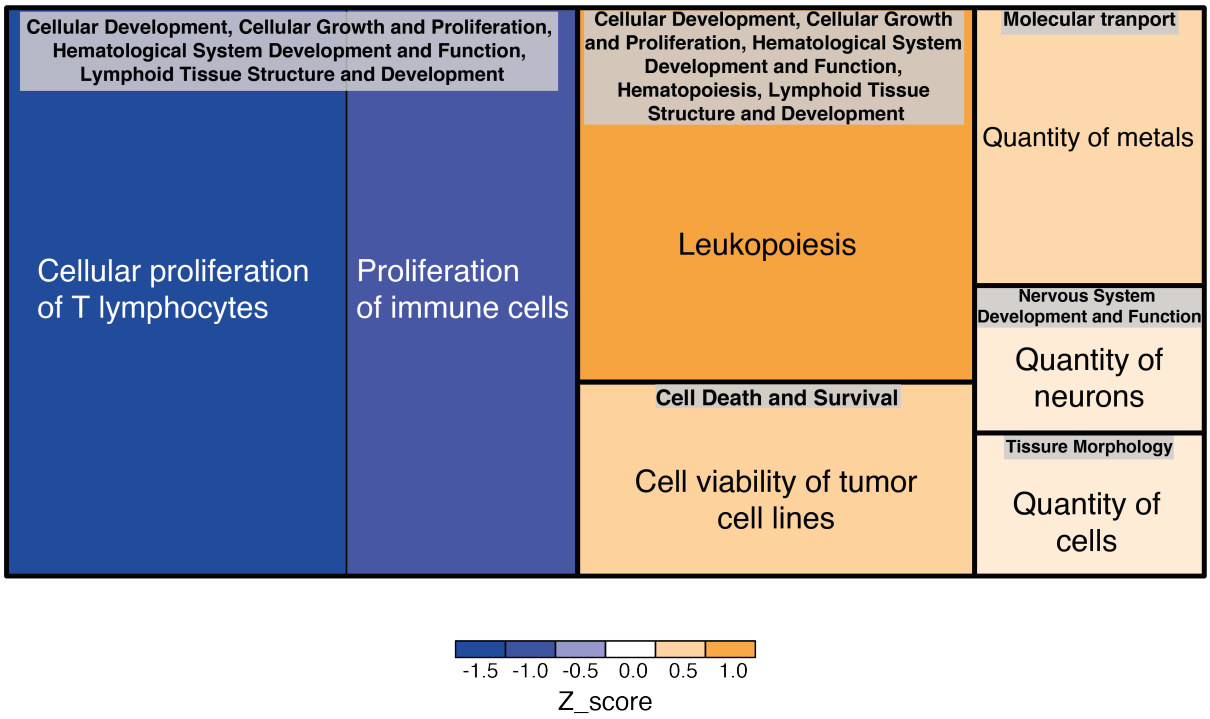

Figure 5.20: IPA Disease and Function Analysis in Healthy Control iAstrocyte

This treemap shows the diseases and functions retrieved from the IPA analysis of HC_IL2vsG data set. Each box represents a biological function or a disease and they are sized and coloured by their z-score (z-score > 0 in the orange colour scale or < 0 in the blue scale). Diseases and functions are clustered by IPA into master categories for which the name is displayed by a grey label.

A similar analysis for sALS astrocytes returned a greater number of diseases and functions being altered and with a computable activation status (Z-score) (**Figure 5.21**). Consistent with the heathy control results, the processes "quantity of metal ion" and "quantity of metal" appeared to be significantly enriched and activated. Moreover, in line with previous analysis, a mild inhibition of proliferative processes involving immune cells was reported ("quantity of B lymphocytes", "quantity of hematopoietic progenitor cells" and "quantity of pre-B lymphocytes"). Surprisingly, terms linked to the formation of different kinds of tumours were enriched (both activated and inhibited), whilst necrosis and apoptosis of epithelial cells appeared to be increased. These data might indicate a possible detrimental effect of IL-2 in sALS astrocyte as these terms

seemed to indicate an activation of cell death mechanisms. To exclude this hypothesis, an in-depth study of the genes included in these cancer and cell death pathways was conducted. A complete list of all the transcript names and functions with the associated fold changes and significance levels is provided in **Appendix 12.** A reduced number of genes were included in the "apoptosis of epithelial tissue" (5 genes) and in the "necrosis of epithelial tissue" (7 genes) pathways, and all of these transcripts were also included in the larger list of 60 genes that were differentially expressed in the three cancer processes ("malignant solid tumour", "non-melanoma solid tumour" and "formation of solid tumour"). Proteins encoded by these genes exerted a variety of different functions (including different transcription regulators, and several receptor subunits) whose alteration has been linked to cancer, whilst their importance in astrocytes is unclear (see **Appendix 12** for a brief summary of each gene function). Amongst these, only two genes (BIK and BMF) were found as having a direct effect on apoptosis by promoting its activation. Their expression appeared to be increased following IL-2 treatment, which might suggest a detrimental effect. However, transcriptional alteration of only two genes is probably not enough to confidently deduce an increase in cellular death. Moreover, given that the previous LDH data did not suggest any increase in cytotoxicity, these results are difficult to interpret and might indicate an activation of genes involved in cell death although this occurs at later time points. Therefore, further investigation is needed to exclude any possible detrimental long-term effects. Interestingly, some genes (FZD7 $\log_2$FC= 5.34, SHISA2 $\log_2$FC= -4.97, WNT3 $\log_2$FC= 4.67) involved in the Wnt pathway were differentially expressed and included in the list of tumour-related processes. This pathway has been shown to play a crucial role in cancer as well as in cellular proliferation (Teo and Kahn, 2010). Therefore, the alteration of the expression of these genes may exert a supportive effect in astrocytes.

Additionally, the IPA analysis also revealed an evident activation of the process "quantity of glycogen" in treated sALS astrocytes compared to untreated. This result is in contrast with what was reported from the Enrichr and REVIGO analysis in sALS astrocytes (suggesting a reduction in glycogen accumulation and an increased glucose synthesis). This mechanism also needs additional research to clarify these apparently contradictory results and to validate any beneficial effect of IL-2 on astrocyte glucose metabolism.

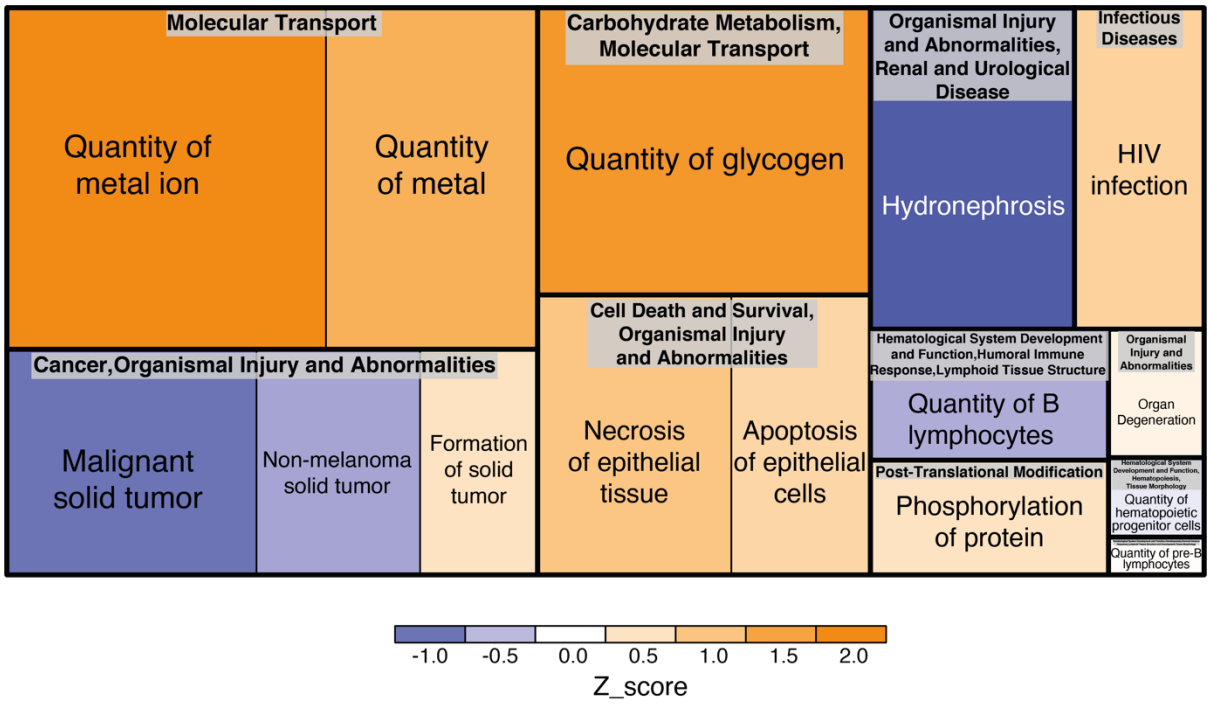

Figure 5.21: IPA Disease and Function Analysis in sALS iAstrocyte

This treemap shows the diseases and functions retrieved from the IPA analysis of SALS_IL2vsG data set. Each box represents a biological function or a disease and they are sized and coloured by their z-score (z-score > 0 in the orange colour scale or < 0 in the blue scale). Diseases and functions are clustered by IPA into master categories for which the name is displayed by a grey label.

Lastly, a disease and function analysis was also conducted in C9 ALS astrocytes (**Figure 5.22**). In line with previous findings, several processes involved in the metabolism of glucose and carbohydrates were altered in these cells following IL-2 treatment. The "accumulation of carbohydrate" was increased, which may reflect the activation of the "quantity of glycogen" in sALS cells. Nonetheless, in C9 astrocytes the "metabolism of polysaccharide" was also increased and mixed alterations in mechanisms involving glucose were reported ("uptake of D-glucose" and "glucose tolerance" being increased and "concentration of D-glucose" and "transport of glucose" being decreased). Therefore, further investigation is also needed in this type of cell to verify a beneficial effect of IL-2 on glucose metabolism and to ascertain that astrocytes are more supportive to MNs following the treatment. Additionally, the

transport and oxidation of lipids was reduced in the C9_IL2vsG comparison. The latter process is particularly interesting because, as lipid oxidation is one of the main consequences of oxidative damage, this might represent an additional indicator of a reduction in the oxidative stress induced by IL-2.

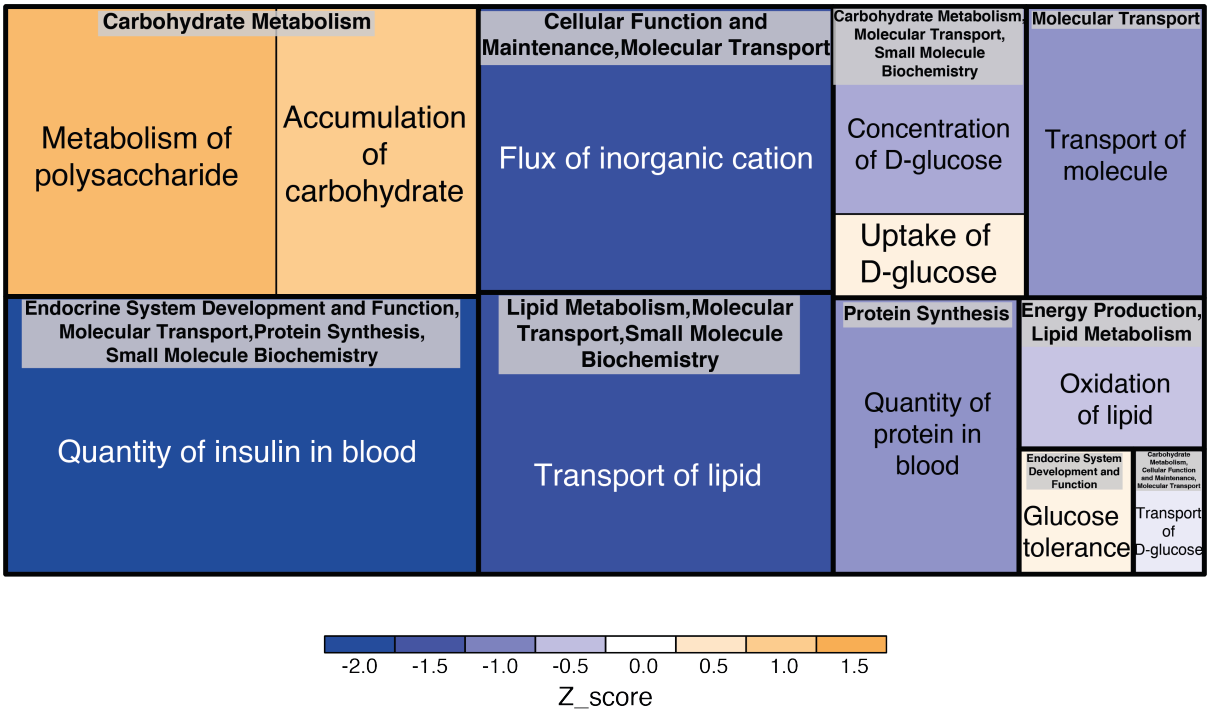

Figure 5.22: IPA Disease and Function Analysis in C9 iAstrocyte

This treemap shows the diseases and functions retrieved from the IPA analysis of C9_IL2vsG data set. Each box represents a biological function or a disease and they are sized and coloured by their z-score (z-score > 0 in the orange colour scale or < 0 in the blue scale). Diseases and functions are clustered by IPA into master categories for which the name is displayed by a grey label.

5.4 The Effects of IL-2 on MN Viability and Morphology

The last aim of this chapter was to assess whether IL-2 treatment had any effects on the viability and morphology of mouse MNs. In particular, these cells were co-cultured with iAstrocytes from one sALS (P17), one patient carrying a *C9orf72* mutation (P78) and one healthy control (155) to evaluate whether the cytokine was able to reduce ALS astrocyte-mediated MN toxicity whilst increasing cell viability. Additionally, given that it has been reported in the literature that IL-2 promoted morphological changes in neurons, including an increase in the branching index and arborization, differences in the number of neurites in treated cells were also investigated.

Importantly, data reported in this section were collected from only one experimental replicate. In fact, despite being attempted six times, just one co-culture experiment was successfully completed. This was due to several technical problems experienced with iAstrocytes and MNs including both bacterial and yeast infections. Due to time constraints, it was therefore not possible to replicate data but the plan is to produce triplicates following completion of the PhD.

Patient-derived astrocytes were firstly treated with IL-2 *in vitro*, then MNs were seeded on top of them and two additional IL-2 treatments were performed in order to allow both iAstrocyte and MNs to interact with the cytokine. Two control conditions were performed: i) Dimethyl Sulfoxide (DMSO, 1:1000) and ii) PBS + 5% glucose solution, in order to exclude the possibility of any effect of glucose contained in the PBS used to dilute IL-2. Cells were imaged at D1 and D3 following MN plating.

Data revealed a trend towards an increase in the number of viable MNs (identified as a cell body with at least one axon) co-cultured with all the three iAstrocyte lines (155, P78 and P17) following treatment with 10nM IL-2 (**Figure 5.23**). This was particularly evident in MNs co-cultured with heathy control astrocytes, which reached statistical significance at both D1 and D3 (One-way ANOVA with Tukey's correction for multiple comparisons). MNs seeded on top of P78 astrocytes (C9orf72-ALS mutant) showed an IL-2 mediated trend increase at D1 whilst a statistically significant difference was

reported at D3 between negative control (DMSO) and IL-2 treated cells. In addition, there was a trend towards significance (Adjusted p-value= 0.054) between the control condition (1:1000, PBS + 5% glucose solution) and IL-2. Less variations were reported in MNs co-cultured with patients 17 (sALS) which only showed a trend towards a viability increment at D1. Importantly, in the presence of all the astrocytic lines, no significant differences in the MN viability were reported between cells treated with either DMSO or PBS + 5% glucose solution. Therefore, the reported increases in MN viability were not mediated by glucose.

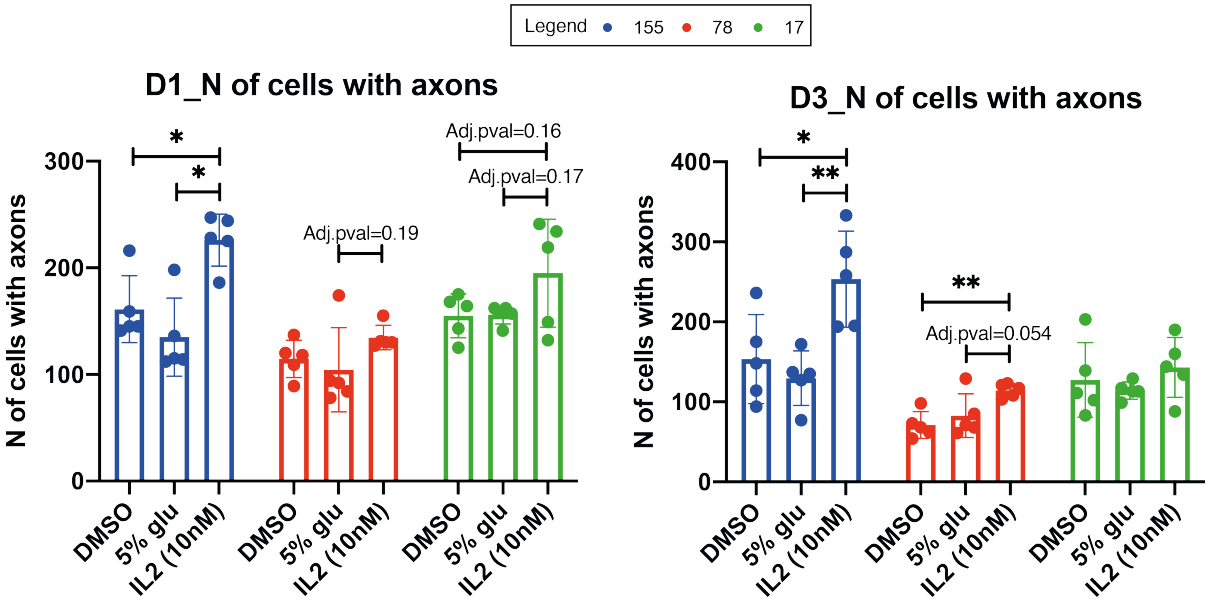

Figure 5.23: The Effect of IL-2 on MN Viability in Co-cultures with iAstrocytes.

These graphs show the number of viable MNs (cells with at least one axon) following co-culture with iAstrocytes (healthy control: 155 in blue, C9 ALS: P78 in red and sALS: P17 in green) for 1 or 3 days and IL-2 treatment (10nM). Additionally, two control conditions were also included: DMSO (1:1000) and PBS + 5% glucose solution (1:1000). Significant (One-way ANOVA with Tukey's correction for multiple comparisons) increases in the number of viable MNs were reported following IL-2 treatment in cells co-cultured with healthy control astrocytes (at D1 and D3) and P78 (only at D3). A trend towards protection was seen in P17. Each dot represents a technical replicate (five technical replicates per each condition) from only one experimental replicate. Mean ± SD are graphed. * : Adjusted p-value < 0.05; ** : Adjusted p-value < 0.01.

In addition, the number of MN neurites were also assessed to test the hypothesis of augmented branching index of the axons and dendritic arborization promoted by IL-2 (**Figure 5.24**). A significant (One-way ANOVA with Tukey's correction for multiple comparisons) increase in the neurite counts of MN co-cultured with the healthy control astrocytes following IL-2 treatment was reported both at D1 and D3. In the presence of P78 astrocytes, a considerable trend toward a significant neurite increment (Adjusted p-value= 0.06, between cells treated with PBS + 5% glucose or IL-2) was registered at D1 while statistical significance was reached at D3, when an increase in neurites was reported in IL-2 treated cells compared to DMSO negative controls. However, an insignificant increase (adjusted p-value= 0.14) was registered between cells treated with PBS + 5% glucose or IL-2. In contrast, no increases in the number of neurites were documented for MN co-cultured with P17.

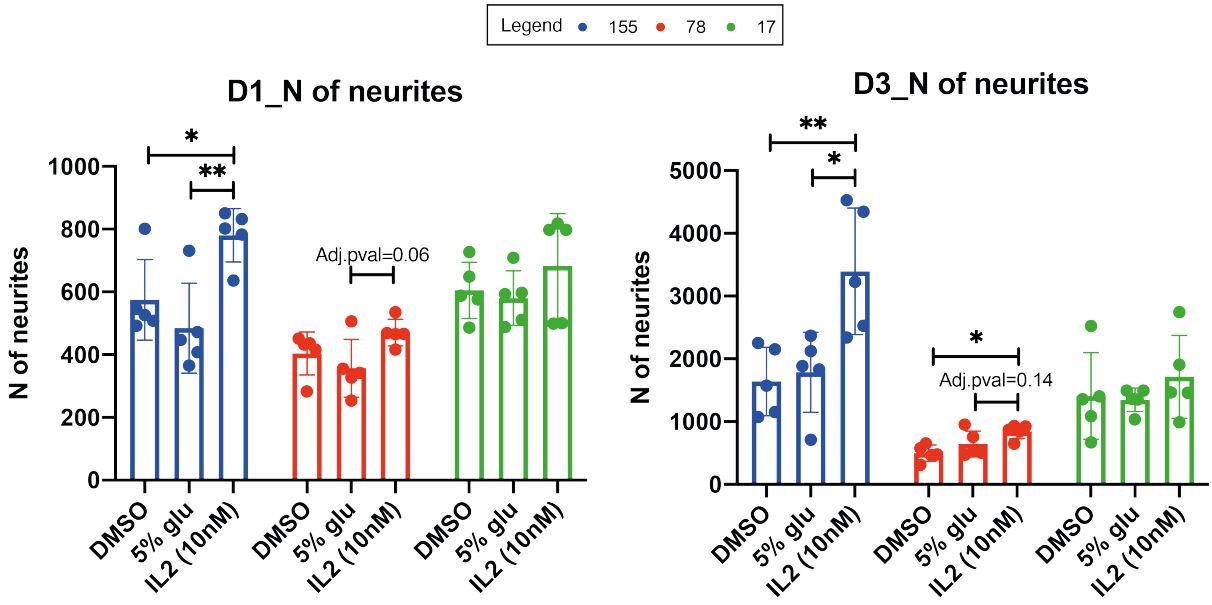

Figure 5.24: The Effect of IL-2 on MN Neurites in Co-cultures with iAstrocytes.

These graphs show the number of neurites detected in MNs co-cultured with iAstrocytes from a healthy control (155 in blue), an ALS patient carrying a C9orf72 mutation (P78 in red) and a sALS (P17 in green) for 1 or 3 days in the presence of either IL-2, PBS + 5% glucose solution or DMSO. Significant (One-way ANOVA with Tukey's correction for multiple comparisons) increases in the number of viable MNs were reported following IL-2 treatment in cells co-cultured with healthy control astrocytes (at D1 and D3) and P78 (only at D3). No statistically significant change was reported in P17. Each dot represents a technical replicate (five technical replicates per each condition) from only one experimental replicate. Mean ± SD are graphed. * : Adjusted p-value < 0.05; ** : Adjusted p-value < 0.01.

In conclusion, these results, although still preliminary, suggest that IL-2 induced a protective and a survival-promoting effect on MNs co-cultured with healthy control astrocytes. Milder effects were generally reported in the presence of ALS astrocytes as only P78 seemed to react to IL-2 by increasing MN viability and the number of neurites. This may suggest that the cytokine is able to affect MN viability or slightly reduce astrocyte-induced toxicity in just a selection of responsive ALS patients.

5.5 Discussion

The objective of this last part of my PhD research was to evaluate the effect of IL-2 on CNS cells, specifically on astrocytes and motor neurons. In fact, this cytokine was previously shown to cross the blood brain barrier and its receptor subunits were found to be widely distributed in different CNS anatomical regions. To this end, induced-neuronal progenitor cells (iNPCs)-derived astrocytes reprogrammed from 3 healthy controls, 3 sporadic ALS and 3 ALS patients carrying a C9orf72 mutation were grown together with healthy murine MNs. Unfortunately, the results reported in this section are considered preliminary as several impediments, mainly related to the Covid-19 pandemic resulting in laboratory closures and limited access, impacted on data collection. Nonetheless, we intend to increase replicates and gather new data in due course following competition of the PhD.

A summary of the results collected in this section of the study is provided below:

1) Firstly, an optimization was performed to identify the best experimental settings for the IL-2 *in vitro* treatment. The basal expression of the IL-2 receptor subunits was investigated via qRT-PCR analysis. Data revealed that, while the subunits IL2RB and IL2RG were consistently detected at generally high levels in all the investigated lines (3 healthy controls, 3 sALS and 3 C9orf72 ALS astrocytes), the expression of IL2RA was barely or not detectable in all the samples. This suggested that the intermediate affinity receptor was the main one present on astrocytes. Different IL-2 concentrations (1, 5, 10, 50 or 100nM), treatment times (1, 4 or 24 hrs) and experimental settings (1 or 10% FBS media) were tested and the expression of genes (*IL2RB*, *MYB*, *CASP3* and *CCND2*) known for being upregulated in response to IL-2 in immune cells was monitored. The best combination of settings able to promote the maximum transcriptional induction was a 4hr long treatment with 10nM IL-2 diluted in media containing 1% FBS.

2) Given that for the treatment optimization the expression of CASP3, a crucial protein implicated in the regulation of apoptosis, was monitored and reported

to be increased with the IL-2 treatment, cytotoxicity assays were performed. These were carried out in order to ascertain that the treatment did not lead to an increase in cell death. Results indicated no significant difference between astrocytes treated with IL-2 and the controls, which suggested that the cytokine administration did not induce cytotoxicity.

3) Subsequently, Oxford Nanopore cDNA sequencing was used to evaluate gene expression changes in response to the optimized IL-2 treatment in 3 healthy controls, 3 ALS patients carrying a C9orf72 mutation and 3 sALS-derived astrocytes. Three different transcriptional analyses were carried out in which, within each astrocyte group (healthy controls, C9orf72 ALS and sALS), IL-2-treated samples were compared to the control condition to find significant DEGs. Interestingly, ALS patient-derived astrocytes showed a greater number of genes being significantly differentially expressed following the IL-2 treatment compared to the healthy controls. In particular, those carrying a C9orf72 mutation seemed to be the most reactive with the greatest transcriptional regulation. Subsequently, gene enrichment analyses were conducted in order to identify biological processes and pathways being altered following IL-2 administration. In particular, two analyses were performed using different software programmes (Enrichr and REVIGO or IPA) to ensure a complete functional interpretation of the differentially expression data sets.

4) Lastly, co-cultures of patient-derived astrocytes and healthy mouse MNs were performed in order to assess whether IL-2 was capable of reducing the astrocyte-induced MN toxicity. Therefore, increases in cell viability were monitored through this assay and, given the evidence in the literature suggesting augmented neuron arborization levels and branching index following IL-2 treatment, MN morphological changes were also examined. Due to COVID-19-related restrictions and to multiple cell culture infections, the co-culture data collected are only preliminary (one replicate) and therefore need further investigation.

To our knowledge, this was the first time that IL-2 was tested in astrocytes and therefore, an initial treatment optimization was necessary. Despite not being able to collect all the necessary experimental replicates and having reported a limited number of statistically significant results, a 4hr long treatment with 10nM IL-2 diluted in media containing 1% FBS was identified as the best combination of treatment settings. This decision was supported by the well-established constant of dissociation of the intermediate affinity receptor (Kd ~10^{-9} M), which is expressed on iNPC-derived astrocytes and that is able to react to nanomolar IL-2 concentrations (Spolski et al., 2018). We appreciate that this range of doses is greater than what was used to stimulate Tregs, which constitutively express the high affinity receptor (Kd ~10^{-11} M). However, it is not possible to exclude any reaction of astrocytes or other CNS cells following peripheral administration of ld-IL-2 given that the cytokine does cross the blood brain barrier and a limited number of high affinity receptor may be also present in these cells despite not being detected via qRT-PCR. Therefore, the objective was to study the *in vitro* reaction of astrocytes to nanomolar doses of IL-2 and to compare these results with future expression data retrieved from the CSF of ALS participants included into another clinical trial (MIROCALS, see chapter 6 for a more detailed description), which also aims to investigate the CNS transcriptomic effects of subcutaneous injection of 2MIU-IL2 in ALS patients. In addition, the decision of conducting the treatment in media contain 1% FBS was supported by the collected data in 10% FBS showing limited effects and also considering a recent study, which suggested that the serum is able to induce an inflammatory-like phenotype in these cells (Perriot et al., 2018). Therefore, we hypothesized that high FBS concentrations might mask the effect of IL-2. In line with this, multiple other research groups chose to use reduced or no FBS in their media when treating astrocytes with different interleukins (see **Table 5.1**). Lastly, the chosen treatment time (4 hrs) is consistent with previous literature indicating short time points (from 2 to 6 hrs) as ideal for monitoring of gene expression changes in astrocyte following treatment with different cytokines (Thelin et al., 2020, Tarassishin et al., 2014, Norden et al., 2014, Jang et al., 2013, Semple et al., 2010, Ma et al., 2010, Burmeister et al., 2019a, Dong et al., 1999).

RNA samples from IL-2 treated and control iAstrocytes were used to produce Oxford Nanopore cDNA sequencing expression data. Quality control analysis revealed a considerably high number of mapped and assigned reads and average read lengths

consistent with full-length transcripts. Unfortunately, while the majority of the samples showed an expected distribution of the per sequence GC content (with a peak at 42-45% which is consistent with the human transcriptome), two samples showed an unexpected additional peak at 35%, which might indicate either a contamination or an enrichment in A/T rich sequences. We appreciate this as a limitation to our analysis and therefore we are now planning to sequence other patient-derived astrocytes and healthy controls to increase the number of replicates. Nonetheless, high Phred quality scores were obtained (~23 in all the samples), which suggested a per base level of sequencing accuracy greater than 99%. A principal component analysis was also carried out in order to visually inspect differences and similarities amongst transcriptional profiles. Surprisingly, four samples belonging to a healthy control (161, both IL-2 treated and control) and a C9orf72-ALS (P201, both IL-2 treated and control) appeared to be grouped and spatially distanced from all the rest of the samples. However, this difference was not the result of a batch effect nor it was not ascribable to gender and age dissimilarities of the fibroblast donors or to differences in the cell culture process (passage number). The spatial separation was also confirmed by multidimensional scaling (MDS), an independent dimensionality reduction technique. Although the removal of these four samples allowed a group separation consistent with the different disease types (healthy control, sALS and C9orf72 ALS), these were not considered as outliers. This decision was reinforced by the fact that an additional analysis revealed very high correlation scores (>0.99) suggesting tight similarities between all the investigated samples. Moreover, the exclusion of 4 out of 18 samples would have potentially biased the subsequent differential expression analysis. Nonetheless, this was considered as a major limitation to our study and, as mentioned before, the aim is to repeat the sequencing using different fibroblast donors and to include those in the transcriptomic analyses to reinforce and validate our results.

Gene expression analyses were performed and surprisingly, the three astrocyte groups appeared to react very differently to the IL-2 treatment. In fact, no genes were identified as commonly differentially expressed in all the three comparisons whilst limited similarities were reported between paired data sets. Interestingly though, despite the limited DEGs in common, some biological processes were found to be similarly altered in all the comparisons. In particular, mechanisms involved in CNS homeostasis, especially myelination and axonogenesis, were upregulated in all the treated astrocyte groups. This suggested a possible protective effect of IL-2 on CNS

homeostasis. Additionally, genes involved in the synaptic vesicle and anterograde transport were increased only in healthy controls and C9orf72 ALS treated astrocytes. This is particularly interesting as accumulating evidence in the ALS literature suggest defects in axonal transport (as reviewed in (De Vos and Hafezparast, 2017)). Additionally, the activation of the IPA term "quantity of neurons" indicated a possible pro-survival effect of IL-2 on neurons which was mediated by the healthy control astrocytes. This is consistent with what was previously reported in the literature by Sarder and colleagues who proposed that IL-2 induced a pro-survival effect which was indirectly mediated by soluble factors released from glial cells (Sarder et al., 1993). Moreover, the canonical pathway analysis in healthy astrocytes revealed "CREB signaling pathway in neurons" as an additional interesting CNS-related mechanism being significantly enriched. This pathway is crucial for the regulation of neuronal plasticity and survival. However, a recent report also showed pivotal protective effects in astrocytes involving the regulation of mitochondrial functions, lipid metabolism and redox protection (Pardo et al., 2017).

Modifications in the oxidative stress response system were also reported in all the three comparisons. In particular, reduction in the ROS biosynthesis and in the oxidative damage-induced cell death mechanisms were documented, together with alteration in the regulation of the oxidative stress response system. Moreover, the IPA analysis of C9orf72 ALS astrocytes treated with IL-2 revealed an inhibition in the oxidation of lipids, one of the main consequences of oxidative stress. This result is in line with previous data from the IMODALS trial indicating an inhibition of processes involved in the production of ROS and reduction in the NRF2 pathway activation at D8. Therefore, this reinforces the hypothesis of an additional beneficial impact of IL-2 on the oxidative state with potential key protective effects on this ALS pathological mechanism.

Both the Enrichr - REVIGO analysis and IPA revealed that several processes involved in immune system homeostasis (such as lymphocyte activation and function and cytokine production) were also modified in all the three comparisons. Despite the challenging interpretation of these alterations, these data suggested that genes known for their activity within the immune system are also expressed in astrocytes and their transcription was regulated by IL-2 in an immune-regulative way. In fact, similarly to the results from the peripheral blood of IMODALS patients, the IL-2 administration did

not induce a general immune suppression but it rather promoted a characteristic immunological reorganization.

Moreover, both enrichment analyses suggested a modification in pathways involved in glucose biosynthesis and storage. This is of striking importance for astrocytes as these cells are responsible for providing neurons with the necessary energy (glucose-lactose shuttle) and for the glucose accumulation into glycogen. As previously mentioned, these mechanisms are impacted in ALS with evidence of reduced glycogen degradation to glucose and increased glycogen production being reported in the literature (Allen et al., 2019b, Li et al., 2019, Dodge et al., 2013). Surprisingly, contrasting results were found in the two gene enrichment analyses. In fact, while the Enrichr and REVIGO sALS data suggested a beneficial alteration characterized by increased gluconeogenesis and reduced glycogen synthesis, opposite results were found from the IPA analysis where the quantity of glycogen seemed to be increased in sALS. Similarly, activation of the "accumulation of carbohydrate" process was increased in C9orf72 ALS, however, this was accompanied by increased uptake of D-glucose and metabolism of polysaccharides. More investigation is therefore needed to elucidate these apparently paradoxical results and to verify any possible beneficial effect on glucose metabolism.

Moreover, the Enrichr and REVIGO analysis of sALS treated astrocytes and the C9orf72 IPA analysis revealed evidence of an alteration in the biosynthesis and cellular response to retinol (also known as vitamin A). This molecule has been previously associated with ALS although contrasting evidence is reported in the literature. In fact, in a recent Chinese study, vitamin A serum levels were found to be increased in ALS patients compared to healthy controls and the authors proposed retinol as a risk factor for this disease (Wang et al., 2014). Nonetheless, in a different report, a selection of MNs from familial and sporadic ALS cases displaying higher retinoic acid receptor β levels appeared to be more resistant to cellular death (Kolarcik and Bowser, 2012). Additionally, a retinoid-free diet in healthy rats was found to cause a range of clinical symptoms similar to ALS (atrophy, muscular weakness and MN loss) (Corcoran et al., 2002) and the treatment of mSOD1 mice with a retinoid X receptor agonist extended their lifespan and reduced reactive astrogliosis (Riancho et al., 2015). Given the modifications induced by IL-2, further investigations will be needed to fully elucidate another potentially interesting effects of this cytokine on CNS cells.

Lastly, albeit being preliminary, encouraging results were reported in co-cultures, which suggested an increase in MN viability in cells co-cultured with both astrocytes derived from a healthy control and from an ALS fibroblast donor carrying a *C9orf72* mutation. Additionally, an augmented number of neurites was reported in the same astrocyte lines. Nonetheless, no significant improvements were seen in MN co-cultured with one sporadic ALS astrocytic line. Taken together, these data suggested a possible impact of IL-2 on ALS astrocyte-induced MN toxicity although this effect may be limited to a number of responsive patients. Unfortunately, as these fibroblasts were biopsied from patients who were not on the IMODALS trial, their systemic and Treg response is unknown and therefore this data on CNS cells cannot be related to an IL-2-induced immune system response. Additionally, the healthy control astrocyte data revealed a possible pro-survival effect of the cytokine on normal cells which is consistent with previous reports in the literature indicating IL-2 as having a protective, survival -promoting effects on healthy neurons (see chapter 1.5) (Sarder et al., 1993).

Chapter 6 – Final Discussion and Future Directions

Amyotrophic lateral sclerosis is a devastating neurodegenerative disease and currently no disease modifying treatment is available. The objective of this study was to evaluate the molecular effects of low-dose interleukin-2 treatment to validate the hypothesis of a protective impact in ALS patients due to the immune modulatory properties of the cytokine. Whilst ld-IL-2 has been previously shown to promote regulatory T cells expansion and induce a physiological immune regulation in other autoimmune disorders (as reviewed in section 1.4), this was the first time ld-IL-2 was trialed in ALS patients and also the first time its gene expression changes were monitored in such individuals over the treatment period.

The majority of this study focused on generating and analysing transcriptional profiles of IMODALS clinical trial participants. Evidence revealed a successful Treg expansion following three treatment cycles with ld-IL-2. In particular, consistent with previous findings reported in the literature (see section 1.4) and with our collaborators' data (Camu et al., 2020), a dose-dependent gene expression reaction was reported. Therefore, 2MIU-IL-2 was proposed as the most effective dose to treat ALS patients. Additionally, evidence of longitudinal transcriptional alterations was documented. Specifically, data were consistent with an evident initial immune suppression (D8) whilst the establishment of an immune regulatory condition (Treg expansion) was achieved at later trial stages (D64), suggesting the existence of a cumulative reaction to successive doses of ld-IL-2. Nonetheless, these effects were not sustained following cessation of the treatment (D85) as the expression of Treg markers was determined to be returning towards baseline levels. Therefore, continuous ld-IL-2 administrations might be required to preserve a Treg expansion in ALS patients.

Interestingly, our data demonstrated the existence of inter-individual differences in patients' abilities to react to the drug. This was in line with previous studies investigating the effects of ld-IL-2 in other autoimmune disorders, which documented some individuals being more responsive than others (Koreth et al., 2011, Koreth et al.,

2016, Saadoun et al., 2011, Rosenzwajg et al., 2020, He et al., 2020, Castela et al., 2014). Therefore, IMODALS patients were classified into low, moderate and high-Treg responders and substantial baseline (D1) differences were reported in their transcriptome with the low responders having a more inflammatory-prone phenotype at time of recruitment. Additionally, a predictive biomarker analysis was conducted and two genes (*TLR9* and *CD27*) were successfully identified as baseline predictors of patient responsiveness (as measured by the number of Tregs at D64) to three cycles of 2MIU IL-2. This result is of particular interest and, if validated, this may be crucial for future precision medicine approaches, to allow patient stratification and the identification of the best therapeutic strategy for each individual. Importantly, the significance of this findings may not be limited to ALS but could impact the pharmacological research of the aforementioned autoimmune disorders that trialed ld-IL-2 and reported inter-individual differences.

A limitation of this study is the small participant group size, which particularly affected the analyses. In particular, we recognise age, sex and genetic background as crucial variables possibly impacting on the ALS transcriptional phenotype. Nonetheless, in such a limited sized cohort, we believed that stratifying for these factors would have considerably reduced the statistical power of our analyses. This limited participant size also substantially affected the proposed predictive biomarker research, which therefore needs validation. Additionally, we appreciate the possibility of genetic variants (i.e. in genes encoding for the IL-2 receptor subunits) underlying the inter-individual difference within patients in terms of Treg-responsiveness to the cytokine. However, although blood for extracting DNA sample was collected as part of the trial, this has not yet been sequenced due to funding restraints and therefore this type of analysis was not yet possible. Lastly, the IMODALS trial was underpowered in detecting any effect on survival as patients were followed-up over a period of only six months. In fact, this was not an aim of this clinical trial, which only focused on the safety and the investigation of the molecular effects of ld-IL-2. Nonetheless, given the evidence in the literature suggesting a significant correlation between Treg number and patient survival (Rentzos et al. 2012, Mantovani et al. 2009, Henkel et al. 2013) and that, in ALS mouse models, Treg expansion ameliorated symptoms and prolonged survival (Beers et al. 2008, 2011, Sheean et al. 2018), it is justified to hypothesise an effect of ld-IL-2 on disease progression.

The aim is to address all these limitations by analysing data from a larger trial called Modifying Immune Response and OutComes in ALS (MIROCALS, NCT03039673), which is currently underway. This randomized (1:1), placebo-controlled, double-blind, parallel group trial will investigate the effects of five cycles of 2MIU IL-2 in a considerably greater cohort of 220 ALS patients over a period of 18 months. This will allow more complex examination of gene expression changes throughout the trial and further investigation on the variability in Treg-response as well as the validation of the robustness of our proposed predictive model. RNA from both peripheral blood and CSF is currently being processed in our laboratory to generate gene expression profiles with the aim of comparing peripheral and central transcriptional changes following repeated ld-IL-2 administrations. In contrast to IMODALS, MIROCALS patients have been recruited at diagnosis, and have been treated with riluzole for three months prior to the start of the ld-IL-2 (or placebo) administration, providing a unique resource to establish the longitudinal effects of riluzole treatment as well as ld-IL-2 in a large, clinically and genetically characterized cohort of patients. One of the primary end points of MIROCALS is the assessment of any increase in patient survival to validate this cytokine as an immune modulatory drug able to reduce the speed of disease progression. The other primary objectives of the trial are to evaluate clinical efficacy using a range of clinical tests and to further validate the safety of the drug. Secondary and explorative outcomes include the identification of biomarkers of drug responder status, deep immune phenotyping, neuroimaging and genomic analysis. Importantly, an extensive genetic characterization of the participants will be carried out providing the chance to associate any variants with high or low Treg-responders.

Considering the IL-2 penetrance across the blood brain barrier, the last part of this work focused on the study of the molecular effects of this cytokine on CNS cells, specifically astrocytes and MNs. Importantly, astrocytes were investigated as they are known to be crucial in the pathogenesis of ALS and as they are also able to modulate different immune system cells, including Tregs (as reviewed in section 1.2b). To our knowledge, this was the first time IL-2 was tested on induced neuronal progenitor cell (iNPC)-derived astrocytes reprogrammed from ALS or healthy control fibroblasts. Therefore, the initial aim was to optimize the treatment and a combination of settings (10nM IL-2 for 4 hrs in media containing 1% FBS) was successfully identified as ideal for these cells. Subsequently, Oxford Nanopore gene expression profiling of these

astrocytes revealed evidence of interesting biological processes and pathways being altered following IL-2 administration. In particular, the activation of processes involved in CNS homeostasis (including myelination and axonogenesis), reduction in oxidative stress with decreased production of ROS and modification in the astrocyte glucose metabolism were reported. All these processes are implicated in ALS and their IL-2-mediated alteration can be protective and potentially able to reduce astrocyte-mediated MN toxicity. This is in line with preliminary data suggesting an increase in MN viability and in neurite numbers in cells co-cultured with an IL-2-treated astrocyte line reprogrammed from an ALS patient carrying a C9orf72 mutation. In contrast, insignificant differences were reported with a sporadic ALS individual. These results may reflect the inter-individual differences observed in the IMODALS trial, where only a selection of participants appeared to be strongly responding to ld-IL-2 compared to the rest of the individuals who showed only a partial response. Unfortunately, this hypothesis could not be verified as fibroblasts from IMODALS patients were not collected and the cells used for iAstrocyte differentiation belonged to different individuals suffering from ALS.

Several limitations and impediments (mainly related to the Covid-19 pandemic) characterized the last part of this work involving CNS cells and therefore we recognize these data as preliminary despite being interesting and encouraging. Specifically, the reduced number of replicates (which particularly affected the co-culture experiments) impacted the ability to draw definite conclusions. Additionally, Oxford Nanopore transcriptomic data revealed unexpected variability in our samples (161 and P201 were spatially distanced from the rest of the samples in the PCA) and this might have reduced the number of identified differentially expressed genes and prevented the identification of potentially interesting altered processes. Therefore, the aim is to address these limitations by increasing the number of replicates and by generating new transcriptomic data from patient-derived astrocytes reprogrammed from other ALS patients and healthy controls to validate our results.

The last part of this PhD study focused on the astrocyte reaction to IL-2. However, in terms of future work, it will be interesting to study this cytokine on ALS patient-derived MNs to investigate whether it exerts any protective effects on the degenerating cells characteristic of the disease.

In conclusion, despite the reported limitations, our data are completely novel and intriguing as the effect of IL-2 in ALS was investigated here for the first time. The results successfully demonstrated a Treg expansion, a concomitant peripheral immune regulation and evidence of activation of CNS protective pathways. This has the potential to reduce the ALS pathological neuroinflammatory condition and possibly to increase patient survival. Additionally, a predictive model was proposed, which, if validated, may be able to stratify patients and select the most responsive ones to ld-IL-2. This could be crucial for future precision medicine approaches focusing on this type of treatment for ALS patients.

PhD outputs

Publications:

1. **Giovannelli I**, Heath P, Shaw PJ, Kirby J. *The involvement of regulatory T cells in amyotrophic lateral sclerosis and their therapeutic potential.* **Amyotroph Lateral Scler Frontotemporal Degener. 2020** Aug;21(5-6):435-444. doi: 10.1080/21678421.2020.1752246. Epub 2020 Jun 2. PMID: 32484719.

2. Boddy SL, **Giovannelli I**, Sassani M, Cooper-Knock J, Snyder MP, Segal E, Elinav E, Barker LA, Shaw PJ, McDermott CJ. *The gut microbiome: a key player in the complexity of amyotrophic lateral sclerosis (ALS)*. **BMC Med. 2021** Jan 20;19(1):13. doi: 10.1186/s12916-020-01885-3. PMID: 33468103; PMCID: PMC7816375. (Shared first authorship).

3. **Giovannelli I**, Bayatti N, Brown A, Wang D, Mickunas M, Camu W, Veyrune JL, Payan C, Garlanda C, Locati M, Juntas-Morales R, Pageot N, Malaspina A, Andreasson U, Suehs C, Saker S, Masseguin C, de Vos J, Zetterberg H, Al-Chalabi A, Leigh PN, Tree T, Bensimon G, Heath PR, Shaw PJ, Kirby J. *Amyotrophic lateral sclerosis transcriptomics reveals immunological effects of low-dose interleukin-2.* **Brain Commun. 2021** Jun 29;3(3):fcab141. doi: 10.1093/braincomms/fcab141. PMID: 34409288; PMCID: PMC8364666.

Conference presentations:

1. **Giovannelli I**, Heath P, Shaw PJ and Kirby J. *Low-dose IL-2 administration in ALS: understanding the transcriptional response to treatment*. **Sheffield Medical School Research Meeting, Sheffield (2019)**. Poster presentation.

2. **Giovannelli I**, Heath P, Shaw PJ and Kirby J. *Low-dose IL-2 administration in ALS: understanding the transcriptional response to treatment*. **European Network to Cure ALS (ENCALS) Meeting, Tours (2019)**. Poster presentation.

3. **Giovannelli I**, Heath P, Shaw PJ and Kirby J. *Low-dose IL-2 administration in ALS: understanding the transcriptional response to treatment*. **Sheffield BRC Training Academy Presentation Day (2019)**. Oral presentation.

4. **Giovannelli I**, Heath P, Shaw PJ and Kirby J. *Exploratory research in amyotrophic lateral sclerosis clinical trials.* **7th MDHRSA Research Forum: Clinical Trial Development (2020)**. Oral presentation.

5. **Giovannelli I**, Heath P, Shaw PJ and Kirby J. *Blood transcriptomics of ALS patients in the IMODALS clinical trial.* **Sheffield BRC Training Academy Presentation Day (2020)**. Oral presentation. Recipient of the 1st prize for the best oral presentation.

6. **Giovannelli I**, Mickunas M, Tree T, Bensimon G, Leigh PN, Heath P, Shaw PJ, Kirby J. *Blood Transcriptomics of ALS Patients in the IMODALS Clinical Trial.* **Motor Neurone Disease Association International Virtual Symposium (2020)**. ePoster presentation.

7. **Giovannelli I**, Shaw A, Myszcznska M, Roome K, Granger S, Destro M, Wan LM, Heath P, Ferraiuolo L, Low-dose interleukin-2 as an immune-modulatory therapeutic strategy for ALS. **European Network to Cure ALS (ENCALS) Virtual Meeting (2021).** ePoster and flash oral presentation.

8. **Giovannelli I**, Heath P, Shaw PJ and Kirby J. Low-dose interleukin-2 and amyotrophic lateral sclerosis: understanding the transcriptional response after treatment. **Neuroscience Institute Autumn Conference 2021.** Oral presentation.

9. **Giovannelli I**, Granger S, Roome K, Destro M, Myszcznska M, Shaw A, Ferraiuolo L, Heath P, Low-dose interleukin-2 as an immune-modulatory therapeutic strategy for ALS. **Motor Neurone Disease Association International Virtual Symposium (December 2021).** Abstract accepted for an ePoster.

Appendix list

All the appendices can be found in attached to this thesis as separate files.

Appendix 1: A selection of the results I obtained analysing data from the IMODALS clinical trial have been published in this original article in the journal Brain Communications.

Appendix 2: Full list of significant ($p < 0.05$ and $1.2 \leq FC \leq -1.2$) DEGs resulted from the comparison 1MIU_vs_Placebo

Appendix 3: Full list of significant ($p < 0.05$ and $1.2 \leq FC \leq -1.2$) DEGs resulted from the comparison 2MIU_vs_Placebo

Appendix 4: Full list of significant ($p < 0.05$) Gene Ontology Biological Processes (GO BP) resulted from the Enrichr analysis of the DEGs retrieved from the Limma comparison ΔD8. Both down and upregulated processes are reported.

Appendix 5: Full list of significant ($p < 0.05$) Gene Ontology Biological Processes (GO BP) resulted from the Enrichr analysis of the DEGs retrieved from the Limma comparison ΔD64. Both down and upregulated processes are reported.

Appendix 6: Table illustrates significantly (p-value<0.05) enriched diseases and functions from ΔD8 differentially expressed gene list analysis using IPA®. For each disease and function term the cluster category is reported together with p-value, z-score, predicted activation state (z-score>2= increased activation, z-score<-2=decreased activation), number of transcripts and their IDs. Data were analysed through the use of IPA (QIAGEN Inc., https://www.qiagenbioinformatics.com/products/ingenuitypathway-analysis).

Appendix 7: Table illustrates significantly (p-value<0.05) enriched diseases and functions from ΔD64 differentially expressed gene list analysis using IPA®. For each disease and function term the cluster category is reported together with p-value, z-score, predicted activation state (z-score>2= increased activation, z-score<-

2=decreased activation), number of transcripts and their IDs. Data were analysed through the use of IPA (QIAGEN Inc., https://www.qiagenbioinformatics.com/products/ingenuitypathway-analysis)

Appendix 8: Table including the 81 discriminatory variables resulting from the Qlucore analysis of the nanoString data. For each transcript, normalized raw count expression is reported for each sample screened. Samples are named by patient ID and the treatment type and date of sample collection (either D1, D8 or D64) is also shown.

Appendix 9: Full list of significant (log2FC ≤ -0.58 or ≥ 0.58 which is equal to 1.5 ≤ FC ≤ -1.5 and p-value <0.05)) DEGs resulted from the comparison HC_IL2vsG.

Appendix 10: Full list of significant (log2FC ≤ -0.58 or ≥ 0.58 which is equal to 1.5 ≤ FC ≤ -1.5 and p-value <0.05)) DEGs resulted from the comparison SALS_IL2vsG.

Appendix 11: Full list of significant (log2FC ≤ -0.58 or ≥ 0.58 which is equal to 1.5 ≤ FC ≤ -1.5 and p-value <0.05)) DEGs resulted from the comparison C9_IL2vsG.

Appendix 12: This table shows all the genes included in 5 IPA diseases and functions, namely: "apoptosis of epithelial tissue" (reported in the table with the letter A), "necrosis of epithelial tissue" (reported as B), "malignant solid tumour" (reported as C), "non-melanoma solid tumour" (reported as D) and "formation of solid tumour" (reported as E). For each gene, the logarithmic fold change (log2FC) and the p-value (comparison SALS_IL2vsG) are reported together with the IPA term. Additionally, a summary of the function exerted by the encoded protein is also included (source: https://www.genecards.org/).

Bibliography

ABE, K., PAN, L. H., WATANABE, M., KATO, T. & ITOYAMA, Y. 1995. Induction of nitrotyrosine-like immunoreactivity in the lower motor neuron of amyotrophic lateral sclerosis. *Neurosci Lett,* 199**,** 152-4.

AEBISCHER, J., CASSINA, P., OTSMANE, B., MOUMEN, A., SEILHEAN, D., MEININGER, V., BARBEITO, L., PETTMANN, B. & RAOUL, C. 2011. IFNγ triggers a LIGHT-dependent selective death of motoneurons contributing to the non-cell-autonomous effects of mutant SOD1. *Cell Death Differ,* 18**,** 754-68.

AL-CHALABI, A., HARDIMAN, O., KIERNAN, M. C., CHIÒ, A., RIX-BROOKS, B. & VAN DEN BERG, L. H. 2016. Amyotrophic lateral sclerosis: moving towards a new classification system. *Lancet Neurol,* 15**,** 1182-94.

AL-SARRAJ, S., KING, A., CLEVELAND, M., PRADAT, P. F., CORSE, A., ROTHSTEIN, J. D., LEIGH, P. N., ABILA, B., BATES, S., WURTHNER, J. & MEININGER, V. 2014. Mitochondrial abnormalities and low grade inflammation are present in the skeletal muscle of a minority of patients with amyotrophic lateral sclerosis; an observational myopathology study. *Acta Neuropathol Commun,* 2**,** 165.

ALEXIANU, M. E., KOZOVSKA, M. & APPEL, S. H. 2001. Immune reactivity in a mouse model of familial ALS correlates with disease progression. *Neurology,* 57**,** 1282-9.

ALLEN, S. P., HALL, B., CASTELLI, L. M., FRANCIS, L., WOOF, R., SISKOS, A. P., KOULOURA, E., GRAY, E., THOMPSON, A. G., TALBOT, K., HIGGINBOTTOM, A., MYSZCZYNSKA, M., ALLEN, C. F., STOPFORD, M. J., HEMINGWAY, J., BAUER, C. S., WEBSTER, C. P., DE VOS, K. J., TURNER, M. R., KEUN, H. C., HAUTBERGUE, G. M., FERRAIUOLO, L. & SHAW, P. J. 2019a. Astrocyte adenosine deaminase loss increases motor neuron toxicity in amyotrophic lateral sclerosis. *Brain,* 142**,** 586-605.

ALLEN, S. P., HALL, B., WOOF, R., FRANCIS, L., GATTO, N., SHAW, A. C., MYSZCZYNSKA, M., HEMINGWAY, J., COLDICOTT, I., WILLCOCK, A., JOB, L., HUGHES, R. M., BOSCHIAN, C., BAYATTI, N., HEATH, P. R., BANDMANN, O., MORTIBOYS, H., FERRAIUOLO, L. & SHAW, P. J. 2019b. C9orf72 expansion within astrocytes reduces metabolic flexibility in amyotrophic lateral sclerosis. *Brain,* 142**,** 3771-3790.

ALMER, G., GUÉGAN, C., TEISMANN, P., NAINI, A., ROSOKLIJA, G., HAYS, A. P., CHEN, C. & PRZEDBORSKI, S. 2001. Increased expression of the pro-inflammatory enzyme cyclooxygenase-2 in amyotrophic lateral sclerosis. *Ann Neurol,* 49**,** 176-85.

ALMER, G., TEISMANN, P., STEVIC, Z., HALASCHEK-WIENER, J., DEECKE, L., KOSTIC, V. & PRZEDBORSKI, S. 2002. Increased levels of the pro-inflammatory prostaglandin PGE2 in CSF from ALS patients. *Neurology,* 58**,** 1277-9.

ALMER, G., VUKOSAVIC, S., ROMERO, N. & PRZEDBORSKI, S. 1999. Inducible nitric oxide synthase up-regulation in a transgenic mouse model of familial amyotrophic lateral sclerosis. *J Neurochem,* 72**,** 2415-25.

ALSULIMAN, A., APPEL, S. H., BEERS, D. R., BASAR, R., SHAIM, H., KAUR, I., ZULOVICH, J., YVON, E., MUFTUOGLU, M., IMAHASHI, N., KONDO, K., LIU, E., SHPALL, E. J. & REZVANI, K. 2016. A robust, good manufacturing practice-

compliant, clinical-scale procedure to generate regulatory T cells from patients with amyotrophic lateral sclerosis for adoptive cell therapy. *Cytotherapy,* 18**,** 1312-24.

ALVES, S., CHURLAUD, G., AUDRAIN, M., MICHAELSEN-PREUSSE, K., FOL, R., SOUCHET, B., BRAUDEAU, J., KORTE, M., KLATZMANN, D. & CARTIER, N. 2017. Interleukin-2 improves amyloid pathology, synaptic failure and memory in Alzheimer's disease mice. *Brain,* 140**,** 826-842.

AMAN, P., PANAGOPOULOS, I., LASSEN, C., FIORETOS, T., MENCINGER, M., TORESSON, H., HÖGLUND, M., FORSTER, A., RABBITTS, T. H., RON, D., MANDAHL, N. & MITELMAN, F. 1996. Expression patterns of the human sarcoma-associated genes FUS and EWS and the genomic structure of FUS. *Genomics,* 37**,** 1-8.

AMIN, K. 2012. The role of mast cells in allergic inflammation. *Respir Med,* 106**,** 9-14.

ANDERSEN, P. M. & AL-CHALABI, A. 2011. Clinical genetics of amyotrophic lateral sclerosis: what do we really know? *Nat Rev Neurol,* 7**,** 603-15.

ANKARCRONA, M., DYPBUKT, J. M., BONFOCO, E., ZHIVOTOVSKY, B., ORRENIUS, S., LIPTON, S. A. & NICOTERA, P. 1995. Glutamate-induced neuronal death: a succession of necrosis or apoptosis depending on mitochondrial function. *Neuron,* 15**,** 961-73.

ANNUNZIATA, P. & VOLPI, N. 1985. High levels of C3c in the cerebrospinal fluid from amyotrophic lateral sclerosis patients. *Acta Neurol Scand,* 72**,** 61-4.

APPEL, S. H., BEERS, D. R. & HENKEL, J. S. 2010. T cell-microglial dialogue in Parkinson's disease and amyotrophic lateral sclerosis: are we listening? *Trends Immunol,* 31**,** 7-17.

APPEL, V., STEWART, S. S., SMITH, G. & APPEL, S. H. 1987. A rating scale for amyotrophic lateral sclerosis: description and preliminary experience. *Ann Neurol,* 22**,** 328-33.

ARAI, T., HASEGAWA, M., AKIYAMA, H., IKEDA, K., NONAKA, T., MORI, H., MANN, D., TSUCHIYA, K., YOSHIDA, M., HASHIZUME, Y. & ODA, T. 2006. TDP-43 is a component of ubiquitin-positive tau-negative inclusions in frontotemporal lobar degeneration and amyotrophic lateral sclerosis. *Biochem Biophys Res Commun,* 351**,** 602-11.

ARNOLD, E. S., LING, S. C., HUELGA, S. C., LAGIER-TOURENNE, C., POLYMENIDOU, M., DITSWORTH, D., KORDASIEWICZ, H. B., MCALONIS-DOWNES, M., PLATOSHYN, O., PARONE, P. A., DA CRUZ, S., CLUTARIO, K. M., SWING, D., TESSAROLLO, L., MARSALA, M., SHAW, C. E., YEO, G. W. & CLEVELAND, D. W. 2013. ALS-linked TDP-43 mutations produce aberrant RNA splicing and adult-onset motor neuron disease without aggregation or loss of nuclear TDP-43. *Proc Natl Acad Sci U S A,* 110**,** E736-45.

AWATSUJI, H., FURUKAWA, Y., NAKAJIMA, M., FURUKAWA, S. & HAYASHI, K. 1993. Interleukin-2 as a neurotrophic factor for supporting the survival of neurons cultured from various regions of fetal rat brain. *J Neurosci Res,* 35**,** 305-11.

AZAM, S., JAKARIA, M., KIM, I. S., KIM, J., HAQUE, M. E. & CHOI, D. K. 2019. Regulation of Toll-Like Receptor (TLR) Signaling Pathway by Polyphenols in the Treatment of Age-Linked Neurodegenerative Diseases: Focus on TLR4 Signaling. *Front Immunol,* 10**,** 1000.

BAHIA EL IDRISSI, N., BOSCH, S., RAMAGLIA, V., ARONICA, E., BAAS, F. & TROOST, D. 2016. Complement activation at the motor end-plates in amyotrophic lateral sclerosis. *J Neuroinflammation,* 13**,** 72.

BAKKAR, N., BOEHRINGER, A. & BOWSER, R. 2015. Use of biomarkers in ALS drug development and clinical trials. *Brain Res,* 1607**,** 94-107.

BALASINGAM, V., TEJADA-BERGES, T., WRIGHT, E., BOUCKOVA, R. & YONG, V. W. 1994. Reactive astrogliosis in the neonatal mouse brain and its modulation by cytokines. *J Neurosci,* 14**,** 846-56.

BANERJEE, R., MOSLEY, R. L., REYNOLDS, A. D., DHAR, A., JACKSON-LEWIS, V., GORDON, P. H., PRZEDBORSKI, S. & GENDELMAN, H. E. 2008. Adaptive immune neuroprotection in G93A-SOD1 amyotrophic lateral sclerosis mice. *PLoS One,* 3**,** e2740.

BANKS, W. A., KASTIN, A. J. & BROADWELL, R. D. 1995. Passage of cytokines across the blood-brain barrier. *Neuroimmunomodulation,* 2**,** 241-8.

BANKS, W. A., NIEHOFF, M. L. & ZALCMAN, S. S. 2004. Permeability of the mouse blood-brain barrier to murine interleukin-2: predominance of a saturable efflux system. *Brain Behav Immun,* 18**,** 434-42.

BARBER, S. C. & SHAW, P. J. 2010. Oxidative stress in ALS: key role in motor neuron injury and therapeutic target. *Free Radic Biol Med,* 48**,** 629-41.

BARNUM, S. R. 1995. Complement biosynthesis in the central nervous system. *Crit Rev Oral Biol Med,* 6**,** 132-46.

BARON, P., BUSSINI, S., CARDIN, V., CORBO, M., CONTI, G., GALIMBERTI, D., SCARPINI, E., BRESOLIN, N., WHARTON, S. B., SHAW, P. J. & SILANI, V. 2005. Production of monocyte chemoattractant protein-1 in amyotrophic lateral sclerosis. *Muscle Nerve,* 32**,** 541-4.

BAUFELD, C., O'LOUGHLIN, E., CALCAGNO, N., MADORE, C. & BUTOVSKY, O. 2017. Differential contribution of microglia and monocytes in neurodegenerative diseases. *J Neural Transm (Vienna)*.

BEADLING, C. & SMITH, K. A. 2002. DNA array analysis of interleukin-2-regulated immediate/early genes. *Med Immunol,* 1**,** 2.

BEAL, M. F., FERRANTE, R. J., BROWNE, S. E., MATTHEWS, R. T., KOWALL, N. W. & BROWN, R. H. 1997. Increased 3-nitrotyrosine in both sporadic and familial amyotrophic lateral sclerosis. *Ann Neurol,* 42**,** 644-54.

BEERS, D. R., HENKEL, J. S., ZHAO, W., WANG, J. & APPEL, S. H. 2008. CD4+ T cells support glial neuroprotection, slow disease progression, and modify glial morphology in an animal model of inherited ALS. *Proc Natl Acad Sci U S A,* 105**,** 15558-63.

BEERS, D. R., HENKEL, J. S., ZHAO, W., WANG, J., HUANG, A., WEN, S., LIAO, B. & APPEL, S. H. 2011a. Endogenous regulatory T lymphocytes ameliorate amyotrophic lateral sclerosis in mice and correlate with disease progression in patients with amyotrophic lateral sclerosis. *Brain,* 134**,** 1293-314.

BEERS, D. R., ZHAO, W., LIAO, B., KANO, O., WANG, J., HUANG, A., APPEL, S. H. & HENKEL, J. S. 2011b. Neuroinflammation modulates distinct regional and temporal clinical responses in ALS mice. *Brain Behav Immun,* 25**,** 1025-35.

BEERS, D. R., ZHAO, W., WANG, J., ZHANG, X., WEN, S., NEAL, D., THONHOFF, J. R., ALSULIMAN, A. S., SHPALL, E. J., REZVANI, K. & APPEL, S. H. 2017. ALS patients' regulatory T lymphocytes are dysfunctional, and correlate with disease progression rate and severity. *JCI Insight,* 2**,** e89530.

BENDOTTI, C., MARINO, M., CHERONI, C., FONTANA, E., CRIPPA, V., POLETTI, A. & DE BIASI, S. 2012. Dysfunction of constitutive and inducible ubiquitin-

proteasome system in amyotrophic lateral sclerosis: implication for protein aggregation and immune response. *Prog Neurobiol,* 97**,** 101-26.
BENVENISTE, E. N., HERMAN, P. K. & WHITAKER, J. N. 1987. Myelin basic protein-specific RNA levels in interleukin-2-stimulated oligodendrocytes. *J Neurochem,* 49**,** 1274-9.
BENVENISTE, E. N. & MERRILL, J. E. 1986. Stimulation of oligodendroglial proliferation and maturation by interleukin-2. *Nature,* 321**,** 610-3.
BETTELLI, E., CARRIER, Y., GAO, W., KORN, T., STROM, T. B., OUKKA, M., WEINER, H. L. & KUCHROO, V. K. 2006. Reciprocal developmental pathways for the generation of pathogenic effector TH17 and regulatory T cells. *Nature,* 441**,** 235-8.
BETTENCOURT, C. & HOULDEN, H. 2015. Exome sequencing uncovers hidden pathways in familial and sporadic ALS. *Nat Neurosci,* 18**,** 611-3.
BEUREL, E., HARRINGTON, L. E., BUCHSER, W., LEMMON, V. & JOPE, R. S. 2014. Astrocytes modulate the polarization of CD4+ T cells to Th1 cells. *PLoS One,* 9**,** e86257.
BITTAR, P. G., CHARNAY, Y., PELLERIN, L., BOURAS, C. & MAGISTRETTI, P. J. 1996. Selective distribution of lactate dehydrogenase isoenzymes in neurons and astrocytes of human brain. *J Cereb Blood Flow Metab,* 16**,** 1079-89.
BLECHER, R., ELLIOTT, M. A., YILMAZ, E., DETTORI, J. R., OSKOUIAN, R. J., PATEL, A., CLARKE, A., HUTTON, M., MCGUIRE, R., DUNN, R., DEVINE, J., TWADDLE, B. & CHAPMAN, J. R. 2019. Contact Sports as a Risk Factor for Amyotrophic Lateral Sclerosis: A Systematic Review. *Global Spine J,* 9**,** 104-118.
BLOKHUIS, A. M., GROEN, E. J., KOPPERS, M., VAN DEN BERG, L. H. & PASTERKAMP, R. J. 2013. Protein aggregation in amyotrophic lateral sclerosis. *Acta Neuropathol,* 125**,** 777-94.
BOGDANOV, M., BROWN, R. H., MATSON, W., SMART, R., HAYDEN, D., O'DONNELL, H., FLINT BEAL, M. & CUDKOWICZ, M. 2000. Increased oxidative damage to DNA in ALS patients. *Free Radic Biol Med,* 29**,** 652-8.
BOPP, T., BECKER, C., KLEIN, M., KLEIN-HESSLING, S., PALMETSHOFER, A., SERFLING, E., HEIB, V., BECKER, M., KUBACH, J., SCHMITT, S., STOLL, S., SCHILD, H., STAEGE, M. S., STASSEN, M., JONULEIT, H. & SCHMITT, E. 2007. Cyclic adenosine monophosphate is a key component of regulatory T cell-mediated suppression. *J Exp Med,* 204**,** 1303-10.
BORTHWICK, G. M., JOHNSON, M. A., INCE, P. G., SHAW, P. J. & TURNBULL, D. M. 1999. Mitochondrial enzyme activity in amyotrophic lateral sclerosis: implications for the role of mitochondria in neuronal cell death. *Ann Neurol,* 46**,** 787-90.
BOWLING, A. C., SCHULZ, J. B., BROWN, R. H. & BEAL, M. F. 1993. Superoxide dismutase activity, oxidative damage, and mitochondrial energy metabolism in familial and sporadic amyotrophic lateral sclerosis. *J Neurochem,* 61**,** 2322-5.
BOYER, O., SAADOUN, D., ABRIOL, J., DODILLE, M., PIETTE, J. C., CACOUB, P. & KLATZMANN, D. 2004. CD4+CD25+ regulatory T-cell deficiency in patients with hepatitis C-mixed cryoglobulinemia vasculitis. *Blood,* 103**,** 3428-30.
BROWNE, S. E., YANG, L., DIMAURO, J. P., FULLER, S. W., LICATA, S. C. & BEAL, M. F. 2006. Bioenergetic abnormalities in discrete cerebral motor pathways presage spinal cord pathology in the G93A SOD1 mouse model of ALS. *Neurobiol Dis,* 22**,** 599-610.

BRUCE, P., AND ANDREW BRUCE. 2017. *Practical Statistics for Data Scientists*. O'Reilly Media.

BRUIJN, L. I., BECHER, M. W., LEE, M. K., ANDERSON, K. L., JENKINS, N. A., COPELAND, N. G., SISODIA, S. S., ROTHSTEIN, J. D., BORCHELT, D. R., PRICE, D. L. & CLEVELAND, D. W. 1997. ALS-linked SOD1 mutant G85R mediates damage to astrocytes and promotes rapidly progressive disease with SOD1-containing inclusions. *Neuron,* 18**,** 327-38.

BURATTI, E. & BARALLE, F. E. 2010. The multiple roles of TDP-43 in pre-mRNA processing and gene expression regulation. *RNA Biol,* 7**,** 420-9.

BURMEISTER, A. R., JOHNSON, M. B. & MARRIOTT, I. 2019a. Murine astrocytes are responsive to the pro-inflammatory effects of IL-20. *Neurosci Lett,* 708**,** 134334.

BURY, J. J., CHAMBERS, A., HEATH, P. R., INCE, P. G., SHAW, P. J., MATTHEWS, F. E., BRAYNE, C., SIMPSON, J. E., WHARTON, S. B. & STUDY, C. F. A. A. 2021. Type 2 diabetes mellitus-associated transcriptome alterations in cortical neurones and associated neurovascular unit cells in the ageing brain. *Acta Neuropathol Commun,* 9**,** 5.

BUTOVSKY, O., SIDDIQUI, S., GABRIELY, G., LANSER, A. J., DAKE, B., MURUGAIYAN, G., DOYKAN, C. E., WU, P. M., GALI, R. R., IYER, L. K., LAWSON, R., BERRY, J., KRICHEVSKY, A. M., CUDKOWICZ, M. E. & WEINER, H. L. 2012. Modulating inflammatory monocytes with a unique microRNA gene signature ameliorates murine ALS. *J Clin Invest,* 122**,** 3063-87.

BUTTI, Z. & PATTEN, S. A. 2018. RNA Dysregulation in Amyotrophic Lateral Sclerosis. *Front Genet,* 9**,** 712.

BYRNE, S., WALSH, C., LYNCH, C., BEDE, P., ELAMIN, M., KENNA, K., MCLAUGHLIN, R. & HARDIMAN, O. 2011. Rate of familial amyotrophic lateral sclerosis: a systematic review and meta-analysis. *J Neurol Neurosurg Psychiatry,* 82**,** 623-7.

CACCAMO, A., MAJUMDER, S., DENG, J. J., BAI, Y., THORNTON, F. B. & ODDO, S. 2009. Rapamycin rescues TDP-43 mislocalization and the associated low molecular mass neurofilament instability. *J Biol Chem,* 284**,** 27416-24.

CALVIO, C., NEUBAUER, G., MANN, M. & LAMOND, A. I. 1995. Identification of hnRNP P2 as TLS/FUS using electrospray mass spectrometry. *RNA,* 1**,** 724-33.

CAMU, W., MICKUNAS, M., VEYRUNE, J. L., PAYAN, C., GARLANDA, C., LOCATI, M., JUNTAS-MORALES, R., PAGEOT, N., MALASPINA, A., ANDREASSON, U., KIRBY, J., SUEHS, C., SAKER, S., MASSEGUIN, C., DE VOS, J., ZETTERBERG, H., SHAW, P. J., AL-CHALABI, A., LEIGH, P. N., TREE, T. & BENSIMON, G. 2020. Repeated 5-day cycles of low dose aldesleukin in amyotrophic lateral sclerosis (IMODALS): A phase 2a randomised, double-blind, placebo-controlled trial. *EBioMedicine***,** 102844.

CAO, X., CAI, S. F., FEHNIGER, T. A., SONG, J., COLLINS, L. I., PIWNICA-WORMS, D. R. & LEY, T. J. 2007. Granzyme B and perforin are important for regulatory T cell-mediated suppression of tumor clearance. *Immunity,* 27**,** 635-46.

CASSINA, P., CASSINA, A., PEHAR, M., CASTELLANOS, R., GANDELMAN, M., DE LEÓN, A., ROBINSON, K. M., MASON, R. P., BECKMAN, J. S., BARBEITO, L. & RADI, R. 2008. Mitochondrial dysfunction in SOD1G93A-bearing astrocytes promotes motor neuron degeneration: prevention by mitochondrial-targeted antioxidants. *J Neurosci,* 28**,** 4115-22.

CASSINA, P., PELUFFO, H., PEHAR, M., MARTINEZ-PALMA, L., RESSIA, A., BECKMAN, J. S., ESTÉVEZ, A. G. & BARBEITO, L. 2002. Peroxynitrite triggers a phenotypic transformation in spinal cord astrocytes that induces motor neuron apoptosis. *J Neurosci Res,* 67**,** 21-9.

CASTELA, E., LE DUFF, F., BUTORI, C., TICCHIONI, M., HOFMAN, P., BAHADORAN, P., LACOUR, J. P. & PASSERON, T. 2014. Effects of low-dose recombinant interleukin 2 to promote T-regulatory cells in alopecia areata. *JAMA Dermatol,* 150**,** 748-51.

CASULA, M., IYER, A. M., SPLIET, W. G., ANINK, J. J., STEENTJES, K., STA, M., TROOST, D. & ARONICA, E. 2011. Toll-like receptor signaling in amyotrophic lateral sclerosis spinal cord tissue. *Neuroscience,* 179**,** 233-43.

CEDARBAUM, J. M., STAMBLER, N., MALTA, E., FULLER, C., HILT, D., THURMOND, B. & NAKANISHI, A. 1999. The ALSFRS-R: a revised ALS functional rating scale that incorporates assessments of respiratory function. BDNF ALS Study Group (Phase III). *J Neurol Sci,* 169**,** 13-21.

CEDERBOM, L., HALL, H. & IVARS, F. 2000. CD4+CD25+ regulatory T cells down-regulate co-stimulatory molecules on antigen-presenting cells. *Eur J Immunol,* 30**,** 1538-43.

CESTRA, G., ROSSI, S., DI SALVIO, M. & COZZOLINO, M. 2017. Control of mRNA Translation in ALS Proteinopathy. *Front Mol Neurosci,* 10**,** 85.

CEYZÉRIAT, K., ABJEAN, L., CARRILLO-DE SAUVAGE, M. A., BEN HAIM, L. & ESCARTIN, C. 2016. The complex STATes of astrocyte reactivity: How are they controlled by the JAK-STAT3 pathway? *Neuroscience,* 330**,** 205-18.

CHEN, E. Y., TAN, C. M., KOU, Y., DUAN, Q., WANG, Z., MEIRELLES, G. V., CLARK, N. R. & MA'AYAN, A. 2013. Enrichr: interactive and collaborative HTML5 gene list enrichment analysis tool. *BMC Bioinformatics,* 14**,** 128.

CHEN, Y., XIA, K., CHEN, L. & FAN, D. 2019. Increased Interleukin-6 Levels in the Astrocyte-Derived Exosomes of Sporadic Amyotrophic Lateral Sclerosis Patients. *Front Neurosci,* 13**,** 574.

CHENG, C. W., LIN, M. J. & SHEN, C. K. 2015. Rapamycin alleviates pathogenesis of a new Drosophila model of ALS-TDP. *J Neurogenet,* 29**,** 59-68.

CHESLOW, L. & ALVAREZ, J. I. 2016. Glial-endothelial crosstalk regulates blood-brain barrier function. *Curr Opin Pharmacol,* 26**,** 39-46.

CHIU, I. M., MORIMOTO, E. T., GOODARZI, H., LIAO, J. T., O'KEEFFE, S., PHATNANI, H. P., MURATET, M., CARROLL, M. C., LEVY, S., TAVAZOIE, S., MYERS, R. M. & MANIATIS, T. 2013. A neurodegeneration-specific gene-expression signature of acutely isolated microglia from an amyotrophic lateral sclerosis mouse model. *Cell Rep,* 4**,** 385-401.

CHIÒ, A., BENZI, G., DOSSENA, M., MUTANI, R. & MORA, G. 2005. Severely increased risk of amyotrophic lateral sclerosis among Italian professional football players. *Brain,* 128**,** 472-6.

CHOI, S. J., HONG, Y. H., KIM, S. M., SHIN, J. Y., SUH, Y. J. & SUNG, J. J. 2020. High neutrophil-to-lymphocyte ratio predicts short survival duration in amyotrophic lateral sclerosis. *Sci Rep,* 10**,** 428.

CLAUS, C., RIETHER, C., SCHÜRCH, C., MATTER, M. S., HILMENYUK, T. & OCHSENBEIN, A. F. 2012. CD27 signaling increases the frequency of regulatory T cells and promotes tumor growth. *Cancer Res,* 72**,** 3664-76.

COADY, T. H. & MANLEY, J. L. 2015. ALS mutations in TLS/FUS disrupt target gene expression. *Genes Dev,* 29**,** 1696-706.

COOPER-KNOCK, J., MOLL, T., RAMESH, T., CASTELLI, L., BEER, A., ROBINS, H., FOX, I., NIEDERMOSER, I., VAN DAMME, P., MOISSE, M., ROBBERECHT, W., HARDIMAN, O., PANADES, M. P., ASSIALIOUI, A., MORA, J. S., BASAK, A. N., MORRISON, K. E., SHAW, C. E., AL-CHALABI, A., LANDERS, J. E., WYLES, M., HEATH, P. R., HIGGINBOTTOM, A., WALSH, T., KAZOKA, M., MCDERMOTT, C. J., HAUTBERGUE, G. M., KIRBY, J. & SHAW, P. J. 2019. Mutations in the Glycosyltransferase Domain of GLT8D1 Are Associated with Familial Amyotrophic Lateral Sclerosis. *Cell Rep,* 26**,** 2298-2306.e5.

COQUE, E., SALSAC, C., ESPINOSA-CARRASCO, G., VARGA, B., DEGAUQUE, N., CADOUX, M., CRABÉ, R., VIRENQUE, A., SOULARD, C., FIERLE, J. K., BRODOVITCH, A., LIBRALATO, M., VÉGH, A. G., VENTEO, S., SCAMPS, F., BOUCRAUT, J., LAPLAUD, D., HERNANDEZ, J., GERGELY, C., VINCENT, T. & RAOUL, C. 2019. Cytotoxic CD8. *Proc Natl Acad Sci U S A,* 116**,** 2312-2317.

COQUET, J. M., RIBOT, J. C., BĄBAŁA, N., MIDDENDORP, S., VAN DER HORST, G., XIAO, Y., NEVES, J. F., FONSECA-PEREIRA, D., JACOBS, H., PENNINGTON, D. J., SILVA-SANTOS, B. & BORST, J. 2013. Epithelial and dendritic cells in the thymic medulla promote CD4+Foxp3+ regulatory T cell development via the CD27-CD70 pathway. *J Exp Med,* 210**,** 715-28.

CORCIA, P., TAUBER, C., VERCOULLIE, J., ARLICOT, N., PRUNIER, C., PRALINE, J., NICOLAS, G., VENEL, Y., HOMMET, C., BAULIEU, J. L., COTTIER, J. P., ROUSSEL, C., KASSIOU, M., GUILLOTEAU, D. & RIBEIRO, M. J. 2012. Molecular imaging of microglial activation in amyotrophic lateral sclerosis. *PLoS One,* 7**,** e52941.

CORCORAN, J., SO, P. L. & MADEN, M. 2002. Absence of retinoids can induce motoneuron disease in the adult rat and a retinoid defect is present in motoneuron disease patients. *J Cell Sci,* 115**,** 4735-41.

COYNE, A. N., ZAEPFEL, B. L. & ZARNESCU, D. C. 2017. Failure to Deliver and Translate-New Insights into RNA Dysregulation in ALS. *Front Cell Neurosci,* 11**,** 243.

COZZOLINO, M. & CARRÌ, M. T. 2012. Mitochondrial dysfunction in ALS. *Prog Neurobiol,* 97**,** 54-66.

COZZOLINO, M., PESARESI, M. G., GERBINO, V., GROSSKREUTZ, J. & CARRÌ, M. T. 2012. Amyotrophic lateral sclerosis: new insights into underlying molecular mechanisms and opportunities for therapeutic intervention. *Antioxid Redox Signal,* 17**,** 1277-330.

CRISAFULLI, S. G., BRAJKOVIC, S., CIPOLAT MIS, M. S., PARENTE, V. & CORTI, S. 2018. Therapeutic Strategies Under Development Targeting Inflammatory Mechanisms in Amyotrophic Lateral Sclerosis. *Mol Neurobiol,* 55**,** 2789-2813.

CRUGNOLA, V., LAMPERTI, C., LUCCHINI, V., RONCHI, D., PEVERELLI, L., PRELLE, A., SCIACCO, M., BORDONI, A., FASSONE, E., FORTUNATO, F., CORTI, S., SILANI, V., BRESOLIN, N., DI MAURO, S., COMI, G. P. & MOGGIO, M. 2010. Mitochondrial respiratory chain dysfunction in muscle from patients with amyotrophic lateral sclerosis. *Arch Neurol,* 67**,** 849-54.

CUDKOWICZ, M. E., SHEFNER, J. M., SCHOENFELD, D. A., ZHANG, H., ANDREASSON, K. I., ROTHSTEIN, J. D. & DRACHMAN, D. B. 2006. Trial of celecoxib in amyotrophic lateral sclerosis. *Ann Neurol,* 60**,** 22-31.

DALMAN, M. R., DEETER, A., NIMISHAKAVI, G. & DUAN, Z. H. 2012. Fold change and p-value cutoffs significantly alter microarray interpretations. *BMC Bioinformatics,* 13 Suppl 2**,** S11.

DE LA ROSA, M., RUTZ, S., DORNINGER, H. & SCHEFFOLD, A. 2004. Interleukin-2 is essential for CD4+CD25+ regulatory T cell function. *Eur J Immunol,* 34**,** 2480-8.

DE VOS, K. J. & HAFEZPARAST, M. 2017. Neurobiology of axonal transport defects in motor neuron diseases: Opportunities for translational research? *Neurobiol Dis,* 105**,** 283-299.

DEITMER, J. W., THEPARAMBIL, S. M., RUMINOT, I., NOOR, S. I. & BECKER, H. M. 2019. Energy Dynamics in the Brain: Contributions of Astrocytes to Metabolism and pH Homeostasis. *Front Neurosci,* 13**,** 1301.

DELGOFFE, G. M., KOLE, T. P., ZHENG, Y., ZAREK, P. E., MATTHEWS, K. L., XIAO, B., WORLEY, P. F., KOZMA, S. C. & POWELL, J. D. 2009. The mTOR kinase differentially regulates effector and regulatory T cell lineage commitment. *Immunity,* 30**,** 832-44.

DENG, H., GAO, K. & JANKOVIC, J. 2014. The role of FUS gene variants in neurodegenerative diseases. *Nat Rev Neurol,* 10**,** 337-48.

DENG, H. X., HENTATI, A., TAINER, J. A., IQBAL, Z., CAYABYAB, A., HUNG, W. Y., GETZOFF, E. D., HU, P., HERZFELDT, B. & ROOS, R. P. 1993. Amyotrophic lateral sclerosis and structural defects in Cu,Zn superoxide dismutase. *Science,* 261**,** 1047-51.

DENG, J., YANG, M., CHEN, Y., CHEN, X., LIU, J., SUN, S., CHENG, H., LI, Y., BIGIO, E. H., MESULAM, M., XU, Q., DU, S., FUSHIMI, K., ZHU, L. & WU, J. Y. 2015. FUS Interacts with HSP60 to Promote Mitochondrial Damage. *PLoS Genet,* 11**,** e1005357.

DINKOVA-KOSTOVA, A. T. & KAZANTSEV, A. G. 2017. Activation of Nrf2 signaling as a common treatment of neurodegenerative diseases. *Neurodegener Dis Manag,* 7**,** 97-100.

DODGE, J. C., TRELEAVEN, C. M., FIDLER, J. A., TAMSETT, T. J., BAO, C., SEARLES, M., TAKSIR, T. V., MISRA, K., SIDMAN, R. L., CHENG, S. H. & SHIHABUDDIN, L. S. 2013. Metabolic signatures of amyotrophic lateral sclerosis reveal insights into disease pathogenesis. *Proc Natl Acad Sci U S A,* 110**,** 10812-7.

DODGE, J. C., TRELEAVEN, C. M., PACHECO, J., COOPER, S., BAO, C., ABRAHAM, M., CROMWELL, M., SARDI, S. P., CHUANG, W. L., SIDMAN, R. L., CHENG, S. H. & SHIHABUDDIN, L. S. 2015. Glycosphingolipids are modulators of disease pathogenesis in amyotrophic lateral sclerosis. *Proc Natl Acad Sci U S A,* 112**,** 8100-5.

DONG, Y., ROHN, W. M. & BENVENISTE, E. N. 1999. IFN-gamma regulation of the type IV class II transactivator promoter in astrocytes. *J Immunol,* 162**,** 4731-9.

DRACHMAN, D. B., FRANK, K., DYKES-HOBERG, M., TEISMANN, P., ALMER, G., PRZEDBORSKI, S. & ROTHSTEIN, J. D. 2002. Cyclooxygenase 2 inhibition protects motor neurons and prolongs survival in a transgenic mouse model of ALS. *Ann Neurol,* 52**,** 771-8.

DU, L., ZHANG, Y., CHEN, Y., ZHU, J., YANG, Y. & ZHANG, H. L. 2017. Role of Microglia in Neurological Disorders and Their Potentials as a Therapeutic Target. *Mol Neurobiol,* 54**,** 7567-7584.

DU, Y., ZHAO, W., THONHOFF, J. R., WANG, J., WEN, S. & APPEL, S. H. 2020. Increased activation ability of monocytes from ALS patients. *Exp Neurol,* 328**,** 113259.

DUFFY, S. S., KEATING, B. A., PERERA, C. J. & MOALEM-TAYLOR, G. 2018. The role of regulatory T cells in nervous system pathologies. *J Neurosci Res,* 96**,** 951-968.

DUPONT, G., DEMARET, J., VENET, F., MALERGUE, F., MALCUS, C., POITEVIN-LATER, F., MOREL, J. & MONNERET, G. 2014. Comparative dose-responses of recombinant human IL-2 and IL-7 on STAT5 phosphorylation in CD4+FOXP3- cells versus regulatory T cells: a whole blood perspective. *Cytokine,* 69**,** 146-9.

EDARAVONE WRITING GROUP 2017. Safety and efficacy of edaravone in well defined patients with amyotrophic lateral sclerosis: a randomised, double-blind, placebo-controlled trial. *Lancet Neurol,* 16**,** 505-512.

EIZENBERG, O., FABER-ELMAN, A., LOTAN, M. & SCHWARTZ, M. 1995. Interleukin-2 transcripts in human and rodent brains: possible expression by astrocytes. *J Neurochem,* 64**,** 1928-36.

ENGELHARDT, J. I. & APPEL, S. H. 1990. IgG reactivity in the spinal cord and motor cortex in amyotrophic lateral sclerosis. *Arch Neurol,* 47**,** 1210-6.

ENGELHARDT, J. I., TAJTI, J. & APPEL, S. H. 1993. Lymphocytic infiltrates in the spinal cord in amyotrophic lateral sclerosis. *Arch Neurol,* 50**,** 30-6.

ENGL, E. & ATTWELL, D. 2015. Non-signalling energy use in the brain. *J Physiol,* 593**,** 3417-29.

FADUL, M. M., HEATH, P. R., COOPER-KNOCK, J., KURZ, J. M., AL-AZZAWI, H. A., ALI, Z., SMITH, T., MATTHEWS, F. E., BRAYNE, C., WHARTON, S. B. & SIMPSON, J. E. 2020. Transcriptomic Analysis of Age-Associated Periventricular Lesions Reveals Dysregulation of the Immune Response. *Int J Mol Sci,* 21.

FALLARINO, F., GROHMANN, U., HWANG, K. W., ORABONA, C., VACCA, C., BIANCHI, R., BELLADONNA, M. L., FIORETTI, M. C., ALEGRE, M. L. & PUCCETTI, P. 2003. Modulation of tryptophan catabolism by regulatory T cells. *Nat Immunol,* 4**,** 1206-12.

FANG, T., AL KHLEIFAT, A., MEURGEY, J. H., JONES, A., LEIGH, P. N., BENSIMON, G. & AL-CHALABI, A. 2018. Stage at which riluzole treatment prolongs survival in patients with amyotrophic lateral sclerosis: a retrospective analysis of data from a dose-ranging study. *Lancet Neurol*.

FARG, M. A., SUNDARAMOORTHY, V., SULTANA, J. M., YANG, S., ATKINSON, R. A., LEVINA, V., HALLORAN, M. A., GLEESON, P. A., BLAIR, I. P., SOO, K. Y., KING, A. E. & ATKIN, J. D. 2014. C9ORF72, implicated in amytrophic lateral sclerosis and frontotemporal dementia, regulates endosomal trafficking. *Hum Mol Genet,* 23**,** 3579-95.

FERRAIUOLO, L., HEATH, P. R., HOLDEN, H., KASHER, P., KIRBY, J. & SHAW, P. J. 2007. Microarray analysis of the cellular pathways involved in the adaptation to and progression of motor neuron injury in the SOD1 G93A mouse model of familial ALS. *J Neurosci,* 27**,** 9201-19.

FERRAIUOLO, L., HIGGINBOTTOM, A., HEATH, P. R., BARBER, S., GREENALD, D., KIRBY, J. & SHAW, P. J. 2011. Dysregulation of astrocyte-motoneuron cross-talk in mutant superoxide dismutase 1-related amyotrophic lateral sclerosis. *Brain,* 134**,** 2627-41.

FERRANTE, R. J., BROWNE, S. E., SHINOBU, L. A., BOWLING, A. C., BAIK, M. J., MACGARVEY, U., KOWALL, N. W., BROWN, R. H. & BEAL, M. F. 1997. Evidence of increased oxidative damage in both sporadic and familial amyotrophic lateral sclerosis. *J Neurochem,* 69**,** 2064-74.

FIEBICH, B. L., BATISTA, C. R. A., SALIBA, S. W., YOUSIF, N. M. & DE OLIVEIRA, A. C. P. 2018. Role of Microglia TLRs in Neurodegeneration. *Front Cell Neurosci,* 12**,** 329.

FISCHER, C., MAZZONE, M., JONCKX, B. & CARMELIET, P. 2008. FLT1 and its ligands VEGFB and PlGF: drug targets for anti-angiogenic therapy? *Nat Rev Cancer,* 8**,** 942-56.

FORSBERG, K., ANDERSEN, P. M., MARKLUND, S. L. & BRÄNNSTRÖM, T. 2011. Glial nuclear aggregates of superoxide dismutase-1 are regularly present in patients with amyotrophic lateral sclerosis. *Acta Neuropathol,* 121**,** 623-34.

FRAY, A. E., INCE, P. G., BANNER, S. J., MILTON, I. D., USHER, P. A., COOKSON, M. R. & SHAW, P. J. 1998. The expression of the glial glutamate transporter protein EAAT2 in motor neuron disease: an immunohistochemical study. *Eur J Neurosci,* 10**,** 2481-9.

FRITH, K., JOLY, A. L., MA, C. S., TANGYE, S. G., LOHSE, Z., SEITZ, C., VERGE, C. F., ANDERSSON, J. & GRAY, P. 2019. The FOXP3Δ2 isoform supports Treg cell development and protects against severe IPEX syndrome. *J Allergy Clin Immunol,* 144**,** 317-320.e8.

GANESALINGAM, J., AN, J., SHAW, C. E., SHAW, G., LACOMIS, D. & BOWSER, R. 2011. Combination of neurofilament heavy chain and complement C3 as CSF biomarkers for ALS. *J Neurochem,* 117**,** 528-37.

GAO, J., WANG, L., LIU, J., XIE, F., SU, B. & WANG, X. 2017. Abnormalities of Mitochondrial Dynamics in Neurodegenerative Diseases. *Antioxidants (Basel),* 6.

GARG, G., TYLER, J. R., YANG, J. H., CUTLER, A. J., DOWNES, K., PEKALSKI, M., BELL, G. L., NUTLAND, S., PEAKMAN, M., TODD, J. A., WICKER, L. S. & TREE, T. I. 2012. Type 1 diabetes-associated IL2RA variation lowers IL-2 signaling and contributes to diminished CD4+CD25+ regulatory T cell function. *J Immunol,* 188**,** 4644-53.

GAROFALO, S., COCOZZA, G., PORZIA, A., INGHILLERI, M., RASPA, M., SCAVIZZI, F., ARONICA, E., BERNARDINI, G., PENG, L., RANSOHOFF, R. M., SANTONI, A. & LIMATOLA, C. 2020. Natural killer cells modulate motor neuron-immune cell cross talk in models of Amyotrophic Lateral Sclerosis. *Nat Commun,* 11**,** 1773.

GAUTIER, G., VERSCHUEREN, A., MONNIER, A., ATTARIAN, S., SALORT-CAMPANA, E. & POUGET, J. 2010. ALS with respiratory onset: clinical features and effects of non-invasive ventilation on the prognosis. *Amyotroph Lateral Scler,* 11**,** 379-82.

GEEVASINGA, N., MENON, P., ÖZDINLER, P. H., KIERNAN, M. C. & VUCIC, S. 2016. Pathophysiological and diagnostic implications of cortical dysfunction in ALS. *Nat Rev Neurol,* 12**,** 651-661.

GELOSO, M. C., CORVINO, V., MARCHESE, E., SERRANO, A., MICHETTI, F. & D'AMBROSI, N. 2017. The Dual Role of Microglia in ALS: Mechanisms and Therapeutic Approaches. *Front Aging Neurosci,* 9**,** 242.

GIOVANNELLI, I., BAYATTI, N., BROWN, A., WANG, D., MICKUNAS, M., CAMU, W., VEYRUNE, J. L., PAYAN, C., GARLANDA, C., LOCATI, M., JUNTAS-MORALES, R., PAGEOT, N., MALASPINA, A., ANDREASSON, U., SUEHS,

C., SAKER, S., MASSEGUIN, C., DE VOS, J., ZETTERBERG, H., AL-CHALABI, A., LEIGH, P. N., TREE, T., BENSIMON, G., HEATH, P. R., SHAW, P. J. & KIRBY, J. 2021. Amyotrophic lateral sclerosis transcriptomics reveals immunological effects of low-dose interleukin-2. *Brain Commun,* 3**,** fcab141.

GIOVANNELLI, I., HEATH, P., SHAW, P. J. & KIRBY, J. 2020. The involvement of regulatory T cells in amyotrophic lateral sclerosis and their therapeutic potential. *Amyotroph Lateral Scler Frontotemporal Degener***,** 1-10.

GONDEK, D. C., LU, L. F., QUEZADA, S. A., SAKAGUCHI, S. & NOELLE, R. J. 2005. Cutting edge: contact-mediated suppression by CD4+CD25+ regulatory cells involves a granzyme B-dependent, perforin-independent mechanism. *J Immunol,* 174**,** 1783-6.

GORDON, P. H., MOORE, D. H., MILLER, R. G., FLORENCE, J. M., VERHEIJDE, J. L., DOORISH, C., HILTON, J. F., SPITALNY, G. M., MACARTHUR, R. B., MITSUMOTO, H., NEVILLE, H. E., BOYLAN, K., MOZAFFAR, T., BELSH, J. M., RAVITS, J., BEDLACK, R. S., GRAVES, M. C., MCCLUSKEY, L. F., BAROHN, R. J., TANDAN, R. & GROUP, W. A. S. 2007. Efficacy of minocycline in patients with amyotrophic lateral sclerosis: a phase III randomised trial. *Lancet Neurol,* 6**,** 1045-53.

GRAD, L. I., ROULEAU, G. A., RAVITS, J. & CASHMAN, N. R. 2017. Clinical Spectrum of Amyotrophic Lateral Sclerosis (ALS). *Cold Spring Harb Perspect Med,* 7.

GRAVES, M. C., FIALA, M., DINGLASAN, L. A., LIU, N. Q., SAYRE, J., CHIAPPELLI, F., VAN KOOTEN, C. & VINTERS, H. V. 2004. Inflammation in amyotrophic lateral sclerosis spinal cord and brain is mediated by activated macrophages, mast cells and T cells. *Amyotroph Lateral Scler Other Motor Neuron Disord,* 5**,** 213-9.

GRINBERG-BLEYER, Y., BAEYENS, A., YOU, S., ELHAGE, R., FOURCADE, G., GREGOIRE, S., CAGNARD, N., CARPENTIER, W., TANG, Q., BLUESTONE, J., CHATENOUD, L., KLATZMANN, D., SALOMON, B. L. & PIAGGIO, E. 2010. IL-2 reverses established type 1 diabetes in NOD mice by a local effect on pancreatic regulatory T cells. *J Exp Med,* 207**,** 1871-8.

GUIDOTTI, G., SCARLATA, C., BRAMBILLA, L. & ROSSI, D. 2021. Tumor Necrosis Factor Alpha in Amyotrophic Lateral Sclerosis: Friend or Foe? *Cells,* 10.

GUSTAFSON, M. P., STAFF, N. P., BORNSCHLEGL, S., BUTLER, G. W., MAAS, M. L., KAZAMEL, M., ZUBAIR, A., GASTINEAU, D. A., WINDEBANK, A. J. & DIETZ, A. B. 2017. Comprehensive immune profiling reveals substantial immune system alterations in a subset of patients with amyotrophic lateral sclerosis. *PLoS One,* 12**,** e0182002.

HAIDET-PHILLIPS, A. M., HESTER, M. E., MIRANDA, C. J., MEYER, K., BRAUN, L., FRAKES, A., SONG, S., LIKHITE, S., MURTHA, M. J., FOUST, K. D., RAO, M., EAGLE, A., KAMMESHEIDT, A., CHRISTENSEN, A., MENDELL, J. R., BURGHES, A. H. & KASPAR, B. K. 2011. Astrocytes from familial and sporadic ALS patients are toxic to motor neurons. *Nat Biotechnol,* 29**,** 824-8.

HANISCH, U. K. & QUIRION, R. 1995. Interleukin-2 as a neuroregulatory cytokine. *Brain Res Brain Res Rev,* 21**,** 246-84.

HANISCH, U. K., SETO, D. & QUIRION, R. 1993. Modulation of hippocampal acetylcholine release: a potent central action of interleukin-2. *J Neurosci,* 13**,** 3368-74.

HARCHA, P. A., GARCÉS, P., ARREDONDO, C., FERNÁNDEZ, G., SÁEZ, J. C. & VAN ZUNDERT, B. 2021. Mast Cell and Astrocyte Hemichannels and Their

Role in Alzheimer's Disease, ALS, and Harmful Stress Conditions. *Int J Mol Sci,* 22.

HARDIMAN, O., AL-CHALABI, A., CHIO, A., CORR, E. M., LOGROSCINO, G., ROBBERECHT, W., SHAW, P. J., SIMMONS, Z. & VAN DEN BERG, L. H. 2017. Amyotrophic lateral sclerosis. *Nat Rev Dis Primers,* 3**,** 17071.

HARTEMANN, A., BENSIMON, G., PAYAN, C. A., JACQUEMINET, S., BOURRON, O., NICOLAS, N., FONFREDE, M., ROSENZWAJG, M., BERNARD, C. & KLATZMANN, D. 2013. Low-dose interleukin 2 in patients with type 1 diabetes: a phase 1/2 randomised, double-blind, placebo-controlled trial. *Lancet Diabetes Endocrinol,* 1**,** 295-305.

HARWOOD, C. A., WESTGATE, K., GUNSTONE, S., BRAGE, S., WAREHAM, N. J., MCDERMOTT, C. J. & SHAW, P. J. 2016. Long-term physical activity: an exogenous risk factor for sporadic amyotrophic lateral sclerosis? *Amyotroph Lateral Scler Frontotemporal Degener,* 17**,** 377-84.

HE, J., ZHANG, R., SHAO, M., ZHAO, X., MIAO, M., CHEN, J., LIU, J., ZHANG, X., JIN, Y., WANG, Y., ZHANG, S., ZHU, L., JACOB, A., JIA, R., YOU, X., LI, X., LI, C., ZHOU, Y., YANG, Y., YE, H., LIU, Y., SU, Y., SHEN, N., ALEXANDER, J., GUO, J., AMBRUS, J., LIN, X., YU, D., SUN, X. & LI, Z. 2020. Efficacy and safety of low-dose IL-2 in the treatment of systemic lupus erythematosus: a randomised, double-blind, placebo-controlled trial. *Ann Rheum Dis,* 79**,** 141-149.

HEATH, P. R. & SHAW, P. J. 2002. Update on the glutamatergic neurotransmitter system and the role of excitotoxicity in amyotrophic lateral sclerosis. *Muscle Nerve,* 26**,** 438-58.

HENKEL, J. S., BEERS, D. R., WEN, S., RIVERA, A. L., TOENNIS, K. M., APPEL, J. E., ZHAO, W., MOORE, D. H., POWELL, S. Z. & APPEL, S. H. 2013. Regulatory T-lymphocytes mediate amyotrophic lateral sclerosis progression and survival. *EMBO Mol Med,* 5**,** 64-79.

HENKEL, J. S., ENGELHARDT, J. I., SIKLÓS, L., SIMPSON, E. P., KIM, S. H., PAN, T., GOODMAN, J. C., SIDDIQUE, T., BEERS, D. R. & APPEL, S. H. 2004. Presence of dendritic cells, MCP-1, and activated microglia/macrophages in amyotrophic lateral sclerosis spinal cord tissue. *Ann Neurol,* 55**,** 221-35.

HENSLEY, K., ABDEL-MOATY, H., HUNTER, J., MHATRE, M., MOU, S., NGUYEN, K., POTAPOVA, T., PYE, Q. N., QI, M., RICE, H., STEWART, C., STROUKOFF, K. & WEST, M. 2006. Primary glia expressing the G93A-SOD1 mutation present a neuroinflammatory phenotype and provide a cellular system for studies of glial inflammation. *J Neuroinflammation,* 3**,** 2.

HEURICH, B., EL IDRISSI, N. B., DONEV, R. M., PETRI, S., CLAUS, P., NEAL, J., MORGAN, B. P. & RAMAGLIA, V. 2011. Complement upregulation and activation on motor neurons and neuromuscular junction in the SOD1 G93A mouse model of familial amyotrophic lateral sclerosis. *J Neuroimmunol,* 235**,** 104-9.

HIGGINS, C. M., JUNG, C. & XU, Z. 2003. ALS-associated mutant SOD1G93A causes mitochondrial vacuolation by expansion of the intermembrane space and by involvement of SOD1 aggregation and peroxisomes. *BMC Neurosci,* 4**,** 16.

HONG, S. & SONG, M. R. 2014. STAT3 but not STAT1 is required for astrocyte differentiation. *PLoS One,* 9**,** e86851.

HOOTEN, K. G., BEERS, D. R., ZHAO, W. & APPEL, S. H. 2015. Protective and Toxic Neuroinflammation in Amyotrophic Lateral Sclerosis. *Neurotherapeutics,* 12**,** 364-75.

HOVDEN, H., FREDERIKSEN, J. L. & PEDERSEN, S. W. 2013. Immune system alterations in amyotrophic lateral sclerosis. *Acta Neurol Scand,* 128**,** 287-96.

HOWLAND, D. S., LIU, J., SHE, Y., GOAD, B., MARAGAKIS, N. J., KIM, B., ERICKSON, J., KULIK, J., DEVITO, L., PSALTIS, G., DEGENNARO, L. J., CLEVELAND, D. W. & ROTHSTEIN, J. D. 2002. Focal loss of the glutamate transporter EAAT2 in a transgenic rat model of SOD1 mutant-mediated amyotrophic lateral sclerosis (ALS). *Proc Natl Acad Sci U S A,* 99**,** 1604-9.

HUANG, Z., DAUER, D. J., HA, G. K., LEWIS, M. H. & PETITTO, J. M. 2009. Interleukin-2 deficiency-induced T cell autoimmunity in the mouse brain. *Neurosci Lett,* 463**,** 44-8.

HUANG, Z., MEOLA, D. & PETITTO, J. M. 2011. Loss of CNS IL-2 gene expression modifies brain T lymphocyte trafficking: response of normal versus autoreactive Treg-deficient T cells. *Neurosci Lett,* 499**,** 213-8.

HUMRICH, J. Y. & RIEMEKASTEN, G. 2019. Low-dose interleukin-2 therapy for the treatment of systemic lupus erythematosus. *Curr Opin Rheumatol,* 31**,** 208-212.

HUNTER, K. E., SPORN, M. B. & DAVIES, A. M. 1993. Transforming growth factor-betas inhibit mitogen-stimulated proliferation of astrocytes. *Glia,* 7**,** 203-11.

INGRE, C., ROOS, P. M., PIEHL, F., KAMEL, F. & FANG, F. 2015. Risk factors for amyotrophic lateral sclerosis. *Clin Epidemiol,* 7**,** 181-93.

ISLAM, M. T. 2017. Oxidative stress and mitochondrial dysfunction-linked neurodegenerative disorders. *Neurol Res,* 39**,** 73-82.

ITALIANI, P. & BORASCHI, D. 2014. From Monocytes to M1/M2 Macrophages: Phenotypical vs. Functional Differentiation. *Front Immunol,* 5**,** 514.

ITO, M., KOMAI, K., MISE-OMATA, S., IIZUKA-KOGA, M., NOGUCHI, Y., KONDO, T., SAKAI, R., MATSUO, K., NAKAYAMA, T., YOSHIE, O., NAKATSUKASA, H., CHIKUMA, S., SHICHITA, T. & YOSHIMURA, A. 2019. Brain regulatory T cells suppress astrogliosis and potentiate neurological recovery. *Nature,* 565**,** 246-250.

ITO, S., BOLLARD, C. M., CARLSTEN, M., MELENHORST, J. J., BIANCOTTO, A., WANG, E., CHEN, J., KOTLIAROV, Y., CHEUNG, F., XIE, Z., MARINCOLA, F., TANIMOTO, K., BATTIWALLA, M., OLNES, M. J., PERL, S., SCHUM, P., HUGHES, T. E., KEYVANFAR, K., HENSEL, N., MURANSKI, P., YOUNG, N. S. & BARRETT, A. J. 2014. Ultra-low dose interleukin-2 promotes immune-modulating function of regulatory T cells and natural killer cells in healthy volunteers. *Mol Ther,* 22**,** 1388-1395.

JANG, E., KIM, J. H., LEE, S., SEO, J. W., JIN, M., LEE, M. G., JANG, I. S., LEE, W. H. & SUK, K. 2013. Phenotypic polarization of activated astrocytes: the critical role of lipocalin-2 in the classical inflammatory activation of astrocytes. *J Immunol,* 191**,** 5204-19.

JIN, M., GÜNTHER, R., AKGÜN, K., HERMANN, A. & ZIEMSSEN, T. 2020. Peripheral proinflammatory Th1/Th17 immune cell shift is linked to disease severity in amyotrophic lateral sclerosis. *Sci Rep,* 10**,** 5941.

JOHANN, S., HEITZER, M., KANAGARATNAM, M., GOSWAMI, A., RIZO, T., WEIS, J., TROOST, D. & BEYER, C. 2015. NLRP3 inflammasome is expressed by astrocytes in the SOD1 mouse model of ALS and in human sporadic ALS patients. *Glia,* 63**,** 2260-73.

JOHNSON, D. A. & JOHNSON, J. A. 2015. Nrf2--a therapeutic target for the treatment of neurodegenerative diseases. *Free Radic Biol Med,* 88**,** 253-267.
JULIAN, T. H., GLASCOW, N., BARRY, A. D. F., MOLL, T., HARVEY, C., KLIMENTIDIS, Y. C., NEWELL, M., ZHANG, S., SNYDER, M. P., COOPER-KNOCK, J. & SHAW, P. J. 2021. Physical exercise is a risk factor for amyotrophic lateral sclerosis: Convergent evidence from Mendelian randomisation, transcriptomics and risk genotypes. *EBioMedicine,* 68**,** 103397.
KALMAR, B. & GREENSMITH, L. 2017. Cellular Chaperones As Therapeutic Targets in ALS to Restore Protein Homeostasis and Improve Cellular Function. *Front Mol Neurosci,* 10**,** 251.
KAMMERL, I. E. & MEINERS, S. 2016. Proteasome function shapes innate and adaptive immune responses. *Am J Physiol Lung Cell Mol Physiol,* 311**,** L328-36.
KAUR, S. J., MCKEOWN, S. R. & RASHID, S. 2016. Mutant SOD1 mediated pathogenesis of Amyotrophic Lateral Sclerosis. *Gene,* 577**,** 109-18.
KAWAMATA, H. & MANFREDI, G. 2010. Mitochondrial dysfunction and intracellular calcium dysregulation in ALS. *Mech Ageing Dev,* 131**,** 517-26.
KAWAMATA, T., AKIYAMA, H., YAMADA, T. & MCGEER, P. L. 1992. Immunologic reactions in amyotrophic lateral sclerosis brain and spinal cord tissue. *Am J Pathol,* 140**,** 691-707.
KEMPURAJ, D., THANGAVEL, R., NATTERU, P. A., SELVAKUMAR, G. P., SAEED, D., ZAHOOR, H., ZAHEER, S., IYER, S. S. & ZAHEER, A. 2016. Neuroinflammation Induces Neurodegeneration. *J Neurol Neurosurg Spine,* 1.
KENNEDY-NASSER, A. A., KU, S., CASTILLO-CARO, P., HAZRAT, Y., WU, M. F., LIU, H., MELENHORST, J., BARRETT, A. J., ITO, S., FOSTER, A., SAVOLDO, B., YVON, E., CARRUM, G., RAMOS, C. A., KRANCE, R. A., LEUNG, K., HESLOP, H. E., BRENNER, M. K. & BOLLARD, C. M. 2014. Ultra low-dose IL-2 for GVHD prophylaxis after allogeneic hematopoietic stem cell transplantation mediates expansion of regulatory T cells without diminishing antiviral and antileukemic activity. *Clin Cancer Res,* 20**,** 2215-25.
KING, A. E., WOODHOUSE, A., KIRKCALDIE, M. T. & VICKERS, J. C. 2016. Excitotoxicity in ALS: Overstimulation, or overreaction? *Exp Neurol,* 275 Pt 1**,** 162-71.
KOLARCIK, C. L. & BOWSER, R. 2012. Retinoid signaling alterations in amyotrophic lateral sclerosis. *Am J Neurodegener Dis,* 1**,** 130-45.
KOPITAR-JERALA, N. 2017. The Role of Interferons in Inflammation and Inflammasome Activation. *Front Immunol,* 8**,** 873.
KORETH, J., KIM, H. T., JONES, K. T., LANGE, P. B., REYNOLDS, C. G., CHAMMAS, M. J., DUSENBURY, K., WHANGBO, J., NIKIFOROW, S., ALYEA, E. P., ARMAND, P., CUTLER, C. S., HO, V. T., CHEN, Y. B., AVIGAN, D., BLAZAR, B. R., ANTIN, J. H., RITZ, J. & SOIFFER, R. J. 2016. Efficacy, durability, and response predictors of low-dose interleukin-2 therapy for chronic graft-versus-host disease. *Blood,* 128**,** 130-7.
KORETH, J., MATSUOKA, K., KIM, H. T., MCDONOUGH, S. M., BINDRA, B., ALYEA, E. P., ARMAND, P., CUTLER, C., HO, V. T., TREISTER, N. S., BIENFANG, D. C., PRASAD, S., TZACHANIS, D., JOYCE, R. M., AVIGAN, D. E., ANTIN, J. H., RITZ, J. & SOIFFER, R. J. 2011. Interleukin-2 and regulatory T cells in graft-versus-host disease. *N Engl J Med,* 365**,** 2055-66.
KOVACS, M., ALAMÓN, C., MACIEL, C., VARELA, V., IBARBURU, S., TARRAGÓ, L., KING, P. H., SI, Y., KWON, Y., HERMINE, O., BARBEITO, L. & TRIAS, E.

2021. The pathogenic role of c-Kit+ mast cells in the spinal motor neuron-vascular niche in ALS. *Acta Neuropathol Commun,* 9**,** 136.
KOVANEN, P. E., YOUNG, L., AL-SHAMI, A., ROVELLA, V., PISE-MASISON, C. A., RADONOVICH, M. F., POWELL, J., FU, J., BRADY, J. N., MUNSON, P. J. & LEONARD, W. J. 2005. Global analysis of IL-2 target genes: identification of chromosomal clusters of expressed genes. *Int Immunol,* 17**,** 1009-21.
KRÄMER, A., GREEN, J., POLLARD, J. & TUGENDREICH, S. 2014. Causal analysis approaches in Ingenuity Pathway Analysis. *Bioinformatics,* 30**,** 523-30.
KRÄMER, T. J., HACK, N., BRÜHL, T. J., MENZEL, L., HUMMEL, R., GRIEMERT, E. V., KLEIN, M., THAL, S. C., BOPP, T. & SCHÄFER, M. K. E. 2019. Depletion of regulatory T cells increases T cell brain infiltration, reactive astrogliosis, and interferon-γ gene expression in acute experimental traumatic brain injury. *J Neuroinflammation,* 16**,** 163.
KUHLE, J., LINDBERG, R. L., REGENITER, A., MEHLING, M., STECK, A. J., KAPPOS, L. & CZAPLINSKI, A. 2009. Increased levels of inflammatory chemokines in amyotrophic lateral sclerosis. *Eur J Neurol,* 16**,** 771-4.
KULESHOV, M. V., JONES, M. R., ROUILLARD, A. D., FERNANDEZ, N. F., DUAN, Q., WANG, Z., KOPLEV, S., JENKINS, S. L., JAGODNIK, K. M., LACHMANN, A., MCDERMOTT, M. G., MONTEIRO, C. D., GUNDERSEN, G. W. & MA'AYAN, A. 2016. Enrichr: a comprehensive gene set enrichment analysis web server 2016 update. *Nucleic Acids Res,* 44**,** W90-7.
KUSHNER, P. D., STEPHENSON, D. T. & WRIGHT, S. 1991. Reactive astrogliosis is widespread in the subcortical white matter of amyotrophic lateral sclerosis brain. *J Neuropathol Exp Neurol,* 50**,** 263-77.
KWIATKOWSKI, T. J., BOSCO, D. A., LECLERC, A. L., TAMRAZIAN, E., VANDERBURG, C. R., RUSS, C., DAVIS, A., GILCHRIST, J., KASARSKIS, E. J., MUNSAT, T., VALDMANIS, P., ROULEAU, G. A., HOSLER, B. A., CORTELLI, P., DE JONG, P. J., YOSHINAGA, Y., HAINES, J. L., PERICAK-VANCE, M. A., YAN, J., TICOZZI, N., SIDDIQUE, T., MCKENNA-YASEK, D., SAPP, P. C., HORVITZ, H. R., LANDERS, J. E. & BROWN, R. H. 2009. Mutations in the FUS/TLS gene on chromosome 16 cause familial amyotrophic lateral sclerosis. *Science,* 323**,** 1205-8.
KWON, I., XIANG, S., KATO, M., WU, L., THEODOROPOULOS, P., WANG, T., KIM, J., YUN, J., XIE, Y. & MCKNIGHT, S. L. 2014. Poly-dipeptides encoded by the C9orf72 repeats bind nucleoli, impede RNA biogenesis, and kill cells. *Science,* 345**,** 1139-45.
LABZIN, L. I., HENEKA, M. T. & LATZ, E. 2018. Innate Immunity and Neurodegeneration. *Annu Rev Med,* 69**,** 437-449.
LACORTE, E., FERRIGNO, L., LEONCINI, E., CORBO, M., BOCCIA, S. & VANACORE, N. 2016. Physical activity, and physical activity related to sports, leisure and occupational activity as risk factors for ALS: A systematic review. *Neurosci Biobehav Rev,* 66**,** 61-79.
LANDUYT, A. E., KLOCKE, B. J., COLVIN, T. B., SCHOEB, T. R. & MAYNARD, C. L. 2019. Cutting Edge: ICOS-Deficient Regulatory T Cells Display Normal Induction of. *J Immunol,* 202**,** 1039-1044.
LAPCHAK, P. A. 1992. A role for interleukin-2 in the regulation of striatal dopaminergic function. *Neuroreport,* 3**,** 165-8.
LAPCHAK, P. A. & ARAUJO, D. M. 1993. Interleukin-2 regulates monoamine and opioid peptide release from the hypothalamus. *Neuroreport,* 4**,** 303-6.

LEE, E. B., LEE, V. M. & TROJANOWSKI, J. Q. 2011. Gains or losses: molecular mechanisms of TDP43-mediated neurodegeneration. *Nat Rev Neurosci,* 13**,** 38-50.
LEE, J. D., KUMAR, V., FUNG, J. N., RUITENBERG, M. J., NOAKES, P. G. & WOODRUFF, T. M. 2017. Pharmacological inhibition of complement C5a-C5a. *Br J Pharmacol,* 174**,** 689-699.
LEE, J. D., LEVIN, S. C., WILLIS, E. F., LI, R., WOODRUFF, T. M. & NOAKES, P. G. 2018. Complement components are upregulated and correlate with disease progression in the TDP-43. *J Neuroinflammation,* 15**,** 171.
LEHMANN, S., ESCH, E., HARTMANN, P., GOSWAMI, A., NIKOLIN, S., WEIS, J., BEYER, C. & JOHANN, S. 2018. Expression profile of pattern recognition receptors in skeletal muscle of SOD1(G93A) ALS mice and sporadic ALS patients. *Neuropathol Appl Neurobiol*.
LEONARD, W. J. & WAN, C. K. 2016. IL-21 Signaling in Immunity. *F1000Res,* 5.
LETIEMBRE, M., LIU, Y., WALTER, S., HAO, W., PFANDER, T., WREDE, A., SCHULZ-SCHAEFFER, W. & FASSBENDER, K. 2009. Screening of innate immune receptors in neurodegenerative diseases: a similar pattern. *Neurobiol Aging,* 30**,** 759-68.
LEVINE, T. P., DANIELS, R. D., GATTA, A. T., WONG, L. H. & HAYES, M. J. 2013. The product of C9orf72, a gene strongly implicated in neurodegeneration, is structurally related to DENN Rab-GEFs. *Bioinformatics, 2*9**,** 499-503.
LI, C., WEI, Q., GU, X., CHEN, Y., CHEN, X., CAO, B., OU, R. & SHANG, H. 2019. Decreased Glycogenolysis by miR-338–3p promotes regional glycogen accumulation within the spinal cord of amyotrophic lateral sclerosis mice. *Front Mol Neurosci,* 12**,** 114.
LIAO, B., ZHAO, W., BEERS, D. R., HENKEL, J. S. & APPEL, S. H. 2012. Transformation from a neuroprotective to a neurotoxic microglial phenotype in a mouse model of ALS. *Exp Neurol,* 237**,** 147-52.
LING, S. C., POLYMENIDOU, M. & CLEVELAND, D. W. 2013. Converging mechanisms in ALS and FTD: disrupted RNA and protein homeostasis. *Neuron,* 79**,** 416-38.
LIU, G., MA, H., QIU, L., LI, L., CAO, Y., MA, J. & ZHAO, Y. 2011. Phenotypic and functional switch of macrophages induced by regulatory CD4+CD25+ T cells in mice. *Immunol Cell Biol,* 89**,** 130-42.
LIU, J. & WANG, F. 2017. Role of Neuroinflammation in Amyotrophic Lateral Sclerosis: Cellular Mechanisms and Therapeutic Implications. *Front Immunol,* 8**,** 1005.
LOBSIGER, C. S., BOILLÉE, S., POZNIAK, C., KHAN, A. M., MCALONIS-DOWNES, M., LEWCOCK, J. W. & CLEVELAND, D. W. 2013. C1q induction and global complement pathway activation do not contribute to ALS toxicity in mutant SOD1 mice. *Proc Natl Acad Sci U S A,* 110**,** E4385-92.
LOGROSCINO, G., TRAYNOR, B. J., HARDIMAN, O., CHIÒ, A., MITCHELL, D., SWINGLER, R. J., MILLUL, A., BENN, E., BEGHI, E. & EURALS 2010. Incidence of amyotrophic lateral sclerosis in Europe. *J Neurol Neurosurg Psychiatry,* 81**,** 385-90.
LONGINETTI, E. & FANG, F. 2019. Epidemiology of amyotrophic lateral sclerosis: an update of recent literature. *Curr Opin Neurol,* 32**,** 771-776.
LOVE, M. I., HUBER, W. & ANDERS, S. 2014. Moderated estimation of fold change and dispersion for RNA-seq data with DESeq2. *Genome Biol,* 15**,** 550.

MA, X., REYNOLDS, S. L., BAKER, B. J., LI, X., BENVENISTE, E. N. & QIN, H. 2010. IL-17 enhancement of the IL-6 signaling cascade in astrocytes. *J Immunol,* 184**,** 4898-906.

MADILL, M., MCDONAGH, K., MA, J., VAJDA, A., MCLOUGHLIN, P., O'BRIEN, T., HARDIMAN, O. & SHEN, S. 2017. Amyotrophic lateral sclerosis patient iPSC-derived astrocytes impair autophagy via non-cell autonomous mechanisms. *Mol Brain,* 10**,** 22.

MADJI HOUNOUM, B., MAVEL, S., COQUE, E., PATIN, F., VOURC'H, P., MAROUILLAT, S., NADAL-DESBARATS, L., EMOND, P., CORCIA, P., ANDRES, C. R., RAOUL, C. & BLASCO, H. 2017. Wildtype motoneurons, ALS-Linked SOD1 mutation and glutamate profoundly modify astrocyte metabolism and lactate shuttling. *Glia,* 65**,** 592-605.

MAGG, T., MANNERT, J., ELLWART, J. W., SCHMID, I. & ALBERT, M. H. 2012. Subcellular localization of FOXP3 in human regulatory and nonregulatory T cells. *Eur J Immunol,* 42**,** 1627-38.

MAGISTRETTI, P. J. & ALLAMAN, I. 2018. Lactate in the brain: from metabolic end-product to signalling molecule. *Nat Rev Neurosci,* 19**,** 235-249.

MAHMOUD, S., GHARAGOZLOO, M., SIMARD, C. & GRIS, D. 2019. Astrocytes Maintain Glutamate Homeostasis in the CNS by Controlling the Balance between Glutamate Uptake and Release. *Cells,* 8.

MAIHÖFNER, C., PROBST-COUSIN, S., BERGMANN, M., NEUHUBER, W., NEUNDÖRFER, B. & HEUSS, D. 2003. Expression and localization of cyclooxygenase-1 and -2 in human sporadic amyotrophic lateral sclerosis. *Eur J Neurosci,* 18**,** 1527-34.

MAILER, R. K. W. 2018. Alternative Splicing of FOXP3-Virtue and Vice. *Front Immunol,* 9**,** 530.

MAJOUNIE, E., RENTON, A. E., MOK, K., DOPPER, E. G., WAITE, A., ROLLINSON, S., CHIÒ, A., RESTAGNO, G., NICOLAOU, N., SIMON-SANCHEZ, J., VAN SWIETEN, J. C., ABRAMZON, Y., JOHNSON, J. O., SENDTNER, M., PAMPHLETT, R., ORRELL, R. W., MEAD, S., SIDLE, K. C., HOULDEN, H., ROHRER, J. D., MORRISON, K. E., PALL, H., TALBOT, K., ANSORGE, O., HERNANDEZ, D. G., AREPALLI, S., SABATELLI, M., MORA, G., CORBO, M., GIANNINI, F., CALVO, A., ENGLUND, E., BORGHERO, G., FLORIS, G. L., REMES, A. M., LAAKSOVIRTA, H., MCCLUSKEY, L., TROJANOWSKI, J. Q., VAN DEERLIN, V. M., SCHELLENBERG, G. D., NALLS, M. A., DRORY, V. E., LU, C. S., YEH, T. H., ISHIURA, H., TAKAHASHI, Y., TSUJI, S., LE BER, I., BRICE, A., DREPPER, C., WILLIAMS, N., KIRBY, J., SHAW, P., HARDY, J., TIENARI, P. J., HEUTINK, P., MORRIS, H. R., PICKERING-BROWN, S., TRAYNOR, B. J., CONSORTIUM, C.-A. F., FTLD/FTLD/ALS, F. R. N. O. & CONSORTIUM, I. 2012. Frequency of the C9orf72 hexanucleotide repeat expansion in patients with amyotrophic lateral sclerosis and frontotemporal dementia: a cross-sectional study. *Lancet Neurol,* 11**,** 323-30.

MALE M., B. J., ROTH D. B., ROITT I. 2006. *Immunology*, Elsevier.

MALEK, T. R. 2008. The biology of interleukin-2. *Annu Rev Immunol,* 26**,** 453-79.

MALEK, T. R. & CASTRO, I. 2010. Interleukin-2 receptor signaling: at the interface between tolerance and immunity. *Immunity,* 33**,** 153-65.

MALIK, R. & WIEDAU, M. 2020. Therapeutic Approaches Targeting Protein Aggregation in Amyotrophic Lateral Sclerosis. *Front Mol Neurosci,* 13**,** 98.

MANDRIOLI, J., D'AMICO, R., ZUCCHI, E., GESSANI, A., FINI, N., FASANO, A., CAPONNETTO, C., CHIÒ, A., DALLA BELLA, E., LUNETTA, C., MAZZINI, L.,

MARINOU, K., SORARÙ, G., DE BIASI, S., LO TARTARO, D., PINTI, M., COSSARIZZA, A. & GROUP, R.-A. I. 2018. Rapamycin treatment for amyotrophic lateral sclerosis: Protocol for a phase II randomized, double-blind, placebo-controlled, multicenter, clinical trial (RAP-ALS trial). *Medicine (Baltimore),* 97**,** e11119.

MANTOVANI, S., GARBELLI, S., PASINI, A., ALIMONTI, D., PEROTTI, C., MELAZZINI, M., BENDOTTI, C. & MORA, G. 2009. Immune system alterations in sporadic amyotrophic lateral sclerosis patients suggest an ongoing neuroinflammatory process. *J Neuroimmunol,* 210**,** 73-9.

MANTOVANI, S., GORDON, R., MACMAW, J. K., PFLUGER, C. M., HENDERSON, R. D., NOAKES, P. G., MCCOMBE, P. A. & WOODRUFF, T. M. 2014. Elevation of the terminal complement activation products C5a and C5b-9 in ALS patient blood. *J Neuroimmunol,* 276**,** 213-8.

MARIN, B., BOUMÉDIENE, F., LOGROSCINO, G., COURATIER, P., BABRON, M. C., LEUTENEGGER, A. L., COPETTI, M., PREUX, P. M. & BEGHI, E. 2017. Variation in worldwide incidence of amyotrophic lateral sclerosis: a meta-analysis. *Int J Epidemiol,* 46**,** 57-74.

MARONGIU, L., GORNATI, L., ARTUSO, I., ZANONI, I. & GRANUCCI, F. 2019. Below the surface: The inner lives of TLR4 and TLR9. *J Leukoc Biol,* 106**,** 147-160.

MATSUOKA, K., KORETH, J., KIM, H. T., BASCUG, G., MCDONOUGH, S., KAWANO, Y., MURASE, K., CUTLER, C., HO, V. T., ALYEA, E. P., ARMAND, P., BLAZAR, B. R., ANTIN, J. H., SOIFFER, R. J. & RITZ, J. 2013. Low-dose interleukin-2 therapy restores regulatory T cell homeostasis in patients with chronic graft-versus-host disease. *Sci Transl Med,* 5**,** 179ra43.

MATTIAZZI, M., D'AURELIO, M., GAJEWSKI, C. D., MARTUSHOVA, K., KIAEI, M., BEAL, M. F. & MANFREDI, G. 2002. Mutated human SOD1 causes dysfunction of oxidative phosphorylation in mitochondria of transgenic mice. *J Biol Chem,* 277**,** 29626-33.

MATUS, S., VALENZUELA, V., MEDINAS, D. B. & HETZ, C. 2013. ER Dysfunction and Protein Folding Stress in ALS. *Int J Cell Biol,* 2013**,** 674751.

MCALPINE, W., SUN, L., WANG, K. W., LIU, A., JAIN, R., SAN MIGUEL, M., WANG, J., ZHANG, Z., HAYSE, B., MCALPINE, S. G., CHOI, J. H., ZHONG, X., LUDWIG, S., RUSSELL, J., ZHAN, X., CHOI, M., LI, X., TANG, M., MORESCO, E. M. Y., BEUTLER, B. & TURER, E. 2018. Excessive endosomal TLR signaling causes inflammatory disease in mice with defective SMCR8-WDR41-C9ORF72 complex function. *Proc Natl Acad Sci U S A,* 115**,** E11523-E11531.

MCCOMBE, P. A., LEE, J. D., WOODRUFF, T. M. & HENDERSON, R. D. 2020. The Peripheral Immune System and Amyotrophic Lateral Sclerosis. *Front Neurol,* 11**,** 279.

MCGILL, R. B. 2020. Monocytes and neutrophils are associated with clinical features in amyotrophic lateral sclerosis. *In:* FREDERIK J STEYN, S. T. N., KATHRYN A THORPE, SUSAN HEGGIE, MARC J RUITENBERG, ROBERT D HENDERSON, PAMELA A MCCOMBE, TRENT M WOODRUFF (ed.). B*rain Communications*.

MCGILL, R. B., STEYN, F. J., NGO, S. T., THORPE, K. A., HEGGIE, S., RUITENBERG, M. J., HENDERSON, R. D., MCCOMBE, P. A. & WOODRUFF, T. M. 2020. Monocytes and neutrophils are associated with clinical features in amyotrophic lateral sclerosis. *Brain Commun,* 2**,** fcaa013.

MCHUGH, R. S., WHITTERS, M. J., PICCIRILLO, C. A., YOUNG, D. A., SHEVACH, E. M., COLLINS, M. & BYRNE, M. C. 2002. CD4(+)CD25(+) immunoregulatory T cells: gene expression analysis reveals a functional role for the glucocorticoid-induced TNF receptor. *Immunity,* 16**,** 311-23.

MEAD, R. J., HIGGINBOTTOM, A., ALLEN, S. P., KIRBY, J., BENNETT, E., BARBER, S. C., HEATH, P. R., COLUCCIA, A., PATEL, N., GARDNER, I., BRANCALE, A., GRIERSON, A. J. & SHAW, P. J. 2013. S[+] Apomorphine is a CNS penetrating activator of the Nrf2-ARE pathway with activity in mouse and patient fibroblast models of amyotrophic lateral sclerosis. *Free Radic Biol Med,* 61**,** 438-52.

MEDINAS, D. B., VALENZUELA, V. & HETZ, C. 2017. Proteostasis disturbance in amyotrophic lateral sclerosis. *Hum Mol Genet,* 26**,** R91-R104.

MEJZINI, R., FLYNN, L. L., PITOUT, I. L., FLETCHER, S., WILTON, S. D. & AKKARI, P. A. 2019. ALS Genetics, Mechanisms, and Therapeutics: Where Are We Now? *Front Neurosci,* 13**,** 1310.

MELLOR, A. L. & MUNN, D. H. 2004. IDO expression by dendritic cells: tolerance and tryptophan catabolism. *Nat Rev Immunol,* 4**,** 762-74.

MEOLA, D., HUANG, Z. & PETITTO, J. M. 2013. Selective Neuronal and Brain Regional Expession of IL-2 in IL2P 8-GFP Transgenic Mice: Relation to Sensorimotor Gating. *J Alzheimers Dis Parkinsonism,* 3**,** 1000127.

MEYER, K., FERRAIUOLO, L., MIRANDA, C. J., LIKHITE, S., MCELROY, S., RENUSCH, S., DITSWORTH, D., LAGIER-TOURENNE, C., SMITH, R. A., RAVITS, J., BURGHES, A. H., SHAW, P. J., CLEVELAND, D. W., KOLB, S. J. & KASPAR, B. K. 2014. Direct conversion of patient fibroblasts demonstrates non-cell autonomous toxicity of astrocytes to motor neurons in familial and sporadic ALS. *Proc Natl Acad Sci U S A,* 111**,** 829-32.

MICHELL-ROBINSON, M. A., TOUIL, H., HEALY, L. M., OWEN, D. R., DURAFOURT, B. A., BAR-OR, A., ANTEL, J. P. & MOORE, C. S. 2015. Roles of microglia in brain development, tissue maintenance and repair. *Brain,* 138**,** 1138-59.

MILLS, K. H. 2004. Regulatory T cells: friend or foe in immunity to infection? *Nat Rev Immunol,* 4**,** 841-55.

MIRON, V. E., BOYD, A., ZHAO, J. W., YUEN, T. J., RUCKH, J. M., SHADRACH, J. L., VAN WIJNGAARDEN, P., WAGERS, A. J., WILLIAMS, A., FRANKLIN, R. J. M. & FFRENCH-CONSTANT, C. 2013. M2 microglia and macrophages drive oligodendrocyte differentiation during CNS remyelination. *Nat Neurosci,* 16**,** 1211-1218.

MISHRA, P. S., DHULL, D. K., NALINI, A., VIJAYALAKSHMI, K., SATHYAPRABHA, T. N., ALLADI, P. A. & RAJU, T. R. 2016. Astroglia acquires a toxic neuroinflammatory role in response to the cerebrospinal fluid from amyotrophic lateral sclerosis patients. *J Neuroinflammation,* 13**,** 212.

MITCHELL, R. M., FREEMAN, W. M., RANDAZZO, W. T., STEPHENS, H. E., BEARD, J. L., SIMMONS, Z. & CONNOR, J. R. 2009. A CSF biomarker panel for identification of patients with amyotrophic lateral sclerosis. *Neurology,* 72**,** 14-9.

MOLL, T., SHAW, P. J. & COOPER-KNOCK, J. 2020. Disrupted glycosylation of lipids and proteins is a cause of neurodegeneration. *Brain,* 143**,** 1332-1340.

MONTECINO-RODRIGUEZ, E., BERENT-MAOZ, B. & DORSHKIND, K. 2013. Causes, consequences, and reversal of immune system aging. *J Clin Invest,* 123**,** 958-65.

MORA, J. S., BRADLEY, W. G., CHAVERRI, D., HERNÁNDEZ-BARRAL, M., MASCIAS, J., GAMEZ, J., GARGIULO-MONACHELLI, G. M., MOUSSY, A., MANSFIELD, C. D., HERMINE, O. & LUDOLPH, A. C. 2021. Long-term survival analysis of masitinib in amyotrophic lateral sclerosis. *Ther Adv Neurol Disord,* 14**,** 17562864211030365.

MORENO-GARCÍA, L., MIANA-MENA, F. J., MORENO-MARTÍNEZ, L., DE LA TORRE, M., LUNETTA, C., TARLARINI, C., ZARAGOZA, P., CALVO, A. C. & OSTA, R. 2021. Inflammasome in ALS Skeletal Muscle:. *Int J Mol Sci,* 22.

MORGAN, B. P. 2015. The role of complement in neurological and neuropsychiatric diseases. *Expert Rev Clin Immunol,* 11**,** 1109-19.

MORI, K., LAMMICH, S., MACKENZIE, I. R., FORNÉ, I., ZILOW, S., KRETZSCHMAR, H., EDBAUER, D., JANSSENS, J., KLEINBERGER, G., CRUTS, M., HERMS, J., NEUMANN, M., VAN BROECKHOVEN, C., ARZBERGER, T. & HAASS, C. 2013. hnRNP A3 binds to GGGGCC repeats and is a constituent of p62-positive/TDP43-negative inclusions in the hippocampus of patients with C9orf72 mutations. *Acta Neuropathol,* 125**,** 413-23.

MORONI, S. C. & ROSSI, A. 1995. Enhanced survival and differentiation in vitro of different neuronal populations by some interleukins. *Int J Dev Neurosci,* 13**,** 41-9.

MOUJALLED, D., GRUBMAN, A., ACEVEDO, K., YANG, S., KE, Y. D., MOUJALLED, D. M., DUNCAN, C., CARAGOUNIS, A., PERERA, N. D., TURNER, B. J., PRUDENCIO, M., PETRUCELLI, L., BLAIR, I., ITTNER, L. M., CROUCH, P. J., LIDDELL, J. R. & WHITE, A. R. 2017. TDP-43 mutations causing amyotrophic lateral sclerosis are associated with altered expression of RNA-binding protein hnRNP K and affect the Nrf2 antioxidant pathway. *Hum Mol Genet,* 26**,** 1732-1746.

MUKAI, K., TSAI, M., STARKL, P., MARICHAL, T. & GALLI, S. J. 2016. IgE and mast cells in host defense against parasites and venoms. *Semin Immunopathol,* 38**,** 581-603.

MURDOCK, B. J., BENDER, D. E., KASHLAN, S. R., FIGUEROA-ROMERO, C., BACKUS, C., CALLAGHAN, B. C., GOUTMAN, S. A. & FELDMAN, E. L. 2016. Increased ratio of circulating neutrophils to monocytes in amyotrophic lateral sclerosis. *Neurol Neuroimmunol Neuroinflamm,* 3**,** e242.

MURDOCK, B. J., FAMIE, J. P., PIECUCH, C. E., RAUE, K. D., MENDELSON, F. E., PIERONI, C. H., INIGUEZ, S. D., ZHAO, L., GOUTMAN, S. A. & FELDMAN, E. L. 2021a. NK cells associate with ALS in a sex- and age-dependent manner. *JCI Insight,* 6.

MURDOCK, B. J., GOUTMAN, S. A., BOSS, J., KIM, S. & FELDMAN, E. L. 2021b. Amyotrophic Lateral Sclerosis Survival Associates With Neutrophils in a Sex-specific Manner. *Neurol Neuroimmunol Neuroinflamm,* 8.

MURDOCK, B. J., ZHOU, T., KASHLAN, S. R., LITTLE, R. J., GOUTMAN, S. A. & FELDMAN, E. L. 2017. Correlation of Peripheral Immunity With Rapid Amyotrophic Lateral Sclerosis Progression. *JAMA Neurol,* 74**,** 1446-1454.

NAGAI, M., RE, D. B., NAGATA, T., CHALAZONITIS, A., JESSELL, T. M., WICHTERLE, H. & PRZEDBORSKI, S. 2007. Astrocytes expressing ALS-linked mutated SOD1 release factors selectively toxic to motor neurons. *Nat Neurosci,* 10**,** 615-22.

NAGOSHI, N., NAKASHIMA, H. & FEHLINGS, M. G. 2015. Riluzole as a neuroprotective drug for spinal cord injury: from bench to bedside. *Molecules,* 20**,** 7775-89.
NAGY, D., KATO, T. & KUSHNER, P. D. 1994. Reactive astrocytes are widespread in the cortical gray matter of amyotrophic lateral sclerosis. *J Neurosci Res,* 38**,** 336-47.
NARDO, G., TROLESE, M. C., VERDERIO, M., MARIANI, A., DE PAOLA, M., RIVA, N., DINA, G., PANINI, N., ERBA, E., QUATTRINI, A. & BENDOTTI, C. 2018. Counteracting roles of MHCI and CD8. *Mol Neurodegener,* 13**,** 42.
NEUMANN, M., KWONG, L. K., TRUAX, A. C., VANMASSENHOVE, B., KRETZSCHMAR, H. A., VAN DEERLIN, V. M., CLARK, C. M., GROSSMAN, M., MILLER, B. L., TROJANOWSKI, J. Q. & LEE, V. M. 2007. TDP-43-positive white matter pathology in frontotemporal lobar degeneration with ubiquitin-positive inclusions. *J Neuropathol Exp Neurol,* 66**,** 177-83.
NIEBRÓJ-DOBOSZ, I., DZIEWULSKA, D. & KWIECIŃSKI, H. 2004. Oxidative damage to proteins in the spinal cord in amyotrophic lateral sclerosis (ALS). *Folia Neuropathol,* 42**,** 151-6.
NIJSSEN, J., COMLEY, L. H. & HEDLUND, E. 2017. Motor neuron vulnerability and resistance in amyotrophic lateral sclerosis. *Acta Neuropathol,* 133**,** 863-885.
NIMMERJAHN, A., KIRCHHOFF, F. & HELMCHEN, F. 2005. Resting microglial cells are highly dynamic surveillants of brain parenchyma in vivo. *Science,* 308**,** 1314-8.
NORDEN, D. M., FENN, A. M., DUGAN, A. & GODBOUT, J. P. 2014. TGFβ produced by IL-10 redirected astrocytes attenuates microglial activation. *Glia,* 62**,** 881-95.
NYGAARD, V., RØDLAND, E. A. & HOVIG, E. 2016. Methods that remove batch effects while retaining group differences may lead to exaggerated confidence in downstream analyses. *Biostatistics,* 17**,** 29-39.
OHL, K. & TENBROCK, K. 2015. Regulatory T cells in systemic lupus erythematosus. *Eur J Immunol,* 45**,** 344-55.
PACHECO, R., GALLART, T., LLUIS, C. & FRANCO, R. 2007. Role of glutamate on T-cell mediated immunity. *J Neuroimmunol,* 185**,** 9-19.
PADUANO, F., GAUDIO, E., MENSAH, A. A., PINTON, S., BERTONI, F. & TRAPASSO, F. 2018. T-Cell Leukemia/Lymphoma 1 (TCL1): An Oncogene Regulating Multiple Signaling Pathways. *Front Oncol,* 8**,** 317.
PAEZ-COLASANTE, X., FIGUEROA-ROMERO, C., SAKOWSKI, S. A., GOUTMAN, S. A. & FELDMAN, E. L. 2015. Amyotrophic lateral sclerosis: mechanisms and therapeutics in the epigenomic era. *Nat Rev Neurol,* 11**,** 266-79.
PANDIYAN, P., ZHENG, L., ISHIHARA, S., REED, J. & LENARDO, M. J. 2007. CD4+CD25+Foxp3+ regulatory T cells induce cytokine deprivation-mediated apoptosis of effector CD4+ T cells. *Nat Immunol,* 8**,** 1353-62.
PANSARASA, O., BORDONI, M., DIAMANTI, L., SPROVIERO, D., GAGLIARDI, S. & CEREDA, C. 2018. SOD1 in Amyotrophic Lateral Sclerosis: "Ambivalent" Behavior Connected to the Disease. *Int J Mol Sci,* 19.
PARDO, A. C., WONG, V., BENSON, L. M., DYKES, M., TANAKA, K., ROTHSTEIN, J. D. & MARAGAKIS, N. J. 2006. Loss of the astrocyte glutamate transporter GLT1 modifies disease in SOD1(G93A) mice. *Exp Neurol,* 201**,** 120-30.
PARDO, L., VALOR, L. M., ERASO-PICHOT, A., BARCO, A., GOLBANO, A., HARDINGHAM, G. E., MASGRAU, R. & GALEA, E. 2017. CREB Regulates

Distinct Adaptive Transcriptional Programs in Astrocytes and Neurons. *Sci Rep,* 7**,** 6390.
PARK, B. S. & MORI, M. 2010. Balancing false discovery and false negative rates in selection of differentially expressed genes in microarrays. *Open Access Bioinformatics,* 2010**,** 1-9.
PEHAR, M., HARLAN, B. A., KILLOY, K. M. & VARGAS, M. R. 2017. Role and Therapeutic Potential of Astrocytes in Amyotrophic Lateral Sclerosis. *Curr Pharm Des,* 23**,** 5010-5021.
PERERA, N. D. & TURNER, B. J. 2016. AMPK Signalling and Defective Energy Metabolism in Amyotrophic Lateral Sclerosis. *Neurochem Res,* 41**,** 544-53.
PERRIOT, S., MATHIAS, A., PERRIARD, G., CANALES, M., JONKMANS, N., MERIENNE, N., MEUNIER, C., EL KASSAR, L., PERRIER, A. L., LAPLAUD, D. A., SCHLUEP, M., DÉGLON, N. & DU PASQUIER, R. 2018. Human Induced Pluripotent Stem Cell-Derived Astrocytes Are Differentially Activated by Multiple Sclerosis-Associated Cytokines. *Stem Cell Reports,* 11**,** 1199-1210.
PESIRIDIS, G. S., LEE, V. M. & TROJANOWSKI, J. Q. 2009. Mutations in TDP-43 link glycine-rich domain functions to amyotrophic lateral sclerosis. *Hum Mol Genet,* 18**,** R156-62.
PETITTO, J. M., HUANG, Z., RAIZADA, M. K., RINKER, C. M. & MCCARTHY, D. B. 1998. Molecular cloning of the cDNA coding sequence of IL-2 receptor-gamma (gammac) from human and murine forebrain: expression in the hippocampus in situ and by brain cells in vitro. *Brain Res Mol Brain Res,* 53**,** 152-62.
PETITTO, J. M., MCNAMARA, R. K., GENDREAU, P. L., HUANG, Z. & JACKSON, A. J. 1999. Impaired learning and memory and altered hippocampal neurodevelopment resulting from interleukin-2 gene deletion. *J Neurosci Res,* 56**,** 441-6.
PETITTO, J. M., MEOLA, D. & HUANG, Z. 2012. Interleukin-2 and the brain: dissecting central versus peripheral contributions using unique mouse models. *Methods Mol Biol,* 934**,** 301-11.
POLI, A., MICHEL, T., THÉRÉSINE, M., ANDRÈS, E., HENTGES, F. & ZIMMER, J. 2009. CD56bright natural killer (NK) cells: an important NK cell subset. *Immunology,* 126**,** 458-65.
POMPL, P. N., HO, L., BIANCHI, M., MCMANUS, T., QIN, W. & PASINETTI, G. M. 2003. A therapeutic role for cyclooxygenase-2 inhibitors in a transgenic mouse model of amyotrophic lateral sclerosis. *FASEB J,* 17**,** 725-7.
QIU, H., LEE, S., SHANG, Y., WANG, W. Y., AU, K. F., KAMIYA, S., BARMADA, S. J., FINKBEINER, S., LUI, H., CARLTON, C. E., TANG, A. A., OLDHAM, M. C., WANG, H., SHORTER, J., FILIANO, A. J., ROBERSON, E. D., TOURTELLOTTE, W. G., CHEN, B., TSAI, L. H. & HUANG, E. J. 2014. ALS-associated mutation FUS-R521C causes DNA damage and RNA splicing defects. *J Clin Invest,* 124**,** 981-99.
RABBITTS, T. H., FORSTER, A., LARSON, R. & NATHAN, P. 1993. Fusion of the dominant negative transcription regulator CHOP with a novel gene FUS by translocation t(12;16) in malignant liposarcoma. *Nat Genet,* 4**,** 175-80.
RAMESH, N. & PANDEY, U. B. 2017. Autophagy Dysregulation in ALS: When Protein Aggregates Get Out of Hand. *Front Mol Neurosci,* 10**,** 263.
RANGANATHAN, R., HAQUE, S., COLEY, K., SHEPHEARD, S., COOPER-KNOCK, J. & KIRBY, J. 2020. Multifaceted Genes in Amyotrophic Lateral Sclerosis-Frontotemporal Dementia. *Front Neurosci,* 14**,** 684.

RANSOHOFF, R. M. 2016. A polarizing question: do M1 and M2 microglia exist? *Nat Neurosci,* 19**,** 987-91.

RATCLIFFE, L. E., VÁZQUEZ VILLASEÑOR, I., JENNINGS, L., HEATH, P. R., MORTIBOYS, H., SCHWARTZENTRUBER, A., KARYKA, E., SIMPSON, J. E., INCE, P. G., GARWOOD, C. J. & WHARTON, S. B. 2018. Loss of IGF1R in Human Astrocytes Alters Complex I Activity and Support for Neurons. *Neuroscience,* 390**,** 46-59.

RATTI, A. & BURATTI, E. 2016. Physiological functions and pathobiology of TDP-43 and FUS/TLS proteins. *J Neurochem,* 138 Suppl 1**,** 95-111.

REAUME, A. G., ELLIOTT, J. L., HOFFMAN, E. K., KOWALL, N. W., FERRANTE, R. J., SIWEK, D. F., WILCOX, H. M., FLOOD, D. G., BEAL, M. F., BROWN, R. H., SCOTT, R. W. & SNIDER, W. D. 1996. Motor neurons in Cu/Zn superoxide dismutase-deficient mice develop normally but exhibit enhanced cell death after axonal injury. *Nat Genet,* 13**,** 43-7.

RENTZOS, M., EVANGELOPOULOS, E., SERETI, E., ZOUVELOU, V., MARMARA, S., ALEXAKIS, T. & EVDOKIMIDIS, I. 2012. Alterations of T cell subsets in ALS: a systemic immune activation? *Acta Neurol Scand,* 125**,** 260-4.

RENTZOS, M., ROMBOS, A., NIKOLAOU, C., ZOGA, M., ZOUVELOU, V., DIMITRAKOPOULOS, A., ALEXAKIS, T., TSOUTSOU, A., SAMAKOVLI, A., MICHALOPOULOU, M. & EVDOKIMIDIS, J. 2010. Interleukin-17 and interleukin-23 are elevated in serum and cerebrospinal fluid of patients with ALS: a reflection of Th17 cells activation? *Acta Neurol Scand,* 122**,** 425-9.

RIANCHO, J., BERCIANO, M. T., RUIZ-SOTO, M., BERCIANO, J., LANDRETH, G. & LAFARGA, M. 2016. Retinoids and motor neuron disease: Potential role in amyotrophic lateral sclerosis. *J Neurol Sci,* 360**,** 115-20.

RIANCHO, J., RUIZ-SOTO, M., BERCIANO, M. T., BERCIANO, J. & LAFARGA, M. 2015. Neuroprotective Effect of Bexarotene in the SOD1(G93A) Mouse Model of Amyotrophic Lateral Sclerosis. *Front Cell Neurosci,* 9**,** 250.

RITCHIE, M. E., PHIPSON, B., WU, D., HU, Y., LAW, C. W., SHI, W. & SMYTH, G. K. 2015. limma powers differential expression analyses for RNA-sequencing and microarray studies. *Nucleic Acids Res,* 43**,** e47.

ROBBERECHT, W. & PHILIPS, T. 2013. The changing scene of amyotrophic lateral sclerosis. *Nat Rev Neurosci,* 14**,** 248-64.

ROBERTSON, J., BEAULIEU, J. M., DOROUDCHI, M. M., DURHAM, H. D., JULIEN, J. P. & MUSHYNSKI, W. E. 2001. Apoptotic death of neurons exhibiting peripherin aggregates is mediated by the proinflammatory cytokine tumor necrosis factor-alpha. *J Cell Biol,* 155**,** 217-26.

RODRÍGUEZ, G. E., GONZÁLEZ, D. M., MONACHELLI, G. M., COSTA, J. J., NICOLA, A. F. & SICA, R. E. 2012. Morphological abnormalities in mitochondria of the skin of patients with sporadic amyotrophic lateral sclerosis. *Arq Neuropsiquiatr,* 70**,** 40-4.

ROLFES, L., SCHULTE-MECKLENBECK, A., SCHREIBER, S., VIELHABER, S., HERTY, M., MARTEN, A., PFEUFFER, S., RUCK, T., WIENDL, H., GROSS, C. C., MEUTH, S. G., BOENTERT, M. & PAWLITZKI, M. 2021. Amyotrophic lateral sclerosis patients show increased peripheral and intrathecal T-cell activation. *Brain Commun,* 3**,** fcab157.

RONCHETTI, S., RICCI, E., PETRILLO, M. G., CARI, L., MIGLIORATI, G., NOCENTINI, G. & RICCARDI, C. 2015. Glucocorticoid-induced tumour necrosis factor receptor-related protein: a key marker of functional regulatory T cells. *J Immunol Res,* 2015**,** 171520.

ROSALES, C. 2018. Neutrophil: A Cell with Many Roles in Inflammation or Several Cell Types? *Front Physiol,* 9**,** 113.

ROSEN, D. R., SIDDIQUE, T., PATTERSON, D., FIGLEWICZ, D. A., SAPP, P., HENTATI, A., DONALDSON, D., GOTO, J., O'REGAN, J. P. & DENG, H. X. 1993. Mutations in Cu/Zn superoxide dismutase gene are associated with familial amyotrophic lateral sclerosis. *Nature,* 362**,** 59-62.

ROSENZWAJG, M., CHURLAUD, G., MALLONE, R., SIX, A., DÉRIAN, N., CHAARA, W., LORENZON, R., LONG, S. A., BUCKNER, J. H., AFONSO, G., PHAM, H. P., HARTEMANN, A., YU, A., PUGLIESE, A., MALEK, T. R. & KLATZMANN, D. 2015. Low-dose interleukin-2 fosters a dose-dependent regulatory T cell tuned milieu in T1D patients. *J Autoimmun,* 58**,** 48-58.

ROSENZWAJG, M., LORENZON, R., CACOUB, P., PHAM, H. P., PITOISET, F., EL SOUFI, K., RIBET, C., BERNARD, C., ARACTINGI, S., BANNEVILLE, B., BEAUGERIE, L., BERENBAUM, F., CHAMPEY, J., CHAZOUILLERES, O., CORPECHOT, C., FAUTREL, B., MEKINIAN, A., REGNIER, E., SAADOUN, D., SALEM, J. E., SELLAM, J., SEKSIK, P., DAGUENEL-NGUYEN, A., DOPPLER, V., MARIAU, J., VICAUT, E. & KLATZMANN, D. 2018. Immunological and clinical effects of low-dose interleukin-2 across 11 autoimmune diseases in a single, open clinical trial. *Ann Rheum Dis*.

ROSENZWAJG, M., SALET, R., LORENZON, R., TCHITCHEK, N., ROUX, A., BERNARD, C., CAREL, J. C., STOREY, C., POLAK, M., BELTRAND, J., AMOUYAL, C., HARTEMANN, A., CORBEAU, P., VICAUT, E., BIBAL, C., BOUGNÈRES, P., TRAN, T. A. & KLATZMANN, D. 2020. Low-dose IL-2 in children with recently diagnosed type 1 diabetes: a Phase I/II randomised, double-blind, placebo-controlled, dose-finding study. *Diabetologia,* 63**,** 1808-1821.

ROTHSTEIN, J. D., MARTIN, L. J. & KUNCL, R. W. 1992. Decreased glutamate transport by the brain and spinal cord in amyotrophic lateral sclerosis. *N Engl J Med,* 326**,** 1464-8.

ROTHSTEIN, J. D., VAN KAMMEN, M., LEVEY, A. I., MARTIN, L. J. & KUNCL, R. W. 1995. Selective loss of glial glutamate transporter GLT-1 in amyotrophic lateral sclerosis. *Ann Neurol,* 38**,** 73-84.

SAADOUN, D., ROSENZWAJG, M., JOLY, F., SIX, A., CARRAT, F., THIBAULT, V., SENE, D., CACOUB, P. & KLATZMANN, D. 2011. Regulatory T-cell responses to low-dose interleukin-2 in HCV-induced vasculitis. *N Engl J Med,* 365**,** 2067-77.

SACCON, R. A., BUNTON-STASYSHYN, R. K., FISHER, E. M. & FRATTA, P. 2013. Is SOD1 loss of function involved in amyotrophic lateral sclerosis? *Brain,* 136**,** 2342-58.

SAMARASINGHE, S., VIRGO, L. & DE BELLEROCHE, J. 1996. Distribution of the N-methyl-D-aspartate glutamate receptor subunit NR2A in control and amyotrophic lateral sclerosis spinal cord. *Brain Res,* 727**,** 233-7.

SANJABI, S., OH, S. A. & LI, M. O. 2017. Regulation of the Immune Response by TGF-β: From Conception to Autoimmunity and Infection. *Cold Spring Harb Perspect Biol,* 9.

SANTOS, R., VADODARIA, K. C., JAEGER, B. N., MEI, A., LEFCOCHILOS-FOGELQUIST, S., MENDES, A. P. D., ERIKSON, G., SHOKHIREV, M., RANDOLPH-MOORE, L., FREDLENDER, C., DAVE, S., OEFNER, R., FITZPATRICK, C., PENA, M., BARRON, J. J., KU, M., DENLI, A. M., KERMAN, B. E., CHARNAY, P., KELSOE, J. R., MARCHETTO, M. C. & GAGE, F. H.

2017. Differentiation of Inflammation-Responsive Astrocytes from Glial Progenitors Generated from Human Induced Pluripotent Stem Cells. *Stem Cell Reports,* 8**,** 1757-1769.

SARDER, M., SAITO, H. & ABE, K. 1993. Interleukin-2 promotes survival and neurite extension of cultured neurons from fetal rat brain. *Brain Res,* 625**,** 347-50.

SARESELLA, M., PIANCONE, F., TORTORELLA, P., MARVENTANO, I., GATTI, A., CAPUTO, D., LUNETTA, C., CORBO, M., ROVARIS, M. & CLERICI, M. 2013. T helper-17 activation dominates the immunologic milieu of both amyotrophic lateral sclerosis and progressive multiple sclerosis. *Clin Immunol,* 148**,** 79-88.

SARLETTE, A., KRAMPFL, K., GROTHE, C., NEUHOFF, N., DENGLER, R. & PETRI, S. 2008. Nuclear erythroid 2-related factor 2-antioxidative response element signaling pathway in motor cortex and spinal cord in amyotrophic lateral sclerosis. *J Neuropathol Exp Neurol,* 67**,** 1055-62.

SASAKI, S., HORIE, Y. & IWATA, M. 2007. Mitochondrial alterations in dorsal root ganglion cells in sporadic amyotrophic lateral sclerosis. *Acta Neuropathol,* 114**,** 633-9.

SASAKI, S., KOMORI, T. & IWATA, M. 2000. Excitatory amino acid transporter 1 and 2 immunoreactivity in the spinal cord in amyotrophic lateral sclerosis. *Acta Neuropathol,* 100**,** 138-44.

SASAKI, S., WARITA, H., ABE, K. & IWATA, M. 2001. Inducible nitric oxide synthase (iNOS) and nitrotyrosine immunoreactivity in the spinal cords of transgenic mice with a G93A mutant SOD1 gene. *J Neuropathol Exp Neurol,* 60**,** 839-46.

SCHIFFER, D., CORDERA, S., CAVALLA, P. & MIGHELI, A. 1996. Reactive astrogliosis of the spinal cord in amyotrophic lateral sclerosis. *J Neurol Sci,* 139 Suppl**,** 27-33.

SCHMIDT, A., OBERLE, N. & KRAMMER, P. H. 2012. Molecular mechanisms of treg-mediated T cell suppression. *Front Immunol,* 3**,** 51.

SEKIZAWA, T., OPENSHAW, H., OHBO, K., SUGAMURA, K., ITOYAMA, Y. & NILAND, J. C. 1998. Cerebrospinal fluid interleukin 6 in amyotrophic lateral sclerosis: immunological parameter and comparison with inflammatory and non-inflammatory central nervous system diseases. *J Neurol Sci,* 154**,** 194-9.

SEMPLE, B. D., FRUGIER, T. & MORGANTI-KOSSMANN, M. C. 2010. CCL2 modulates cytokine production in cultured mouse astrocytes. *J Neuroinflammation,* 7**,** 67.

SETO, D., KAR, S. & QUIRION, R. 1997. Evidence for direct and indirect mechanisms in the potent modulatory action of interleukin-2 on the release of acetylcholine in rat hippocampal slices. *Br J Pharmacol,* 120**,** 1151-7.

SHAW, P. J., INCE, P. G., FALKOUS, G. & MANTLE, D. 1995. Oxidative damage to protein in sporadic motor neuron disease spinal cord. *Ann Neurol,* 38**,** 691-5.

SHEEAN, R. K., MCKAY, F. C., CRETNEY, E., BYE, C. R., PERERA, N. D., TOMAS, D., WESTON, R. A., SCHELLER, K. J., DJOUMA, E., MENON, P., SCHIBECI, S. D., MARMASH, N., YERBURY, J. J., NUTT, S. L., BOOTH, D. R., STEWART, G. J., KIERNAN, M. C., VUCIC, S. & TURNER, B. J. 2018. Association of Regulatory T-Cell Expansion With Progression of Amyotrophic Lateral Sclerosis: A Study of Humans and a Transgenic Mouse Model. *JAMA Neurol*.

SHELLIKERI, S., KARTHIKEYAN, V., MARTINO, R., BLACK, S. E., ZINMAN, L., KEITH, J. & YUNUSOVA, Y. 2017. The neuropathological signature of bulbar-onset ALS: A systematic review. *Neurosci Biobehav Rev,* 75**,** 378-392.

SHEN, Y., LIU, S. S., ZHAN, M. Y., LUO, J. H. & ZHU, L. J. 2010. Interleukin-2 enhances dendritic development and spinogenesis in cultured hippocampal neurons. *Anat Rec (Hoboken),* 293**,** 1017-23.

SHIMIZU, J., YAMAZAKI, S., TAKAHASHI, T., ISHIDA, Y. & SAKAGUCHI, S. 2002. Stimulation of CD25(+)CD4(+) regulatory T cells through GITR breaks immunological self-tolerance. *Nat Immunol,* 3**,** 135-42.

SHIMOJO, M., IMAI, Y., NAKAJIMA, K., MIZUSHIMA, S., UEMURA, A. & KOHSAKA, S. 1993. Interleukin-2 enhances the viability of primary cultured rat neocortical neurons. *Neurosci Lett,* 151**,** 170-3.

SIMPSON, E. P., HENRY, Y. K., HENKEL, J. S., SMITH, R. G. & APPEL, S. H. 2004. Increased lipid peroxidation in sera of ALS patients: a potential biomarker of disease burden. *Neurology,* 62**,** 1758-65.

SIMÓN-SÁNCHEZ, J., DOPPER, E. G., COHN-HOKKE, P. E., HUKEMA, R. K., NICOLAOU, N., SEELAAR, H., DE GRAAF, J. R., DE KONING, I., VAN SCHOOR, N. M., DEEG, D. J., SMITS, M., RAAPHORST, J., VAN DEN BERG, L. H., SCHELHAAS, H. J., DE DIE-SMULDERS, C. E., MAJOOR-KRAKAUER, D., ROZEMULLER, A. J., WILLEMSEN, R., PIJNENBURG, Y. A., HEUTINK, P. & VAN SWIETEN, J. C. 2012. The clinical and pathological phenotype of C9ORF72 hexanucleotide repeat expansions. *Brain,* 135**,** 723-35.

SIVANDZADE, F., PRASAD, S., BHALERAO, A. & CUCULLO, L. 2019. NRF2 and NF-κB interplay in cerebrovascular and neurodegenerative disorders: Molecular mechanisms and possible therapeutic approaches. *Redox Biol,* 21**,** 101059.

SKAPER, S. D., FACCI, L., ZUSSO, M. & GIUSTI, P. 2018. An Inflammation-Centric View of Neurological Disease: Beyond the Neuron. *Front Cell Neurosci,* 12**,** 72.

SMITH, E. F., SHAW, P. J. & DE VOS, K. J. 2019. The role of mitochondria in amyotrophic lateral sclerosis. *Neurosci Lett,* 710**,** 132933.

SPOLSKI, R., LI, P. & LEONARD, W. J. 2018. Biology and regulation of IL-2: from molecular mechanisms to human therapy. *Nat Rev Immunol,* 18**,** 648-659.

STA, M., SYLVA-STEENLAND, R. M., CASULA, M., DE JONG, J. M., TROOST, D., ARONICA, E. & BAAS, F. 2011. Innate and adaptive immunity in amyotrophic lateral sclerosis: evidence of complement activation. *Neurobiol Dis,* 42**,** 211-20.

STAATS, K. A., HERNANDEZ, S., SCHÖNEFELDT, S., BENTO-ABREU, A., DOOLEY, J., VAN DAMME, P., LISTON, A., ROBBERECHT, W. & VAN DEN BOSCH, L. 2013. Rapamycin increases survival in ALS mice lacking mature lymphocytes. *Mol Neurodegener,* 8**,** 31.

STEPHENSON, J., NUTMA, E., VAN DER VALK, P. & AMOR, S. 2018. Inflammation in CNS neurodegenerative diseases. *Immunology*.

STOMMEL, E. W., COHEN, J. A., FADUL, C. E., COGBILL, C. H., GRABER, D. J., KINGMAN, L., MACKENZIE, T., CHANNON SMITH, J. Y. & HARRIS, B. T. 2009. Efficacy of thalidomide for the treatment of amyotrophic lateral sclerosis: a phase II open label clinical trial. *Amyotroph Lateral Scler,* 10**,** 393-404.

STOPFORD, M. J., ALLEN, S. P. & FERRAIUOLO, L. 2019. A High-throughput and Pathophysiologically Relevant Astrocyte-motor Neuron Co-culture Assay for Amyotrophic Lateral Sclerosis Therapeutic Discovery. *Bio Protoc,* 9.

SUH, J. H., SHENVI, S. V., DIXON, B. M., LIU, H., JAISWAL, A. K., LIU, R. M. & HAGEN, T. M. 2004. Decline in transcriptional activity of Nrf2 causes age-related loss of glutathione synthesis, which is reversible with lipoic acid. *Proc Natl Acad Sci U S A,* 101**,** 3381-6.

SUPEK, F., BOŠNJAK, M., ŠKUNCA, N. & ŠMUC, T. 2011. REVIGO summarizes and visualizes long lists of gene ontology terms. *PLoS One,* 6**,** e21800.

SURLES, T. A. C. J. G. 2007. Model-Dependent Variance Inflation Factor Cutoff Values. Quality Engineering.

SWINDELL, W. R., KRUSE, C. P. S., LIST, E. O., BERRYMAN, D. E. & KOPCHICK, J. J. 2019. ALS blood expression profiling identifies new biomarkers, patient subgroups, and evidence for neutrophilia and hypoxia. *J Transl Med,* 17**,** 170.

TAN, C. F., EGUCHI, H., TAGAWA, A., ONODERA, O., IWASAKI, T., TSUJINO, A., NISHIZAWA, M., KAKITA, A. & TAKAHASHI, H. 2007. TDP-43 immunoreactivity in neuronal inclusions in familial amyotrophic lateral sclerosis with or without SOD1 gene mutation. *Acta Neuropathol,* 113**,** 535-42.

TAN, E., LYNN, D. J., AMATO, A. A., KISSEL, J. T., RAMMOHAN, K. W., SAHENK, Z., WARMOLTS, J. R., JACKSON, C. E., BAROHN, R. J. & MENDELL, J. R. 1994. Immunosuppressive treatment of motor neuron syndromes. Attempts to distinguish a treatable disorder. *Arch Neurol,* 51**,** 194-200.

TANAKA, M., KIKUCHI, H., ISHIZU, T., MINOHARA, M., OSOEGAWA, M., MOTOMURA, K., TATEISHI, T., OHYAGI, Y. & KIRA, J. 2006. Intrathecal upregulation of granulocyte colony stimulating factor and its neuroprotective actions on motor neurons in amyotrophic lateral sclerosis. *J Neuropathol Exp Neurol,* 65**,** 816-25.

TANG, Q., ADAMS, J. Y., PENARANDA, C., MELLI, K., PIAGGIO, E., SGOUROUDIS, E., PICCIRILLO, C. A., SALOMON, B. L. & BLUESTONE, J. A. 2008. Central role of defective interleukin-2 production in the triggering of islet autoimmune destruction. *Immunity,* 28**,** 687-97.

TARASSISHIN, L., SUH, H. S. & LEE, S. C. 2014. LPS and IL-1 differentially activate mouse and human astrocytes: role of CD14. *Glia,* 62**,** 999-1013.

TATEISHI, T., YAMASAKI, R., TANAKA, M., MATSUSHITA, T., KIKUCHI, H., ISOBE, N., OHYAGI, Y. & KIRA, J. 2010. CSF chemokine alterations related to the clinical course of amyotrophic lateral sclerosis. *J Neuroimmunol,* 222**,** 76-81.

TEO, J. L. & KAHN, M. 2010. The Wnt signaling pathway in cellular proliferation and differentiation: A tale of two coactivators. *Adv Drug Deliv Rev,* 62**,** 1149-55.

THELIN, E. P., HALL, C. E., TYZACK, G. E., FROSTELL, A., GIORGI-COLL, S., ALAM, A., CARPENTER, K. L. H., MITCHELL, J., TAJSIC, T., HUTCHINSON, P. J., PATANI, R. & HELMY, A. 2020. Delineating Astrocytic Cytokine Responses in a Human Stem Cell Model of Neural Trauma. *J Neurotrauma,* 37**,** 93-105.

THONHOFF, J. R., BEERS, D. R., ZHAO, W., PLEITEZ, M., SIMPSON, E. P., BERRY, J. D., CUDKOWICZ, M. E. & APPEL, S. H. 2018. Expanded autologous regulatory T-lymphocyte infusions in ALS: A phase I, first-in-human study. *Neurol Neuroimmunol Neuroinflamm,* 5**,** e465.

TOKUDA, E., TAKEI, Y. I., OHARA, S., FUJIWARA, N., HOZUMI, I. & FURUKAWA, Y. 2019. Wild-type Cu/Zn-superoxide dismutase is misfolded in cerebrospinal fluid of sporadic amyotrophic lateral sclerosis. *Mol Neurodegener,* 14**,** 42.

TOLLERVEY, J. R., CURK, T., ROGELJ, B., BRIESE, M., CEREDA, M., KAYIKCI, M., KÖNIG, J., HORTOBÁGYI, T., NISHIMURA, A. L., ZUPUNSKI, V., PATANI, R., CHANDRAN, S., ROT, G., ZUPAN, B., SHAW, C. E. & ULE, J. 2011. Characterizing the RNA targets and position-dependent splicing regulation by TDP-43. *Nat Neurosci,* 14**,** 452-8.

TRIAS, E., IBARBURU, S., BARRETO-NÚÑEZ, R., VARELA, V., MOURA, I. C., DUBREUIL, P., HERMINE, O., BECKMAN, J. S. & BARBEITO, L. 2017.

Evidence for mast cells contributing to neuromuscular pathology in an inherited model of ALS. *JCI Insight,* 2.
TRIAS, E., KING, P. H., SI, Y., KWON, Y., VARELA, V., IBARBURU, S., KOVACS, M., MOURA, I. C., BECKMAN, J. S., HERMINE, O. & BARBEITO, L. 2018. Mast cells and neutrophils mediate peripheral motor pathway degeneration in ALS. *JCI Insight,* 3.
TSUBOI, Y. & YAMADA, T. 1994. Increased concentration of C4d complement protein in CSF in amyotrophic lateral sclerosis. *J Neurol Neurosurg Psychiatry,* 57**,** 859-61.
TSUDA, M., KOHRO, Y., YANO, T., TSUJIKAWA, T., KITANO, J., TOZAKI-SAITOH, H., KOYANAGI, S., OHDO, S., JI, R. R., SALTER, M. W. & INOUE, K. 2011. JAK-STAT3 pathway regulates spinal astrocyte proliferation and neuropathic pain maintenance in rats. *Brain,* 134**,** 1127-39.
TURNER, M. R., CAGNIN, A., TURKHEIMER, F. E., MILLER, C. C., SHAW, C. E., BROOKS, D. J., LEIGH, P. N. & BANATI, R. B. 2004. Evidence of widespread cerebral microglial activation in amyotrophic lateral sclerosis: an [11C](R)-PK11195 positron emission tomography study. *Neurobiol Dis,* 15**,** 601-9.
TYZACK, G. E., LUISIER, R., TAHA, D. M., NEEVES, J., MODIC, M., MITCHELL, J. S., MEYER, I., GREENSMITH, L., NEWCOMBE, J., ULE, J., LUSCOMBE, N. M. & PATANI, R. 2019. Widespread FUS mislocalization is a molecular hallmark of amyotrophic lateral sclerosis. *Brain,* 142**,** 2572-2580.
VAN DYKE, J. M., SMIT-OISTAD, I. M., MACRANDER, C., KRAKORA, D., MEYER, M. G. & SUZUKI, M. 2016. Macrophage-mediated inflammation and glial response in the skeletal muscle of a rat model of familial amyotrophic lateral sclerosis (ALS). *Exp Neurol,* 277**,** 275-282.
VANCE, C., ROGELJ, B., HORTOBÁGYI, T., DE VOS, K. J., NISHIMURA, A. L., SREEDHARAN, J., HU, X., SMITH, B., RUDDY, D., WRIGHT, P., GANESALINGAM, J., WILLIAMS, K. L., TRIPATHI, V., AL-SARAJ, S., AL-CHALABI, A., LEIGH, P. N., BLAIR, I. P., NICHOLSON, G., DE BELLEROCHE, J., GALLO, J. M., MILLER, C. C. & SHAW, C. E. 2009. Mutations in FUS, an RNA processing protein, cause familial amyotrophic lateral sclerosis type 6. *Science,* 323**,** 1208-1211.
VANDE VELDE, C., MCDONALD, K. K., BOUKHEDIMI, Y., MCALONIS-DOWNES, M., LOBSIGER, C. S., BEL HADJ, S., ZANDONA, A., JULIEN, J. P., SHAH, S. B. & CLEVELAND, D. W. 2011. Misfolded SOD1 associated with motor neuron mitochondria alters mitochondrial shape and distribution prior to clinical onset. *PLoS One,* 6**,** e22031.
VARGAS, M. R. & JOHNSON, J. A. 2010. Astrogliosis in amyotrophic lateral sclerosis: role and therapeutic potential of astrocytes. *Neurotherapeutics,* 7**,** 471-81.
VENT-SCHMIDT, J., HAN, J. M., MACDONALD, K. G. & LEVINGS, M. K. 2014. The role of FOXP3 in regulating immune responses. *Int Rev Immunol,* 33**,** 110-28.
VERBER, N. S., SHEPHEARD, S. R., SASSANI, M., MCDONOUGH, H. E., MOORE, S. A., ALIX, J. J. P., WILKINSON, I. D., JENKINS, T. M. & SHAW, P. J. 2019. Biomarkers in Motor Neuron Disease: A State of the Art Review. *Front Neurol,* 10**,** 291.
VERKHRATSKY, A. & NEDERGAARD, M. 2018. Physiology of Astroglia. *Physiol Rev,* 98**,** 239-389.
VERKHRATSKY, A., PARPURA, V., PEKNA, M., PEKNY, M. & SOFRONIEW, M. 2014. Glia in the pathogenesis of neurodegenerative diseases. *Biochem Soc Trans,* 42**,** 1291-301.

VIELHABER, S., KUNZ, D., WINKLER, K., WIEDEMANN, F. R., KIRCHES, E., FEISTNER, H., HEINZE, H. J., ELGER, C. E., SCHUBERT, W. & KUNZ, W. S. 2000. Mitochondrial DNA abnormalities in skeletal muscle of patients with sporadic amyotrophic lateral sclerosis. *Brain,* 123 (Pt 7)**,** 1339-48.

VIGNALI, D. A., COLLISON, L. W. & WORKMAN, C. J. 2008. How regulatory T cells work. *Nat Rev Immunol,* 8**,** 523-32.

VIRGO, L. & DE BELLEROCHE, J. 1995. Induction of the immediate early gene c-jun in human spinal cord in amyotrophic lateral sclerosis with concomitant loss of NMDA receptor NR-1 and glycine transporter mRNA. *Brain Res,* 676**,** 196-204.

VIVIER, E., TOMASELLO, E., BARATIN, M., WALZER, T. & UGOLINI, S. 2008. Functions of natural killer cells. *Nat Immunol,* 9**,** 503-10.

WAGUESPACK, P. J., BANKS, W. A. & KASTIN, A. J. 1994. Interleukin-2 does not cross the blood-brain barrier by a saturable transport system. *Brain Res Bull,* 34**,** 103-9.

WANG, H. A., LEE, J. D., LEE, K. M., WOODRUFF, T. M. & NOAKES, P. G. 2017. Complement C5a-C5aR1 signalling drives skeletal muscle macrophage recruitment in the hSOD1. *Skelet Muscle,* 7**,** 10.

WANG, R., YANG, B. & ZHANG, D. 2011. Activation of interferon signaling pathways in spinal cord astrocytes from an ALS mouse model. *Glia,* 59**,** 946-58.

WANG, W., LI, L., LIN, W. L., DICKSON, D. W., PETRUCELLI, L., ZHANG, T. & WANG, X. 2013. The ALS disease-associated mutant TDP-43 impairs mitochondrial dynamics and function in motor neurons. *Hum Mol Genet,* 22**,** 4706-19.

WANG, Y., JIN, S., SONOBE, Y., CHENG, Y., HORIUCHI, H., PARAJULI, B., KAWANOKUCHI, J., MIZUNO, T., TAKEUCHI, H. & SUZUMURA, A. 2014. Interleukin-1β induces blood-brain barrier disruption by downregulating Sonic hedgehog in astrocytes. *PLoS One,* 9**,** e110024.

WEBSTER, C. P., SMITH, E. F., BAUER, C. S., MOLLER, A., HAUTBERGUE, G. M., FERRAIUOLO, L., MYSZCZYNSKA, M. A., HIGGINBOTTOM, A., WALSH, M. J., WHITWORTH, A. J., KASPAR, B. K., MEYER, K., SHAW, P. J., GRIERSON, A. J. & DE VOS, K. J. 2016. The C9orf72 protein interacts with Rab1a and the ULK1 complex to regulate initiation of autophagy. *EMBO J,* 35**,** 1656-76.

WEIDUSCHAT, N., MAO, X., HUPF, J., ARMSTRONG, N., KANG, G., LANGE, D. J., MITSUMOTO, H. & SHUNGU, D. C. 2014. Motor cortex glutathione deficit in ALS measured in vivo with the J-editing technique. *Neurosci Lett,* 570**,** 102-7.

WHANGBO, J. S., KIM, H. T., MIRKOVIC, N., LEONARD, L., PORYANDA, S., SILVERSTEIN, S., KIM, S., REYNOLDS, C. G., RAI, S. C., VERRILL, K., LEE, M. A., MARGOSSIAN, S., DUNCAN, C., LEHMANN, L., HUANG, J., NIKIFOROW, S., ALYEA, E. P., ARMAND, P., CUTLER, C. S., HO, V. T., BLAZAR, B. R., ANTIN, J. H., SOIFFER, R. J., RITZ, J. & KORETH, J. 2019a. Dose-escalated interleukin-2 therapy for refractory chronic graft-versus-host disease in adults and children. *Blood Adv,* 3**,** 2550-2561.

WHANGBO, J. S., KIM, H. T., NIKIFOROW, S., KORETH, J., ALHO, A. C., FALAHEE, B., KIM, S., DUSENBURY, K., FIELDS, M. J., REYNOLDS, C. G., ALYEA, E. P., ARMAND, P., CUTLER, C. S., HO, V. T., ANTIN, J. H., SOIFFER, R. J. & RITZ, J. 2019b. Functional analysis of clinical response to low-dose IL-2 in patients with refractory chronic graft-versus-host disease. *Blood Adv,* 3**,** 984-994.

WIEDEMANN, F. R., MANFREDI, G., MAWRIN, C., BEAL, M. F. & SCHON, E. A. 2002. Mitochondrial DNA and respiratory chain function in spinal cords of ALS patients. *J Neurochem,* 80**,** 616-25.

WIEDEMANN, F. R., WINKLER, K., KUZNETSOV, A. V., BARTELS, C., VIELHABER, S., FEISTNER, H. & KUNZ, W. S. 1998. Impairment of mitochondrial function in skeletal muscle of patients with amyotrophic lateral sclerosis. *J Neurol Sci,* 156**,** 65-72.

WIKENHEISER, D. J. & STUMHOFER, J. S. 2016. ICOS Co-Stimulation: Friend or Foe? *Front Immunol,* 7**,** 304.

WILMS, H., SIEVERS, J., DENGLER, R., BUFLER, J., DEUSCHL, G. & LUCIUS, R. 2003. Intrathecal synthesis of monocyte chemoattractant protein-1 (MCP-1) in amyotrophic lateral sclerosis: further evidence for microglial activation in neurodegeneration. *J Neuroimmunol,* 144**,** 139-42.

WINKELS, H., MEILER, S., LIEVENS, D., ENGEL, D., SPITZ, C., BÜRGER, C., BECKERS, L., DANDL, A., REIM, S., AHMADSEI, M., HARTWIG, H., HOLDT, L. M., HRISTOV, M., MEGENS, R. T. A., SCHMITT, M. M., BIESSEN, E. A., BORST, J., FAUSSNER, A., WEBER, C., LUTGENS, E. & GERDES, N. 2017. CD27 co-stimulation increases the abundance of regulatory T cells and reduces atherosclerosis in hyperlipidaemic mice. *Eur Heart J,* 38**,** 3590-3599.

WOODRUFF, T. M., COSTANTINI, K. J., CRANE, J. W., ATKIN, J. D., MONK, P. N., TAYLOR, S. M. & NOAKES, P. G. 2008. The complement factor C5a contributes to pathology in a rat model of amyotrophic lateral sclerosis. *J Immunol,* 181**,** 8727-34.

WYLEZINSKI, L. S. & HAWIGER, J. 2016. Interleukin 2 Activates Brain Microvascular Endothelial Cells Resulting in Destabilization of Adherens Junctions. *J Biol Chem,* 291**,** 22913-22923.

XIE, L., CHOUDHURY, G. R., WINTERS, A., YANG, S. H. & JIN, K. 2015. Cerebral regulatory T cells restrain microglia/macrophage-mediated inflammatory responses via IL-10. *Eur J Immunol,* 45**,** 180-91.

XIE, L. & YANG, S. H. 2015. Interaction of astrocytes and T cells in physiological and pathological conditions. *Brain Res,* 1623**,** 63-73.

YADAV, M., STEPHAN, S. & BLUESTONE, J. A. 2013. Peripherally induced tregs - role in immune homeostasis and autoimmunity. *Front Immunol,* 4**,** 232.

YAMANAKA, K. & KOMINE, O. 2018. The multi-dimensional roles of astrocytes in ALS. *Neurosci Res,* 126**,** 31-38.

YANG, Q., JIAO, B. & SHEN, L. 2020. The Development of C9orf72-Related Amyotrophic Lateral Sclerosis and Frontotemporal Dementia Disorders. *Front Genet,* 11**,** 562758.

YASOJIMA, K., TOURTELLOTTE, W. W., MCGEER, E. G. & MCGEER, P. L. 2001. Marked increase in cyclooxygenase-2 in ALS spinal cord: implications for therapy. *Neurology,* 57**,** 952-6.

ZHANG, H., TAN, C. F., MORI, F., TANJI, K., KAKITA, A., TAKAHASHI, H. & WAKABAYASHI, K. 2008. TDP-43-immunoreactive neuronal and glial inclusions in the neostriatum in amyotrophic lateral sclerosis with and without dementia. *Acta Neuropathol,* 115**,** 115-22.

ZHANG, R., GASCON, R., MILLER, R. G., GELINAS, D. F., MASS, J., HADLOCK, K., JIN, X., REIS, J., NARVAEZ, A. & MCGRATH, M. S. 2005. Evidence for systemic immune system alterations in sporadic amyotrophic lateral sclerosis (sALS). *J Neuroimmunol,* 159**,** 215-24.

ZHANG, X., LI, L., CHEN, S., YANG, D., WANG, Y., WANG, Z. & LE, W. 2011. Rapamycin treatment augments motor neuron degeneration in SOD1(G93A) mouse model of amyotrophic lateral sclerosis. *Autophagy,* 7**,** 412-25.

ZHAO, D. M., THORNTON, A. M., DIPAOLO, R. J. & SHEVACH, E. M. 2006. Activated CD4+CD25+ T cells selectively kill B lymphocytes. *Blood,* 107**,** 3925-32.

ZHAO, W., BEERS, D. R. & APPEL, S. H. 2013. Immune-mediated mechanisms in the pathoprogression of amyotrophic lateral sclerosis. *J Neuroimmune Pharmacol,* 8**,** 888-99.

ZHAO, W., BEERS, D. R., HOOTEN, K. G., SIEGLAFF, D. H., ZHANG, A., KALYANA-SUNDARAM, S., TRAINI, C. M., HALSEY, W. S., HUGHES, A. M., SATHE, G. M., LIVI, G. P., FAN, G. H. & APPEL, S. H. 2017. Characterization of Gene Expression Phenotype in Amyotrophic Lateral Sclerosis Monocytes. *JAMA Neurol,* 74**,** 677-685.

ZHAO, W., BEERS, D. R., LIAO, B., HENKEL, J. S. & APPEL, S. H. 2012. Regulatory T lymphocytes from ALS mice suppress microglia and effector T lymphocytes through different cytokine-mediated mechanisms. *Neurobiol Dis,* 48**,** 418-28.

ZHAO, W., BEERS, D. R., THONHOFF, J. R., THOME, A. D., FARIDAR, A., WANG, J., WEN, S., ORNELAS, L., SAREEN, D., GOODRIDGE, H. S., SVENDSEN, C. N. & APPEL, S. H. 2020. Immunosuppressive Functions of M2 Macrophages Derived from iPSCs of Patients with ALS and Healthy Controls. *iScience,* 23**,** 101192.

ZHENG, J., CHAN, P. L., LIU, Y., QIN, G., XIANG, Z., LAM, K. T., LEWIS, D. B., LAU, Y. L. & TU, W. 2013. ICOS regulates the generation and function of human CD4+ Treg in a CTLA-4 dependent manner. *PLoS One,* 8**,** e82203.

ZHOU, L., LOPES, J. E., CHONG, M. M., IVANOV, I. I., MIN, R., VICTORA, G. D., SHEN, Y., DU, J., RUBTSOV, Y. P., RUDENSKY, A. Y., ZIEGLER, S. F. & LITTMAN, D. R. 2008. TGF-beta-induced Foxp3 inhibits T(H)17 cell differentiation by antagonizing RORgammat function. *Nature,* 453**,** 236-40.

ZHOU, Y., ZHOU, B., PACHE, L., CHANG, M., KHODABAKHSHI, A. H., TANASEICHUK, O., BENNER, C. & CHANDA, S. K. 2019. Metascape provides a biologist-oriented resource for the analysis of systems-level datasets. *Nat Commun,* 10**,** 1523.

ZINSZNER, H., SOK, J., IMMANUEL, D., YIN, Y. & RON, D. 1997. TLS (FUS) binds RNA in vivo and engages in nucleo-cytoplasmic shuttling. *J Cell Sci,* 110 (Pt 15)**,** 1741-50.

ZONDLER, L., MÜLLER, K., KHALAJI, S., BLIEDERHÄUSER, C., RUF, W. P., GROZDANOV, V., THIEMANN, M., FUNDEL-CLEMES, K., FREISCHMIDT, A., HOLZMANN, K., STROBEL, B., WEYDT, P., WITTING, A., THAL, D. R., HELFERICH, A. M., HENGERER, B., GOTTSCHALK, K. E., HILL, O., KLUGE, M., LUDOLPH, A. C., DANZER, K. M. & WEISHAUPT, J. H. 2016. Peripheral monocytes are functionally altered and invade the CNS in ALS patients. *Acta Neuropathol,* 132**,** 391-411.

ZORN, E., NELSON, E. A., MOHSENI, M., PORCHERAY, F., KIM, H., LITSA, D., BELLUCCI, R., RADERSCHALL, E., CANNING, C., SOIFFER, R. J., FRANK, D. A. & RITZ, J. 2006. IL-2 regulates FOXP3 expression in human CD4+CD25+ regulatory T cells through a STAT-dependent mechanism and induces the expansion of these cells in vivo. *Blood,* 108**,** 1571-9.

ZOU, Y. H., GUAN, P. P., ZHANG, S. Q., GUO, Y. S. & WANG, P. 2020. Rofecoxib Attenuates the Pathogenesis of Amyotrophic Lateral Sclerosis by Alleviating Cyclooxygenase-2-Mediated Mechanisms. *Front Neurosci,* 14**,** 817.
ZOU, Z. Y., ZHOU, Z. R., CHE, C. H., LIU, C. Y., HE, R. L. & HUANG, H. P. 2017. Genetic epidemiology of amyotrophic lateral sclerosis: a systematic review and meta-analysis. *J Neurol Neurosurg Psychiatry,* 88**,** 540-549.
ZUCCHI, E., BONETTO, V., SORARÙ, G., MARTINELLI, I., PARCHI, P., LIGUORI, R. & MANDRIOLI, J. 2020. Neurofilaments in motor neuron disorders: towards promising diagnostic and prognostic biomarkers. *Mol Neurodegener,* 15**,** 58.
ÇETIN, G., KLAFACK, S., STUDENCKA-TURSKI, M., KRÜGER, E. & EBSTEIN, F. 2021. The Ubiquitin-Proteasome System in Immune Cells. *Biomolecules,* 11.